

Alma Mater Studiorum – Università di Bologna

DOTTORATO DI RICERCA IN

Chimica

Ciclo XXX

Settore Concorsuale: 03/C1

Settore Scientifico Disciplinare: CHIM/06

Dynamic stereochemistry of chiral axes.
Design and synthesis of stable atropisomers.

Presentata da: Luca Prati

Coordinatore Dottorato

Prof. Aldo Roda

Supervisore

Prof. Andrea Mazzanti

Co-supervisore

Dr. Michele Mancinelli

Esame finale anno 2018

Abstract

In organic chemistry, dynamic processes involving the conformational exchange are ubiquitous phenomena that occur even in the simplest molecule. The study of the preferential disposition of functional groups and the definition of new interaction is therefore, of vital importance in order to foresee the spatial shape of organic molecules.

In the following work, this has been accomplished by: first, an *in silico* DFT analysis of the conformers, second an experimental evaluation of the relative stability of the predicted conformers using the Dynamic-NMR, Dynamic-HPLC, and kinetic studies, and last the assessment of the potential absolute configuration by mean Electronic Circular Dichroism spectroscopy.

The work herein reported finally aim to define the border between unstable conformations and stable ones (configurations). This border has been explored from both sides: 1) the stereodynamic side, that includes low energy process where the stereochemistry is not stable due to a low energy barrier. In this context are analysed molecules displaying long range interactions where only conformational changes are considered; 2) the stereostable side, where the energy barrier between conformers is high enough to generate distinct molecules. In this framework, the design and the synthesis of stereogenic axes in scaffold that cannot bear conventional stereogenic centre are reported.

This work gives a well-rounded view of the conformational analysis of organic molecules providing new insight in the interaction within stereolabile conformations as well as the generation of new stereostable conformers by the insertion of steric demanding groups.

Chirality is in the eyes of the beholder.

Contents

1	INTRODUCTION	1
1.1	CHIRALITY	1
1.2	NOMENCLATURE AND CLASSIFICATION	2
1.3	STEREOCHEMICAL DESCRIPTORS	6
1.4	SYMMETRY AND TIME SCALE: DYNAMIC STEREOCHEMISTRY	6
1.5	DYNAMIC STEREOCHEMISTRY AND CHIRAL AXES	8
1.6	DYNAMIC STEREOCHEMISTRY AND CHIRAL PROPELLERS	18
	REFERENCES	20
2	DYNAMIC STEREOCHEMISTRY ANALYSIS AND METHODOLOGIES	23
2.1	DYNAMIC NUCLEAR MAGNETIC RESONANCE (D-NMR)	23
2.2	DYNAMIC HIGH PERFORMANCE LIQUID CHROMATOGRAPHY (D-HPLC)	27
2.3	KINETIC STUDIES	29
2.4	THEORETICAL MODELS	31
2.4.1	DENSITY FUNCTIONAL THEORY	32
2.4.2	TRANSITION STATES	34
2.5	ELECTRONIC CIRCULAR DICHROISM: CONFIGURATION AND CONFORMATION ANALYSIS	36
2.5.1	EXCITON COUPLING	39
2.5.2	QUANTUM-MECHANICAL CALCULATIONS.	41
	REFERENCES	42
3	AIM OF THE RESEARCH	45
4	DYNAMIC STEREOCHEMISTRY AND CONFORMATIONAL ANALYSIS	47
4.1	LONG-RANGE BONDING/NONBONDING INTERACTIONS: A DONOR–ACCEPTOR RESONANCE STUDIED BY DYNAMIC NMR	47
4.2	NEW AZO-DECORATED N-PYRROLIDINYLTIAZOLES: SYNTHESIS, PROPERTIES AND AN UNEXPECTED REMOTE SUBSTITUENT EFFECT TRANSMISSION.	55
4.3	COMPUTATIONAL AND D-NMR ANALYSIS OF THE CONFORMATIONAL ISOMERS AND STEREODYNAMICS OF SECONDARY 2,2'-BISANILIDES	59

REFERENCES	71
5 CHASE FOR NEW ATROPISOMERS	73
5.1 CONFORMATIONAL ANALYSIS AND ABSOLUTE CONFIGURATION OF AXIALLY CHIRAL 1-ARYL AND 1,3-DIARYL-XANTHINES.	73
5.2 TETRASUBSTITUTED CYCLOPENTADIENONES AS SUITABLE ENANTIOPURE LIGANDS WITH AXIAL CHIRALITY.	88
REFERENCES	103
6 APPENDIX	105
6.1 STUDY OF 1,8 NAPHTHALENE DERIVATIVES AS SENSORS FOR NUCLEOBASES AND CHIRAL PRIMARY AMINE	105
6.1.1 NUCLEOBASES SENSING	105
6.1.2 CHIRAL PRIMARY AMINE SENSING	108
REFERENCES	110
7 EXPERIMENTAL SECTION	111
7.1 LONG-RANGE BONDING/NONBONDING INTERACTIONS: A DONOR-ACCEPTOR RESONANCE STUDIED BY DYNAMIC NMR	111
7.1.1 SYNTHETICAL PROCEDURE	111
7.1.2 DYNAMIC NMR	121
7.2 NEW AZO-DECORATED N-PYRROLIDINYLTIAZOLES: SYNTHESIS, PROPERTIES AND AN UNEXPECTED REMOTE SUBSTITUENT EFFECT TRANSMISSION	128
7.2.1 DYNAMIC NMR	128
7.3 COMPUTATIONAL AND DNMR ANALYSIS OF THE CONFORMATIONAL ISOMERS AND STEREODYNAMICS OF SECONDARY 2,2'-BISANILIDES	129
7.3.1 SYNTHETICAL PROCEDURE	130
7.4 CONFORMATIONAL ANALYSIS AND ABSOLUTE CONFIGURATION OF AXIALLY CHIRAL 1-ARYL AND 1,3-DIARYL-XANTHINES	136
7.4.1 KINETIC STUDIES	137
7.4.2 SYNTHETIC PROCEDURES	145
7.4.3 ASSIGNMENT OF ABSOLUTE CONFIGURATION	159
7.5 TETRASUBSTITUTED CYCLOPENTADIENONES AS SUITABLE ENANTIOPURE LIGANDS WITH AXIAL CHIRALITY	166
7.5.1 SYNTHETIC PROCEDURE	167

1 Introduction

1.1 Chirality

Chirality is a pervading property of the universe. It is a feature of nature spanning from the living being to the inanimate world of light and elementary particles.¹

In chemistry, in particular it is followed the definition provided by IUPAC: “The geometric property of a rigid object (or spatial arrangement of points or atoms) of being non-superimposable on its mirror image; such an object has no symmetry elements of the second kind (a mirror plane, $\sigma = S_1$, a centre of inversion, $i = S_2$, a rotation-reflection axis, S_{2n}). If the object is superimposable on its mirror image the object is described as being achiral.”²

This definition is particularly true at molecular level in which chirality allows the generations of enantiomers that are mirror images one of the other but not superimposable. While in an achiral environment an enantiomeric couple has the same chemical and physical properties, in a chiral one they can display striking different behaviour. This effect is magnified in the living beings, where there is a high concentration of chiral elements (from the helix of the double strand of the DNA to the L-amino acid abundance), and is displayed a high sensitivity towards the interaction with single enantiomers. On this regards, fragrance and drugs can well exemplify the susceptibility of the biological systems towards chiral object.

For instance, limonene ((\pm)-1-methyl-4-(prop-1-en-2-yl)cyclohex-1-ene) exists as *S* and *R* enantiomers that interact differently with our body and respectively each enantiomer are responsible for the scent of lemon and orange (Figure 1.1.1a).

Unfortunately, the importance of chirality in synthetic drugs was taken much more into consideration when negative side effects showed up. Thalidomide was a drug prescribed to pregnant women in the 1960s as anti-nausea. While the *R* enantiomer was active to alleviate nausea, its mirror image, the *S* enantiomer was a teratogen agent. Undisclosed the side effects, the drug was approved as a mixture 50:50 of the *R* and the *S* enantiomer (racemic) and it has caused hundreds of cases of severe birth defects³ (Figure 1.1.1b).

Since then, the stereochemical behaviour of biologically active compound has gained increasingly attention and many sophisticated ways of enantioselective synthesis were designed. Moreover, once the globally and health related importance of chirality and its wide range of applicability was realised, researchers have focused their attention in study new type of molecular chirality in which it is explored the limits to determine the non “*superimposability*” of a molecule with its mirror image.

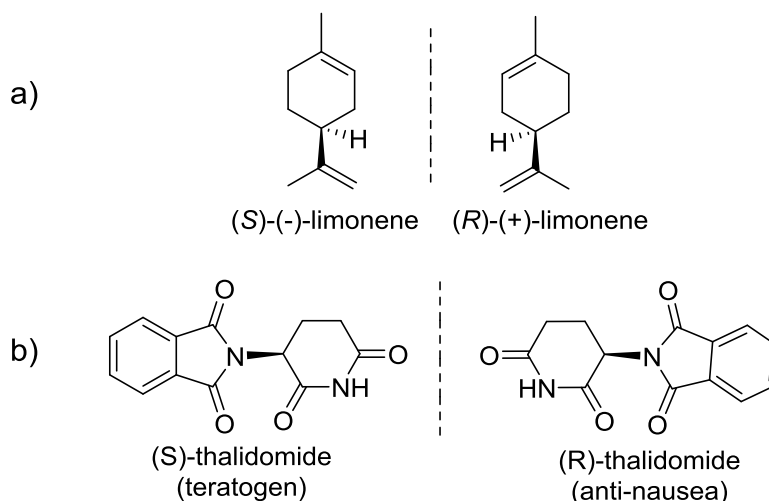


Figure 1.1.1 Structure of chiral biological active molecules

1.2 Nomenclature and classification

Due to the different activity of enantiomers it is of crucial importance to discriminate them in a chemical system. Although this detection may appear trivial it is not always straightforward to define the chirality of a chemical object. Therefore, it is important to have in mind how to detect and classify the chiral systems.

Taking as example two compounds with the same molecular formula they are considered constitutional isomers if they do not have the same connectivity between the atoms (as in 2-nitro and 3-nitro toluene). On the contrary, stereoisomers display the same connectivity but differs in the disposition of atoms in the space. It is noteworthy that are formally considered stereoisomers also the different disposition resulting from the rotation around a single bond, as the four stereoisomers conceivable for the *n*-butane (Figure 1.2.1).

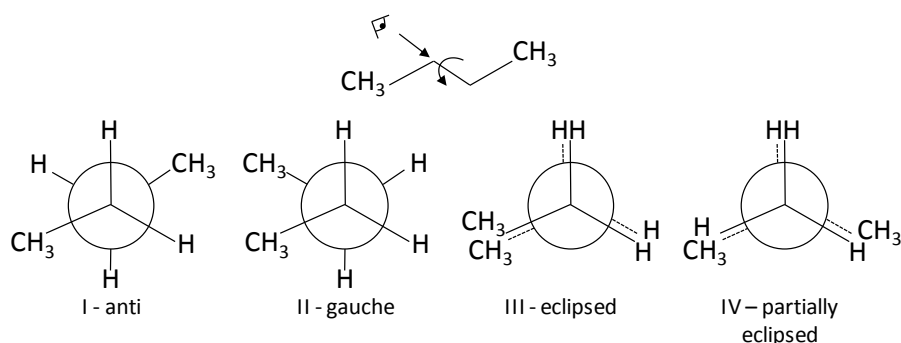


Figure 1.2.1 Stereoisomers determined by the rotation around a single bond of *n*-butane

A stereoisomer that are non-superimposable with its mirror image is called enantiomer otherwise it is identified as diastereoisomer. The geometrical conditions requested for a chemical system to have its mirror image non-superimposable with itself identify chirality in that system. These conditions

can be described as a lack of some symmetry element² (mirror plane and/or centre of inversion) and can be achieved in chemical system by the presence of a stereogenic units (Figure 1.2.2).

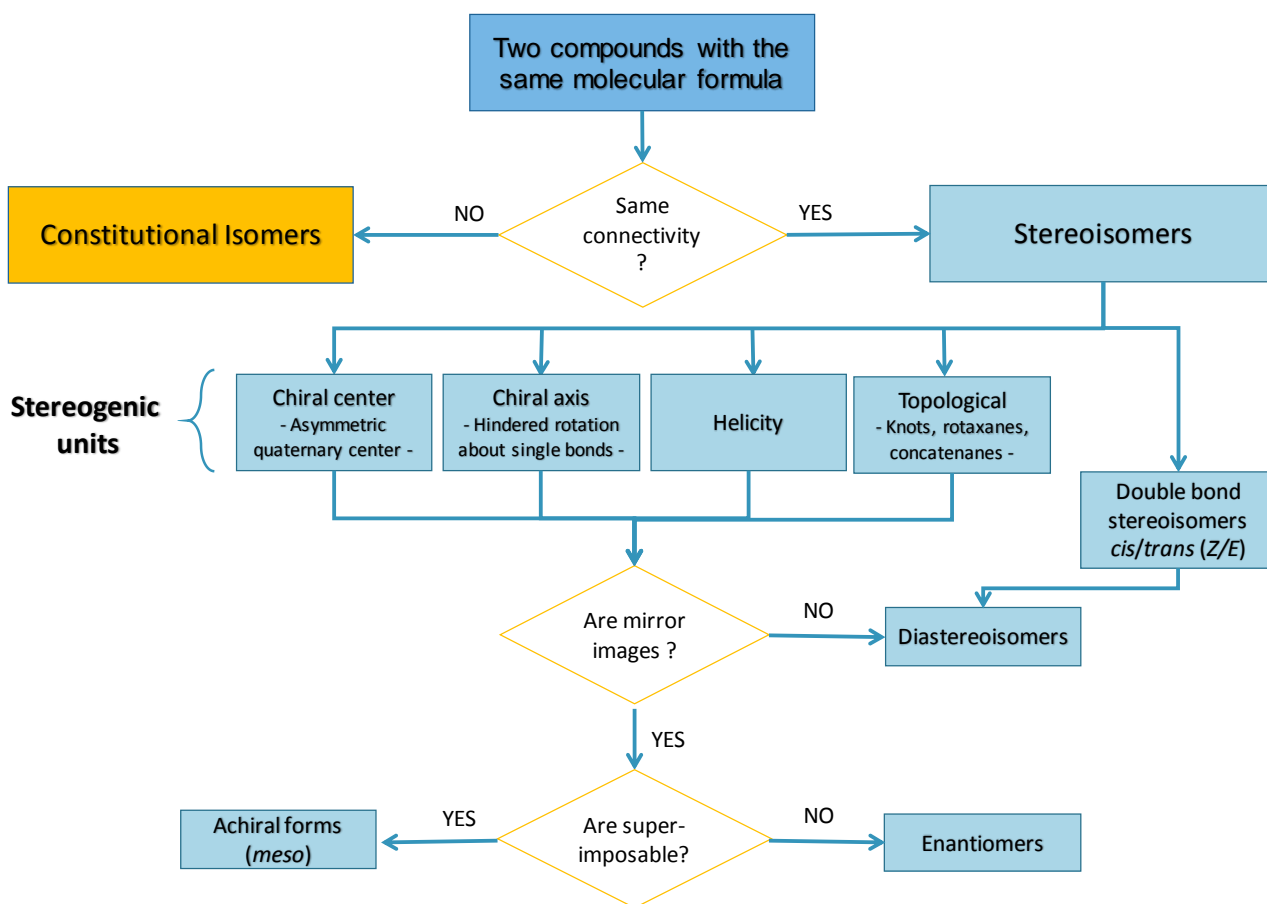


Figure 1.2.2 Classification of chiral molecules

A stereogenic centre is the most common among the stereogenic units and it is identified by a single atom that carries four different substituents (Figure 1.2.3a). Chiral axes, instead, are identified by stereoisomers that can be interconverted by rotation about single bonds with a rotational barrier high enough to avoid interconversion at room temperature (Figure 1.2.3b).⁴ Such enantiomers, where the rotational barrier is higher than 24-25 kcal/mol, are called atropisomers.

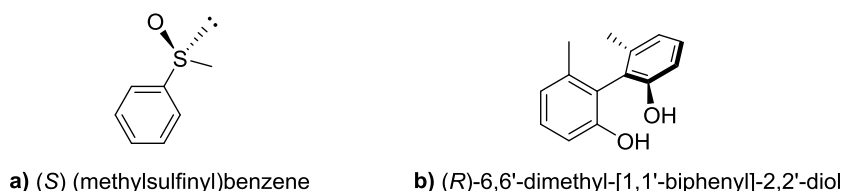


Figure 1.2.3 a) Chiral molecule displaying chiral centre. b) Chiral molecule displaying chiral axes

Stereogenic units such as chiral axes and helicity identify enantiomers that are topologically equivalent, where it is possible to interconvert the two without crossing or breaking bonds. While in chiral axes the distinction is made by merely the rotation around a bond, left-handed and right-handed helical molecules interconvert by the unwind and rewind of the helix. Although such structures can

be found more easily in polymers and bio-polymers like DNA, there are a handful of examples in which helix can be formed in small molecules and their stereodynamic needs to be considered (Figure 1.2.4).

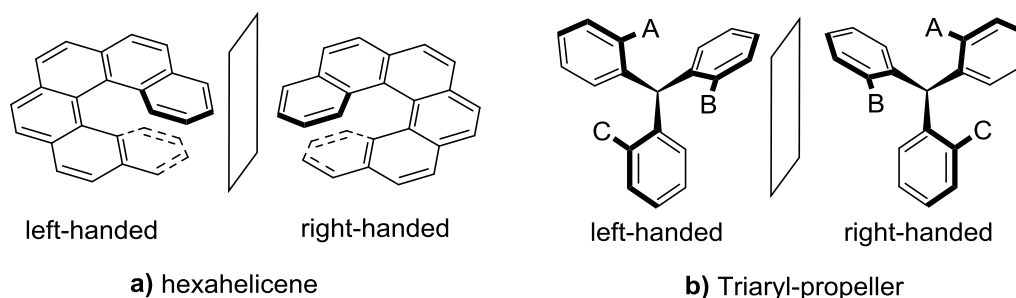


Figure 1.2.4 a) Chiral helicene. b) chiral triaryl propeller

Helicenes⁵ (Figure 1.2.4a) possess a twist in the highly conjugated aromatic system due to an overlap of the benzene rings. The steric clash generates two distinct molecules with a left-handed helix and right-handed ones respectively. While the helicenes display only helical chirality, propeller like molecules such as tri-arylmethane shows three different stereogenic units, namely, a chiral centre, chiral axes and helicity (Figure 1.2.4b). Correspondingly, 2^3 stereoisomers due to the three chiral axes are generated, the CH group generates a chiral centre doubling the number of possible stereoisomers, and lastly the possible stereoisomers can be counted as large as $2^5 = 32$ due to the arrangement of the aryls group as right- or left-handed helix.

The latter derived from the helical disposition of the blades (*i.e.* the aryl substituent around the chiral centre) and is often referred to as propeller chirality. The steric requirements impose the skewed disposition of the blades respect to the central CH, moreover the arrangement of the aryl rings is co-dependent and undergo energetically correlated movement.

The stereoisomers conceivable in a triaryl-propeller are greatly influenced by the nature of the substituents. In the case of identity between A, B and C⁶ the chiral centre is lost and, despite the presence of stereogenic units, some of the possible stereoisomers are not chiral due to the rising of symmetry elements in the molecule. In these cases, the molecule retains its stereogenic units however it is not chiral. It is a *meso* form.

In fact, although in most of the cases stereogenic units generate chiral molecules the lack of symmetry element has never to be overlooked. The presence of one or more of this units it is not an assurance of chirality.

A *meso* compound is defined as a particular compound that has always at least two stereogenic units and between all the conceivable stereoisomers it is the achiral member(s) of a set of diastereoisomers which also includes one or more chiral members.⁷

In Figure 1.2.5 Top are analysed the possible stereoisomers derived from the two chiral centre of 1,2-dimethylcyclopropane. Once the methyl groups lay on the same side of the cyclopropane (*cis*) a symmetry plane is generated and the resulting diastereoisomer is achiral and its mirror image is superimposable to itself. Analogously, in Figure 1.2.5 Bottom is reported a *meso* compound generated by two stereogenic axes, also in this case the molecule gains a plane of symmetry once the 2-methyl-1-naphthyl substituent lay on the same side of the plane defined by the maleimide core.⁸

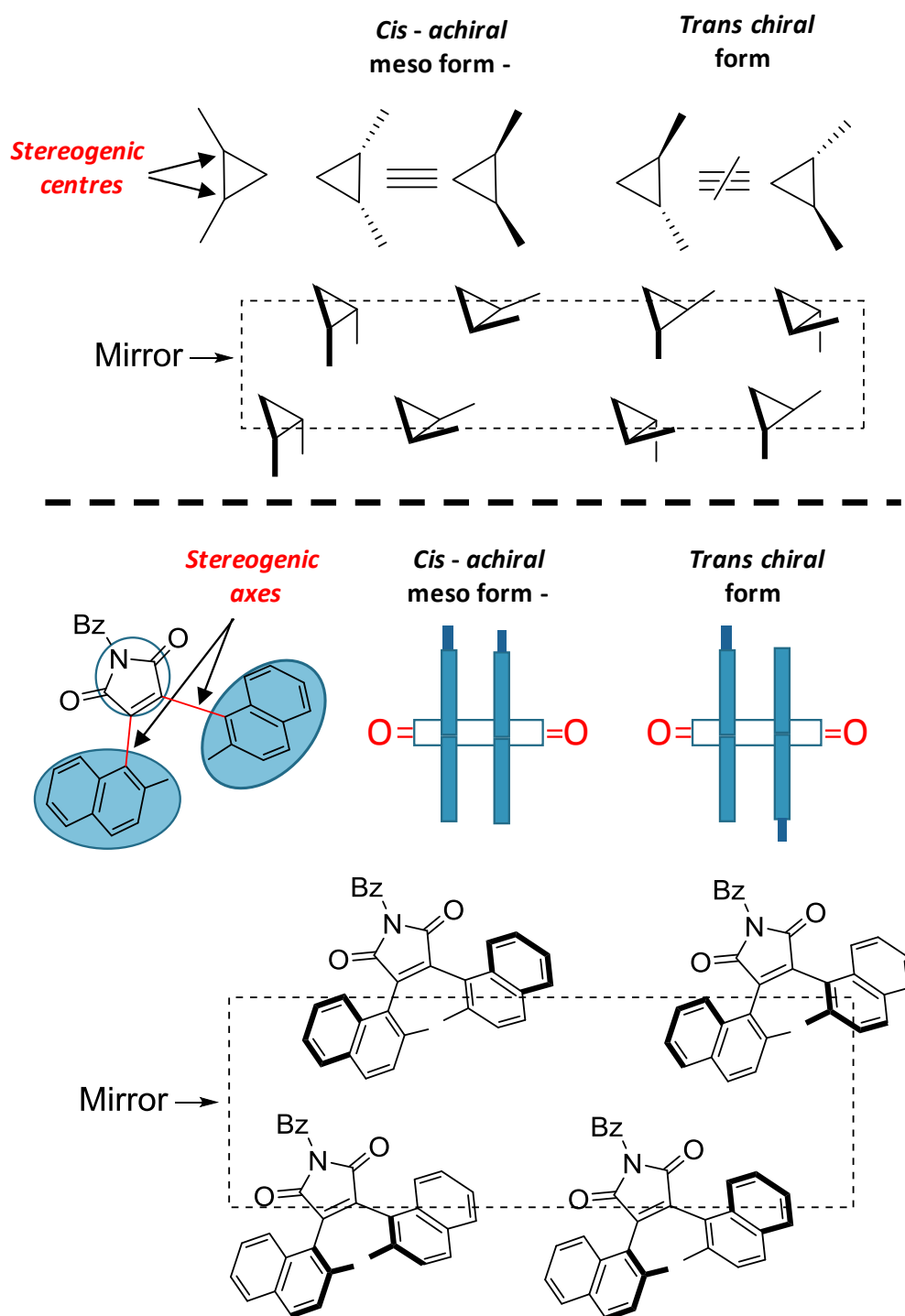


Figure 1.2.5 Top: stereochemistry of 1,2-dimethylcyclopropane Bottom: stereochemistry of 1-benzoyl-3,4-bis(2-methylnaphthalen-1-yl)-1H-pyrrole-2,5-dione

1.3 Stereochemical descriptors

A discussion about stereochemistry needs a clear distinction about stereochemical descriptor. While for chiral centre the *R* and *S* descriptors are well known and defined, there is a lack of clarity in the descriptor *P* and *M* related to molecules carrying chiral axis and/or helix.

Chiral axes generate stereoisomers that are related one to the other by the rotation around a single bond, therefore, the absolute configuration of these molecules should be related to the dihedral angle involved in the rotation. A dihedral angle is identified by four points and defines the torsion angle between two planes. The choice of those four points is crucial to define a descriptor linked to a dihedral angle. An example is reported in Figure 1.3.1 where the four points are described as a chain of atoms **a-b-c-d**, and the torsion angle is the dihedral between the plane identified by the atoms **a, b, c** and the one identified by **b, c, d** (from -180° to $+180^\circ$).

In the assignment of absolute configuration of chiral axis, the **b** and **c** points are placed on the chiral axis while **a** and **d** are the substituent of highest priority (selected with the Cahn–Ingold–Prelog rules) on each side of the bond. Looking from the closest (**a**) and moving along the shortest path to the substituent of highest priority on the other side (**d**), the absolute configuration is assigned *P* (Positive dihedral angle) for clockwise and *M* (Minus, as negative torsion angle) for counter clockwise.

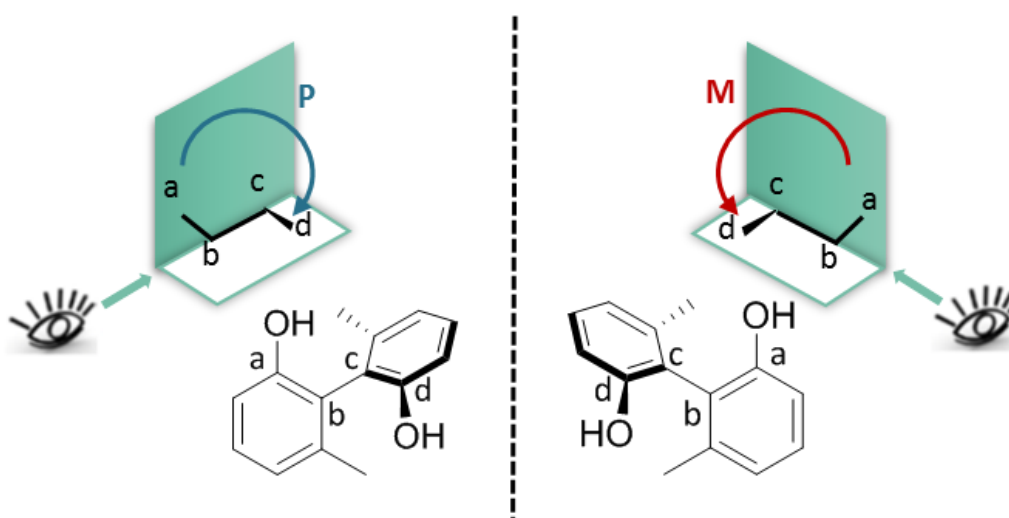


Figure 1.3.1 Left: *P* descriptor representation and (*P*)-6,6'-dimethyl-[1,1'-biphenyl]-2,2'-diol. Right: *M* descriptor representation and (*M*)-6,6'-dimethyl-[1,1'-biphenyl]-2,2'-diol.

The *P* and *M* descriptors are commonly used also to describe helicity, in which *P* stands for a right-handed helix, while *M* stands for a left-handed one.

1.4 Symmetry and time scale: Dynamic stereochemistry

It is much simpler to look at a molecule as a rigid object, dictate the symmetry rules presented in Paragraph 1.1 and therefore define its chirality. However, real molecules rotate, stretch, shrink, rock, bend their angles, torsional angles and bonds. Therefore, often exist a series of continuously

interconverting conformational isomers of a single molecule. If this process is relatively slow with respect to the time scale of the observation, it is necessary to take into consideration the motion of the object in the analysis of the symmetry element of the molecule.

For instance, an amine with three different substituents in its pyramidal form is chiral, however it rapidly interconverts into its enantiomer, passing through a sp^2 trigonal planar hybridization state. The process is so fast that it is not possible to appreciate the chirality of each pyramidal form and the overall system appears to be achiral. In this case the molecule results achiral due to slowness of the observation method, Figure 1.4.1.

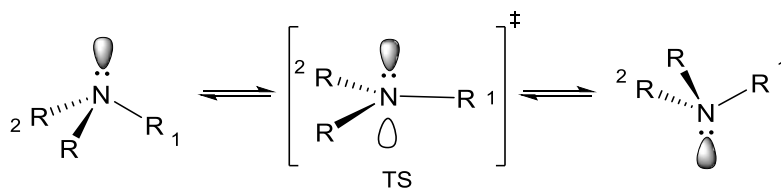


Figure 1.4.1 Enantiomers interconversion of an amine with three different substituents passing through a sp^2 hybridized trigonal planar state.

Chiral diaminocyclohexanes are widely used in chiral organo and organometallic catalysis,^{9,10,11} however only the 1,2 or 1,3-*trans* isomers are used. The chair inversion (passing through the boat conformation) in the *trans* molecules does not produce the relative mirror image, but only provides the exchange of the axial/equatorial positions. While, 1,3-*cis* isomer possess a plane of symmetry and is achiral, the 1,2-*cis* isomer can be considered inherently chiral. However, the ring flipping transforms one enantiomer into its mirror image and it is not possible to isolate neither of them. Analogously, to the three-substituted amine, also in this case the chirality of the system is related to the time scale of the observation (Figure 1.4.2).

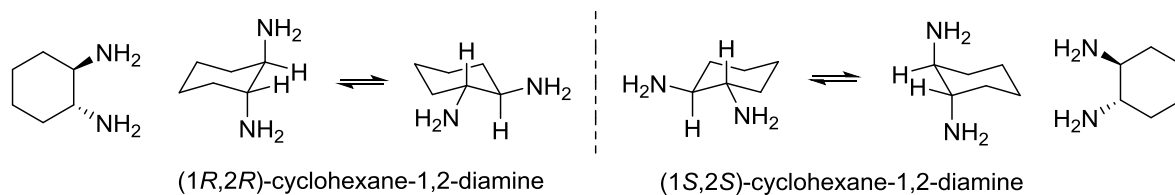
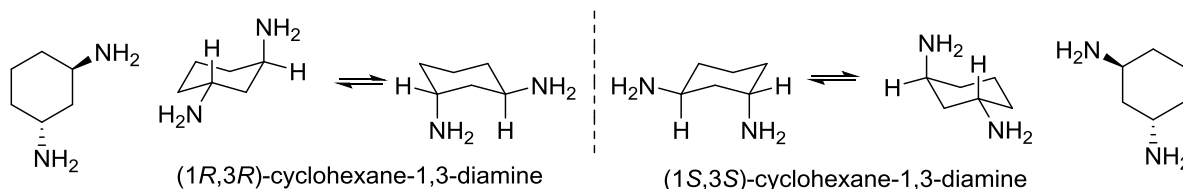
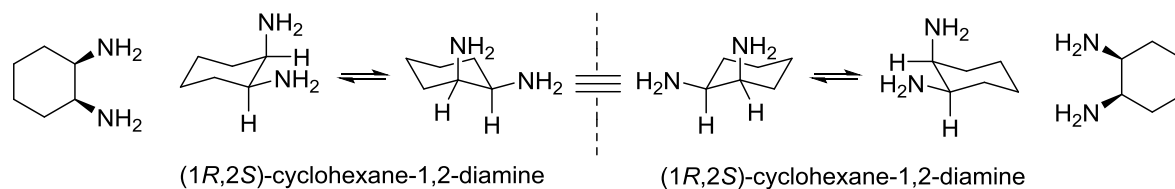
1,2 *trans* diaminecyclohexane

 1,3 *trans* diaminecyclohexane

 1,2 *cis* diaminecyclohexane


Figure 1.4.2 Top and center: 1,2 and 1,3 *trans* diaminecyclohexane and their non-superimposable mirror image; Bottom: 1,2 *cis* diaminecyclohexane in which the ring flipping transforms one enantiomers into the other.

1.5 Dynamic Stereochemistry and chiral axes

As the rapid interconversion of three substituted amines or the chair inversion of cyclohexane, the rotation around a bond is a time-dependent process. When the rotating bond is a chiral axis, the rotation implies racemization. Therefore, depending on the rotational stability of the chiral axis, the half-lives of the stable conformations can dramatically change between minutes to years, depending on the magnitude of several factors: steric hindrance, electronic influences, temperature, solvent, etc. It is quite straightforward that the definition of what is an atropisomers is not trivial. The first observation of this phenomenon has been reported in 1922 by Christie and Kenner with the separation of the 6,6'-dinitroniphenyl-2,2'-dicarboxylic acid and its 4,4',6,6'-tetranitrobiphenyl derivatives by crystallization with salt of 10,11-dimethoxystrychnine, while the same procedure for biphenyl-2,2'-dicarboxylic acid fails due to the fast rotation about the 1,1' bond.¹²

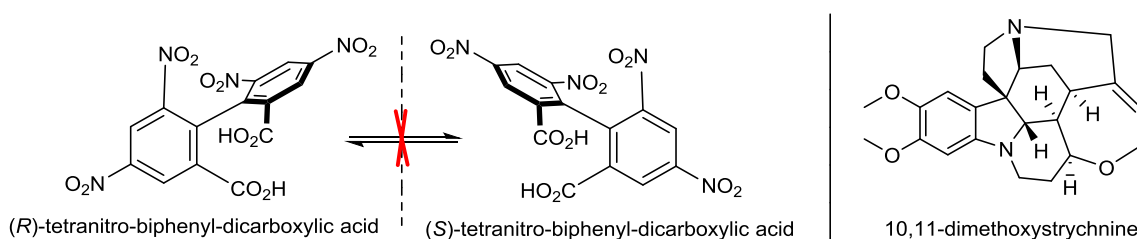


Figure 1.5.1 (*R*) and (*S*) -4,4',6,6'-tetranitro-[1,1'-biphenyl]-2,2'-dicarboxylic acid first resolved by Christie and Kenner by derivatization with 10,11-dimethoxystrychnine

The term “atropisomer” was later coined by Kuhn from the word **a** (α) = not and **tropos** ($\tau\rho\omicron\pi\omicron\sigma$) = rotate identifying those stereoisomers that arise from the not-rotation of a single bond.¹³ However, this first attempt of definition does not sets any boundaries about the stability of the atropisomers and the energy barrier related to the stereogenic axis rotation. Based on these observations, Oki⁴ refined the definition of atropisomer: it is as a conformer that upon bond rotation interconverts slowly enough (rotational barrier 21.8 kcal/mol at 25 °C)¹⁴ to be observed and eventually physically resolved.

Nowadays, this concept is still not exhaustively defined, but it is commonly related to conformers separated by an energy barrier involved in the rotation of a chiral axis that at least permits a half-life time of 1000 s (at 298 K) and that allows, eventually, the physical resolution of the enantiomers.

Recently a very useful map of stereogenic axes stability has been proposed by LaPlante (Figure 1.5.2) for the field of drug discovery.¹⁵ According to his evaluation, compounds can be divided in three classes based on rotational energy barriers.

- **Class 1** the molecules which belong to this class possess relatively fast axial rotation rates (to the order of nanoseconds to few seconds) displaying not even observable (at +25°C) stereoisomers related to the rotation around a single bond and therefore can be intended as single entities. The energy barriers involved are generally lower than 19 kcal/mol and the compounds belonging to the Class 1 cannot be identified as a atropisomer.
- **Class 2** These compounds have metastable situation in which the rotational barriers are between 20 kcal/mol and 30 kcal/mol and the half-life time ($t_{1/2}$) spans from few minutes to years. Molecules with these features are expected to show some observable indication of the presence of atropisomers. However, the less stable components of this class cannot always be physically resolved (at +25 °C). With this criterion, this class can be divided further in to two subclasses:
 - **Class 2a:** $20 \text{ kcal/mol} \leq \Delta E_{\text{rot}} \leq 23 \text{ kcal/mol}$ in which the two enantiomers can be clearly detected, and in some cases even resolved, but the racemization process is fast enough to consider them enantiomerically pure only for several seconds (at +25 °C) then the complete racemization occurs at most in 1 hour. Such fast process makes the single enantiomer existence elusive and for most of the practical application the compounds can be considered a single entity.
 - **Class 2b:** $23 \text{ kcal/mol} < \Delta E_{\text{rot}} < 30 \text{ kcal/mol}$ in this sub-class the enantiomers can be detected, resolved and stored as single enantiomerically pure atropisomer at +25 °C for hours or even weeks.

- **Class 3** compounds are those with half-life time in the order of years. These are chiral stable compounds with a $\Delta E_{\text{rot}} \geq 30$ kcal/mol and the single enantiomers can be considered kinetically stable. Therefore, little to no axial rotation is expected to occur at +25 °C.

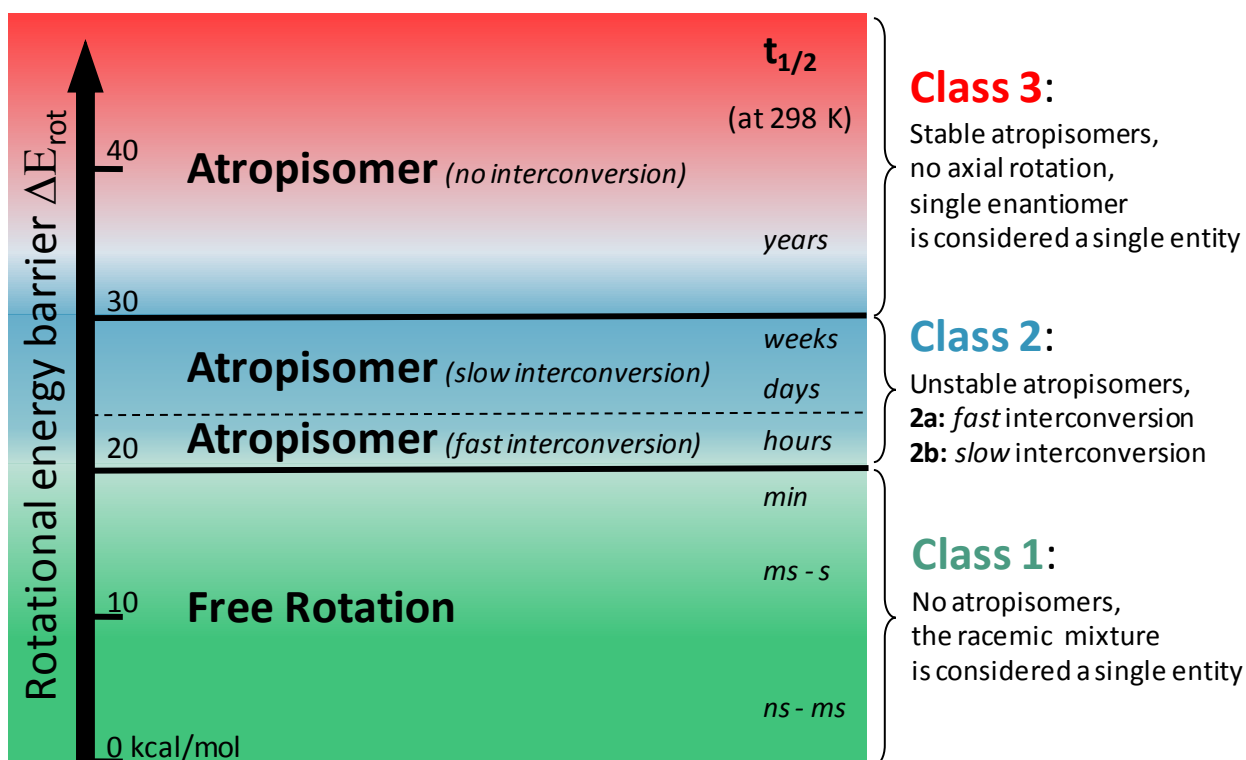


Figure 1.5.2 Rotational energy barrier map with relative half-life time ($t_{1/2}$) at 298 K of the single atropisomer. [Reprinted (adapted) with permission from *ChemMedChem*, 2011, 6, 503-513. Copyright (2011) WILEY-VCH Verlag GmbH & Co. KGaA]

The classification depicted by LaPlante is not intended to be a rigid classification but a gradual passage from a zone of instability to a zone of stability of chiral axis.

Moreover, although useful, this classification lack of some considerations:

1. The state of the compound has a high impact on the rotational barrier, for instance a compound in solution has generally a lower rotational barrier than in solid state. In addition, each solid state (*i.e.* crystalline forms, amorphous forms) has his rotational barrier related to the packing of the crystalline structure. In this manuscript, the energies of the rotational barrier are considered in solution unless otherwise stated.
2. The stability consideration proposed for the detection and resolution of atropisomers are intended at room temperature (+25 °C). In fact, as any kinetic process, the rotation of a bond is highly influenced by the temperature. In particular, the half-life time of a single atropisomer is inversely proportional to the temperature. Therefore, by changing the temperature is possible, on one hand to racemize some Class 3 compounds and on the other to detected chirality in some Class 1 compounds.

With this consideration and this map in hand is possible to explore the parameters that influence the magnitude of a rotational energy barrier and how this energy is identified.

On this regard, it is very useful to imagine the energy profile of a molecule along the rotation around the stereogenic axis. One of the simplest case is the 2,2'-disubstituted biphenyls (Figure 1.5.3). In the ground states (GS) the phenyl rings are in a skewed disposition, where the dihedral angle (φ) is neither 0° nor $\pm 90^\circ$ reaching a compromise between the minimization of the steric repulsion and the maximization of the aromatic resonance stabilization. The latter would be maximized by a coplanar situation (0°) but it would also cause a high hindered structure due to the clash of the *ortho* substituent (in 2' or in 6' position) on the other phenyl ring. While the steric repulsion would be minimized in an orthogonal situation ($\pm 90^\circ$) the stabilization due to π -electron overlap would be completely lost. Thus, each atropisomer of 2,2'-disubstituted biphenyl molecules usually populate ground states with torsional angles that span from 30° to 80° and from 100° to 150° , depending on the relative disposition of the 2,2' group. The *anti* disposition is usually the most stable¹⁶ and see the *ortho* groups on the opposite side respect to the chiral axis, while the *syn* disposition has the *ortho* substituents on the same side.

The orthogonal arrangement among the two phenyl rings represent a local maximum of the energy corresponding to the transition state (TS) between the *anti* and the *syn* disposition. Meanwhile, the coplanar arrangement represents the transition state between one atropisomer and its mirror image. This disposition can be achieved with two opposite rotation: a 0° rotation in which the two 2,2' groups clash one on the top of the other; or with a 180° rotation in which each R group has a steric interaction with the H on the other phenyl ring (*i.e.* 2, 6' and 2', 6 R-H steric clash). The latter situation displays a lower steric repulsion resulting in an energetically favoured TS. The rotational energy barrier is defined as the energy difference between the most stable (*i.e.* the most populated) GS and the most stable TS, it can be more precisely defined as the difference between free Gibbs energies $\Delta G_{\text{rot}}^\ddagger$, Figure 1.5.3.

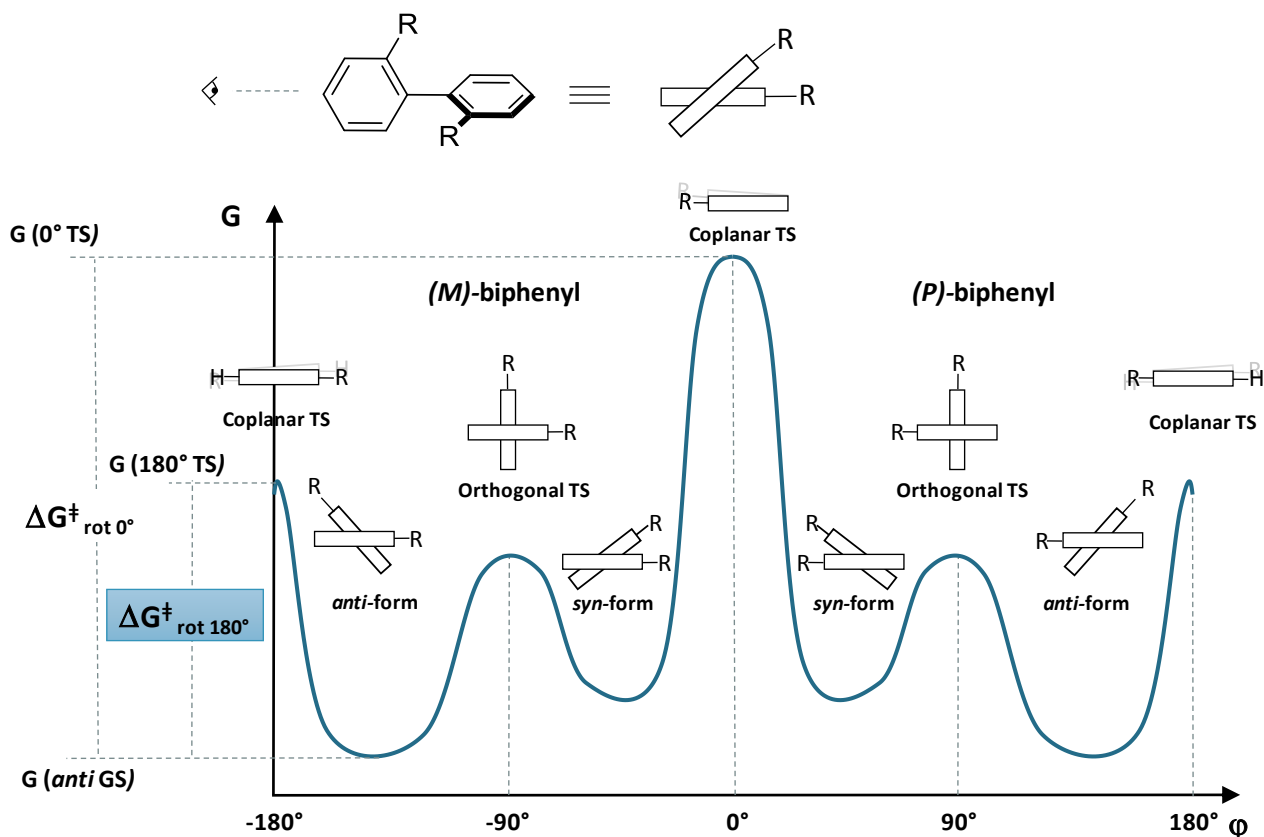


Figure 1.5.3 Energy profile of 2,2'-disubstituted biphenyls. In blue is highlighted the lowest rotational energy barrier: $\Delta G_{\text{rot } 180^\circ}^\ddagger$.

The entity of the $\Delta G_{\text{rot}}^\ddagger$ is therefore defined by the energies level of the lowest coplanar TS (LC-TS) and of the lowest GS (L-GS). It is straightforward that any modification in the magnitude of the $\Delta G_{\text{rot}}^\ddagger$ implies a stabilization or destabilization of LC-TS and/or L-GS.

The biaryl system is a good starting point to evaluate the parameters that modify the energy level of the LC-TS and L-GS. The energy barrier to the atropisomerization of biphenyl can be easily related to the bulkiness of the substituents. In fact, the rotation of chiral axis in a crowded system implies a high steric hindrance and the generation of a high energy (*i.e.* distorted) LC-TS. The LC-TS of 2,2'-disubstituted-biphenyls (Figure 1.5.3) minimized the steric hindrance pairing the most bulky substituent on one ring with the hydrogen on the other. In a 2-isopropyl-2'-R-substituted biphenyl the replacement of R = O-Me with more steric demanding group raises the $\Delta G_{\text{rot}}^\ddagger$ proportionally to the size of the latter. Therefore, it is possible to determine which are the steric requirement to develop a stable atropisomer (R = *t*-Bu, $\Delta G_{\text{rot}}^\ddagger = 32.7$ kcal/mol). Altogether the measurement of the rotational energy barrier provides indirectly the measurement of the steric size of the functional groups R, where: OMe < CF₃ < *i*-Pr < *t*-Bu, Figure 1.5.4 A.¹⁷

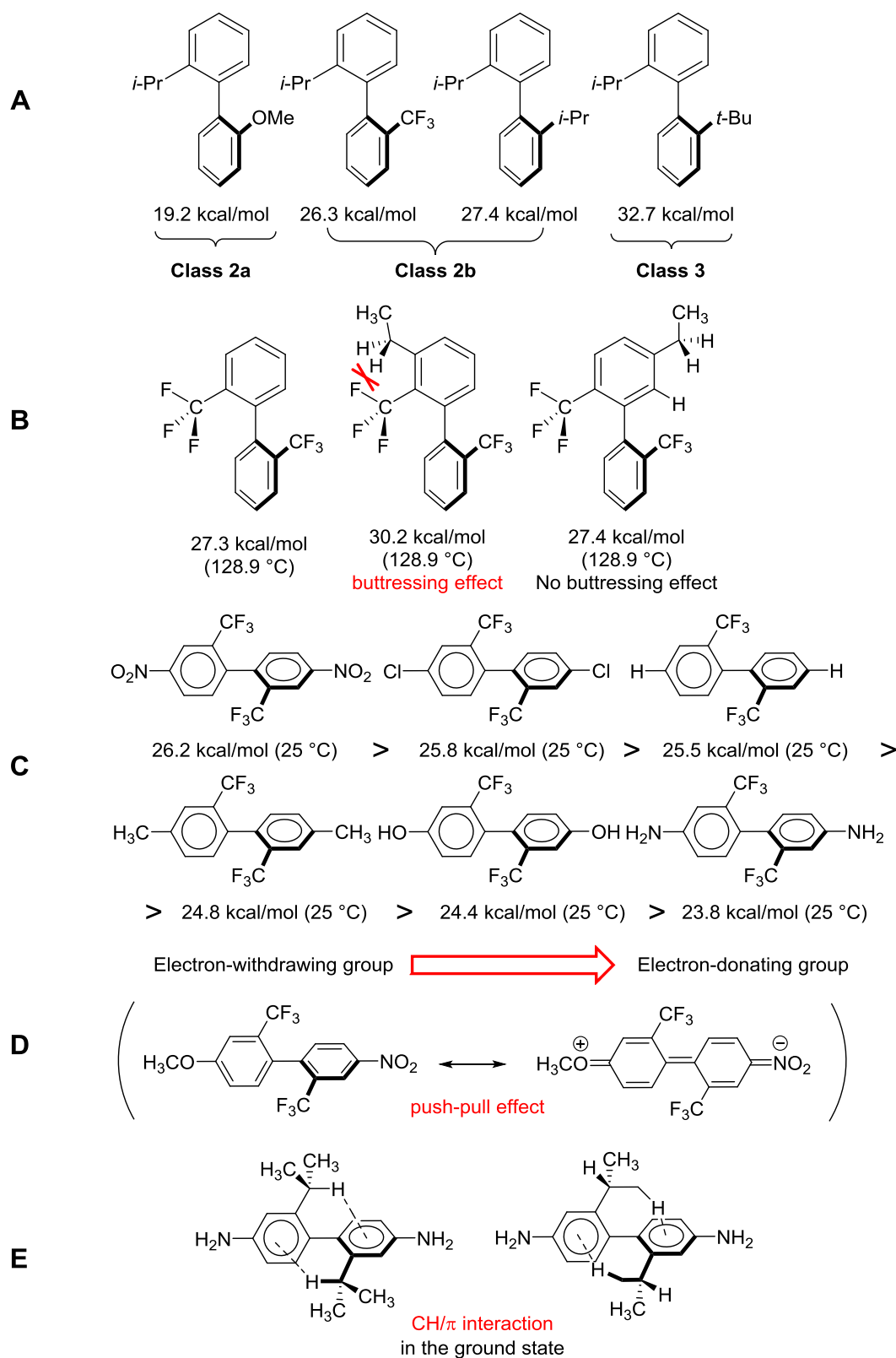


Figure 1.5.4 **A** Dependence of the rotation barrier with increasing demanding steric group in 2,2'-disubstituted biphenyls. **B** Buttering effect of *meta* ethyl substituent in 2,2'-bis(trifluoromethyl)biphenyl. **C** Electronic effect of *para* substituent in 4,4'-disubstituted 2,2'-bis(trifluoromethyl)biphenyl. **D** 4-methoxy-4'-nitro-2,2'-bis(trifluoromethyl)biphenyl push-pull effect and its planar zwitterionic state **E** CH/π interaction occurring in 4,4'-diamino-2,2'-diisopropylbiphenyl.

Also, the *meta* substituent in respect to the chiral axis exhibit an effect on LC-TS, the so-called buttering effect. In which, the *meta* substituent reduces the flexibility of the adjacent *ortho*

substituent reducing the degree of freedom of the latter during the rotation about the chiral axis. Incorporation of a relatively small ethyl group into the *meta*-position of the 2,2'-bis(trifluoromethyl)biphenyl raises the $\Delta G_{\text{rot}}^{\ddagger}$ from 27.3 kcal/mol to 30.2 kcal/mol (Figure 1.5.4 **B**). This is mainly a steric effect that is related to the size both the *meta* and the *ortho*-positions substituents. In fact, the introduction of the ethyl group on the other *meta* position (*C*-5) does not modify consistently the rotational barrier of the system (27.4 kcal/mol), Figure 1.5.4 **B**.

Although the steric effects play an important role in the determination of the stability of the chiral axis, also the electronic effects needed to be considered. During the studies of the rotational barrier of a series of 2,2'-bis(trifluoromethyl)biphenyls, Wolf and collaborators^{18,19,20} noted that electron-withdrawing group located on the 4,4' position stabilize the ground states while the electron-donating groups decrease the $\Delta G_{\text{rot}}^{\ddagger}$. The latter groups are able to increase the electron density on the *C*-1 and *C*-1' weakening the pivotal bond and facilitate the out-of-plane bending. On the other hand, the electron-withdrawing groups lower the negative charge on the 1,1' position obstructing the out-of-plane bending and therefore, stabilize the L-GS. The order established by Wolf of stabilizing *para*-substituents is: $\text{F} \approx \text{NO}_2 > \text{Cl} > \text{CF}_3 > \text{NH}_3^+ > \text{Br} \approx \text{H} > \text{CH}_3 > \text{OCH}_3 > \text{OH} > \text{NHAc} \gg \text{NH}_2$ (Figure 1.5.4 **C**). Once an electron-withdrawing group and an electron-donating group are placed in the 4 and 4' positions respectively, a push pull effect generates an almost planar partial double bond in 1,1' position stabilizing the LC-TS and therefore decreasing the rotational energy barrier (Figure 1.5.4 **D**). Although these trends can be widely confirmed in biphenyls, some alkyl biaryls that undergo to CH/ π interaction could develop opposite trend than the one previously exposed. This is the case of alkyl substituted 2,2'-diisopropylbiphenyl where an electron withdrawing group allows the rotation while an electron donating group, such as an amino, increase the rotational barrier. In this case the electronic effect influences the GS lowering its energy. In fact, the hydrogens of the *i*-Pr groups have the right geometry to interact with the π cloud of the adjacent phenyl ring only in the ground state (*i.e.* not periplanar position). Therefore, the ground state is stabilized by those functional group able to increase the electron density on the aromatic ring and accordingly the $\Delta G_{\text{rot}}^{\ddagger}$ increase (Figure 1.5.4 **E**).

It is worth to be noted from Figure 1.5.4 that the $\Delta G_{\text{rot}}^{\ddagger}$ is influenced by the temperature. At +25 °C the rotational barrier of 2,2'-bis(trifluoromethyl)biphenyl is 25.5 kcal/mol, while at +128.9 °C it is 27.3 kcal/mol. This is generated by a negative entropic contribution to the energy of the TS, where the compromised rotational freedom generates a more ordered state. Although the entropic effects are always present, in most of the case in which is involved the rotation of a chiral axis the entropic factor is negligible with respect to the enthalpy.

Tertiary aryl-amides with *ortho* aromatic substituent display a not orthogonal disposition with respect to the phenyl plane. Depending on the steric hindrance of the amide and the *ortho* substituents, rotation around the carbonyl and the aryl ring ($C_{ar}-C_{co}$) can be restricted generating atropisomers. Moreover, in the $C_{co}-N$, an electronic effect occurs, the rotation is partially blocked due to the partial double bond nature and it is possible to correlate the two isomerization process. When the kinetic constants for the rotations $C_{ar}-C_{co}$ ($k_{Car-Cco}$) and $C_{co}-N$ (k_{Cco-N}) are about the equal, the two process occurs with similar rates and their movement are correlated. Meanwhile when the $k_{Car-Cco} > k_{Cco-N}$ the Ar-CO is fast due to low steric demanding *ortho* substituents and the movement are not correlated. On the other hand, with *ortho*-aryl bulky group the $k_{Car-Cco} < k_{Cco-N}$ and the Ar-CO rotation occurs only geared with the CO-N rotation while the latter can experience some independent movement, Figure 1.5.5.^{21,22} In the case of the N-substituted anilides beside the eventual N- C_{aryl} atropisomerization process, the restrict rotation around the CO-N axis determine an *E/Z* isomerism of the amide bond that can arrange the carbonyl group on one side (*Z*) or the other (*E*) of the phenyl ring.²³ Therefore, with an *ortho* bulky aryl substituent the anilides show two stereodynamic process: *E/Z*- isomerization and atropisomerization (Figure 1.5.5).²⁴ Although less common, also in this case are possible geared movements between the two stereomutations.²⁵

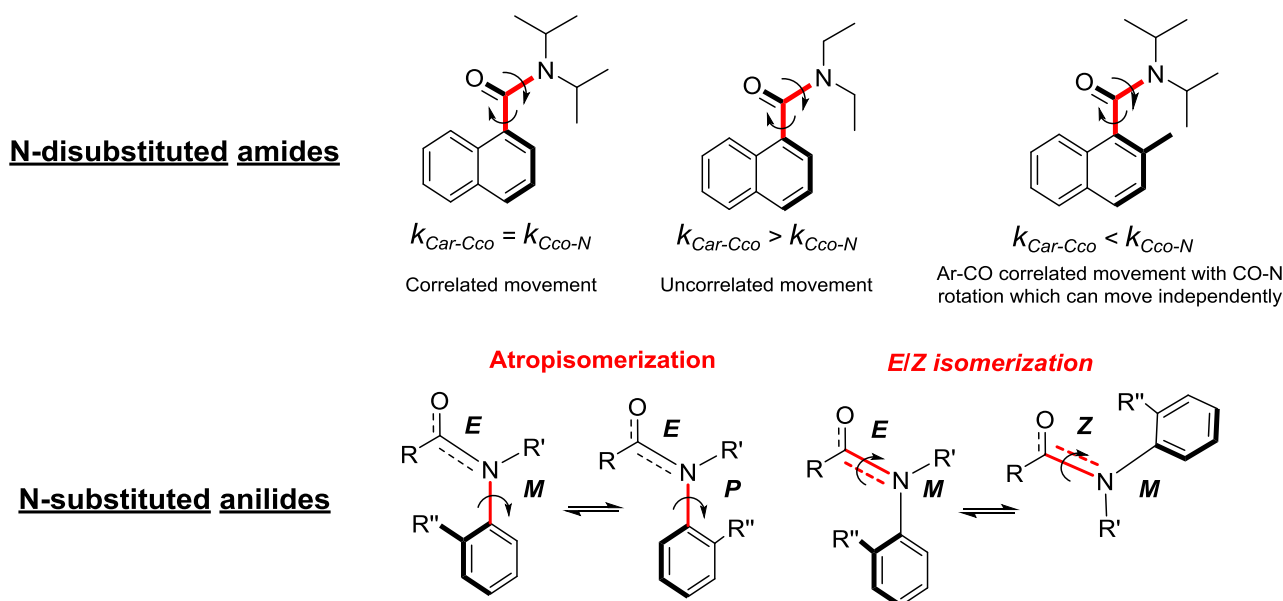


Figure 1.5.5 Stereodynamic of: top, N-disubstituted amides displaying the interdependence of the rotation around the $C_{ar}-C_{co}$ and the $C_{co}-N$ axes; bottom, N-substituted anilides and the two stereodynamic process occurring.

The formation, also transient, of an interaction (even if with a bond order < 1) between the two scaffolds at each side of a chiral axis (bridge effect) can significantly compromise the conformation stability of the chiral compound. The steric considerations on rotational barrier exposed previously define that a four substituted biaryl system should has a stable chiral conformation. However, if the bridge effect occurs the atropisomerization could happen also at room temperature. This is reported

in 1-(2-hydroxy-4,6-dimethylphenyl)-2-naphthaldehyde^{26,27} where the hemiacetal resulting from the aldehyde and hydroxy substituents in the 2,2' position allows the rotation of the chiral axis leading to a surprisingly low $\Delta G_{\text{rot}}^{\ddagger} = 23.7$ kcal/mol (Figure 1.5.6 A).

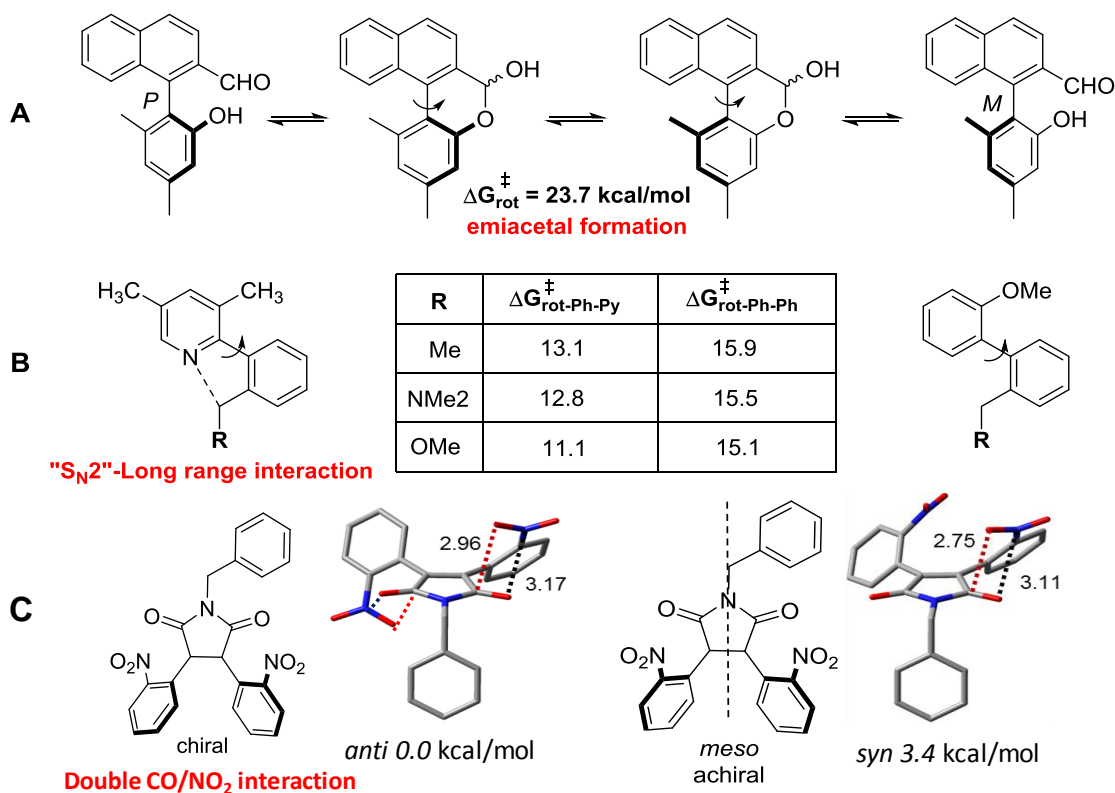


Figure 1.5.6 **A** hemiacetal formation in 1-(2-hydroxy-4,6-dimethylphenyl)-2-naphthaldehyde and its relatively low rotational barrier. **B** Long range interaction in the phenyl-pyridine system with S_N2 geometry and the effects on the $\Delta G_{\text{rot}}^{\ddagger}$ of an electron-withdrawing R substituent compared to the biphenyl analogous. **C** 3,4-bisnitrophenyl-maleimide *anti* chiral populated form and not populated *meso* achiral one. The solid tubular structure and their relative energy are calculated at ω B97XD/6-311++G(2d,p) level. Distances in Å.

Similar effect has been reported for an aryl-pyridine system in which a S_N2 interaction in the TS occurs between an electron poor methylene system and the electron rich nitrogen on the pyridine. This leads, depending on the electron-withdrawing power of the substituent on the methylene, to a more stable TS and therefore to a lower rotational barrier than the biphenyls analogous, in which the $\Delta G_{\text{rot}}^{\ddagger}$ is driven only by steric effects, Figure 1.5.6 B.²⁸

These particular interactions may have high power in the discrimination between diastereoisomers; this is the case of the maleimide molecules studied by Mazzanti and collaborator.²⁹ The 3,4-bis-nitrophenyl-maleimides considered, bearing two non-symmetrical aryl systems, generate a *syn meso* form and a chiral *anti* form. However, only the *anti* diastereoisomer is present due to a newly discovered NO₂/CO interaction that stabilized the ground state of the *anti* conformation making the *syn* conformation completely unstable and therefore, not populated (Figure 1.5.6 C).

In medicinal chemistry, the presence of one or more semi-stable chiral axes can makes the drug discovery campaigns more complex due to the formation of temperature instable stereoisomers.

Therefore, more often the chiral axes are eliminated by using more rigid and conformationally constrained structures. This is the case of a NK1 antagonist where a full bridge bond is inserted into the drug scaffold between the amide moiety and the steric demanding 2,3-disubstituted naphthyl group to remove the cumbersome presence of two chiral axes.³⁰ This expedient resolves altogether the chiral axis due to: the partial double bond nature of the amide bond and the steric hindrance of the naphthyl moiety, Figure 1.5.7.

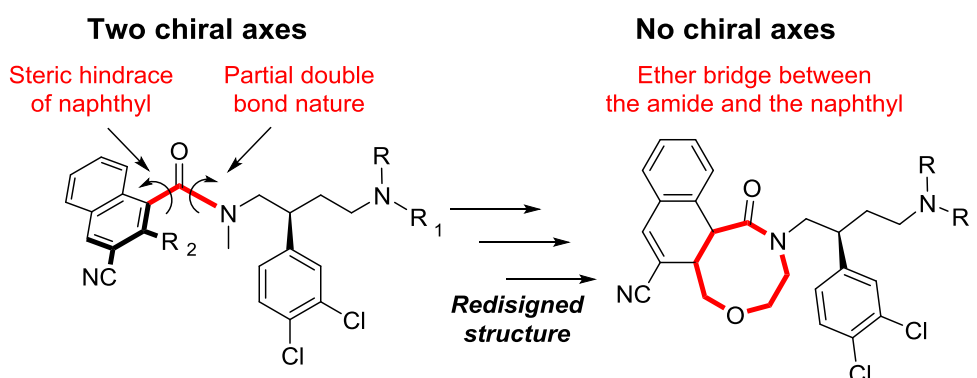


Figure 1.5.7 Removal of chiral axes in a NK1 antagonist through the introduction of a bridge between the naphthyl and the amide moiety

On the contrary, in the case of vancomycin the several stereochemical features are essential to the antibiotic properties of this scaffold. During the multistep total synthesis of this natural occurring macrocycle³¹ the undesired *M* diastereoisomer resulted from the synthesis is simply transformed in the *P* target diastereoisomer by heating the *M* diastereoisomer at +55 °C, Figure 1.5.8.

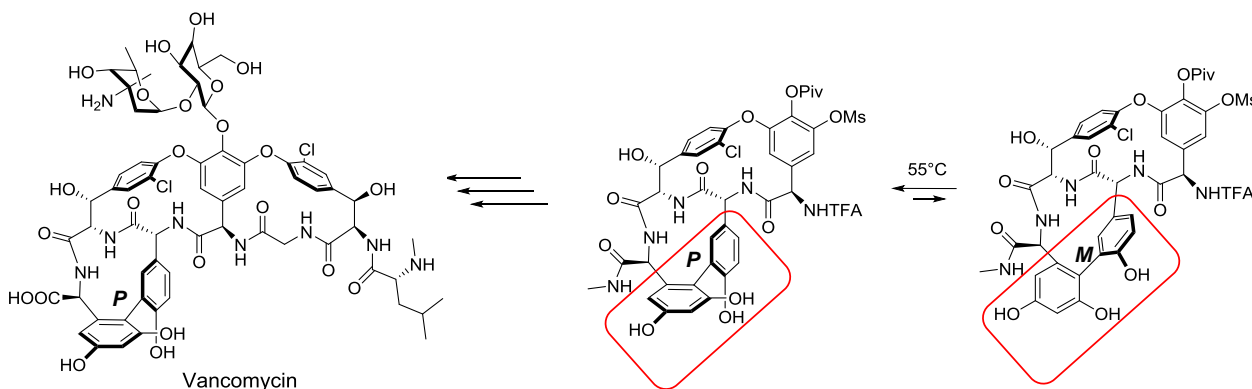


Figure 1.5.8 Vancomycin and its synthetic precursor. A temperature of 55 °C is sufficient to convert the instable *M* diastereoisomer to the stable one.

In fact, rather being influenced by the sterical demanding element, the chirality of the aglycone precursor is controlled by the whole architecture of the scaffold. Therefore, to foresee the conformational stability of chiral axes is not only of academic interest but it is involved and sometimes requested in such biological active molecules.

1.6 Dynamic stereochemistry and chiral propellers

In most of the cases, conformations arise due to concerted movement, in which two different part of a molecule moves simultaneously in a unique process. Therefore, the passage from one conformation to another can, not only occur by the rotation around one bond as previously described, but also through a synchronous movement of two or more parts of the molecule. This system is usually compared to a cog in a geared mechanism in which every cog (*i.e.* moving part of the molecule) cannot move independently.

One of the simplest example is benzophenone, in which the two phenyl rings act as two blade of a propeller that flip around the hub represented by the sp^2 -hybridized carbon. Although this movement has been computationally simulated³² the low activation energy of this process makes practically impossible to experimentally observe the stereomutation. As previously stated and widely reported in literature, hindered systems display an increased interconversion barrier. Lunazzi and coworkers³³ reported the stereomutation analysis of a series of dimesityl derivative of benzophenone. The work provided proofs of the existence of the *M* and *P* conformation, where the two mesityl rings are symmetrically skewed with respect to the carbonyl plane and in which the methyls in the *ortho* positions are diastereotopic. The interconversion process was found to occur via correlated rotation of the two mesityl rings (cog wheel effect) with activation energy of 4.6 kcal/mol. This path is by far the more energetically favoured with respect to the independent movement of the two mesityl rings. For instance, in the asymmetric and apparently less crowded analogous phenyl mesityl ketone the interconversion barriers were found higher than the more hindered dimesityl analogous.³⁴ This apparent contradiction is due to the lack of a concerted movement during the rotation around the C-C axes. The absence of the cog wheel effect makes the two-aryl ring rotation independent one from other and each ring displays a rotational barrier (13.7 kcal/mol and 15.2 kcal/mol for phenyl and mesityl respectively). In a two-ring propeller correlated movement can occur as conrotatory or disrotatory. The comparison between the experimental and the computed rotational barriers pointed out that the interconversion in the dimesityl system occurs with a disrotatory one-flip movement, where one ring is orthogonal while the other is parallel to the plane identified by the carbonyl. On the other hand, the 2 possible conrotatory movements (zero and two ring flip) have a higher energy due to simultaneous orthogonal (two-ring flip) or parallel (zero-ring flip) disposition of both aryl ring, Figure 1.6.1.

The study performed on dynamic stereochemistry in atropisomerism and chiral propellers have paved the way to the recent development in the field of molecular motor.³⁵ Unidirectional molecular motor as the ones developed by Feringa and coworkers^{35a} were possible thanks to the knowledge gained on

the preferential conformation and stereodynamic of organic molecules, and therefore represents the perfect summary of the all the studies on the subject.

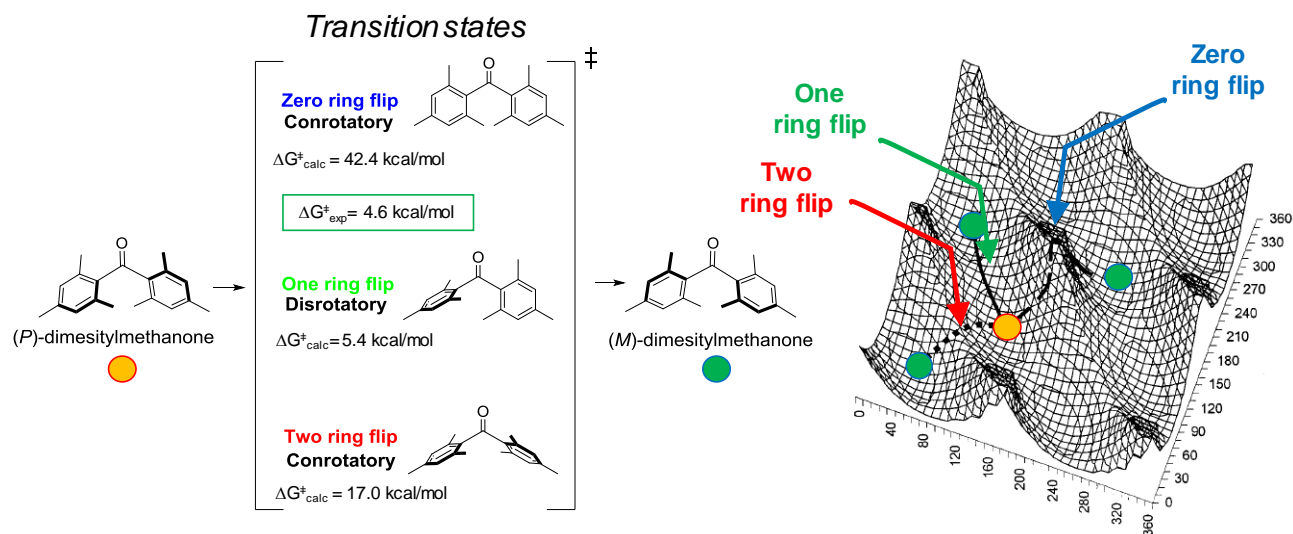


Figure 1.6.1 Dimesityl ketone stereomutation pathways and the relative potential energy map computed as a function of the two Ar-CO dihedral angles (MMFF-94 force field). The ground states of the energetically equal enantiomeric conformers are represented as circle and the transition state are located at the edge of each pathway. [Reprinted (adapted) with permission from *J. Org. Chem.*, **2001**, 66, 488-495. Copyright (2001) American Chemical Society]

The designed motors are light-driven and are derived from overcrowded chiral alkenes in which the steric demanding group are not completely coplanar to the double bond plane. On one side of the double bond is located the stator (thioxanthene) while on the other the rotor (benzothiochromene). In order to have a unidirectional movement is essential an ambivalent behaviour of the rotor with both conformational flexibility and chiral stability. The rotation around the C-C double bond is driven by a controlled series of thermal and photochemical process in which only one motion, controlled by the chiral centre and the helical conformation, is available. The whole process is composed by four steps (as a four-stroke engine): two of photoisomerization and two of thermal helix inversion. Since the interconversion transforms between diastereoisomers both the directions of the motion are populated but with different percentage depending on the Boltzmann distribution, making the motion unidirectional with 26.6% of total efficiency. In other words, 26.6% of the starting molecules make the complete rotation around the stator in one direction, Figure 1.6.2.

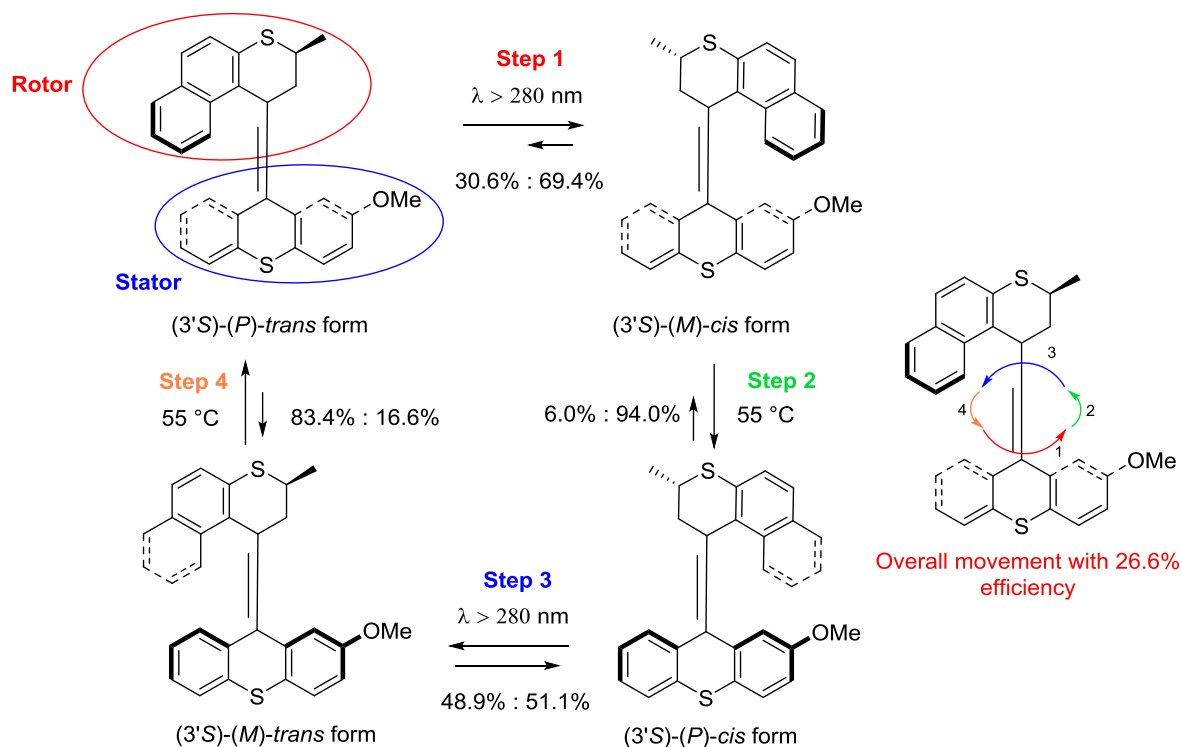


Figure 1.6.2 Four-stroke unidirectional molecular motor of the rotor around the stator designed by Feringa and coworkers.

References

- Goldhaber M., Grodzins L., Sunyar A. W. *Physical Review* **1958**, *109*(3), 1015–1017.
- McNaught A. D., Wilkinson A. *IUPAC. Compendium of Chemical Terminology*, 2nd ed. (the "Gold Book"). Blackwell Scientific Publications, Oxford (**1997**).
- a) Bren L., *FDA Consumer, Cover Story "Frances Oldham Kelsey: FDA Medical Reviewer Leaves Her Mark on History"*, **2001**, *35*(2); b) Fabro S., Smith R. L., Williams R. T. *Nature* **1967**, *215*, 296–297.
- Oki M. *Top. Stereochem.* **1984**, *14*, 1–81.
- Martin R. H. *Angew. Chem. Int. Ed. Engl.* **1974**, *13*, 649–660.
- Bartlett J. *J. Am. Chem. Soc.* **1942**, *64*, 1837–1840.
- PAC, **1996**, *68*, 2193–2211 (Basic terminology of stereochemistry (IUPAC Recommendations 1996)).
- Ambrogio M., Ciogli A., Mancinelli M., Ranieri S., Mazzanti A. *J. Org. Chem.*, **2013**, *78*(8), 3709–3719.
- Bennani Y. L., Hanessian S. *Chem. Rev.* **1997**, *97*(8), 3161–3196.
- Kurahashi T., Hada M., Fujii H. *J. Am. Chem. Soc.* **2009**, *131*(34), 12394–12405.
- Mei K., Jin M., Zhang S., Li P., Liu W., Chen X., Xue F., Duan W., Wang W. *Org. Lett.*, **2009**, *11*(13), 2864–2867.
- Christie G.H., Kenner J. *J. Chem Soc.* **1922**, *121*, 614–620.
- Kuhn R. In: Freudenberg, K. (ed.) *Stereochemie*, Deuticke, Leipzig, **1933**, 803–810.
- The racemization process can be described with a kinetic equation of the first order, therefore the half-life time ($t_{1/2}$) is independent from the concentration and is only a function of the kinetic constant ($t_{1/2} = \ln 2/k$). With a $t_{1/2} = 1000 \text{ s}$ the racemization occurs with kinetic constant $k \approx 7 \cdot 10^{-4} \text{ s}^{-1}$ and has an energy barrier at 298 K of $\approx 21,76 \text{ kcal/mol}$.
- Laplante S. P., Edwards P. J., Fader L. D., Jakalian, A., Hucke, O. *ChemMedChem*, **2011**, *6*, 503–513.
- Roberts R. M. G. *Magn. Reson. Chem.* **1985**, *23*, 52–54.
- Masson E. *Org. Biomol. Chem.*, **2013**, *11*, 2859.
- Wolf C., Köning W., Roussel C. *Liebigs Ann.*, **1995**, 781–785.
- Wolf C., Hochmuth D. H., Köning W., Roussel C. *Liebigs Ann.*, **1996**, 357–363.
- Weseloh G., Wolf C., Köning W. *Angew. Chem. Int. Ed. Engl.*, **1995**, *34*, 1635–1636.
- Clayden J., McCarthy C., Helliwell M., *Chem. Commun.* **1999**, 2059–2060.
- Clayden J., Westlund N., Wilson F. X., *Tetrahedron Lett.* **1999**, *40*, 7883–7887.
- Curran D. P., Qi H., Geib S.J., DeMello N. C. *J. Am. Chem. Soc.*, **1994**, *116*, 3131–3132.
- Chupp J. P., Olin J. F. *J. Org. Chem.* **1967**, *32*, 2297–2303.

- ²⁵ Curran D. P., Hale G. R., Geib S. J., Balog A., Cass Q. B., Degani A. L. G., Hernandez M. Z., Freitas L. C. G. *Tetrahedron: Asymm.*, **1997**, 8, 3955-3975.
- ²⁶ Bringmann G., Hartung T., *Liebigs Ann.*, **1994**, 313-316
- ²⁷ Bringmann G., Vitt D., Kraus J., Breuning M. *Tetrahedron*, **1998**, 54, 10691-10698
- ²⁸ Ruzziconi R., Lepri S., Buonerba F., Schlosser M., Mancinelli M., Ranieri S., Prati L., Mazzanti A. *Org. Lett.* **2015**, 17, 2740-2743.
- ²⁹ Chiarucci M., Ciogli A., Mancinelli M., Ranieri S., Mazzanti A. *Angew. Chem. Int. Ed.* **2014**, 53, 5405-5409.
- ³⁰ a) Albert J. S., Aharony D., Andisik D., Barthlow H., Bernstein P. R., Bialecki R. A., Dedinas R., Dembofsky B. T., Hill D., Kirkland K., Koether G. M., Kosmider B. J., Ohnmacht C., Palmer W., Potts W., Rumsey W., Shen L., Shenvi A., Sherwood A., Warwick P. J., Russell K. *J. Med. Chem.* **2002**, 45, 3972-3983. b) Albert J. S., Ohnmacht C., Bernstein P. R., Rumsey W., Aharony D., Masek B. B., Dembofsky B. T., Koether G. M., Potts W., Evenden J. L. *Tetrahedron*, **2004**, 60, 4337-4347.
- ³¹ a) Evans D. A., Wood M. R., Trotter B. W., Richardson T. I., Barrow J. C., Katz J. L. *Angew. Chem. Int. Ed.* **1998**, 37, 2700-2704; b) Evans D. A., Dinsmore C. J., Watson P. S., Wood M. R., Richardson T. I., Trotter B. W., Katz T. R. *Angew. Chem. Int. Ed.* **1998**, 37, 2704-2708. c) Burns N. N., Krylovam I. N., Hannoush, R. N., Barab P. S. *J. Am. Chem. Soc.*, **2009**, 131, 9172-9173.
- ³² a) Abraham R. J., Haworth I. H. *J. Chem. Soc., Perkin Trans. 2* **1988**, 1429. b) Rappoport Z., Biali S. E., Kaftory M. *J. Am. Chem. Soc.* **1990**, 112, 7742.
- ³³ Grilli S., Lunazzi L., Mazzanti A., Casarini D., Femoni C., *J. Org. Chem.* **2001**, 66, 488-495.
- ³⁴ Casarini D., Lunazzi L., Verbeek R., *Tetrahedron* **1996**, 52, 2471.
- ³⁵ a) Feringa B. L., *Angew. Chem. Int. Ed.*, **2017**, 56, 11060-11078; b) Stoddart J.F. *Angew. Chem. Int. Ed.* **2017**, 56, 11094 - 11125; c) Sauvage J. P., *Angew. Chem. Int. Ed.* **2017**, 56, 11080-11093.

Dynamic stereochemistry of chiral axes. Design and synthesis of stable atropisomers.

2 Dynamic Stereochemistry analysis and methodologies

The importance of the conformational stability of organic molecules are beyond the simple academic research and involved the whole organic chemistry field. Therefore, methods have been established to foresee and determine the dynamic stereochemical properties of such compounds. Among those, Dynamic Nuclear Magnetic Resonance (D-NMR) and Dynamic High Performance Liquid Chromatography (D-HPLC) arose as the most useful experimental methods, and computational studies performed with Density Functional Theory model (DFT) are nowadays widely used as theoretical support.

2.1 Dynamic Nuclear Magnetic Resonance (D-NMR)

NMR is able to observe the conformational exchange of chemical species that happens at a rate sufficiently low to observe separate anisochronous signals, in the milliseconds-seconds region:

$$t = \frac{\sqrt{2}}{2\pi \Delta\nu}$$

where:

t = conformational exchange time (s);

$\Delta\nu$ = chemical shift difference (in Hz) without exchange.

This equation states that two exchanging nuclei can display different chemical shifts when they occupy two positions with different magnetic environment for a time longer than the conformational exchange time (t).

In order to make compatible the time scale of the NMR acquisition to the kinetic process involved, the spectra are usually recorded at different temperature and the observed line shape is the result of the conformational process taking place within the NMR time scale.

As first example, we can consider dimethylformamide (DMF).¹ This molecule displays a hindered rotation around the C-N axis due to the partial double bond nature of the amide functional group. When the rotation is slow in the NMR time scale, each methyl experiences a magnetically different environment for a time long enough to be detected by the NMR, resulting with two different signals. Once the temperature is raised the process occurs faster and the signals broaden until the coalescence point is reached. At this temperature, the two diastereoisomers are no longer distinguishable, and only one broad peak is observable. The D-NMR investigation on DMF is described in Figure 2.1.1 where it is summarized the evolution of the line shape of an uncoupled dynamic two site system.

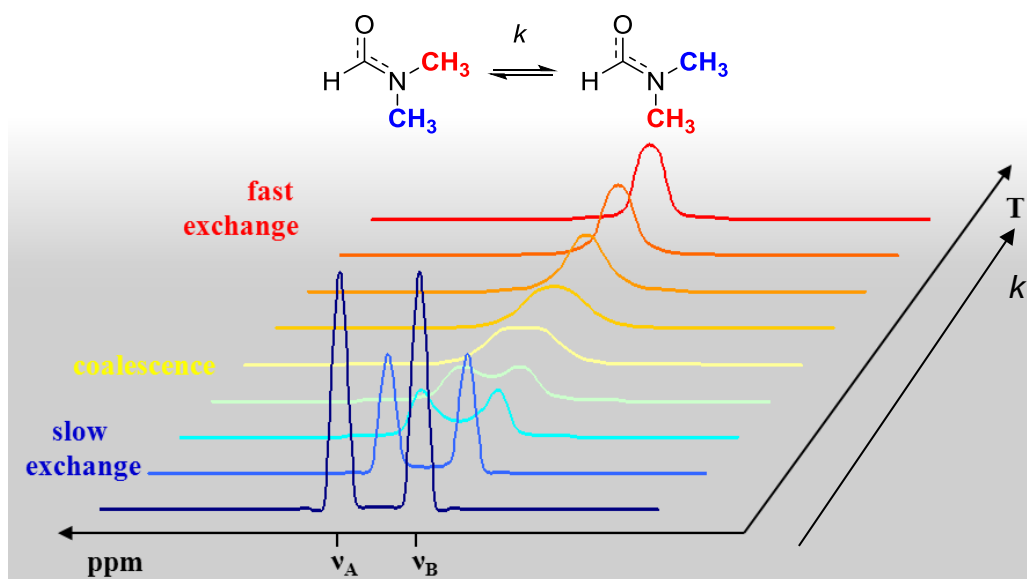


Figure 2.1.1 D-NMR profile of an uncoupled dynamic two site system.

On the other hand, when the conformational process results in the formation of two conformational diastereoisomers, and in particular when the temperature is low enough to freeze their interconversion they are observed as “standard” diastereoisomers, and all the NMR techniques are available for their structural identification. As an example, 1,8-di-*o*-tolylanthracene has two different conformation due to the relative disposition of the *o*-tolyl moieties that can be *anti* or *syn* with respect to the anthracene plane.²

At relatively low temperature (+85.5 °C) both the methyl peaks belonging to each diastereoisomer are observed (unequally populated). Analogously to the DMF case, on raising the temperature also the interconversion rate is faster, until the coalescence is reached (+136 °C). The NMR spectra recorded at different temperature provide a qualitative indication of the magnitude of the ΔG^\ddagger . However, to obtain a measure of the energy of activation involved in the process is necessary to extrapolate the kinetic constant from the D-NMR analysis.

The *coalescence method* can be used only in the simplest system in which two nuclei in absence of any coupling, with equal intensity (50:50 population) undergo to chemical exchange and eventually coalesce with the temperature. The DMF system respect these parameters (Figure 2.1.2). Therefore, the first order interconversion rate constant can be calculated as

$$k_{Tc} = \pi \frac{\Delta\nu}{\sqrt{2}} \quad (\text{Eq. 2.1})$$

Where k_{Tc} is the rate constant at the coalescence temperature Tc and $\Delta\nu$ is the chemical shift difference (Hz) without exchange (at low temperature).

However more complicate cases can occur in which the species displays different thermodynamic stability and more complicate NMR with several coupling constants.^{3,4,5,6}

In these cases, the kinetic constant is derived by *line shape simulation* analysis of the D-NMR spectra. This method allows to handle mathematical models that can simulate second-order spectra and quite complex spin systems (up to 11 nuclei).⁷ To use this method, first a simulated spectrum is obtained where the dynamic processes are blocked ($k \approx 0$), then the line shape at higher temperatures are simulated by simple changing the values of the rate constants. However, corrections need to be made to consider the temperature dependence of J couplings, chemical shifts and conformers ratio. The best value of the kinetic constant at each temperature is then found by simple comparison of the *in silico* simulated and the experimental line shape of the spectrum.

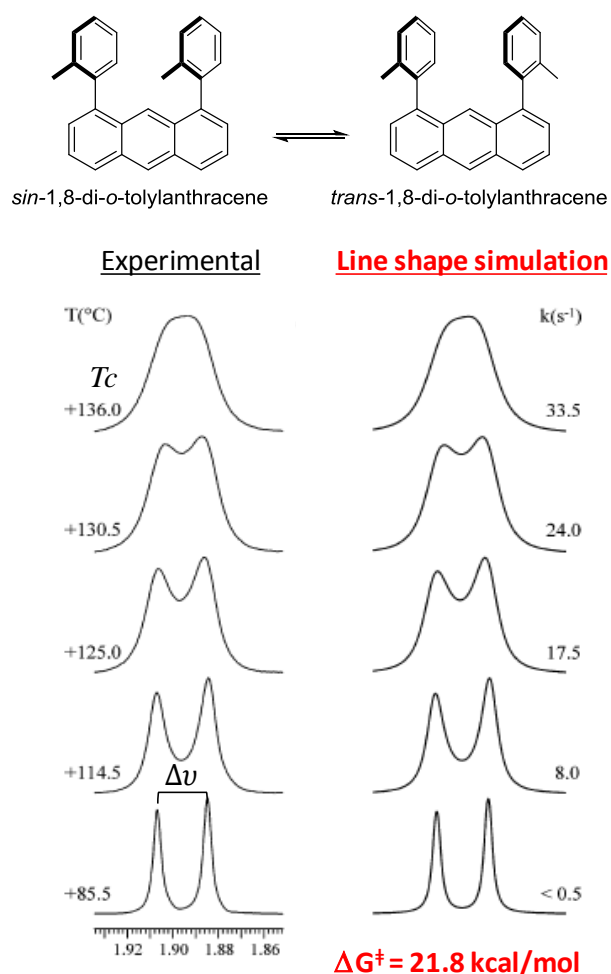


Figure 2.1.2 Left: ^1H NMR methyl signals of 1,8-di-*o*-tolylantracene (600 MHz in DMF- d_7) as a function of temperature. Right: Line shape simulation obtained with the rate constants and the ΔG^\ddagger obtained. [Reprinted (adapted) with permission from *J. Org. Chem.* **2007**, 72, 5391. Copyright 2007 American Chemical Society]

Conformational processes as the ones involved in an axis rotation, are usually a first-order process, and therefore they are not dependent upon concentration. Eventually, the free energy of activation can be extracted by means of the derived Eyring equation⁸ in the case where T is expressed in Kelvin and ΔG^\ddagger in kcal/mol.

$$\Delta G^\ddagger = 4.574 \times 10^{-3} \times T \left(\log_{10} \frac{T}{k} + 10.318 \right) \quad (\text{Eq. 2.2})$$

In the case of the 1,8-di-*o*-tolylanthracene only line shape simulation is applicable (the *syn*: *anti* population is not exactly 50:50 Figure 2.1.2). The line shape simulation is more precise because it provides a mean value of the ΔG^\ddagger overall the temperature analysed. Moreover, it can reveal the entropic contribution by analysing the variation of the ΔG^\ddagger value at different temperatures. However, in most of the cases where a conformational process is involved, the free energy of activation is found invariant with the temperature, thus making the entropic contribution negligible, or below the experimental uncertainty.

The D-NMR approach can determine energy values between about 4.5 and about 22 kcal/mol by line shape simulation. The range of energies that can be studied is limited by the NMR time scale, the resolution of the spectrum, the technical range of temperatures the spectrometer can handle, which is from about -180 °C to +160 °C, and it is limited also by the deuterated solvent (melting or boiling point).

Conformational diastereoisomers, as the 1,8-di-*o*-tolylanthracene, are directly recognizable in a standard NMR analysis due to their different spectroscopic properties. This is not the case for enantiomers and atropisomer in which the two specular images have the same NMR spectra. However, in some cases NMR can detect whether the system is chiral or not. In fact, diastereotopic groups as the methyls in a *iso*-propyl (*i*-Pr) or the protons in a methylene (CH₂) display different chemical shift when they are placed in a chiral environment. This is particularly useful in the case of interconverting atropisomers. With these *probe* of chirality, in fact the signal of diastereotopic group follows an analogous evolution of a mixture of interconverting diastereoisomers. In this case, line shape simulation is essential due to the presence of coupled system and its complexity (Figure 2.1.3). Although useful D-NMR, has a limited range of energy detectable. Therefore, is possible to study the compound that belong to the Class 1 and partially to the Class 2 of LaPlante (see Introduction 1.4).⁹ The racemization of slow interconverting atropisomers ($\Delta G^\ddagger > 22$ kcal/mol) is not accessible with this technique. In these cases, other techniques as Dynamic High Performance Liquid Chromatography (D-HPLC) or kinetic studies can be applied.

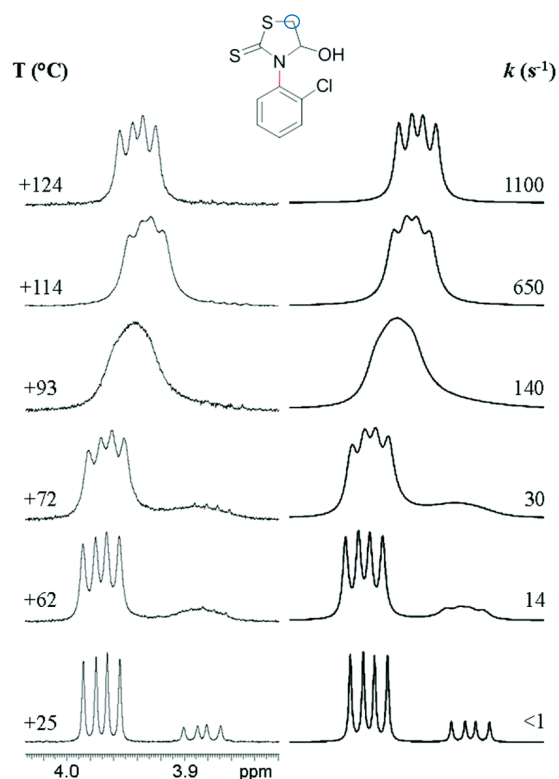


Figure 2.1.3 D-NMR (600MHz DMSO-*d*6) and line shape simulation of 3-arylthiazolidine-2-thiones¹⁰. The diastereotopic signal of the CH₂ serves as a *probe* of chirality. [Reproduced (adapted) with permission from *Org. Biomol. Chem.* **2016**, *14*, 11137. Copyright (2016) Royal Society of Chemistry]

2.2 Dynamic High Performance Liquid Chromatography (D-HPLC)

The recent development of HPLC and UPLC with the introduction of Chiral Stationary Phase (CSP) expanded in the recent years the application of this technique to stereodynamic measures.

High performance liquid chromatography can be easily applied to the study of stereo labile compounds. Chromatograms are collected at variable temperature in order to follow the interconversion of stereo labile species. D-HPLC is complementary to the D-NMR in fact:

1. Enantiomers or atropisomer that interconvert can be analysed without the presence of a *probe* of chirality.
2. The rotational barrier of more stereochemical stable system can be measured reaching the free energy rotational barrier of 25-26 kcal/mol.

An example is reported in the analysis of the rotational barrier of 3-(naphthalen-1-yl)thiazole-2(3*H*)-thione performed by Ciogli and coworkers (Figure 2.2.1).¹⁰

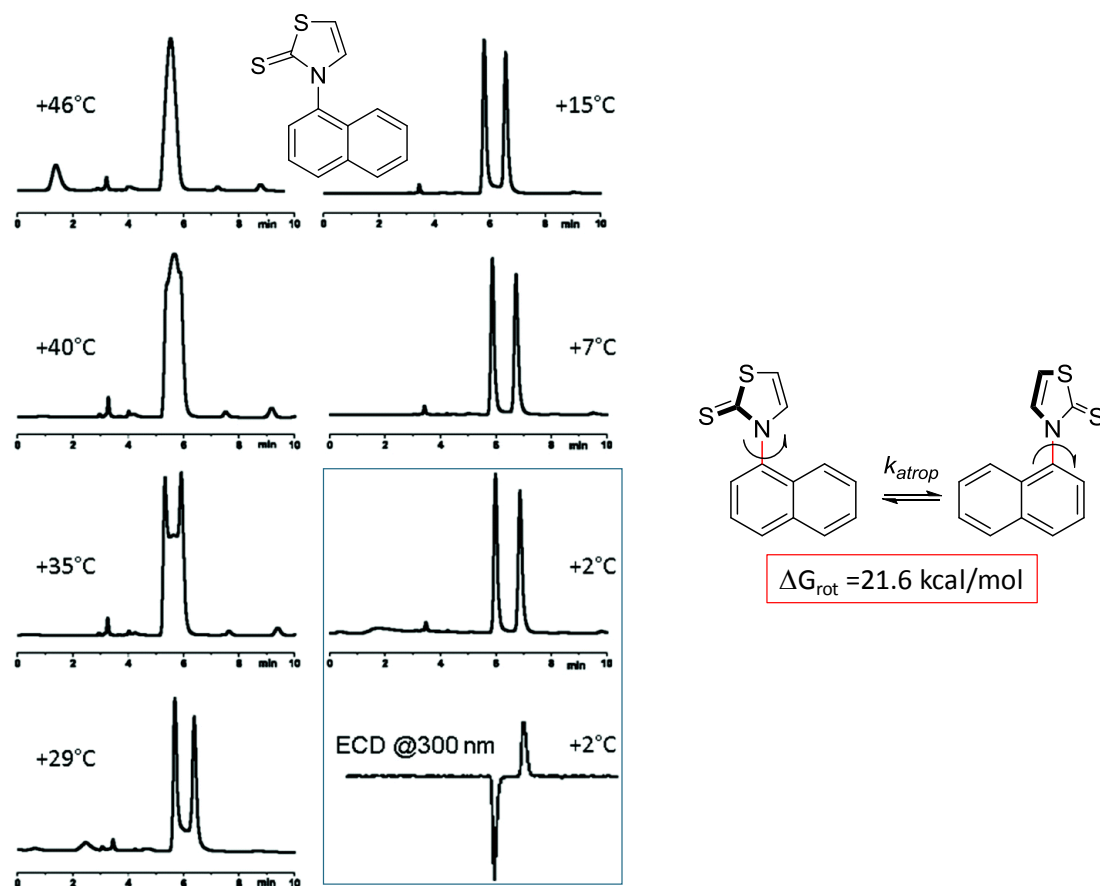


Figure 2.2.1 D-HPLC coupled with single-wavelength ECD analysis performed on 3-(naphthalen-1-yl)thiazole-2(3H)-thione. Column: *R, R* Whelk-O1, 250 × 4.6 mm I.D., eluent: *n*-hexane : dichloromethane 70 : 30 +2% MeOH, flow rate: 1.0 ml min⁻¹, UV detection at 254 nm. [Reproduced (adapted) with permission from *Org. Biomol. Chem.* **2016**, *14*, 11137. Copyright (2016) Royal Society of Chemistry]

This molecule is the dehydrated form of the 3-arylthiazolidine-2-thione shown in Figure 2.1.3, and its rotational barrier cannot be analysed with D-NMR due to the absence of a *probe* of chirality, moreover, its rotational energy is close to the upper limit for D-NMR analysis. Therefore, D-HPLC analysis has been employed (Figure 2.2.1). Using a chiral column, the atropisomers generated by the hindered rotation of the 1-naphthyl group are perfectly separated at +2 °C, as shown by the opposite peaks in the ECD signals detected at 300 nm. Once the temperature is raised, the rotation starts to occur in column while eluting. The competition between atropisomerization and resolution generates elution profiles with a plateau between the peaks. The height of the plateau increases with the temperature, until the stereodynamic process has a faster rate than the separation, and it is possible to observe peaks coalescence at +40 °C. Analogously to the D-NMR, in the D-HPLC the kinetic constant is evaluated through line shape simulation of the chromatograms recorded at different temperature. Although different methods can be applied to reproduce the line shape (theoretical plate model,¹¹ continuous flow model¹²) one of the most reliable is the stochastic model,¹³ where the separation is described through a time dependent function, that can be simulated with an appropriate software.

D-HPLC plays an important role substituting the D-NMR technique when the chemical system defects of diastereotopic nuclei and when rotational barrier is higher than 21 kcal/mol (to avoid performing D-NMR at temperature over + 140 °C). However, thermodynamic limits and the liquid phase issues hamper the possibility to explore the high energy atropisomer ($\Delta G^\ddagger > 26$ kcal/mol).

To study systems in which the stereodynamic processes involved have half-life time of days to years are necessary high energy technique. Dynamic Gas Chromatography (D-GC) works analogously to D-HPLC but can reach higher temperature, enabling the determination of the rotational barrier of stable atropisomer ($\Delta G^\ddagger > 25$ kcal/mol)¹⁴. However, this technique requires particular conditions: 1) a Chiral Gas Chromatography column in which the stationary phase is typically composed by an enantiopure molecule such as β -cyclodextrins or camphorate complex of Ni(II);¹⁵ 2) organic molecule stable at high temperature typical required in a GC analysis. For these reasons to high rotational barrier D-GC is not a widely spread technique and instead are used discontinuous analysis in which the kinetic development is speeded up at high temperature and then analysed at room temperature (where $k \approx 0$).

2.3 Kinetic studies

The combination of D-NMR and D-HPLC can determine the extent of stereodynamic process that occurs with energy between 4.5 kcal/mol and 26 kcal/mol. However, to understand the magnitude of rotational barrier of more stereochemical stable chiral molecules is of crucial importance to get information about the retention of chirality of slow interconverting atropisomers. Dynamic analyses cannot follow high energy process, therefore to monitor such systems are used discontinuous technique, in which an isolated atropisomer is racemized at high temperature and then analysed at room temperature, where $k \approx 0$ and is possible to take *snapshots* of this interconversion process.

Mancinelli and coworkers analysed the atropisomerization barrier of a series of 2,1-borazaronaphthalenes.¹⁶ In one case the barrier was found too high for D-HPLC and D-NMR techniques. Therefore, the slow interconverting enantiomers were resolved in CSP-HPLC and then a small amount of the enantiopure compound were placed at high temperature. Small aliquots were then collected and injected at room temperature in HPLC at different times (Figure 2.3.1).

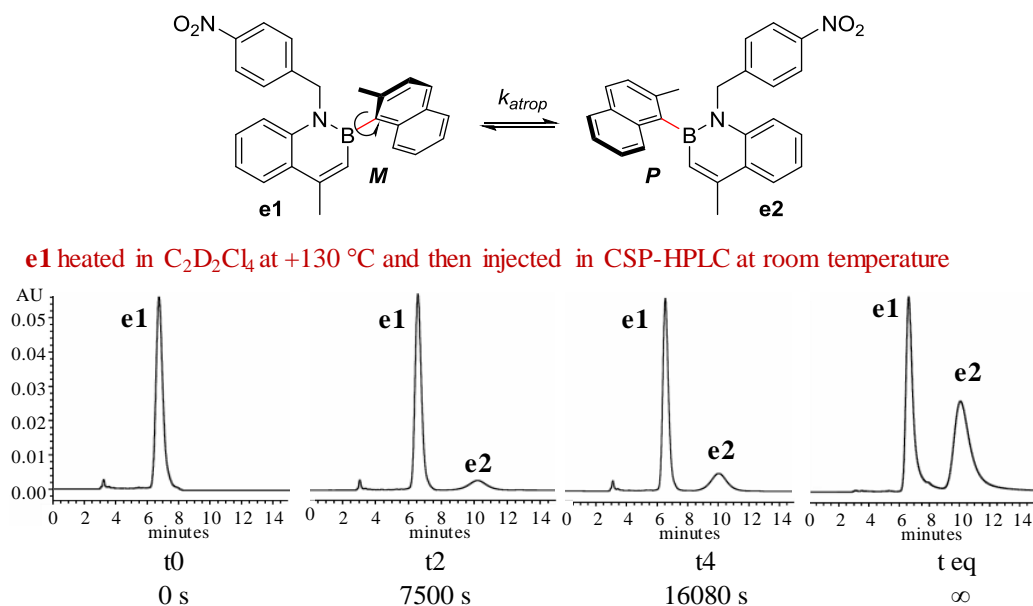


Figure 2.3.1 Racemization of **e1** at +130 °C followed by CSP-HPLC (Lux Cellulose-2 5 μ m, 250 \times 10 mm, 5 mL/min, *n*-hexane : *i*-PrOH = 9 :1). [Reproduced (adapted) with permission from *Org. Lett.* **2016**, 18(11), 2692. Copyright (2016) America Chemical Society].

From the chromatograms reported it is possible to observe the racemization process occurring at high temperature, until the equilibrium is reached. In any racemization process, due to the equal nature of the compounds involved, the rate constant of interconversion of each enantiomer will be the same in both the directions. Therefore, the kinetic equation derived considering a first order process at the equilibrium is found independent from the initial concentration of the atropisomer.

$$\ln(x_{eq} - x) = -2k_{rac}t + \ln x_{eq} \quad (\text{Eq. 2.3})$$

where:

x is the molar fraction of **e2**

x_{eq} is the molar fraction of **e2** at the equilibrium ($x_{eq} = 0.50$)

Extrapolating x from the area of **e2** in the chromatograms and plotting $\ln(x_{eq} - x)$ respects the time (t), the kinetic constant can be obtained through the analysis of the slope, the kinetic constant and therefore the magnitude of the energy barrier involved is determined (33.0 kcal/mol). Furthermore, performing experiment at different temperature is possible to validate the data obtained and to evaluate any entropic contribution to the ΔG^\ddagger (Figure 2.3.2).

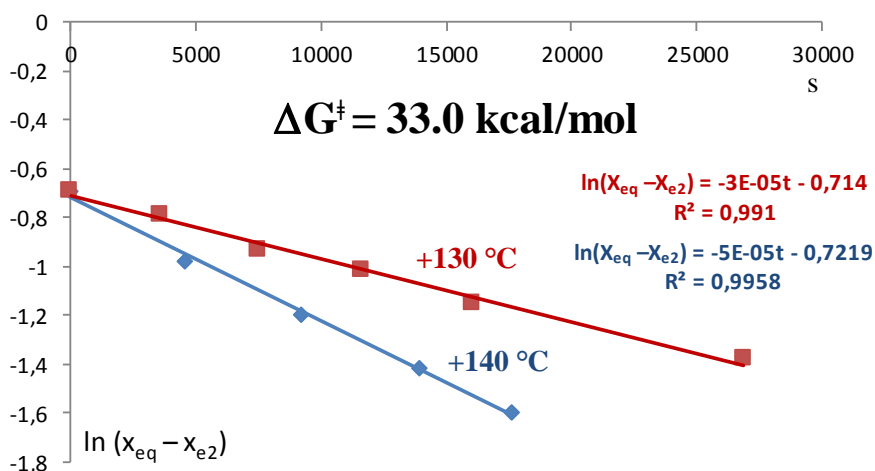


Figure 2.3.2 Plot of the kinetic equation of the atropisomerization of **e1** respect $\ln(x_{\text{eq}} - x)$ at two temperature $+130 \text{ }^\circ\text{C}$ and $+140 \text{ }^\circ\text{C}$ and the rotational energy derived. [Reproduced (adapted) with permission from *Org. Lett.* **2016**, 18(11), 2692. Copyright (2016) America Chemical Society].

2.4 Theoretical models

The introduction of kinetic studies enlarges the whole range of stereodynamic process that occurs from 4.5 kcal/mol to 35 kcal/mol (with half-life time of several years). Although this interval is large it does not cover the conceivable energy barrier of all the stereodynamic process. Moreover, the experimental analysis described have some requisite: peculiar structural motif, solubility in organic solvent, availability of particular deuterated solvent, stability at high temperature, separation of the single stereoisomers among the others. On the other hand, *in silico* computational methods can analyse whatever stereodynamic process might occur in the system, without the condition dictated by the experimental technique. Furthermore, computational methods can be useful prior the synthesis in the design of the molecule and investigate the steric requirement needed to obtain stable atropisomers. Molecular mechanics such as MM3,¹⁷ MMX,¹⁸ MMFF,¹⁹ Amber²⁰ have been the only computational methods available during the early '90. The computational times were quite short and the results obtained quite accurate. However, some limitations of these technique were disclosed when the calculation of transition states were performed. In particular, the geometry of transition state needed to be manually built, and the energy was calculated as a single point energy without further optimization. Therefore, even if the transition state was found there were no indication regarding the presence of a more stable transition state, and the computational analysis proceed essentially with a *trial and error* approach.

The Density Functional Theory (DFT) was introduced in the late 60's by Hohenberg and Kohn,²¹ with their two theorems they gave central importance to the electron density, which they state is the only responsible for the potential and thus all properties of the system, including the many-body wave function. In particular, their hypothesis involves the dependence of the proprieties of the systems (*i.e.*

the ground state) only on the electronic density, which is a function of the three spatial coordinates (x, y, z) . The basic idea of DFT is that for a collection of electrons and nuclei the ground state molecular energy, the wavefunction and all other molecular electronic properties are uniquely determined by the electron probability density $\rho(x, y, z)$, a function of three variables, in which the ground state energy, E_0 , is a functional of the density ρ : $E_0 = F[\rho]$.²³

Hohenberg and Kohn demonstrated that the combination of the appropriate functional with the electron density provides the molecular energy, moreover, the density was demonstrated to follow the variational principle (it can describe the lowest eigenstate), and a mathematical approach to the energy calculation was proposed.²² Kohn-Sham Density Functional Theory (DFT) has the great advantage of considering the electronic correlation, improving performance and accuracy with respect to other computational methods, at a reasonable computational cost.²³

In recent years, the availability of inexpensive high-performance servers and manageable software (Gaussian 09,²⁴ and Spartan²⁵) has allowed high-level calculations to be performed in a reasonable amount of time for molecules containing up to 50–100 atoms.

DFT is a ground-breaking technique because other than the more accurate investigation of the ground state it answers to mechanistic question through the analysis of the energy and geometry of the transition states, that can be unambiguously identified by the analysis of the vibrational states (Paragraph 2.4.2).

2.4.1 Density Functional Theory

The Hartree-Fock (HF) approach consists in searching of an approximation to the ground-state of the N-electron problem by minimizing the total-energy wave-function functional (Eq. 2.4) allowing only N-electron Slater determinants (Eq 2.5) as variational functions.²⁶

$$E[\Psi] = \frac{\langle \Psi | H | \Psi \rangle}{\langle \Psi | \Psi \rangle} \quad (\text{Eq. 2.4})$$

$$\Phi_{\alpha_1, \dots, \alpha_N}(x_1, \dots, x_N) := \frac{1}{\sqrt{N!}} \begin{pmatrix} \varphi_{\alpha_1}(x_1) & \cdots & \varphi_{\alpha_N}(x_1) \\ \vdots & \ddots & \vdots \\ \varphi_{\alpha_1}(x_N) & \cdots & \varphi_{\alpha_N}(x_N) \end{pmatrix} \quad (\text{Eq. 2.5})$$

Where:

- Ψ is the wave function for N-electron system $\Psi(x_1, \dots, x_N)$, where x is a single electron degree of freedom.
- $\Phi_{\alpha_1, \dots, \alpha_N}(x_1, \dots, x_N)$ is the Slater determinant for N electron with φ_α electron states. For instance, the one electron orbital the Slater determinant simplify in $\Phi_\alpha(x) = \varphi_\alpha(x)$, while for N = 2 the determinant is $\Phi_{\alpha_1, \alpha_2}(x_1, x_2) = \frac{(\varphi_{\alpha_1}(x_1)\varphi_{\alpha_2}(x_2) - \varphi_{\alpha_1}(x_2)\varphi_{\alpha_2}(x_1))}{\sqrt{2}}$

In the HF theory, the energy can be described as a linear combination:

$$E_{HF} = V + \langle hP \rangle + \frac{1}{2} \langle PJ(P) \rangle - \frac{1}{2} \langle PK(P) \rangle \quad (\text{Eq. 2.6})$$

where

- V is the nuclear repulsion energy.
- P is the density matrix describing the statistical ensemble of several quantum states.
- $\langle hP \rangle$ is the one-electron (kinetic and potential) energy.
- $\frac{1}{2} \langle PJ(P) \rangle$ is the classical coulomb repulsion of the electrons.
- $-\frac{1}{2} \langle PK(P) \rangle$ is the terms corresponding to the exchange energy (Pauli repulsion) that results from the quantum nature of electrons and is due to the exchange symmetry of the Ψ of indistinguishable particle.

The density functional theory proposed by Kohn and Sham replace the exchange energy for a single determinant with a more general functional: the exchange-correlation functional, which include terms for both the electron correlation and exchange energies. The energy in this case can be formulated as

$$E_{KS} = V + \langle hP \rangle + \frac{1}{2} \langle PJ(P) \rangle + EX[P] + EC[P] \quad (\text{Eq. 2.7})$$

where $EC[P]$ is the correlation functional and $EX[P]$ is the exchange functional.

The functionals ($EC[P]$ and $EX[P]$) normally used in DFT are integrals of function of density and eventually its gradient. Different methods were developed to propose an adequate function to evaluate correctly the exchange-correlation functionals. Among the others hybrid functionals became popular in the late '90 the introduction of B3LYP. This type of functionals linearly combines the HF exchange with the DFT exchange-correlation functionals, leading to integrals that can be solved only by numerical methods, but having a much wider application especially in the field of organic chemistry.

A common DFT approach in the calculation involving a single molecule is to define which functional has to be employed (hybrid, pure, etc.) and the basis set.²⁷ The functional, as described previously, is needed to define the approximation to consider the exchange and correlation energy. The E_{HF} and E_{KS} are reachable only with an infinite set of atomic orbitals. To mathematically describe each orbital, a combination of multiple Gaussian-Type Orbital (GTO) that approximate the more computationally expensive Slater-type (STO) was adopted. To define the orbitals of an atom, a combination of GTOs (basis function) can be attributed to each occupied orbital. This defines a basis set of orbitals for that atom, and in particular this particular basis set is the *minimum basis* (single-zeta). *Minimum basis sets* are always inadequate to describe the interaction between atoms. Therefore, multiple basis functions for each orbital can be assigned. Due to the chemical importance of the valence orbital in making bonds,

these orbitals are usually described by multiple basis function. One of the most common approach is the double-zeta split-valence basis set, where the core orbitals are described with a single-zeta set (only the occupied orbital are taken in consideration), and the valence orbital are described with double-zeta set, doubling the number of basis function for each orbital occupied. In the Pople notation,²⁸ these basis set are described in the form of three number: A-BCg. Where for A is intended the number of GTO assigned to the core shell and the last two number indicate the double zeta composition of the valence orbitals (*i.e.* two basis functions each), where the first is composed by a linear combination of B GTOs, while the second is composed by a linear combination of C GTOs. The notation A-BCDg simply add another basis function to the valence shell orbital that would be composed by D GTOs. One of the most common double-zeta split-valence basis set in DFT calculation of organic molecules is 6-31G. The carbon atom with this basis set is described by:

- 6 GTOs for the $1s^2$ core shell orbital;
- 3 GTOs for the $2s^2, 2p_x, 2p_y, 2p_z$ valence shell orbitals;
- Additionally, 1 GTO for the $2s^2, 2p_x, 2p_y, 2p_z$ valence shell orbitals.

However, the flexibility of GTO is restricted and with these function is not possible to well describe electronic dispersion present in organic molecule, therefore are usually added polarization and diffusion function.

The polarization functions add basis function to the atoms in the valence shell allowing for charge polarization away from the atomic distribution to occur. In the Pople notation these function can be denoted with “*”, “**” or “(d)”, “(d,p)” respectively. The symbols “*” or “(d)” indicate in the case of the carbon atom the addition of 6 d-type basis function for the heavy atom to hybridize the valence orbitals, while “**” or “(d,p)” designate 6 d-type basis function for the heavy atoms and 3 p-type basis function for the hydrogen.

The diffusion functions are added to allow the electron to expand when some net charge is present (ions). To arrange this diffusion, some additional basis functions are added: one for each valence orbital. In the case of the carbon atom, can be added four diffusion functions 1 s-type and 3 p-type (denoted with “+” in Pople notation). This can be expanded to the hydrogen (1 s-type diffusion functions) using the “++” notation.

2.4.2 Transition states

The evaluation of transition state (TS) structures and energies is a central point for stereodynamic analysis, because it represents the energy barriers involved in the process. Young states that a saddle point (TS) structure is mathematically defined as “*the geometry that has zero derivative of energy with respect to moving every one of the nuclei, and has positive second derivative energy for all but*”

one geometric movement".²⁹ In other words, a transition state links two energy minima (ground states) and represents a maximum of energy in the direction of the reaction path, but it is a minimum for all the other movements, Figure 2.4.1.

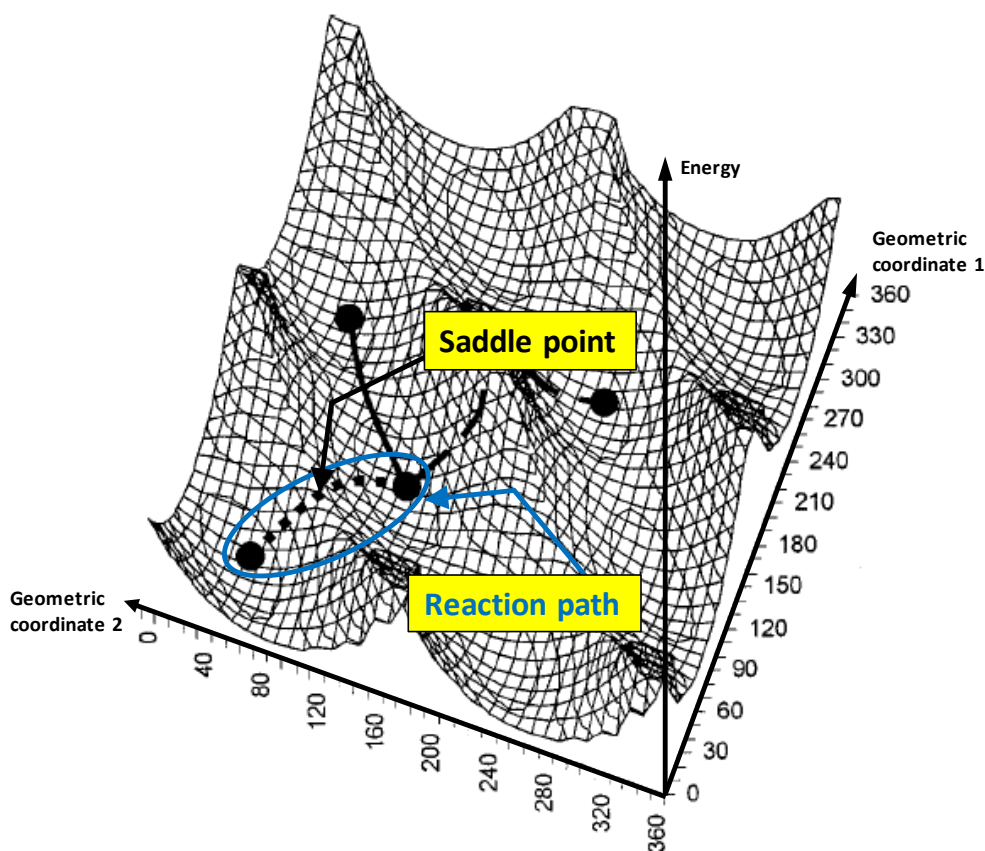


Figure 2.4.1 Potential energy surface. The saddle point is indicated by the black arrow. Dotted line and blue circle indicate the reaction path, and full dot represent the energy minima (ground state). [Reprinted (adapted) with permission from *J. Org. Chem.*, **2001**, 66, 488-495. Copyright (2001) American Chemical Society]

The computation of vibrational frequency verifies whether the stationary point found in the energy map is a saddle point (TS). This is connected to the definition of the TS itself proposed by Young, the second derivative of the potential energy surface (PES) in a saddle point corresponds to an imaginary frequency, and the related vibrational motion corresponds to the motion that bring the molecule from one energy minima to the another.³⁰

The simplest mathematical description of the movement of a diatomic molecule is the simple harmonic motion. In this description, can be easily derived the connection between imaginary frequency of vibration and the individuation of the saddle point, Figure 2.4.2.

Simple harmonic motion

Potential energy	<p style="text-align: center;"><i>Saddle point conditions</i></p> $\frac{dE_p}{dx} = kx = 0$ <p style="text-align: center;"><i>“zero derivative of energy”</i></p> $\frac{d^2E_p}{dx^2} = k < 0$ <p style="text-align: center;"><i>“positive second derivative energy for all but one geometric movement”</i></p> <p style="text-align: center;"><i>Saddle point consequence</i></p> <p style="text-align: center;"><i>if $k < 0$ ω is imaginary</i></p>
$E_p = \frac{1}{2} kx^2$	
Frequency	
$\omega = \sqrt{\frac{k}{m}}$	

Figure 2.4.2 Connection between imaginary frequency and saddle point individuation.

Unfortunately, in the case of intramolecular transformations, such as axis rotation or geared movement the magnitude of the imaginary vibrational frequency is small and it can be difficult to find. On the other hand, in these conformational processes the transition state geometry is much simpler to hypothesize due to the rigidity of the scaffold respect to intermolecular transformation where the molecules have more degrees of freedoms. Therefore, the TS are usually easier to find respect more flexible molecules.

The application of DFT in the study of atropisomers and the possibility to easily individuate the transition state allow to widen the rotational energy barrier analysable and to compare the computed barrier with the experimental one obtained with D-NMR, D-HPLC or kinetic studies. Moreover, with a valid DFT method is possible to design the molecule in order to modulate its stereodynamic behaviour.

2.5 Electronic Circular Dichroism: configuration and conformation analysis

Electronic Circular Dichroism (ECD) analyses the different capability of chiral molecule to absorb right or left circularly polarized radiation (R-CPL and L-CPL respectively Figure 2.5.1) at wavelength compatible with electronic excitation (UV-VIS, 180 nm to 600 nm). Racemic or not chiral molecules do not distinguish between left or right circularly polarized light and absorb both with the same extend leading to a flat ECD spectrum.

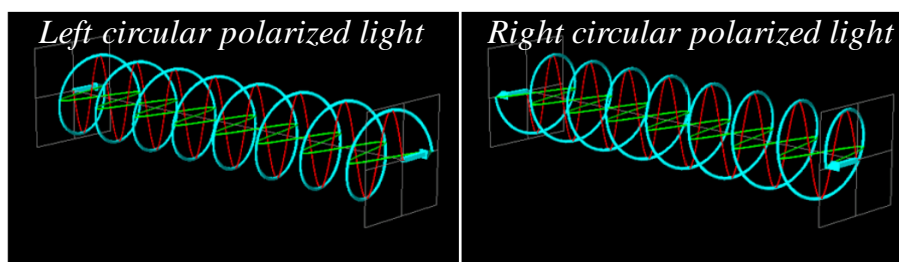


Figure 2.5.1 Left: Left circular polarized light (L-CPL). Right: Right circular polarized light (R-CPL)

The CD signal is composed by the difference: $CD = A^L - A^R$. Namely, the difference between the absorbance of left circular polarized light and the right circular polarized light that is usually expressed in the difference of molar attenuation coefficient for the L and R CPL of the chiral media: $\Delta\varepsilon = \varepsilon^L - \varepsilon^R = CD/cl$ because it is independent by the concentration c and the path length l .

The absorbance of light implies the presence of a chromophore and its related electronic transition. The ECD signal is therefore subjected to the existence of an absorption band to which can be associated a Cotton Effect (CE) that determines a positive or negative ECD band. (Figure 2.5.2 Top). The preferential absorbance of L-CPL or R-CPL from a circular polarized light by the chiral substance, rotate the elliptical polarization of the CPL, since one electromagnetic field vector (right or left, \mathbf{E}_R and \mathbf{E}_L respectively) of the light is absorbed and then does not propagate as fast as the other, generating an out of phase interaction between the two components (L and R CPL) and therefore a signal in terms of $\Delta\varepsilon$.³¹

The different absorbance of one of the CPL component determines the rotation of the elliptical polarization, in other words the rotation of the plane of oscillation of the Electronic Resultant Vector (\mathbf{E}) of the \mathbf{E}_R and \mathbf{E}_L . This rotation can be measured directly in degree as an angle α (rotatory power) and its measure in function of the wavelength is the Optical Rotation Dispersion (ORD) plot of the molecule, that is usually displayed as specific rotatory power $[\alpha]_\lambda = \alpha / cl$ (Figure 2.5.2).

The Electronic Circular Dichroism directly measures the ellipticity (θ) of the ellipsoid plane of oscillation of \mathbf{E} defined as $\theta = \arctg(b/a)$ and expressed in millidegree (mdeg) where b and a are the semi-axes minor and major of the ellipse respectively (Figure 2.5.2). The correlation with the $\Delta\varepsilon$ can be easily derived; in fact, if θ is small $\text{tg}\theta \cong \theta = (b/a) = 32.98 * CD$ when CD is expressed in degree. Usually the ECD spectra are reported as the variation of $\Delta\varepsilon$ or $[\theta] = \theta/cl = 3298 \Delta\varepsilon \left[\frac{\text{degree} * \text{cm}^2}{\text{dmol}} \right]$ in function of the wavelength (Figure 2.5.2).

The source of the rotation of the plane of oscillation of \mathbf{E} is the rotational strength of the molecule at that wavelength, which is directly proportional to electric and magnetic transition dipole moments μ and M respectively.

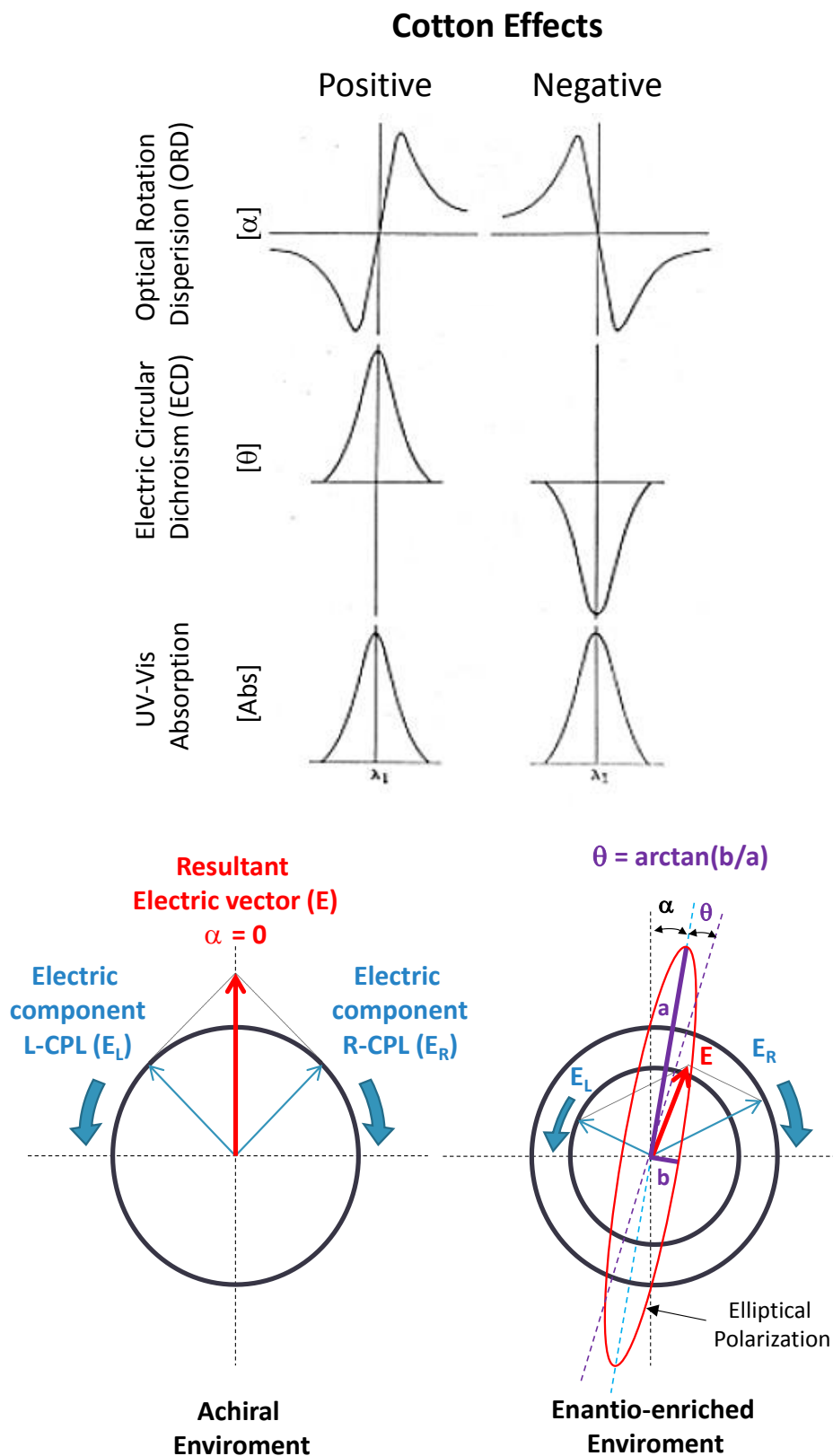


Figure 2.5.2 Top. Effect of Cotton Effect on different spectroscopic technique. Bottom. Behaviour of the resultant electric component of the CPL (\mathbf{E}) in achiral environment and in the presence of an enantiomer and the relative rotation of the plane of oscillation of \mathbf{E} .

In brief, the ECD signal is a consequence of the rotation of the oscillation plane of \mathbf{E} determined by the rotational strength that is dependent by the magnitude and the angles of the transient magnetic

and electric moments, defined, at least the latter, by the nature and disposition of the chromophores in the molecular structure. In this regard, the ECD signal reflects the electronic environment of each chromophore and gives important information about the conformation³² moreover, the ECD spectrum is opposite for a pair of enantiomers,³³ which renders this technique an ideal candidate for the determination of absolute configuration (AC).³⁴

2.5.1 Exciton coupling³⁵

One of the most popular method to perform the analysis of the AC is the exciton coupling. When two or more strong absorbing chromophores are present and not conjugate in a chiral molecule their electric transient dipole moments (ETDMs) generate a split in the electronic excited states that result in a change in the UV absorption and ECD spectra. Such response allows the determination of the disposition and lastly the AC of the chromophore through the exciton coupling method (Figure 2.5.3).

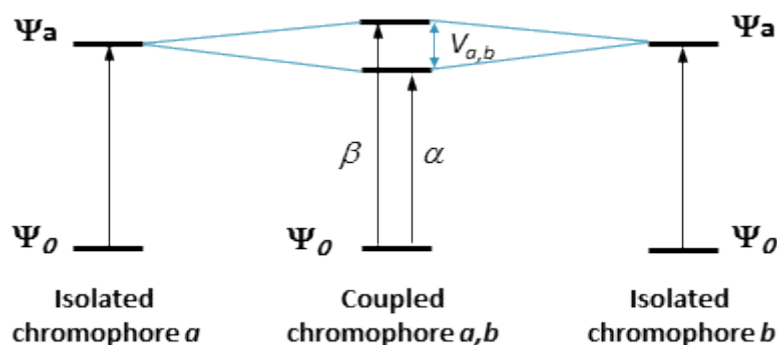


Figure 2.5.3 Ground states Ψ_0 and excited states Ψ_a of isolated and coupled chromophore, in the latter an exciton is generated and the Ψ_a splits in α and β states with Davydov split ($V_{a,b}$)

An exciton is generated when the excitations of two (or more) not-conjugate and spatially near chromophores with an intense π - π^* absorption with equal or similar wavelength (*i.e.* energy) of excitation cannot occur independently. Thus, the excitation of each chromophore delocalized in the system generating an exciton that can interact and couple with each other giving rise, in the case of two chromophore, to a characteristic ECD band with opposite sign and comparable amplitude at different wavelength (ECD exciton couplet). This difference in wavelength between the two maximum of the exciton coupled is the Davydov splitting ($V_{a,b}$).^{36,37}

In Figure 2.5.4 is represented an example of an exciton coupling occurring in di-*p*-benzoate cyclohexane derivative. In this case, where there are two close and equal chromophore the absorption wavelength is equal and the Davydov splitting results symmetric. Thus, the ECD exciton couplet is clearly detected as sequence of first a positive and then a negative CE of equal amplitude and area. The sequence of positive and negative CE is dictated by the relative disposition of the chromophore in the molecule. In fact, if the electron transient dipole moments (ETDM) on the long axis of the chromophores constitute a clock-wise screw passing by the shortest path from the

nearest to the farthest chromophore, the ECD shows first positive, then negative CE, with inversion of CD sign at the same wavelength of the maximum UV absorbance of the chromophore (Positive Exciton Chirality). On the contrary, if the ETDM are arranged in a counter-clock wise screw the ECD displays first a negative then a positive CE with inversion of CD sign at the same wavelength of the maximum UV absorbance of the chromophore (Negative Exciton Chirality), Figure 2.5.4.

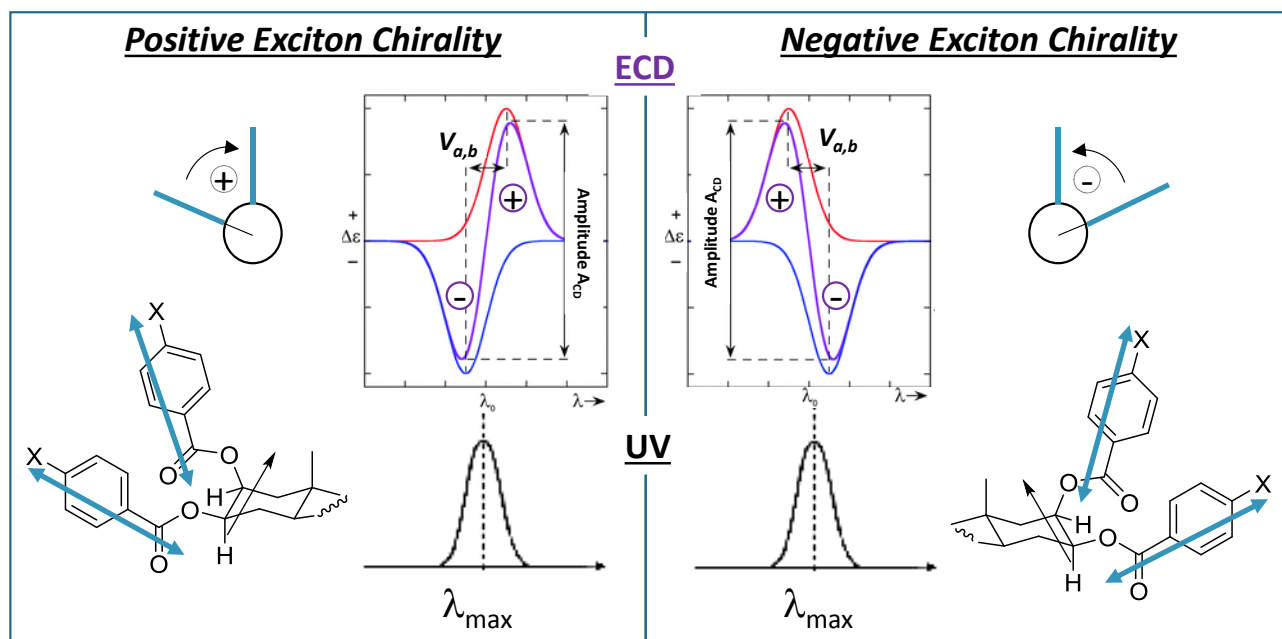


Figure 2.5.4 Positive and Negative Exciton Chirality of two identical chromophores in enantiomers of *p*-benzoate cyclohexane derivative, the H are in *syn* with respect to the ester carbonyl and the latter is in *s-trans* conformation.

The relevant properties of the ECD exciton couplet can be described as follows:

- The amplitude of the CD (A_{CD}) is inversely proportional to the square of the distance between the chromophores maintaining equal the angle between them.
- The amplitude (A_{CD}) is also a function of the dihedral angle between two transition moments, where the maximum A_{CD} is generally obtained when the angle is equal at 70° .³⁸
- The A_{CD} is proportional to the square of the coefficient of molar extinction ϵ of the chromophore. Therefore, to have a strong ECD exciton couplet are indicated chromophores that undergo to strong $\pi-\pi^*$ absorptions.
- If the Cotton Effects have the same rotational strength with the opposite sign for the α and β states, the two Cotton Effect are called conservative and therefore the sum of the integrated areas is equal to zero.
- The rotational strength, defined by the electric and magnetic transition dipole moments μ and M , is origin-independent and is a physically observable quantity.

The exciton coupling chirality method can be expanded with some approximations to system more complicated with two or more different chromophores to obtain the AC. However, this method is not

applicable when the experimental ECD contains multiple bands, due to the presence chromophores with a manifold of electronic transitions or in flexible molecules. Although is not always applicable, this technique can, with relative ease in a rigid system where the chromophore orientation is known, determine the absolute configuration of molecule with accuracy comparable to the X-ray analysis.

2.5.2 Quantum-Mechanical calculations.

When the system present multiple chromophores with flexible conformations, the absolute configuration (AC) is usually determined by comparison of the experimental ECD spectrum to a computed one. In fact, modern computational techniques, are able to simulate the ECD spectrum for a single enantiomer calculating the rotational strength (R) of each transition (once are established the electronic (μ) and magnetic (M) operators of the dipole moments) with the Rosenfeld equation (Eq. 2.8).³⁹

$$R = Im\{\langle 0|\mu|a\rangle \cdot \langle \sigma|M|a\rangle\} \quad (\text{Eq. 2.8})$$

Where:

- Im denotes the imaginary parts of the terms in brackets,
- $\langle \rangle$ notation stands for integration over the configuration space,
- 0 and a are the wavefunctions of the ground state and excited state respectively.

Simply speaking, Eq. 2.7 indicates that the rotational strength R is the imaginary part of the scalar product between the electric and magnetic transition dipole moments.

To perform such calculation, various functionals for Time Dependent DFT (TD-DFT) were developed. The most commons ones are hybrid functional such as BH&HLYP,⁴⁰ M06-2X,⁴¹ ω B97XD that includes empirical dispersion,⁴² and CAM-B3LYP that includes long range correction using the Coulomb Attenuating Method.⁴³ TD-DFT needs a large orbital space in order to calculate electronic transition, therefore large basis sets are usually taken into account, one of the most reliable and used is the 6-311++G(2d,p) basis set that proved to be sufficiently accurate at a reasonable computational cost.⁴⁴ However, the best performance in terms of electronic transition, with an higher computational cost is represented by Dunning's correlation consistent basis sets with double, triple, quadruple, quintuple-zeta and sextuple-zeta (cc-pVDZ, cc-pVTZ, cc-pVQZ, cc-pV5Z, cc-pV6Z) that automatically contains the polarization and diffusion function.⁴⁵

A single molecule can populate different conformations as ground state without changing its chirality. Since the CD timescale is extremely short, in this case the experimental ECD spectrum is determined by linear combination of ECD spectra of each conformation weighted by their population (*i.e.* the energy). In order to simulate the experimental ECD spectrum properly, all the stable conformations need to be found and their ECD spectra calculated. Then the weighted computed spectrum is obtained

considering the Boltzmann distribution and then this spectrum is compared with the experimental one.⁴⁶ As example of this kind of approach, herein the determination of the absolute configuration of three highly flexible natural products with remarkable biological activity is reported by the means of a combination of experimental (in solution and in solid state) and calculated ECD spectra.⁴⁷

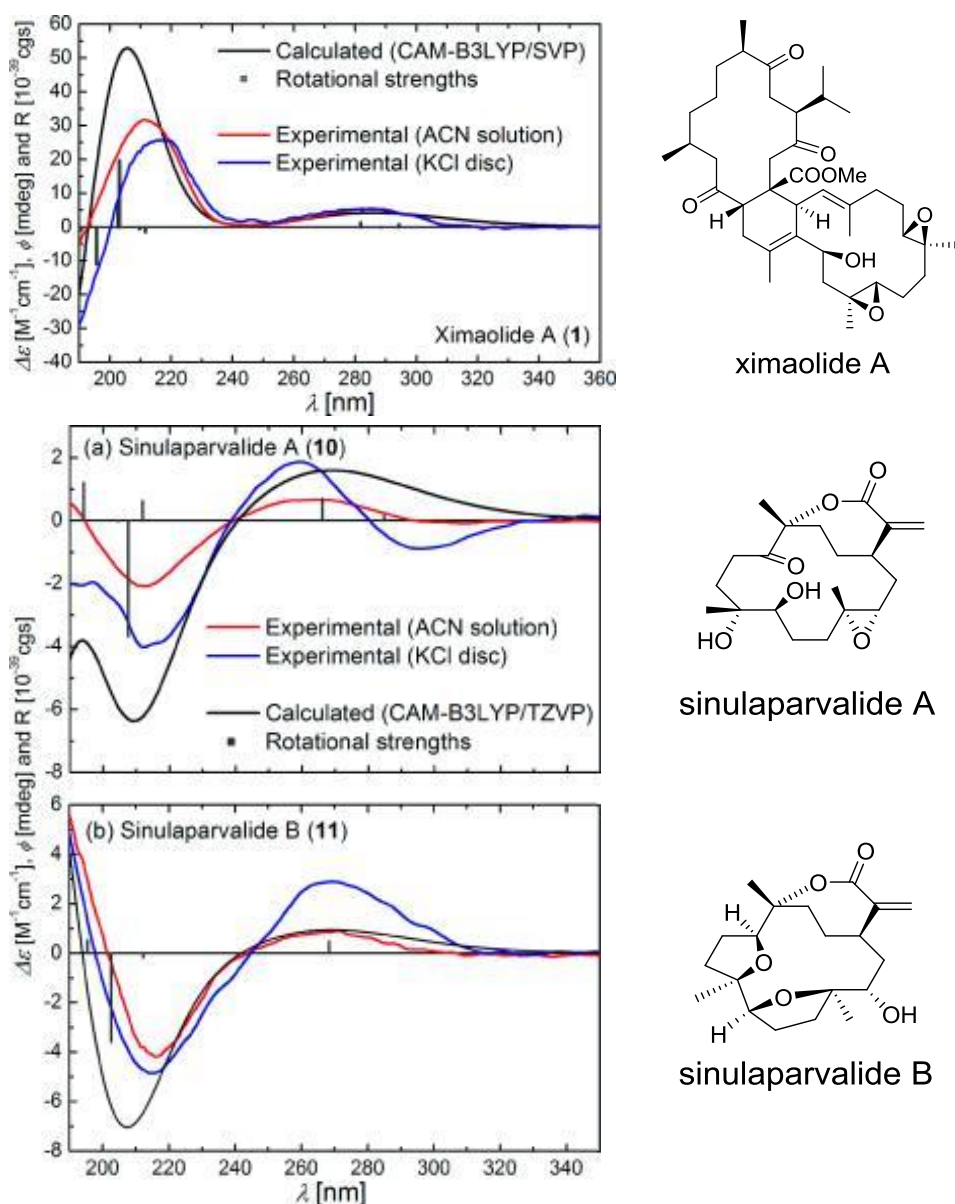


Figure 2.5.5 Electronic Circular Dichroism spectra of ximaolide A, sinularparvalide A and B and determination of the absolute configuration by comparison of experimental and computed ECD spectra. [Reproduced with permission from *Eur. J. Org. Chem.* **2012**, 6722. Copyright (2011) WILEY-VCH Verlag GmbH & Co. KGaA]

References

- ¹ Gutowsky H. S., Holm C. H. *J. Chem. Phys.* **1956**, *25*, 1228.
- ² Lunazzi L., Mancinelli M., Mazzanti A. *J. Org. Chem.* **2007**, *72*, 5391.
- ³ Toyota S., Makino T. *Tetrahedron Lett.* **2003**, *44*, 7775-7778.
- ⁴ Guerra A., Lunazzi L., *J. Org. Chem.* **1995**, *60*, 7959-7965.
- ⁵ Casarini D., Coluccini C., Lunazzi L., Mazzanti A., Rompietti R., *J. Org. Chem.* **2004**, *69*, 5746-5748.

- ⁶ Gasparrini F., Lunazzi L., Mazzanti A., Pierini M., Pietrusiewicz K. M., Villani C. *J. Am. Chem. Soc.* **2000**, *122*, 4776-4780.
- ⁷ Brown J. H.; Bushweller C. H., Mastergabin J. C. QCPE Program No. 633, **1993**.
- ⁸ Eyring H., Polanyi M. Z. *Phys. Chem. Abt. B* **1931**, *12*, 279.
- ⁹ Laplante S. P., Edwards P. J., Fader L. D., Jakalian A., Hucke O. *ChemMedChem*, **2011**, *6*, 503-513.
- ¹⁰ Ciogli A., Kumar S. V., Mancinelli M., Mazzanti A., Perumal S., Severi C., Villani C. *Org. Biomol. Chem.* **2016**, *14*, 11137.
- ¹¹ Jung M., Schurig V. *J. Am. Chem. Soc.* **1992**, *114*, 529-534.
- ¹² Pirkle W. H., Schreiner J. L. *J. Org. Chem.* **1981**, *46*, 4988-4991.
- ¹³ a) Cirilli R., Costi R., Di Santo R., La Torre F., Pierini M., Siani G. *Anal. Chem.*, **2009**, *81*, 3560; b) Veciana J., Crespo, M. I. *Angew. Chem. Int. Ed.* **1991**, *30*, 74-77; c) Krupcik J., Oswald P., Majek P., Sandra P., Armstrong D. W. *J. Chromatogr. A* **2003**, *1000*, 779-800.
- ¹⁴ a) Shurig V., Bürkle W. *J. Am. Chem. Soc.* **1982**, *104*, 7573-7580; b) Bürkle W., Karfunkel H., Shurig V. *J. Chromatogr.* **1984**, *288*, 1-14.
- ¹⁵ a) Jung N., Shurig V. *J. Am. Chem. Soc.* **1992**, *114*, 529-534; b) Trapp O., Shurig V. *Chirality*, **2002**, *14*, 465-470.
- ¹⁶ Mazzanti A., Mercanti E., Mancinelli M. *Org. Lett.*, **2016**, *18* (11), 2692-2695.
- ¹⁷ Allinger N. L., Yuh Y. H., Lii J. H. *J. Am. Chem. Soc.* **1989**, *111*, 8551-8566.
- ¹⁸ PCMODEL, v9, Serena Software, Bloomington, IN (USA).
- ¹⁹ Halgren T. A. *J. Comput. Chem.* **1996**, *17*, 520-552.
- ²⁰ Weiner S. J., Kollman P. A., Case D. A., Singh U. C., Ghio C., Alagona G., Profeta S., Weiner P. *J. Am. Chem. Soc.* **1984**, *106*, 765-784.
- ²¹ Hohenberg P., Kohn W. *Phys. Rev.* **1964**, *136*, B864-B871.
- ²² Kohn W., Sham L. J. *Phys. Rev.* **1965**, *140*, A1133-A1138.
- ²³ a) Koch W., Holthausen M. C. *A Chemist's Guide to Density Functional Theory*, Wiley-VCH, Weinheim, 2nd ed., **2002**; b) *A Primer in Density Functional Theory* (Eds.: Fiolhais, C.; Nogueira, F.; Marques, M.), Springer-Verlag, Heidelberg, **2003**.
- ²⁴ Frisch M. J., Trucks G. W., Schlegel H. B., Scuseria G. E., Robb M. A., Cheeseman J. R., Scalmani G., Barone V., Mennucci B., Petersson G. A., Nakatsuji H., Caricato M., Li X., Hratchian H.P., Izmaylov A. F., Bloino J., Zheng G., Sonnenberg J. L., Hada M., Ehara M., Toyota K., Fukuda R., Hasegawa J., Ishida M., Nakajima T., Honda Y., Kitao O., Nakai H., Vreven T., Montgomery J. A. Jr., Peralta J. E., Ogliaro F., Bearpark M., Heyd J. J., Brothers E., Kudin K. N., Staroverov V. N., Kobayashi R., Normand J., Raghavachari K., Rendell A., Burant J. C., Iyengar S. S., Tomasi J., Cossi M., Rega N., Millam N. J., Klene M., Knox J. E., Cross J. B. Bakken V., Adamo C., Jaramillo J., Gomperts R., Stratmann R. E., Yazyev O., Austin A. J., Cammi R., Pomelli C., Ochterski J. W., Martin R. L., Morokuma K., Zakrzewski V. G., Voth G. A., Salvador P., Dannenberg J. J., Dapprich S., Daniels A. D., Farkas O., Foresman J. B., Ortiz J. V., Cioslowski J., Fox D. J. Gaussian 09, rev D.01; Gaussian, Inc.: Wallingford, CT, **2009**.
- ²⁵ *Spartan 08*, Wavefunction Inc., Irvine, CA (USA).
- ²⁶ Pavarini E., Koch E., Van Den Brink J., Sawatzky G.(eds.) *Quantum Materials: Experiments and Theory Modeling and Simulation Vol. 6* Forschungszentrum Jülich, **2016**.
- ²⁷ a) Pople J. A. *Angew. Chem. Int. Ed.* **1999**, *38*, 1894-1902; b) Kohn W. *Rev. Mod. Phys.* **1999**, *71*, 1253-1267.
- ²⁸ Ditchfield R., Hehre W. J., Pople J. A. *J. Chem. Phys.* **1971**, *54* (2), 724-728.
- ²⁹ Young D. *Computational Chemistry*, **2001**, *17*, 147-158, Wiley Interscience, New York.
- ³⁰ a) *Gaussview 4.1.2*, Gaussian Inc., Wallingford CT, USA; b) *MOLDEN 4.6*, available at <http://www.cmbi.ru.nl/molden/>. See: Schaftenaar G., Noordik, J. H. *J. Comput. Aided Mol. Design* **2000**, *14*, 123-134.
- ³¹ a) Berova N., Nakanishi K., Woody R. W. *Circular Dichroism: principles and applications*, Wiley & Sons, 2nd edition, **2000**; b) Mislow K. *Introduction to Stereochemistry*, Benjamin W. A., Inc, **1965**.
- ³² Pescitelli G., Di Bari L., Berova N. *Chem. Soc. Rev.* **2011**, *40*, 4603-4625.
- ³³ Barron L. D., *Molecular Light Scattering and Optical Activity*, Cambridge University Press, Cambridge, 2nd edition **2004**.
- ³⁴ Berova N., Di Bari L., Pescitelli G., *Chem. Soc. Rev.* **2007**, *36*, 914-931.
- ³⁵ Berova N., Nakanishi K., Chapter 12 in *Circular Dichroism: Principles and Applications, Second Edition*. Edited by Berova N., Nakanishi K., Woody R. W, **2000**, 337, John Wiley & Sons.
- ³⁶ Davydov A. S. *Zhur. Eksptl. I Teoret. Fiz.* **1948**, *18*, 210.
- ³⁷ Davydov A. S. *Theory of Molecular Excitations*, McGraw-Hill, New York, **1962**.
- ³⁸ Berova, N., Ellestad G. A., Harada N., *Characterization by Circular Dichroism Spectroscopy*, in *Comprehensive Natural Products II-Chemistry and Biology*, Eds. Mander L., Lui H. W., Elsevier, Oxford, **2010**, *9*, 91-146.

³⁹ Rosenfeld L. *Z. Physik* **1928**, *52*, 161.

⁴⁰ In Gaussian 09 the BH&HLYP functional has the form: $0.5 * E_X^{HF} + 0.5 * E_X^{LSDA} + 0.5 * \Delta E_X^{Becke88} + E_C^{LYP}$

⁴¹ Zhao Y., Truhlar D. G. *Theor. Chem. Acc.* **2008**, *120*, 215-241.

⁴² Chai J. D., Head-Gordon M. *Phys. Chem. Chem. Phys.* **2008**, *10*, 6615-6620.

⁴³ Yanai T., Tewand D., Handy N. *Chem. Phys. Lett.* **2004**, *393*, 51-57.

⁴⁴ a) Cera G., Chiarucci M., Mazzanti A., Mancinelli M., Bandini M. *Org. Lett.*, **2012**, *14*, 1350-1353; b) Pesciaioli F., Righi P., Mazzanti A., Bartoli G., Bencivenni G. *Chem. Eur. J.*, **2011**, *17*, 2842-2845; c) Duce S., Pesciaioli F., Gramigna L., Bernardi L., Mazzanti A., Ricci A., Bartoli G., Bencivenni G. *Adv. Synt. Catal.*, **2011**, *353*, 860-864; d) Bernardi L., Comes-Franchini M., Fochi M., Leo V., Mazzanti A., Ricci A. *Adv. Synt. Catal.*, **2010**, *352*, 3399-3406.

⁴⁵ Kendall R. A., Dunning T. H., Harrison R. J. *J. Chem. Phys.* **1992**, *96*, 6796-6806.

⁴⁶ Marques M. A. L., Gross E. K. U. *Annu. Rev. Phys. Chem.*, **2004**, *55*, 427-455.

⁴⁷ Kurtán T., Jia R., Li Y., Pescitelli G., Guo Y.W. *Eur. J. Org. Chem.* **2012** 6722-6728.

3 Aim of the research

There is a huge variety of molecules that can display stereodynamic behaviour along an axis. The systems that are taken in consideration in this manuscript well exemplify the variety of application that such stereodynamic structure can reach. The molecular systems presented can be in fact used: to generate steric scale of substituents, to find new and unexpected long range intramolecular interactions that can have a wider and general implication, to introduce chirality into scaffold that cannot bear an ordinary chiral centre and can be used as new enantiopure stable drugs or ligands, or to develop new stereodynamic sensor for biologically relevant molecules.

Consequently, the Ph.D. work herein presented is divided in:

- Chapter 4, where is discussed the analysis of stereodynamic rotation around a C-C or C-N bond in different molecules to elucidate their conformational behaviour and to provide new insight about weak interaction within their system;
- Chapter 5, where is analysed the development and the steric requirement need to produce stable stereogenic axis and therefore stable atropisomers (belonging to the Class 3 of LaPlante, see Introduction 1.4). This different type of stereogenic units is recently gaining importance and represent a new and challenging type of chirality that can introduce chirality into scaffolds that cannot bear ordinary stereogenic centre;
- Appendix where is presented an ongoing project, developed in collaboration with the Prof. Christian Wolf at the Georgetown University, about 1,8 disubstituted naphthalene as stereodynamic sensor for nucleobases or chiral primary amine.

Dynamic stereochemistry of chiral axes. Design and synthesis of stable atropisomers.

4 Dynamic stereochemistry and conformational analysis

The three-dimensional arrangement of the functional groups in a molecule can determine its chemical and biological behaviour. On this regard, it is of extreme importance to determine the most energetically favoured conformation of functional groups in organic molecules, in order to determine properties and reactivity. Many studies and methodology were developed to understand the different arrangement of organic molecules.¹ The study of stereodynamic chiral axis allows to monitor the conformational arrangement of molecules, quantifying the dependency on steric and electronic parameters.²

4.1 Long-Range Bonding/Nonbonding Interactions: A Donor–Acceptor Resonance Studied by Dynamic NMR³

The study of energy barriers that involves the rotation around one hindered bond is directly connected to the steric parameters of the substituents in the nearest environment of that bond.

One of the first method to assess the steric bulkiness of substituents is the *A* value⁴ in which is considered the preferential axial or equatorial disposition of the substituent in cyclohexanes. A more advanced and precise research was performed by the seminar work of Sternhell and coworkers,⁵ who studied the rotational barriers of 6-aryl-1,1,5-trimethylindans system by D-NMR (see Paragraph 2.1). However, with these scaffolds and experimental settings it was not possible to explore the steric bulkiness of small substituent, therefore an additional hindrance *Y* (an OMe or Me groups) is needed in position 5, and then individual steric bulkiness was calculated as a difference between the experimental rotational barrier and an interaction constant $I^{OMe/Me-H}$ due to the presence of the *Y* group. Trying to avoid the dependence of an interaction constant, Schlosser, Mazzanti and Ruzziconi⁶ performed a series of works in which they studied a 3'-2-disubstitued-1,1'-biphenyl with D-NMR at very low temperatures, thus eliminating the need for the interaction constant and finding the steric interaction of small substituents referred to the hydrogen. More recently, Roussel and coworkers^{2d} explored the rotational barrier of atropisomers (from stereolabile to stable) of N-(*o*-substitued-aryl)thiazoline-2-thione by means of D-HPLC and kinetic studies (see Paragraph 2.2 and 2.3) and defined a steric scale, developed by thermal racemization of atropisomers, independent by chiral probe or interaction constant.

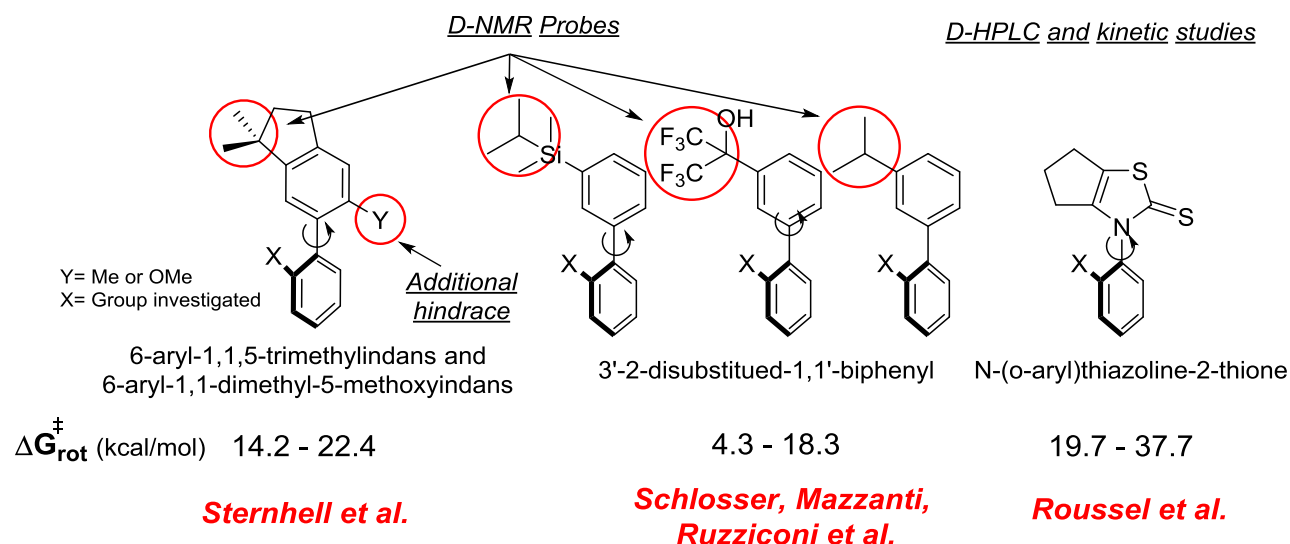
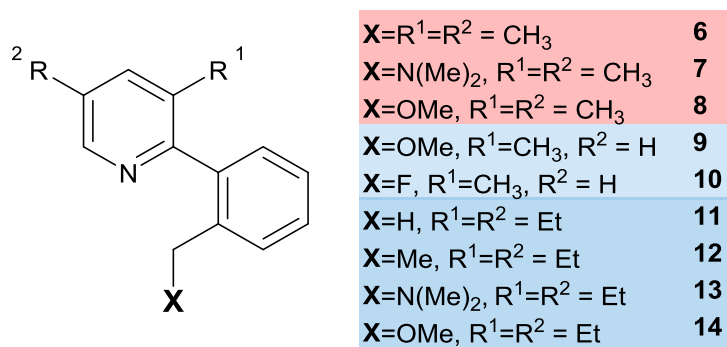


Figure 4.1.1 Scaffold use to define steric scale, the rotational barrier explored and the techniques used.

Starting from these major works and deepening the interest on very small substituent⁷ a new series of simple pyridyl-benzyl derivates were synthesized and studied (**6-14**, Figure 4.1.2). Considering the literature regarding the relation on the steric bulkiness and rotational barrier, a particular series of these new compounds behaved in an unexpected way displaying a long-range interaction that perturbs the expected rotational barriers related to the steric bulkiness of substituents.


 Figure 4.1.2 Pyridyl-benzyl derivatives **1-14**.

Some compounds of the 2-(2-(X-substituted-methyl)phenyl)pyridine series displayed different rotational barrier depending on the nature of the X substituent (Figure 4.1.3). For instance, the methyl (X=H) derivative (**11**) showed a rotational barrier of 13.7 kcal/mol in line with the steric hindrance consideration, however when X was changed to a methoxy group (**14**) the determination with D-NMR pointed out a barrier of 12.6 kcal/mol. The $\Delta G_{\text{rot}}^{\ddagger}$ of **14** with respect to the one found for **11** is not compatible with the above steric scale in which a methoxy group is surely larger than a simple hydrogen.

To explain such unusual feature a computational analysis of the rotational barrier was performed on a model system (**1-5** in Figure 4.1.3) at ω B97XD/6-31G(d) level of theory.

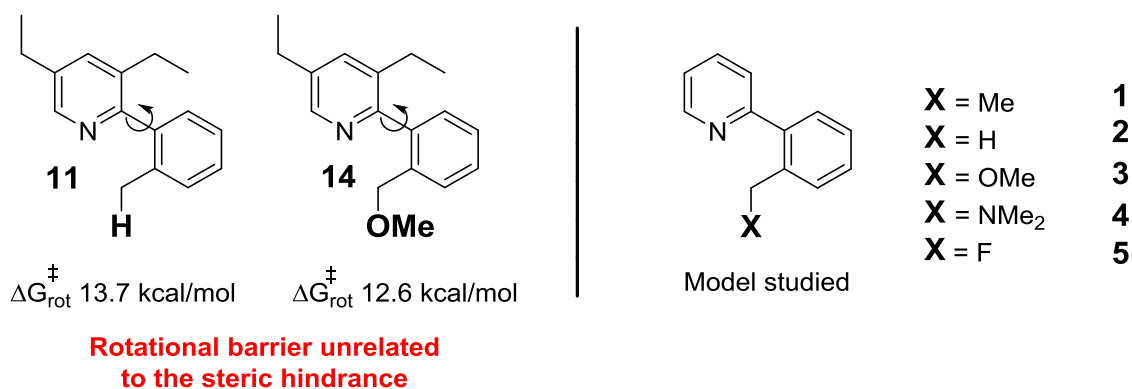


Figure 4.1.3 Left: **11** and **14** and their respective rotational barrier is unrelated to the steric hindrance. Right: Model system used for the computational analysis

The analysis of the geometry of the ground states and transition states (TS) revealed the presence of two valid TS involved in the rotation of the 2-(1'-phenyl)-pyridine bond. One has the dihedral angle (N-C2-C1'-C2') close to 0° (TS0), while the second corresponds to an angle close to 180° (TS180), therefore, the rotation of the benzyl moiety towards the lone pair of the nitrogen or towards the C-H, respectively (Figure 4.1.4).

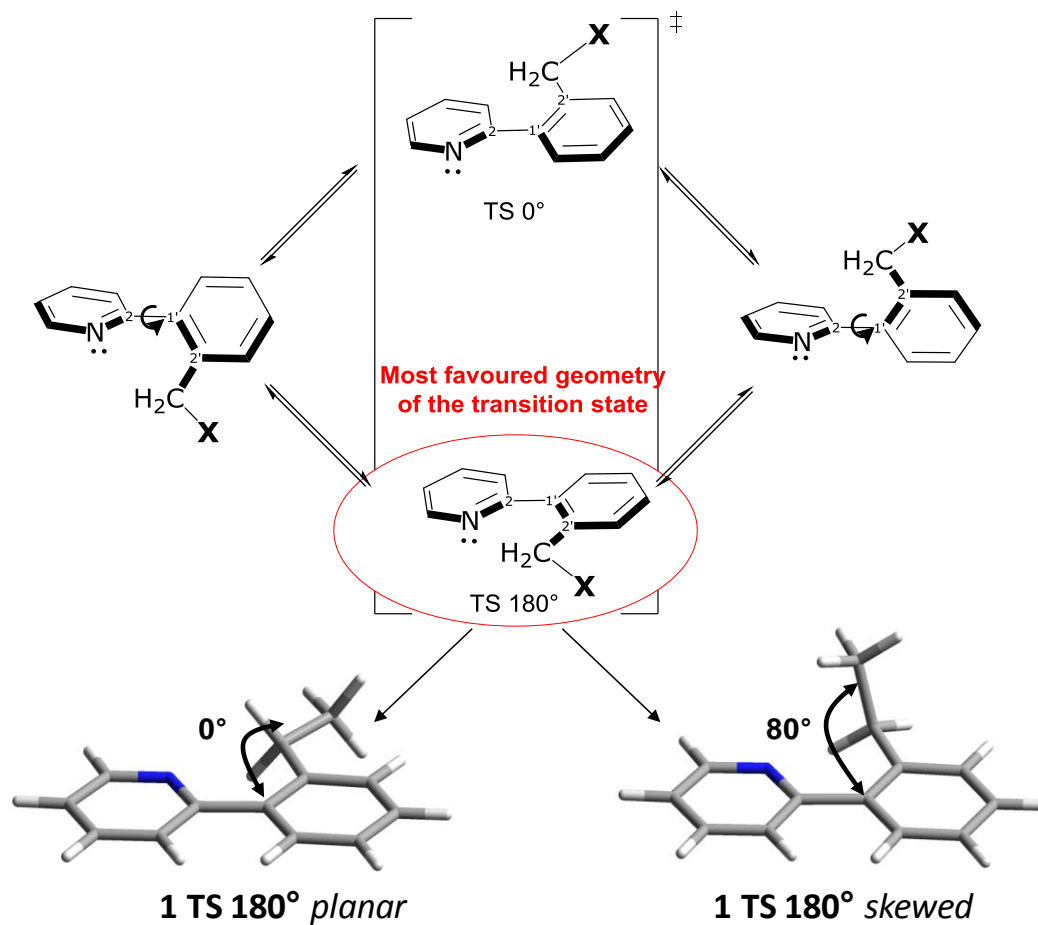


Figure 4.1.4 The two conceivable transition states occurring during the rotation (TS 0° and TS 180°) and the relative two possible ethyl group dispositions. [Reprinted (adapted) with permission from *Org. Lett.* 17, 2015, 2740-2743. Copyright (2015) American Chemical Society].

As the steric scale dictates, the lowest TS was found occurring with a TS180 geometry. Furthermore, in the TS180 the CH₂-X fragment can adopt two geometries, one *planar* in which the X substituent lay in the plane identified by the phenyl ring and one *skewed* where the X is tilted out of the aryl plane of about 80° (Figure 4.1.4). To esteem the contribution of the lone pair of the pyridine, the energies were recalculated (as single points) at the higher CCSD(T)/6-31+G(d)// ω B97XD/6-31G(d) level of theory.⁸ The rotational barrier found in case of **1** was equal to the experimental one proving the reliability of these calculation (Table 4.1.1). Moreover, these results pointed out again that when X=H (**2**) the rotational barrier was higher than in the case in which X was a more sterically demanding substituent such as a methoxy or a fluorine group (**3** and **5**, Table 4.1.1).

Table 4.1.1 Experimental and calculated torsional barriers for 2-arylpyridines. Calculations at the CCSD(T)/6-31+G(d)// ω B97XD/6-31G(d) level (energies in kcal/mol). Values in bold indicate the preferred transition state. [Reprinted (adapted) with permission from (R. Ruzziconi, *et al. Org. Lett.* 17, 2015, 2740-2743). Copyright (2015) American Chemical Society.]

Compound	X	exptl. value	planar TS	skewed TS	ΔE pl-sk ^a
1	Me	5.9 ^b	8.4	6.2	+2.2
2	H	-	5.9 ^c	5.9 ^c	0 ^c
3	OMe	-	4.9	6.7	-1.8
4	NMe ₂	4.8	6.8	6.6	+0.2
5	F	-	4.0	6.9	-2.9

^a a positive value indicates a favoured skewed transition state. ^b See ref. 7. ^c For **2** there is only one geometry of TS 180°

A close inspection of the geometries of the respective lowest TS showed that, while the conformations of the methyl and partially of the dimethylamine (**1** and **4**) substituents were skewed, the conformations preferred by the methoxy and fluorine were planar (**3** and **5**). This discrepancy in the preferred geometry of TS can explain the inverted steric scale found in **11** and **14** and in **2** and **3**, **5**. It is possible, in fact, to hypothesize a stabilizing interaction occurring in the TS between the lone pair of the nitrogen an electron demanding methylene group. In fact, on the contrary of the methyl and hydrogen, the methoxy and fluorine groups are able to remove charge from the α carbon favouring long-range stabilizing interaction that lowers the transition state and therefore the rotational barrier (Figure 4.1.5). On this perspective, the planar TS state occurring in **3** and **5** resemble much of S_N2 intermediate, where the nucleophile group (N lone pair) need to be on the same plane of the electrophile (X group).

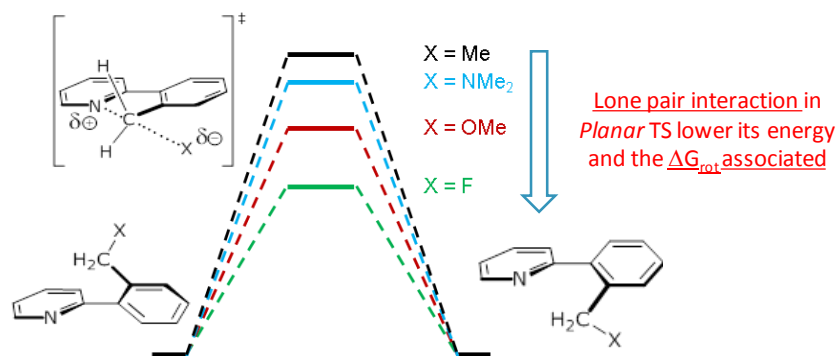


Figure 4.1.5 Schematic representation of the rotational barrier trend, implying the same energy for the GS of different pyridine derivative. [Reprinted (adapted) with permission from *Org. Lett.* 17, 2015, 2740-2743. Copyright (2015) American Chemical Society].

As consequence of this resemblance this long-range interaction can be defined as a resonance between a bonding (**B**) and non-bonding (**NB**) limiting structures. Although, the participation of lone pair on the nitrogen of a pyridine is commonly see in the reactivity of this aromatic ring (Minisci reaction, etc.), in the exceptional case here occurring the lone pair interacts with an atom four interposed bonds away without any conjugation effect (Figure 4.1.6). Due to the uncommon nature of this interaction experimental confirmations were needed.

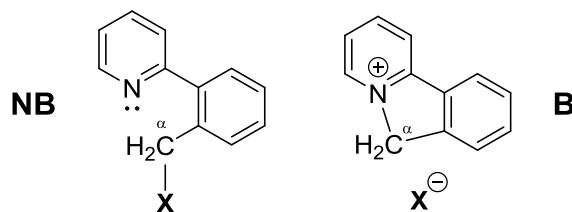
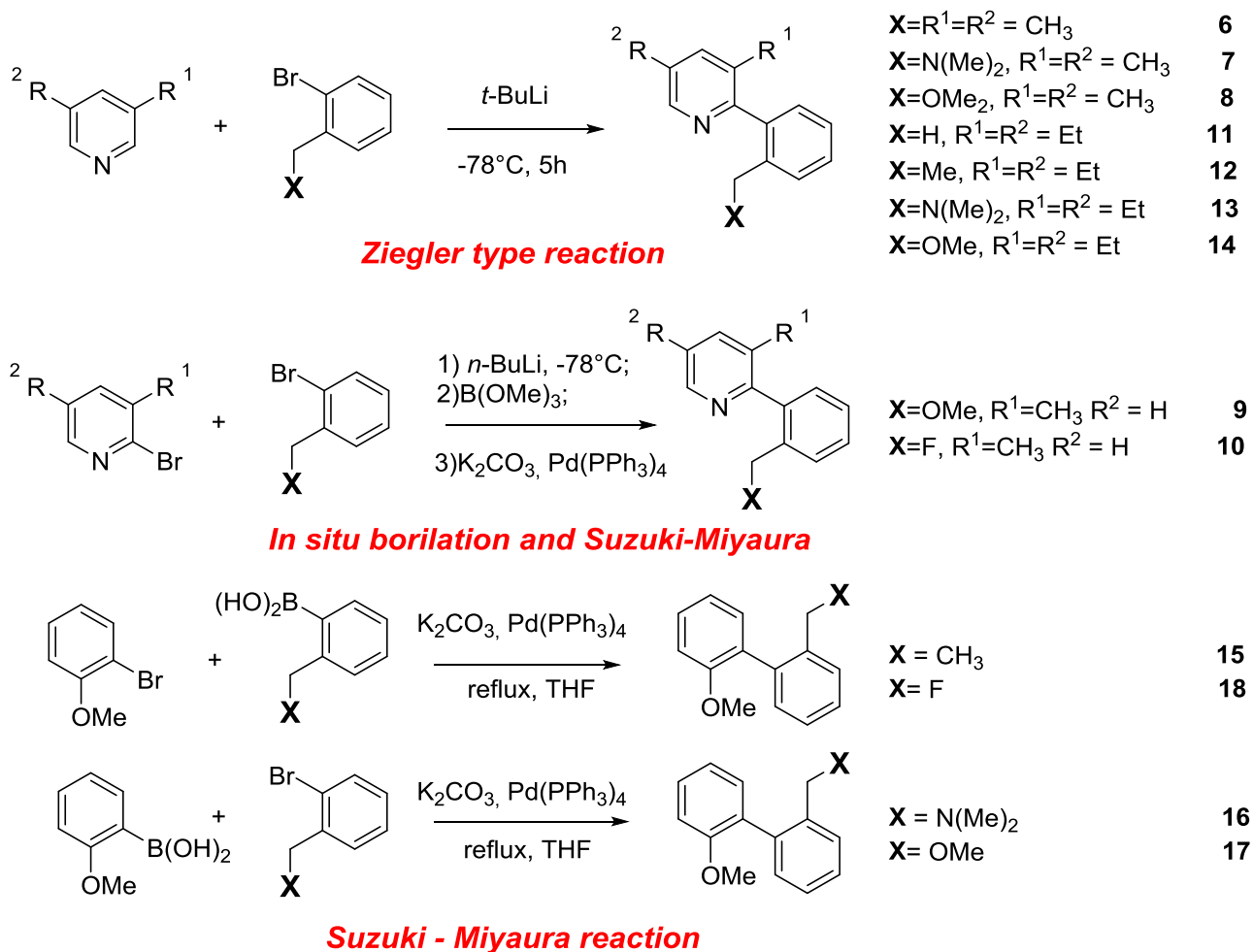


Figure 4.1.6 Non-Bonding (**NB**) and Bonding (**B**) limiting structure occurring with the long-range lone pair - methylene interaction. [Reprinted (adapted) with permission from *Org. Lett.* 17, 2015, 2740-2743. Copyright (2015) American Chemical Society].

The compounds **6-8**, and **11-14**, were synthesized by Ziegler-type addition⁹ starting from 3,5-dimethylpyridine, and 3,5-diethylpyridine, respectively, and the appropriate phenyllithium derivative. The compound **9** and **10** containing the methoxy and fluorine atom was synthesized by Suzuki-Miyaura coupling¹⁰ because the Ziegler protocol yields only, especially in the case of **10**, to the cyclized form **B** due to intramolecular attack of the lithium-amide on the methylene carbon (Figure 4.1.7, detailed experimental procedures are reported in Paragraph 7.1).


 Figure 4.1.7 Synthetical routes adopted to obtain **6-18**.

Once the products were synthesized the rotational barrier were determined by D-NMR analysis and line shape simulation (Figure 4.1.8). In all the molecules the evolution of the diastereotopic methylene signal with the temperature is followed (see Paragraph 7.1.2).

In the case of **11**, once the rotation is blocked (in the NMR time scale) at -28°C , the AB system is shown, then by raising the temperature it first coalesces at $+4^\circ\text{C}$ then at room temperature, become one signal, implying a fast rotation in which the NMR is no longer able to distinguish the chiral environment. The line shape simulation is then able to extract the kinetic constant and determine the experimental calculated energy (see Paragraph 2.1).

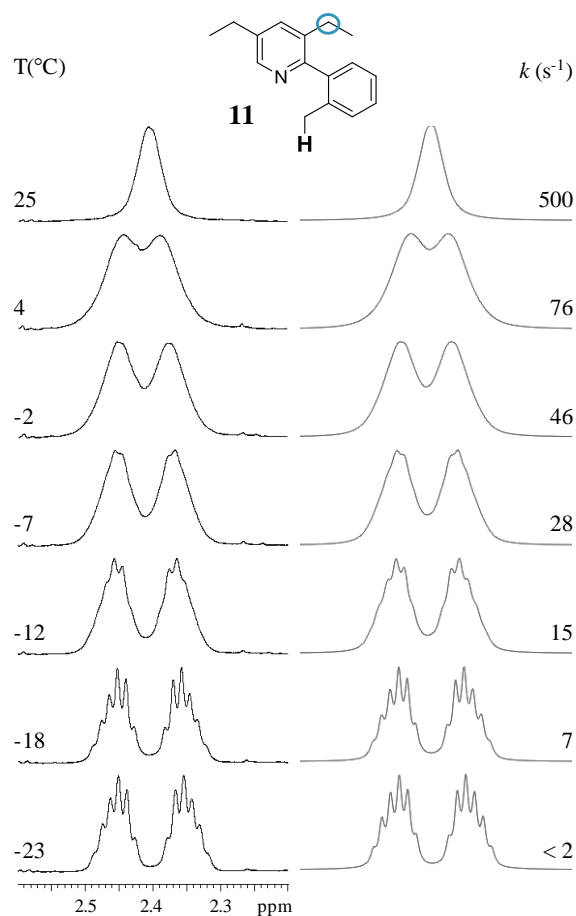


Figure 4.1.8 ^1H D-NMR spectra of CH_2 signal of **11** at 600 MHz in CD_2Cl_2 (left) and line shape simulation and corresponding derived rate constant (right). [Reprinted (adapted) with permission from *Org. Lett.* 17, 2015, 2740-2743. Copyright (2015) American Chemical Society].

The experimental and calculated rotational energies collected are displayed in Table 4.1.2. From the reported values is straightforward to correlate the different rotational barrier with the leaving group tendency of X. In the series where R_1 and R_2 are the same is possible to see the decrease of rotational barrier upon increase of leaving group tendency of X (series **6-8**, **9-10**, and **11-14**). Moreover, the comparison of **8** with **9** demonstrate that a hindrance in position 5 does not influence the $\Delta G_{\text{rot}}^\ddagger$ at any extend.

When $\text{X}=\text{H}$ the diastereotopic nuclei are lost, therefore, to evaluate the contribution of a hydrogen on the rotational barrier, the series **11-14** were synthesized where R_1 and R_2 are ethyl group that serves as chirality probes. Again, in this series is possible to evaluate the dependency of the rotational barrier on the leaving group tendency of X. In both series, **6-8** and **11-14** the tendency of the dimethylamino group (**7** and **13** respectively) does not differ clearly from the respective ethyl derivatives. This is due principally to the coordination in the GS of the lone pair of the dimethylamino group to the electron poor carbon in position 2 of the pyridine ring lowering the energy of the GS and overall rising the barrier (see CH/π interaction Figure 1.5.4 E).

As expected from the hypothesis of limiting structure in Figure 4.1.6, when the X= Br and the X=Cl derivatives were synthesized by Suzuki-Miyaura reaction from 2-pyridine boronic acid or 2-bromopyridine with the respective 2-bromobenzyl halides or [2-(halo-methyl)phenyl]boronic acid, they yielded only the cyclized product **B** 6H-pyrido[2,1-*a*]isoindol-5-inium halides.

Table 4.1.2 Experimental and calculated rotational barriers for compounds **6-18**. Calculations at the CCSD(T)/6-31+G(d)// ω B97XD/6-31G(d) level of theory (energies in kcal/mol). [Reprinted (adapted) with permission from *Org. Lett.* 17, 2015, 2740-2743. Copyright (2015) American Chemical Society].

Compound	R ¹	R ²	X	Experimental barrier	Calculated barrier	ΔE planar-skewed ^a
6	Me	Me	Me	13.1	13.1	2.3
7	Me	Me	NMe ₂	12.8	14.7	0.0
8	Me	Me	OMe	11.1	12.4	-1.4
9	Me	H	OMe	10.9	12.2	-1.4
10	Me	H	F	8.8	10.5	-3.4
11	Et	Et	H	13.7	-	-
12	Et	Et	Me	14.4	-	-
13	Et	Et	NMe ₂	14.7	-	-
14	Et	Et	OMe	12.6	-	-
15	-	-	Me	15.9	18.9	2.1
16	-	-	NMe ₂	15.5	18.8	3.1
17	-	-	OMe	15.1	17.7	2.4
18	-	-	F	15.1	17.9	1.5

^a a positive value indicates a favoured skewed transition state.

Despite all these confirmations, another proof of the presence of a long-range interaction were provided by the analogous biphenyls **15-18** easily synthesized by Suzuki-Miyaura reaction. In this series, the lone pair of the pyridine was simulated by an ortho methoxy group, however both the experimental and calculated rotational barrier proved to be almost independent by the nature of the X substituent, and the *in silico* calculation showed only a skewed TS180 geometry for the TS, proving that the planar disposition is a proper feature of the long-range interaction determined by the presence of the lone pair of the pyridine. This work at first glance has a really limited scope, but if one thinks how the weak interactions, as the H-bond, π - π and halogen-halogen interactions, are fundamental for the construction of an ordered supramolecular structure and scaffold;¹¹ the discovery of any new intra and inter molecular interaction, as this long-range interaction, can open new strategies and technique to impose order to a vast number of molecules.

4.2 New azo-decorated N-pyrrolidinylthiazoles: synthesis, properties and an unexpected remote substituent effect transmission.¹²

Following the same consideration used to explore the long-range interaction in phenyl-pyridine system (Paragraph 4.1) a study on a new series N-pyrrolidinylthiazole was performed.

This study was performed as a following project of the work on stable Wheland-Meisenheimer intermediate¹³ changing the electrophile from 4,6-dinitrobenzofuroxan **DNBF** to a diazonium salt **21a-g** and using as nucleophile both bis (**19**) or mono (**20**) substituted pyrrolidyl-thiazole in position 4 and 2 (Figure 4.2.1).

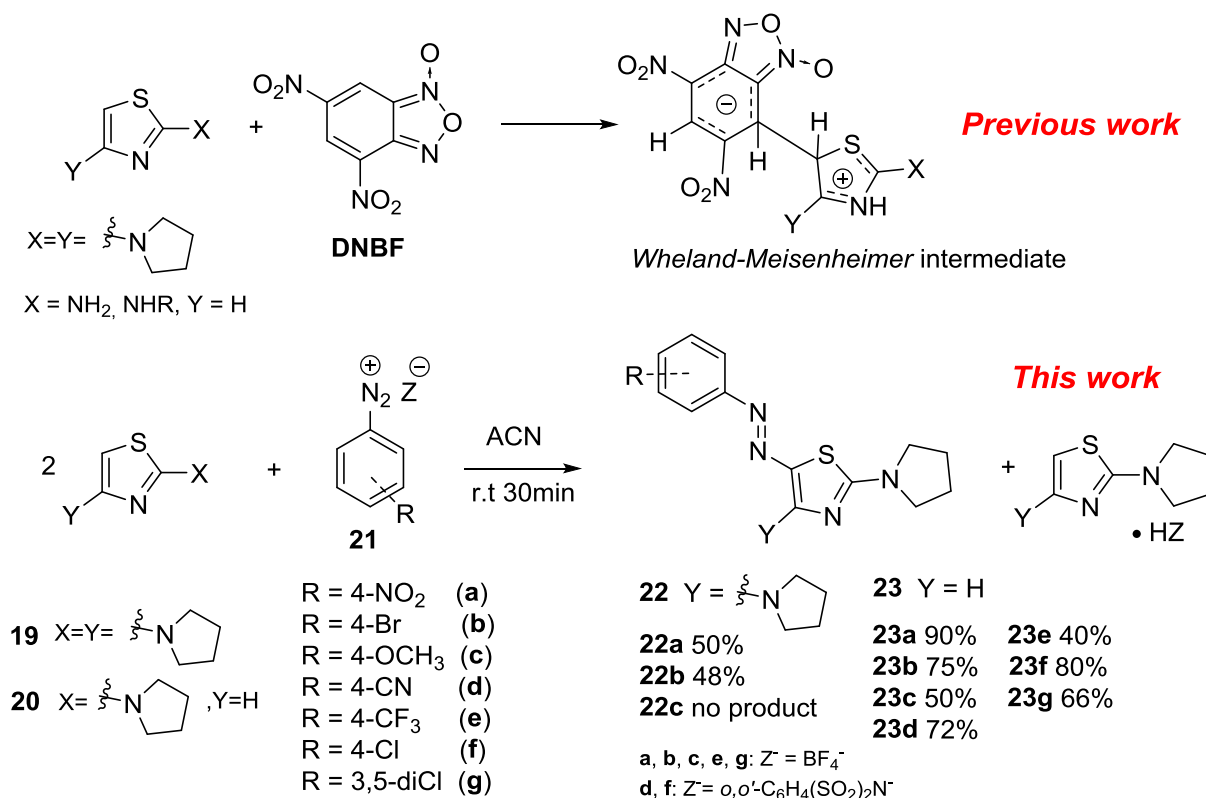


Figure 4.2.1 Top: previous work on the isolation of Wheland-Meisenheimer intermediate. Bottom: current work on reaction between diazonium salt and thiazole and synthesis of product **22a-b** and **23a-g**. [Reprinted (adapted) with permission from *Org. Biomol. Chem.*, **2016**, *14*, 7061. Copyright (2016) Royal Society of Chemistry].

The exceptional reactivity of the **19** made impossible to isolate or even to detect the Wheland intermediate **A** deriving from the attack of the nucleophile position 5 of **19** to the diazonium salt **21** (Figure 4.2.2). Instead the formation of a protonated form of the thiazole **19H** was detected that immediately after the formation of the desired intermediate **A** helps to rearomatize the thiazole ring removing the proton and leading to the formation of products **22a-c**. This reactivity of **19** is mainly due to its ability to delocalize a positive charge on the two free lone pair of the pyrrolidyl rings. The compound **20**, on the other hand, bearing only one pyrrolidyl ring can stabilize the Wheland intermediate without helping in the rearomatization as instead happen with **19**.

As expected, the reaction with **20** is slower and with less side products leading almost exclusively to the corresponding products **23a-g**. Despite this, it was only possible to detect in NMR experiment a resonance between **20** and its protonate form while the positive adduct **B** remains elusive (Figure 4.2.2).

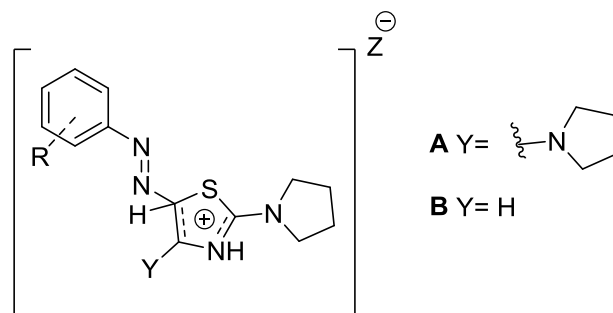


Figure 4.2.2 Positive Wheland intermediate of the reaction between the thiazole and the diazo-aryl salt.

A close inspection of the NMR spectra of **23a-c** at +27 °C revealed that the methylene signal in the α position of the pyrrolidine ring broadens at different extent in function of the substituent on the phenyl ring. Since the *para* position is the only difference between **23a-c**, the broadening of the methylene signal must be connected to an electronic effect of this group, that enhance the double bond nature of the C-N bond slowing down the rotation around the C-N axis and therefore differentiate at the NMR the two alpha positions of the pyrrolidine ring (analogously to the DMF, see Paragraph 2.1). This partial double bond nature is further proved by X-Ray diffraction on **23a** where the C₁-N₄ bond (1.330 Å) is shorter than a usual C₁₀-N₄ (1.475 Å) highlighting a partial double bond nature of this bond also in solid state (Figure 4.2.3).

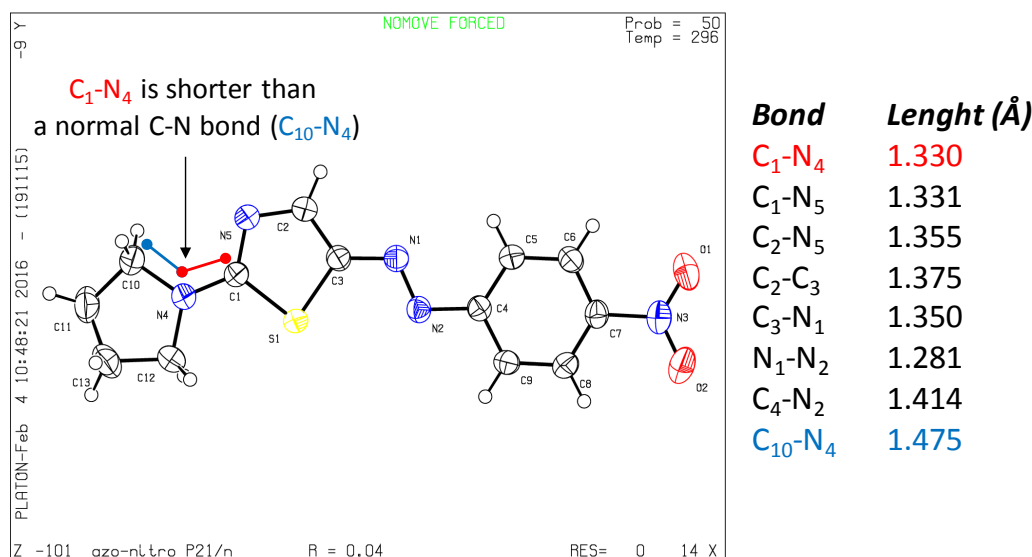


Figure 4.2.3 X-ray structure of **23a** and the relative bond length (Å). The C₁-N₄ bond is shorter than a normal single C-N bond. [Reprinted (adapted) with permission from *Org. Biomol. Chem.*, **2016**, *14*, 7061. Copyright (2016) Royal Society of Chemistry].

Two hypotheses were taken in consideration: 1) a positive mesomeric effect (+M) where the lone pair of the para substituent is delocalized all the way through the C1-N4; or 2) a negative mesomeric effect (-M), where an electron poor substituent recall the lone pair on the pyrrolidine nitrogen forming a resonance form with a partial double bond (Figure 4.2.4).

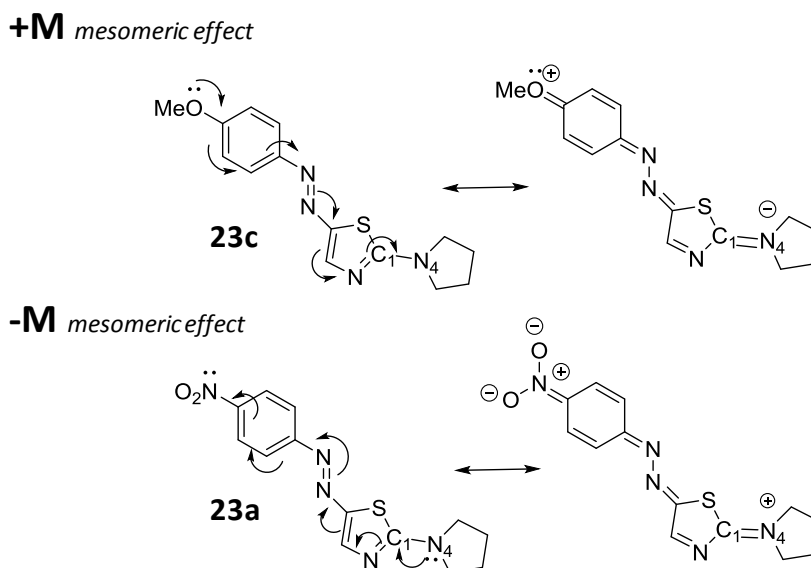


Figure 4.2.4 Mesomeric effects of **23c** (+M) and **23a** (-M) ending up as partial double bond on the C₁-N₄ bond

Although the +M hypothesis imply an improbable negative tetra-coordinate nitrogen, the mechanism needed to be verified. Thus, D-NMR analysis of **23a** and **23c** were performed and the rotational barrier around the C₁-N₄ was derived by line-shape simulation assuming a kinetic equation of the reversible first order (Figure 4.2.5). These analyses revealed that the **23a** has a higher rotational barrier with respect to **23c** (14.2 kcal/mol and 12.9 kcal/mol respectively), indicating, as expected, a stronger double bond formation with an electron withdrawing group rather than with an electron donating and verifying the negative mesomeric (-M) hypothesis.

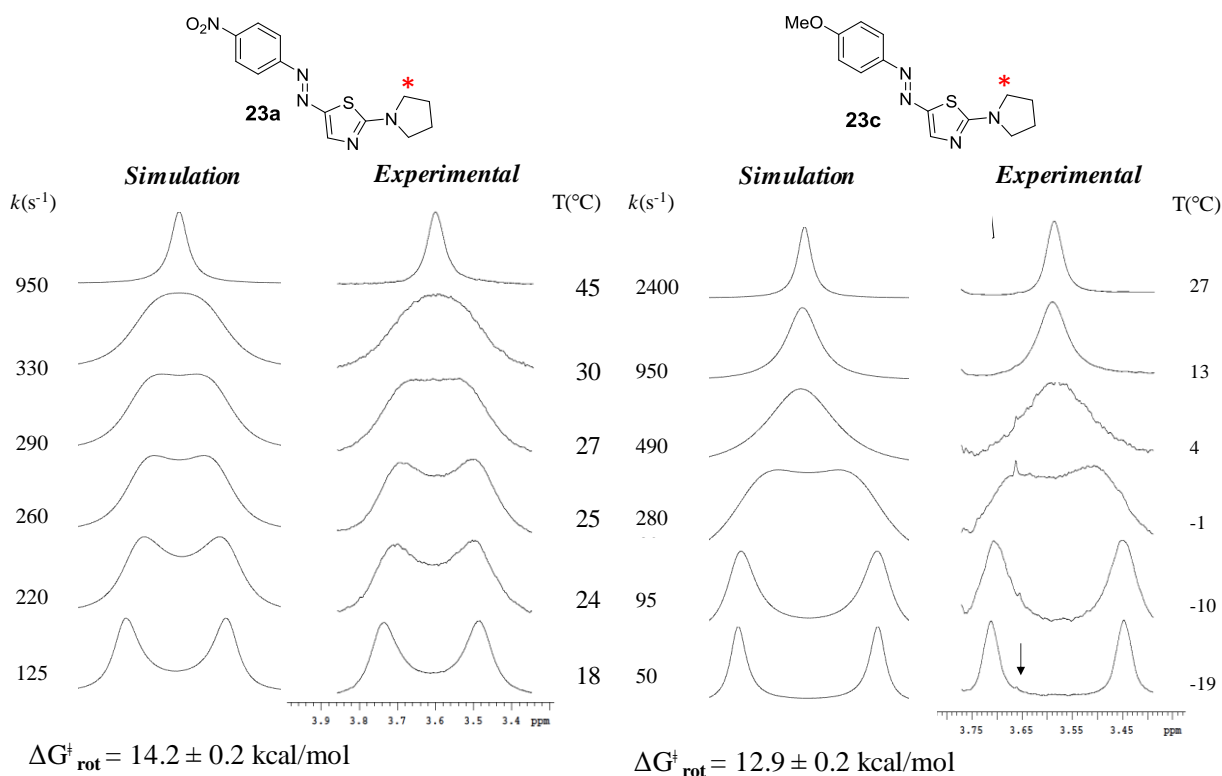
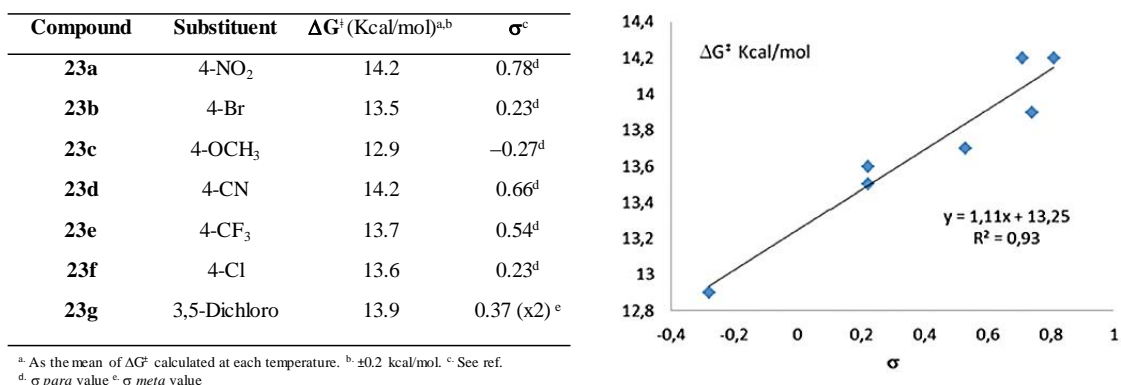


Figure 4.2.5 D-NMR spectra recorded in CDCl_3 at 600 MHz of **23a** (left) and **23c** (right) and their respective line shape simulated spectra and rotational barrier. The arrow in **23c** experimental spectrum indicates an impurity. [Reprinted (adapted) with permission from *Org. Biomol. Chem.*, **2016**, *14*, 7061. Copyright (2016) Royal Society of Chemistry].

To further prove the electronic effect of the *para* substituent on the $\text{C}_1\text{-N}_4$ bond, the D-NMR and line shape simulation were performed on all the compound synthesized (**23a-g**, Figure 4.2.5 and Paragraph 7.2.1). The rotational barrier derived are reported in Figure 4.2.6, in which is possible to observe that the $\Delta G^\ddagger_{\text{rot}}$ increases on going from less to more electron-withdrawing substituents. Moreover, in Figure 4.2.6 are also reported the σ Hammett parameter of each substituent,¹⁴ they were found to be linearly correlated to the energy involved in the rotation of the $\text{C}_1\text{-N}_4$ bond, further relating the mesomeric nature of the substituent on the azo-moiety ring to the double bond entity of the thiazole-pyrrolidinyl bond.



^a As the mean of ΔG^\ddagger calculated at each temperature. ^b ± 0.2 kcal/mol. ^c See ref. ^d σ *para* value ^e σ *meta* value

Figure 4.2.6 Left: experimental energy barrier for the rotation of the pyrrolidinyl ring and the respective Hammett constant for each substituent. Right: Rotational barrier of **23a-g** correlated to the σ Hammett parameter. [Reprinted (adapted) with permission from *Org. Biomol. Chem.*, **2016**, *14*, 7061. Copyright (2016) Royal Society of Chemistry].

4.3 Computational and D-NMR Analysis of the Conformational Isomers and Stereodynamics of Secondary 2,2'-Bisanilides

The disposition in space of functional groups in an organic framework is directly connected to its reactivity and physical properties. Organic amides are a particular functional group that can undergo a *E/Z* isomerism, due to the partial double bond nature of the C-N bond and hindered rotation around the carbonyl-carbon axis. On this regard, stereodynamic behavior of this group have been detected and investigated in tertiary amide moiety showing restricted rotation about the aryl-carbonyl and carbonyl-nitrogen bonds and their correlation (see Figure 1.5.5).¹⁵

Anilides are a particular class of amide derived from organic oxoacid by replacing an OH group by the NPh group or derivative formed by ring substitution.¹⁶ In other words, in the anilides the nitrogen is directly linked to an aryl group and therefore the stereodynamic process involved can occur along the C_{aryl}-N and the N-C_{carbonyl} axes (atropisomerization and *E/Z* isomerization, respectively, see Figure 1.5.5).¹⁷

The interest in the anilides goes beyond their particular stereodynamic, anilides, in fact, finds application: 1) as analgesic, especially in the paracetamol family (propacetamol, acetanilide, phenacetin); 2) as auxiliary groups in asymmetric synthesis reported by Curran and Clayden, where the anilides moiety aids to retain or transfer axial chirality in organic radicals passing by a meta-stable C-N atropisomer (Figure 4.3.1).^{17,18}

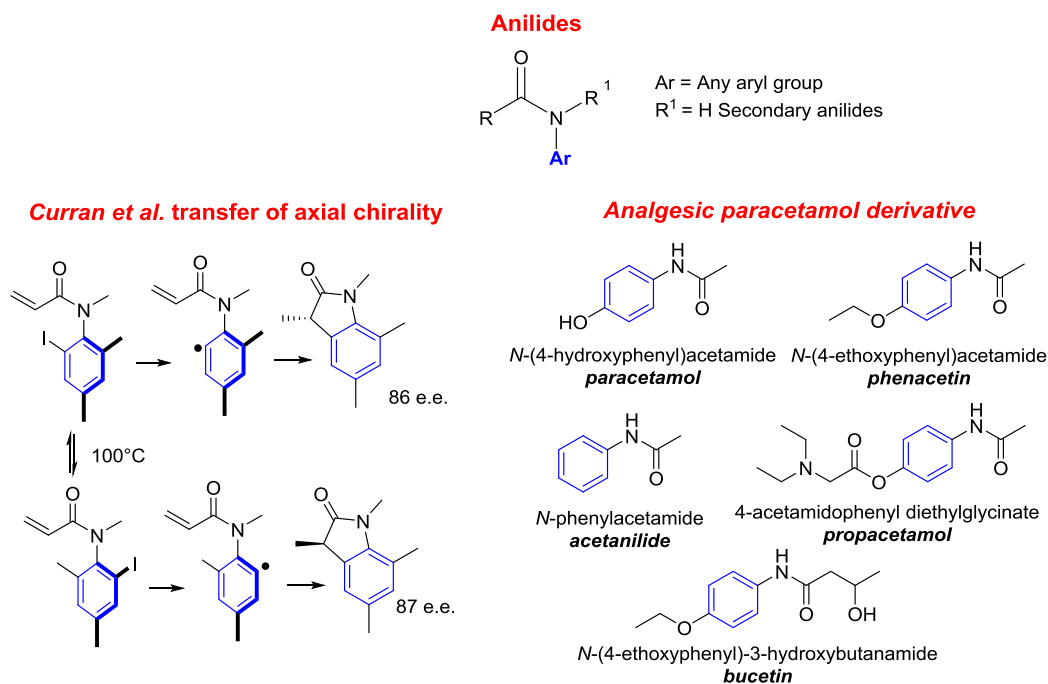


Figure 4.3.1 Anilides, structure and application in asymmetric synthesis and drug derivatives.

Although the wide application of this structural motif, its stereodynamic remains not exhaustively studied.¹⁹

Both for this reason, and following a previous work on 2,2'-binaphthalene-1,1'-diol (**24**),²⁰ where the dynamic stereochemistry of the hindered rotation of the two ester-aryl moieties and the naphthyl-naphthyl bond was reported, the stereodynamic of 2,2'-bisanilides analogous of **24** (**25-33**) were investigated (Figure 4.3.2).²¹

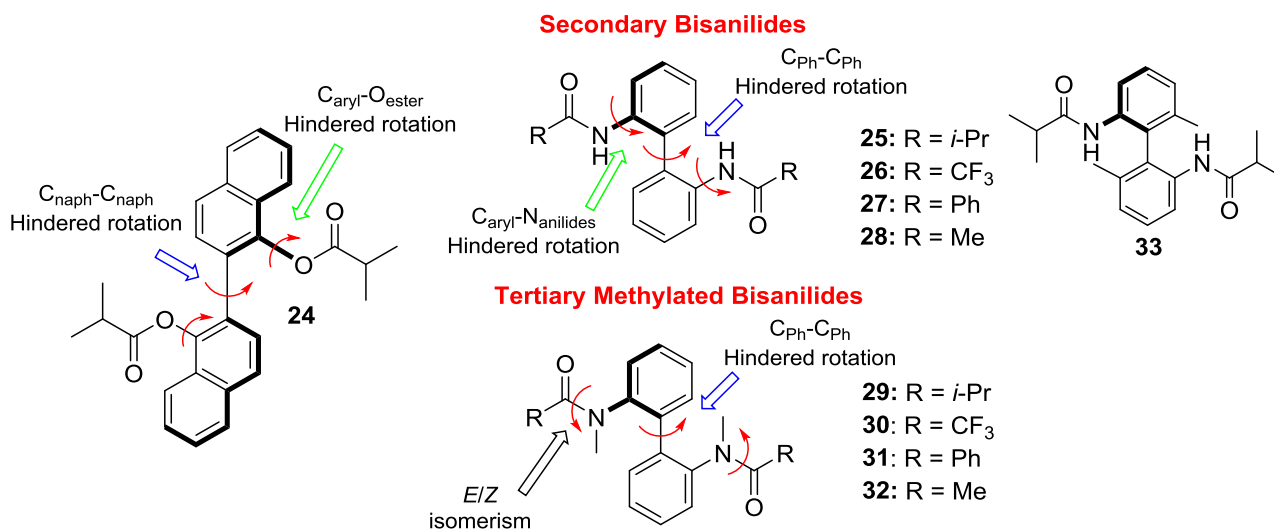


Figure 4.3.2 Structure of 2,2'-binaphthalene-1,1'-diol diisobutyrate **24**, and structural analogues bisanilides **25-33** investigated.

The ¹H-NMR of **25** was recorded (in a mixture 5/1 v/v of CDFCl₃/CDF₂Cl) from -47 °C down to -139 °C. At first, it showed for the diastereotopic methyl of isopropyl group an anisochronous doublet related to chiral environment associated to the slow aryl-aryl rotation in the NMR timescale. Then, once the temperature was further decreased (-128 °C), instead of detecting the expected conformational diastereoisomer corresponding to the $C_{\text{aryl}}-N$ bond hindered rotation a new series of peak emerged directly from the baseline, indicating the formation of dynamic new species in solution. A detailed inspection of the aliphatic region of the spectra revealed the presence of two species with 80:20 ratio, in which the major shows four methyls and 2 CH while the minor displays only two CH₃ and one methine. This can be ascribed to the simultaneous presence of two species: a symmetric one (C₂ symmetry) in which the methyl and CH of each phenyl ring have the same magnetic environment and an asymmetric one (C₁ symmetry) in which each methyl and methine have a different chemical shift (Figure 4.3.3). Considering an identical rate constant for the interconversion of one signal of the symmetric species into two signals of the asymmetric one and *vice versa*, a line shape simulation was performed in the range between -97 °C to -107 °C. An energy of activation related to the exchange between the two conformations were calculated as large as 8.6 ± 0.2 kcal/mol considering a reversible first order kinetics (Figure 4.3.4 left).

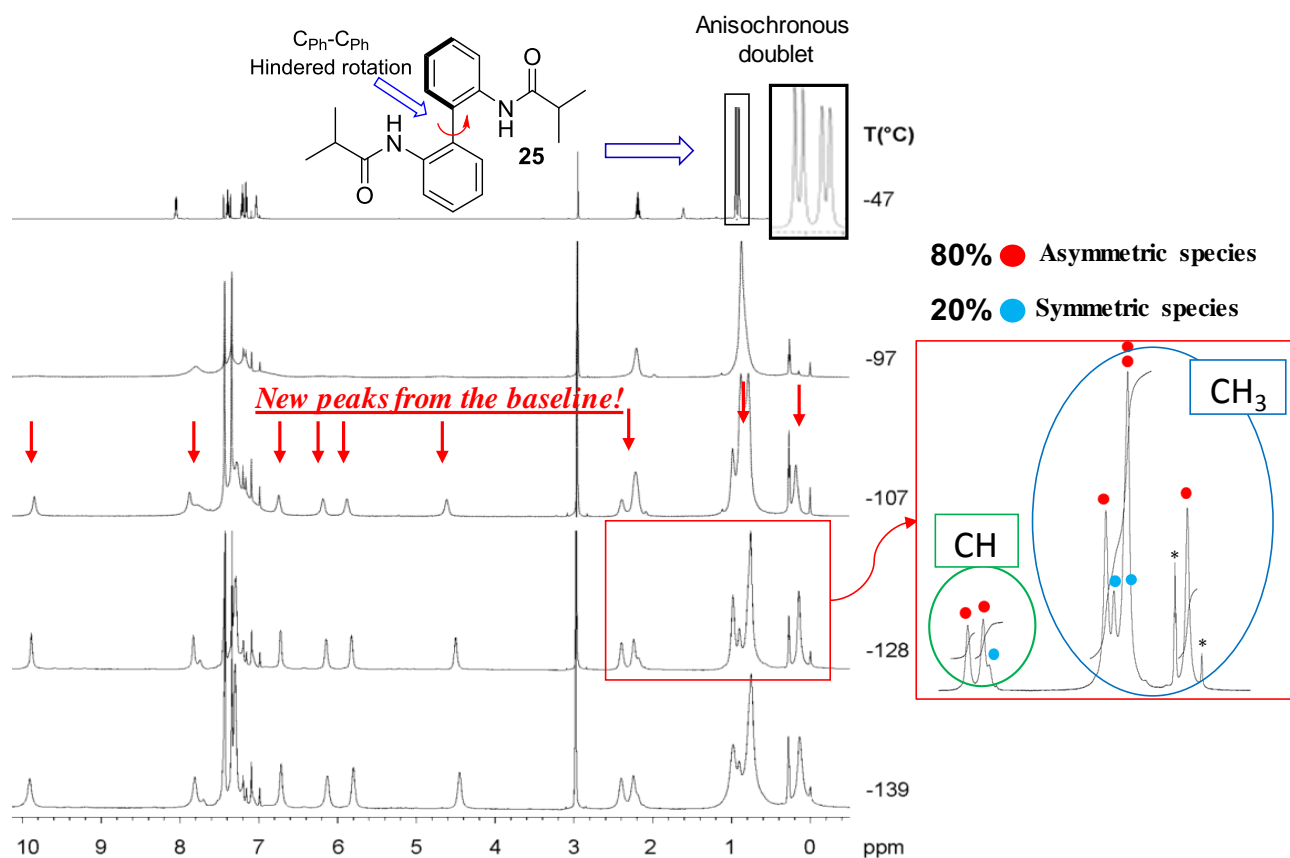


Figure 4.3.3 Temperature dependence of the ^1H NMR spectra of **25** (600 MHz in $\text{CDFCl}_2/\text{CDF}_2\text{Cl}$ 5/1 v/v). [Reprinted (adapted) with permission from *J. Org. Chem.* **2016**, *81*, 89. Copyright (2016) American Chemical Society].

However, the change on lowering the temperature of the ratio between the two conformations is related to a ΔH° of -4.1 kcal/mol and a ΔS° of -25 cal/mol K for the conversion of the C_2 to the C_1 conformations (Figure 4.3.4 right).

The deuterated Freon solvent is useful to reach extremely low temperature with NMR spectroscopy; however, it lacks polarity. To study the response of **25** at low temperature in a much polar solvent, the D-NMR was performed again in deuterated Freon in presence of about 3 equivalents of CD_3OD . The NMR spectra recorded (Figure 7.3.1) show similar results, however the peaks emerged from the baseline at lower temperature with respect to the sample without CD_3OD . This behaviour indicates an interference of polar solvent during the generation of the dynamic species.

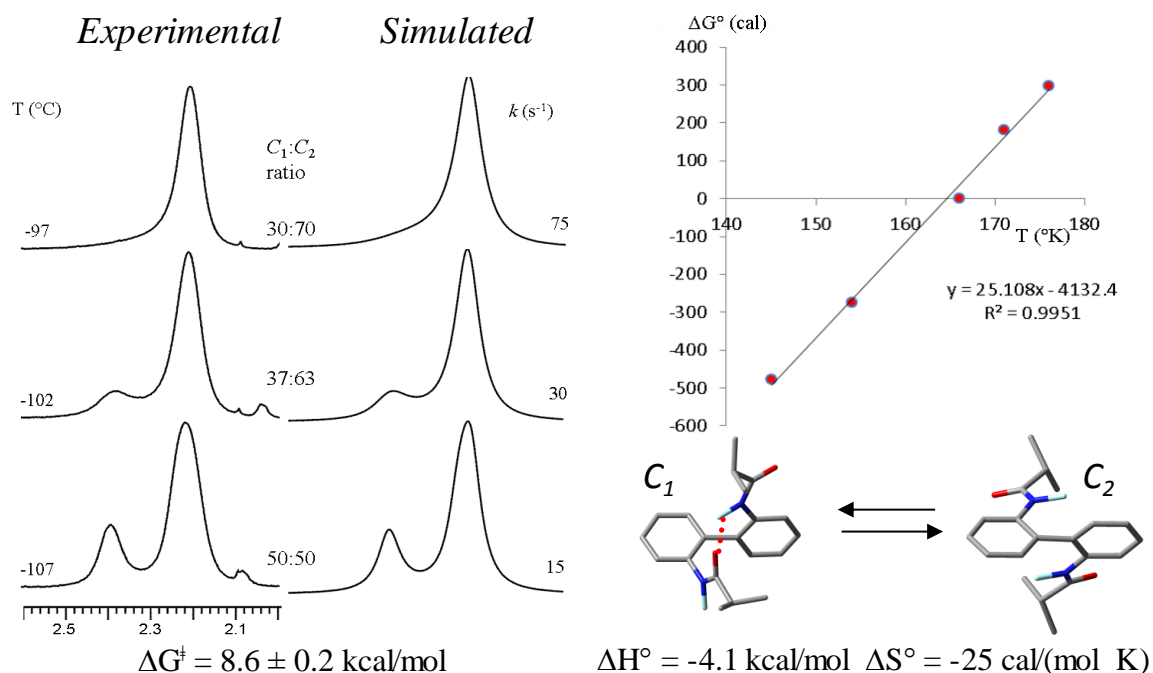


Figure 4.3.4 Line shape simulation and thermodynamic data for the exchange between C_1 and C_2 conformers of the compound **25**. [Reprinted (adapted) with permission from *J. Org. Chem.* **2016**, *81*, 89. Copyright (2016) American Chemical Society].

In order to see if this behaviour can be extended to other derivatives of the secondary 2-2' bisanilides, the products **26-28** were synthesized and analysed. As expected, on lowering the temperature also **26-28** display a new series of peaks emerging from the baseline, although the intensity and the temperature of formation of the new species are different (Figure 4.3.10).

X-ray diffraction on single crystal of **25** and **28** obtained by slow evaporation of a CHCl_3 and acetonitrile solutions respectively, revealed that in solid-state the amides do not lay in the plane of the phenyl ring in order to form an *intramolecular* hydrogen bond between the two amide moieties with a global C_1 symmetry (Figure 4.3.5 **A**). On the other hand, X-ray analysis on single crystals of **27** (from CHCl_3) showed a completely different conformation, in which the molecule can arrange in two different C_2 conformers that dispose the amide moiety with dihedral angle $\text{H-N-C}_2\text{-C}_1$ of 31.4° and -121.7° respectively in order to form an *intermolecular* hydrogen bond connecting the CO with the NH of the nearest molecule (Figure 4.3.5 **B**). The dissimilar X-ray structures between the different derivatives highlight that the solid-state conformations are separated by small energy differences and both intramolecular and intermolecular interaction can be obtained.

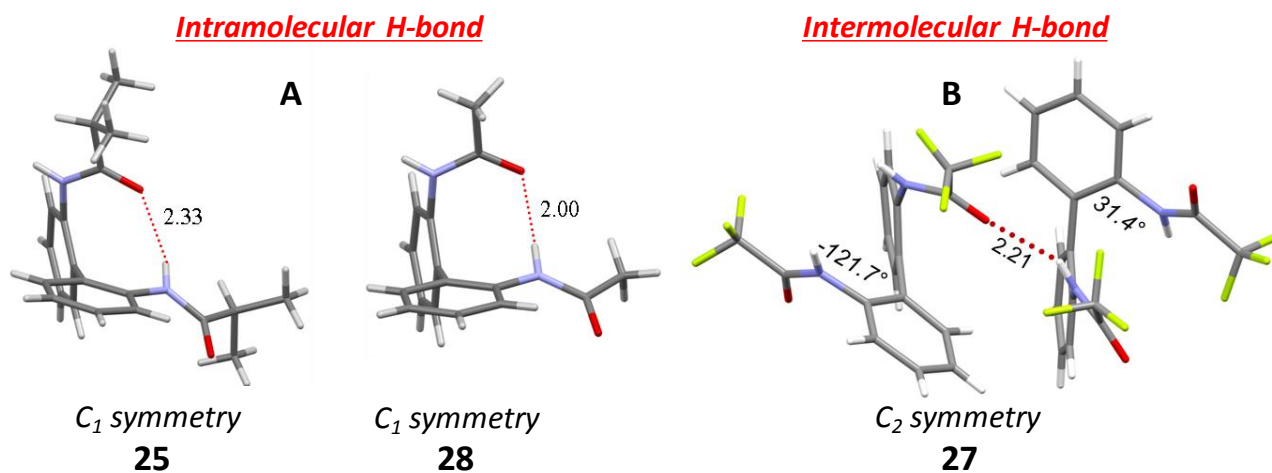


Figure 4.3.5 X-ray determined structures of A) **25** and **28** displaying an intramolecular H-bond B) **27** displaying an intermolecular H-bond between the carbonyl and the NH of the neighbour molecule. [Reprinted (adapted) with permission from *J. Org. Chem.* **2016**, *81*, 89. Copyright (2016) American Chemical Society].

Still, the nature of the new peaks arising at low temperature in the ¹H-NMR of **25-28** remains unknown. These X-ray structures, showing an intra- or inter-molecular H-bond suggested the existence of such interaction also in solution, this hypothesis can explain the NMR pattern showed at low temperature in two different scenarios (Figure 4.3.6):

1. **The formation of an intramolecular H-bond** with *C*₁ geometry similar to the one found in solid-state for **25** and **28** that breaks the molecular symmetry generating an asymmetric species responsible for the four methyl and two methine peaks. In this perspective, the conformer with *C*₁ geometry would be in equilibrium with a *C*₂ symmetric species responsible for the two methyl and one methine peaks.
2. **The formation of an intermolecular H-bond** in which the formation of the dimer (with a similar geometry of the one found for **27** in solid state) would explain the main set of peaks (asymmetric one) found at low temperature, while the co-presence of the monomer would be attributed to the minor symmetric species.

In principle, both scenarios cannot be ruled out merely on the basis of these information, therefore a set of more accurate experimental and theoretical analysis were designed.

Theoretical investigation of the **intramolecular H-bond** scenario led to the identification of two conformations: one with a *C*₂ symmetry where the amide lies in the plane of the phenyl ring (**C₂-NH-*in***) without any hydrogen bonding and another with a *C*₁ symmetry similar to the ones observed in the X-ray of **25** and **28**, where the amide is skewed with respect to the phenyl ring and undergoes an intramolecular H-bond with the amide on the other aryl system (**C₁-H-bond**). However, the computational analysis performed with different functionals and the basis set 6-31G(d) led to different results (Table 4.3.1). In fact, while B3LYP suggested the **C₂-NH-*in*** as the most stable conformation,

the M06-2X functional led to an almost equally populated situation between **C₂-NH-in** and **C₁-H-bond**, and when the ω B97XD functional was used the **C₁-H-bond** was no longer populated (it was no longer an energy minimum). Without producing any valuable result in the intramolecular H-bond scenario, the theoretical investigations were further focused on the *intermolecular H-bond* hypothesis and therefore to the formation of dimers.

Due to the presence of the hindered rotation about the C_{Ph}-C_{Ph} axis is necessary to take into consideration two type of dimers: a *homodimer*, where are present two bisanilides with the same axial chirality, or a *heterodimer*, where are employed the two bisanilides with opposite chirality. While with a homodimer the conceivable geometry would lead to conformations with a C₂ or a C₁ global symmetry, in the case of the heterodimer the accessible symmetry would be C_i and C_s. The DFT investigation of the dimers hypothesis revealed two stable conformations for both cases with similar energy. B3LYP and M06-2X was explored while ω B97XD was ruled out due to its incapability to find the intramolecular interaction in the intramolecular scenario.

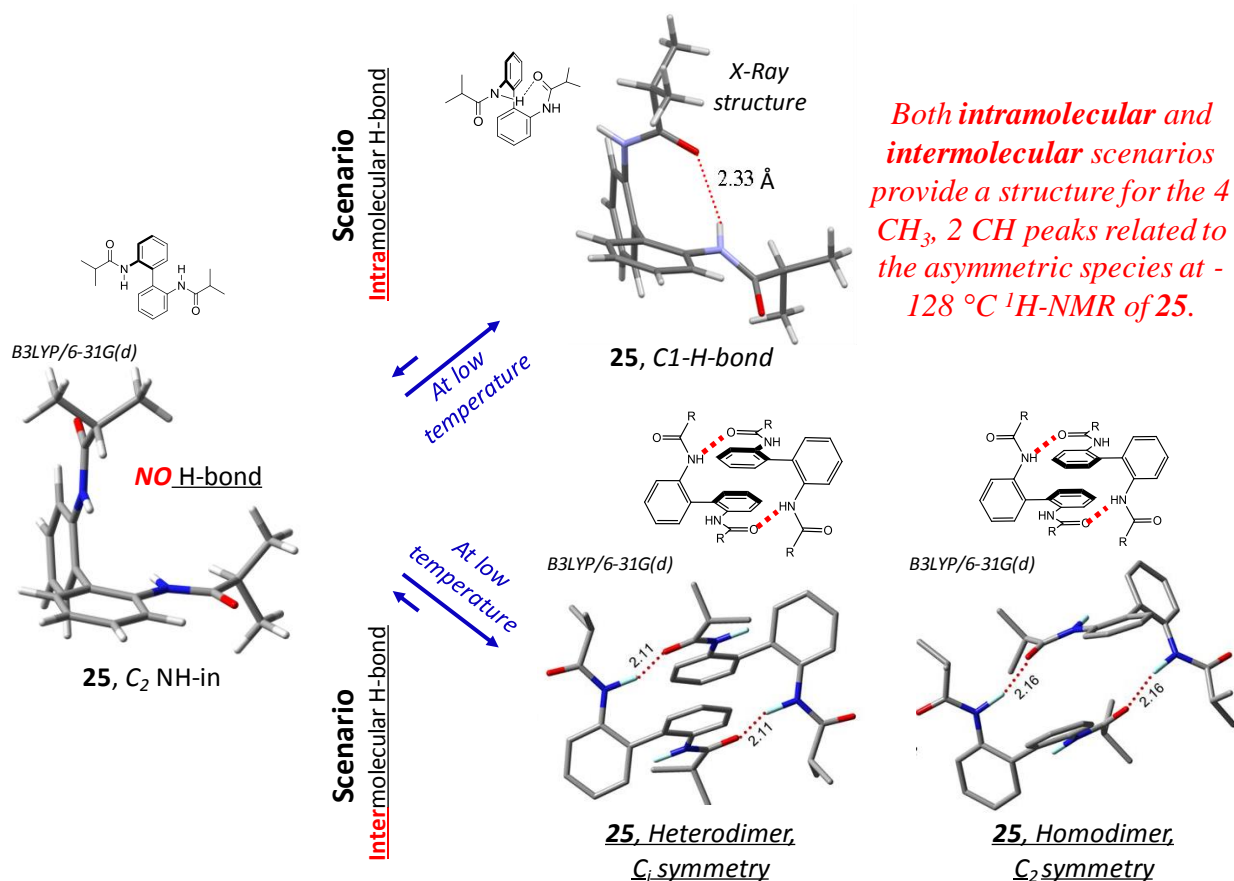


Figure 4.3.6 Structures related to the intramolecular H-bond and intermolecular H-bond scenarios of **25**, derived from X-ray or from DFT calculations.

The heterodimer (C_i symmetry) results more stable respect to the homodimer (C₂ symmetry) with both functional: by 0.5 kcal/mol and by 2.7 kcal/mol at B3LYP/6-31G(d) and M06-2X/6-31G(d) level of theory, respectively. Both structures resulted in agreement with the ¹H-NMR analysis at -128 °C

displaying two different isopropyl groups for each molecule that lead to four methyl peaks once considered the intrinsic diastereotopicity of this moiety. The calculated gain in energy obtained from the formation of a dimer²² is 6.8 kcal/mol for the heterodimer and 5.0 kcal/mol for the homodimer at B3LYP/6-31G(d) level of theory (21.3 kcal/mol and 18.3 kcal/mol with M06-2X respectively). Expanding these studies also to **26-28** was noted a not clear trend for the stability of homo and heterodimers and a huge difference between the dimerization energies calculated with the two functionals (Table 4.3.1) that finally did not allow to a consistent explanation of this scenario.

Table 4.3.1 .TOP: Computational data for the C₂-NH-*in* and C₁-H-bond conformations of **25**. BOTTOM: Dimers energies and dimerization energies for **25-28**. Dimerization energies E_{Dim} were calculated with counterpoise correction. [Reprinted (adapted) with permission from *J. Org. Chem.* **2016**, *81*, 89. Copyright (2016) American Chemical Society].

Intramolecular H-bond – C₂-NH-*in* and C₁-H-bond DFT energies of **25**

Conformation	Method	Energy (a.u.)	ΔE (kcal/mol)
C ₂ -NH- <i>in</i>	B3LYP/6-31G(d)	-1036.596083	0.00
C ₁ -H-bond	B3LYP/6-31G(d)	-1036.591816	2.68
C ₂ -NH- <i>in</i>	M06-2X/6-31G(d)	-1036.185695	0.00
C ₁ -H-bond	M06-2X/6-31G(d)	-1036.185473	0.13
C ₂ -NH- <i>in</i>	ωB97XD/6-31G(d)	-1036.281224	0.08
C ₁ -H-bond	ωB97XD/6-31G(d)	-1036.281361 ^a	0.00

Intermolecular H-bond – Dimers DFT energies (E) and Energy gain for the Dimerization (E_{dim.}) In kcal/mol of **25-28**.

Compounds	B3LYP/6-31G(d)				M06-2X/6-31G(d)			
	<i>Heterodimer</i>		<i>Homodimer</i>		<i>Heterodimer</i>		<i>Homodimer</i>	
	E	E _{Dim.}	E	E _{Dim.}	E	E _{Dim.}	E	E _{Dim.}
25	0.00	-6.8	0.50	-5.0	0.00	-21.3	2.67	-18.3
26	0.75	-5.5	0.00	-0.6	0.54	-17.2	0.00	-13.1
27	5.55	-4.3	0.00	-1.6	0.31	-24.0	0.00	-17.7
28	0.00	-8.6	2.03	-6.4	0.00	-18.0	1.16	-17.8

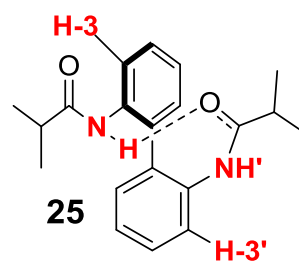
^a This geometry degenerates to the C₂-NH-*in*.

Since in both scenario the computed energy differences were not conclusive in the indication of a preferred system, the NMR chemical shifts were considered. The NH and the H3 moieties of each phenyl ring can display different chemical shifts once an H-bond process is occurring. In fact, the low temperature signals at 9.9 ppm and 4.5 ppm could be attributed to the H-bond (NH) and free NH (NH) respectively that once the temperature is raised collapse at the average chemical shift of these two peaks (7.0 ppm while the experimental is around 7.2 ppm). Although is not possible to have an experimental support for these consideration, it is worth to explore *in silico* this possibility.

Calculations were performed both on the dimer and on the monomers (**C₂-NH-in** and **C₁-H-bond**) at GIAO-B3LYP/6-311++G-(2d,p)//B3LYP/6-31G(d) level of theory. The results showed different chemical shifts for **C₁-H-bond** and the dimers of the NHs or the H-3s depending if they are involved in the H-bond or not (Table 4.3.2). In particular **C₁-H-bond** displayed the higher NHs split as can be supposed due to the more shielded arrangement of the NH not involved in the H-bond in this conformation. Moreover, the H-3 in the dimers is found in an environment where the carbonyls almost lay in the plane of aryl therefore the formation of the dimer should move the H-3 signal at higher ppm. In other words, in the dimers the carbonyl does not change its orientation remaining near the H-3, instead in **C₁-H-bond** the carbonyl is moved away from the H-3', leaving the H-3' in a much electron rich environment as the calculation suggest (upfield shift of H-3'). The experimental D-NMR showed an upfield of the H-3 on lowering the temperature indicating a behaviour more consistent with the intramolecular H-bond formation.

Table 4.3.2 Calculated Chemical shift at GIAO-B3LYP/6-311++G-(2d,p)//B3LYP/6-31G(d) for 25

Conf. 25	NH	NH'	H-3	H-3'
C₁-H-bond	8.1	6.5	9.0	7.4
C₂-NH-in	6.7	6.7	9.5	9.5
Heterodimer	8.7	7.5	9.5	9.0
Homodimer	8.2	7.5	9.0	8.5



However, this indication is far from be conclusive. To collect more experimental evidence the infrared spectrum of **25** was recorded (Figure 4.3.7). Despite it was recorded at room temperature, the faster time scale of IR vs NMR might be helpful in detecting the split in NH or C=O region due to the two conformations observed also in the NMR. Interestingly in the NH region was observed two bands, one sharp at 3415 cm⁻¹ and one broad at 3340 cm⁻¹ that can be connected to an N-H that is in equilibrium between the free form and the H-bond respectively.

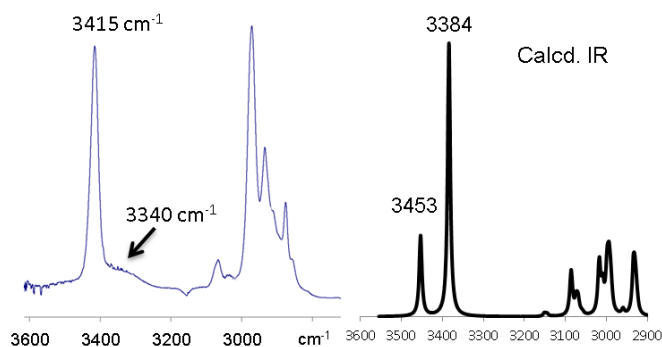


Figure 4.3.7 IR region of the N-H stretching region of the spectrum and calculated IR spectrum of **25** for the same spectral region at the B3LYP/6-31G(d) level. [Reprinted (adapted) with permission from *J. Org. Chem.* **2016**, *81*, 89. Copyright (2016) American Chemical Society].

Although this region can be strongly affected by the presence of the water the calculated IR spectrum at B3LYP/6-31G(d) level of theory confirms that an NH H-bond interaction generate two bands where the one found at lower frequency is the one involved in an H-bond. Although this experiment confirms that the NH undergoes to an H-bond equilibrium, it was not able to discriminate between the intramolecular and intermolecular H-bond scenario.

The IR spectrum and the evidence collected with the $^1\text{H-NMR}$ at low temperature with three equivalents of CD_3OD , indicate that the conformations rely on the presence of H-bonds, and more specifically a polar solvent seems to interfere with the formation of this interaction whether it comes from a monomer that undergoes to intramolecular H-bond or a dimer formed by intermolecular hydrogen bonding. In order to study this interference a titration with $\text{DMSO-}d_6$ tracked by NMR spectroscopy at room temperature was performed. When aliquot of $\text{DMSO-}d_6$ was added to a solution of **25** in CDCl_3 the NMR spectra shows a large upfield shift (0.4 ppm) for the H-3 and an even more large downfield shift for the NH (1 ppm). All the other signals did not show any significative change of the chemical shift (Figure 4.3.8).

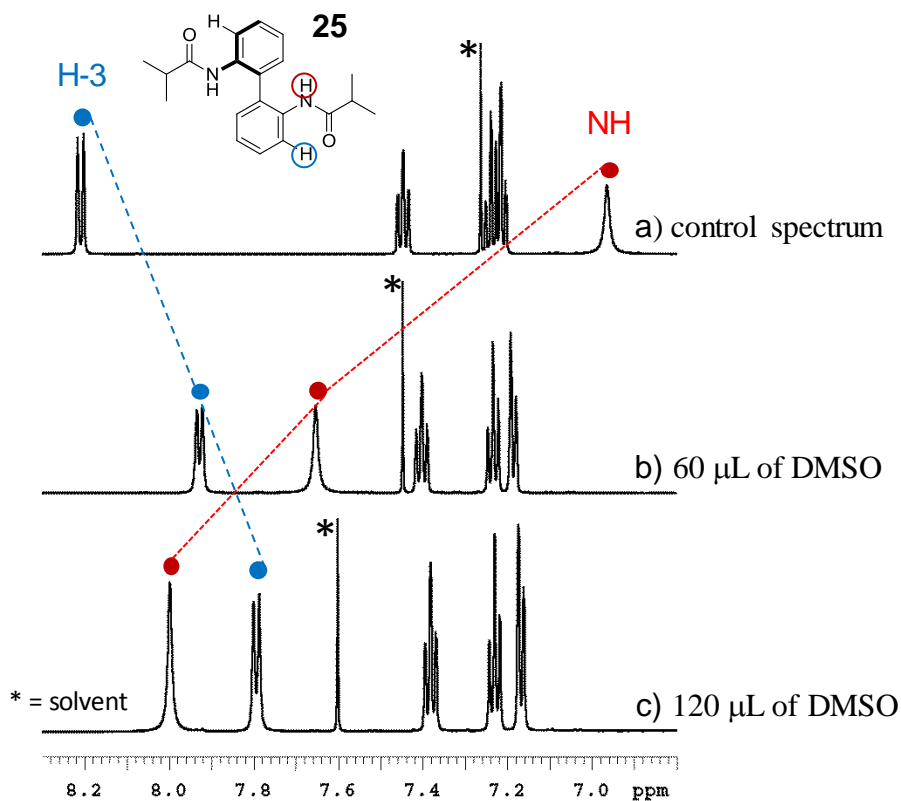


Figure 4.3.8 $\text{DMSO-}d_6$ titration followed by $^1\text{H NMR}$ of bisanilide **25** in CDCl_3 (600 MHz, 25°C). The concentration of **25** is maintained 0.04 M. [Reprinted (adapted) with permission from *J. Org. Chem.* **2016**, *81*, 89. Copyright (2016) American Chemical Society].

A modelling of the system was performed at B3LYP/6-31G(d) level of theory considering the mono and double interaction of one or two DMSO molecule with one or two NH respectively. The energy stabilization deriving from the NH- DMSO interaction was found to be -8.3 kcal/mol and -16.4

kcal/mol for the mono and the double adduct respectively.²³ The theoretical investigation pointed out that the adducts display the geometry of the **C₁-H-bond** conformation that upon solvation move the carbonyl out of the plane. This explain the downfield shift of the H-3 that now found itself far from the C=O with respect to the **C₂-NH-*in*** conformation.

To elucidate the DMSO titration experiments and the relative theoretical model obtained, a solute or bis-solute system was proposed (Figure 4.3.9). In this view at room temperature there is a fast exchange between the **C₂-NH-*in*** stabilized by the amide conjugation and **C₁-H-bond** stabilized by the intramolecular bond leading to a mediated NMR spectra. Once the temperature is decreased the equilibrium rate decreases and the signal of both conformations can be discriminated. The hydrogen acceptor solvent disrupts this equilibrium firstly coordinate one of the two free NH, then, when the amount of polar solvent increases, both the NH ending up forming a bis-solute that completely sequesters the bisanilide from the **C₂-NH-*in*** ↔ **C₁-H-bond** equilibrium.

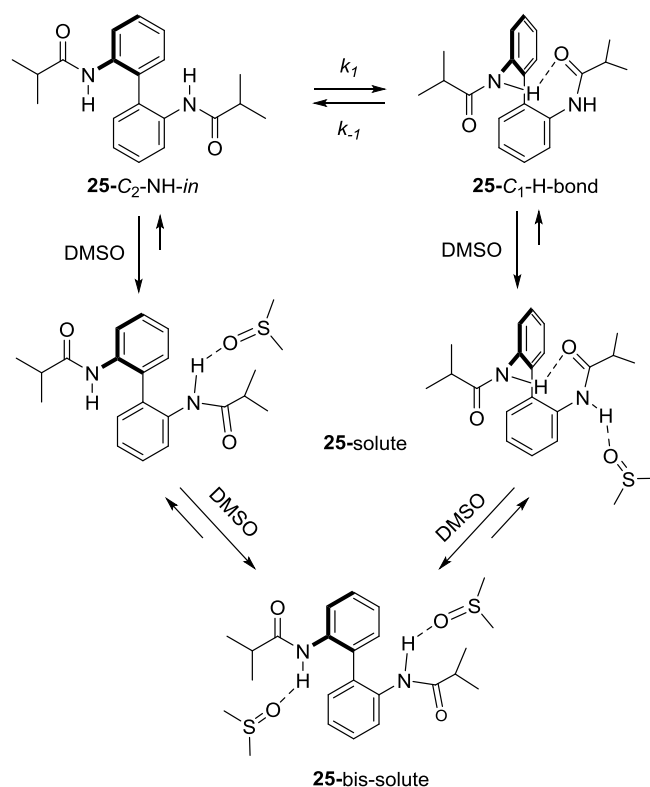


Figure 4.3.9 Model to explain the dynamic interaction of **25** with DMSO in solution. [Reprinted (adapted) with permission from *J. Org. Chem.* **2016**, *81*, 89. Copyright (2016) American Chemical Society].

The interaction with the solvent plays an important role in determining magnitude of the conformational split at the NMR at low temperature. In fact, analysing the behaviour of **25-28** at low temperature is possible to note that the amount of the asymmetric conformer (H-bond conformer) decrease in the series (Figure 4.3.10). In the *intramolecular H-bond* scenario the R substituent is an obstacle to the disrupting solvent coordination of the amide moiety, therefore bulky R substituent protect the amide moiety from the solvent favouring the intramolecular coordination. On the other

hand, in the *intermolecular H-bond* scenario the formation of dimers (and therefore the asymmetric species) is obstructed by R bulky substituent that in this geometry crowds the interdimeric space. In other words, for the dimers there should be an inverse proportion between the bulkiness of R substituent and the amount of asymmetric species found at low temperature. The exactly opposite experimental tendency found in **25-28** (Figure 4.3.10) is a strong evidence that support the intramolecular H-bond scenario.

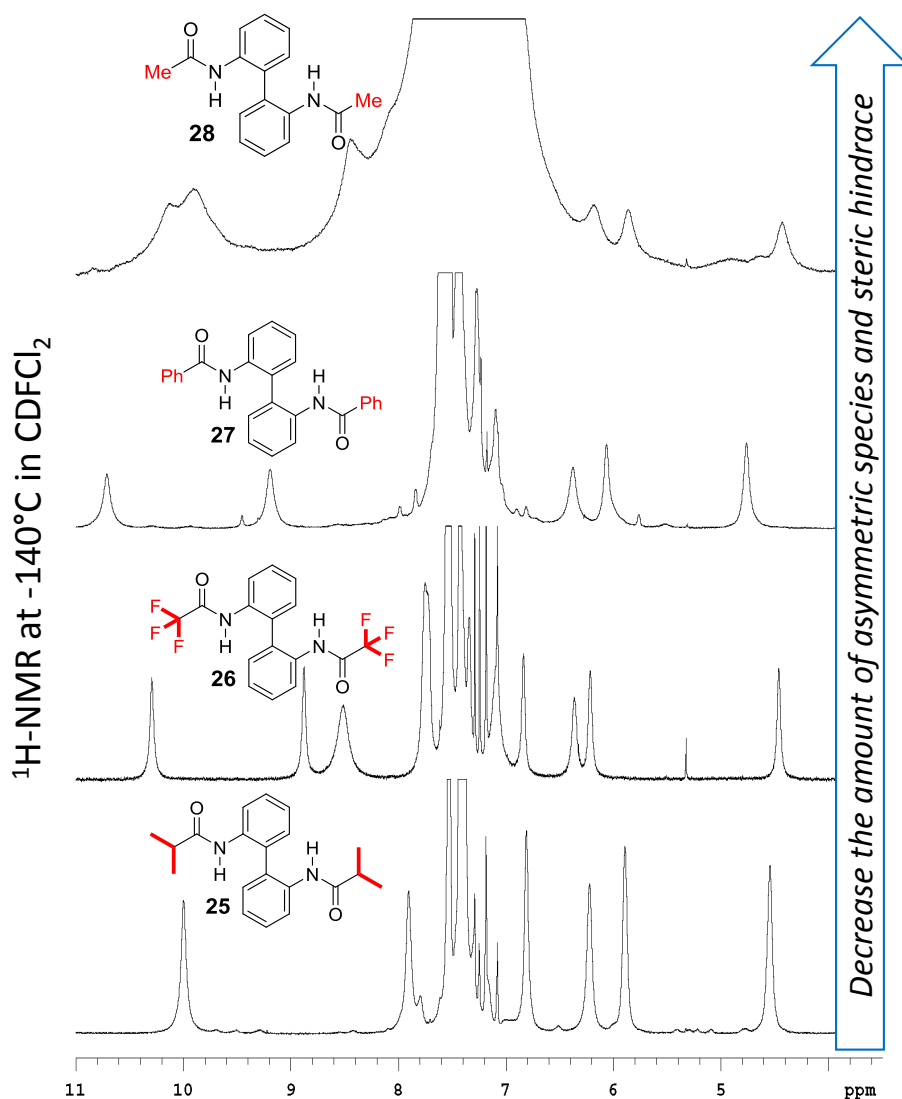


Figure 4.3.10 ^1H NMR spectra of compounds **25-28** acquired at $-140\text{ }^\circ\text{C}$ (600 MHz in $\text{CDCl}_2/\text{CDF}_2\text{Cl}$). [Reprinted (adapted) with permission from *J. Org. Chem.* **2016**, *81*, 89. Copyright (2016) American Chemical Society].

The dimeric structures feature two molecules of bisanilides in **C₂-NH-*in*** where the dihedral angle between the two phenyl subunits is almost 90° , on the other hand the intramolecular H-bond relies on the possibility of the $\text{C}_{\text{Ph}}-\text{C}_{\text{Ph}}$ bond to rotate passing by an almost 90° **C₂-NH-*in*** (as supported by the X-ray analysis) to a much closer angle in **C₁-H-bond**.

To corroborate these considerations (*M*)-**33** was synthesized starting from enantiopure (*M*)-6,6'-dimethyl-2,2'-diaminobiphenyl and its proton NMR was recorded at low temperature (Figure 4.3.11

Left). This molecule having a tetra-*ortho*-substituted biphenyl unit cannot rotate the $C_{Ph}-C_{Ph}$ existing in fact as a couple of atropisomers with a dihedral angle approximately of 90° .

The 1H -NMR low temperature spectra of (*M*)-**33** and its racemate in $CDCl_2$ were strikingly different from the one recorded for compounds **25-28**. In fact, in these cases were only possible to observe a downfield shift of the amide and an upfield shift of the neighbouring H-3. It was not detected the formation of any asymmetric species.

The formation of the dimer is not obstructed by the more rigid scaffold of **33**, yet it was not detected any new species emerging from the baseline. Therefore, to rationalize this result is necessary to consider only the intramolecular H-bond as a possible scenario, where the constrains imposed by the fixed $C_{Ph}-C_{Ph}$ angle impede the realization of the C_1-H -bond conformation and therefore the intramolecular H-bond.

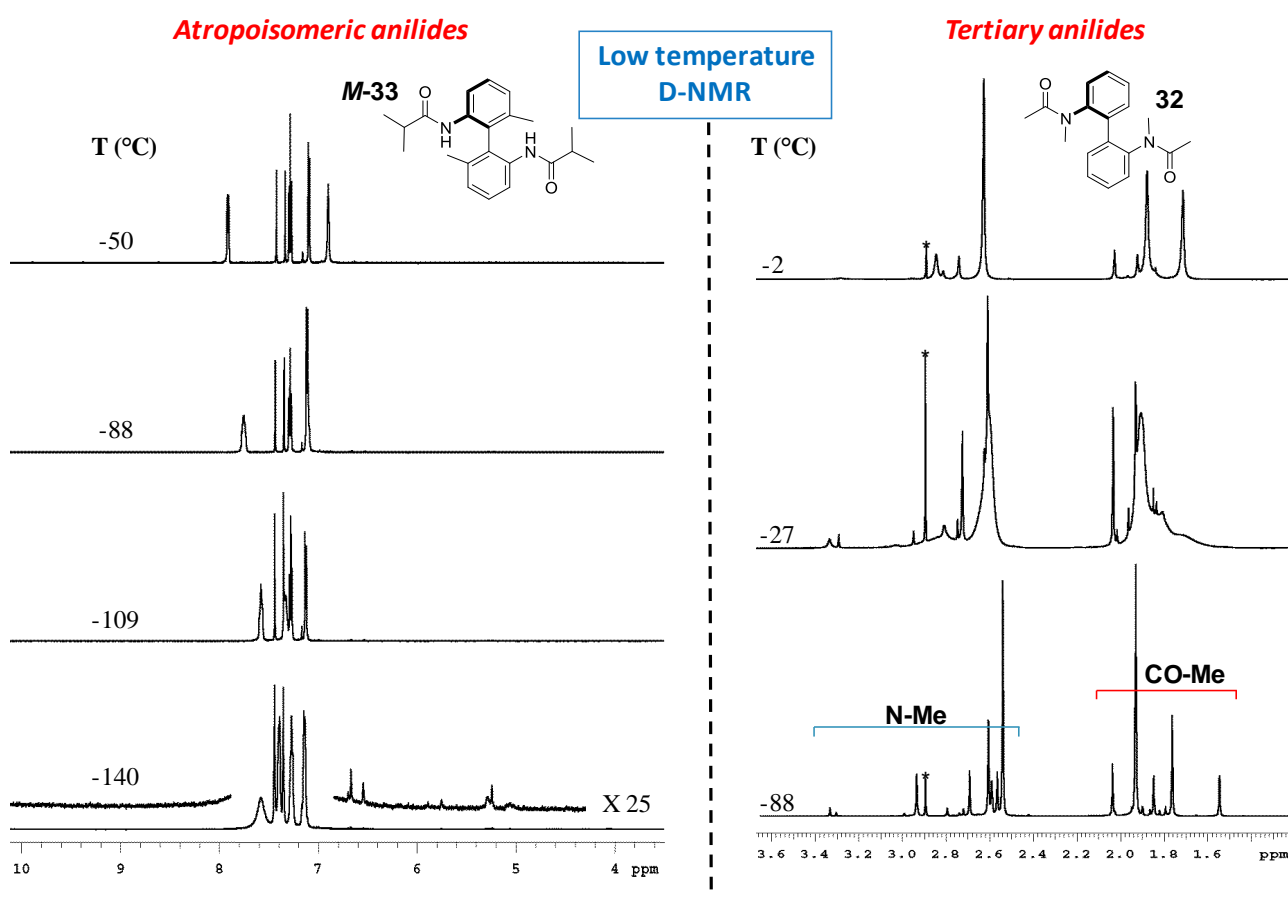


Figure 4.3.11 Left: D-NMR of **33** (600 MHz in $CDCl_2/CDCl_2$). No detection of any asymmetric species. Right: D-NMR of tertiary anilide **32** (600 MHz in $CDCl_2/CDCl_2$). [Reprinted (adapted) with permission from *J. Org. Chem.* **2016**, *81*, 89. Copyright (2016) American Chemical Society].

To completely rule out the dimer formation, DOSY experiment²⁴ of **25** and **33** were performed in $C_2D_2Cl_4$. The results of DOSY performed in both diluted and concentrated solution highlighted a small radius for the all the samples (around 2.30:1 with respect to the solvent radius); since the

dimerization should involve an increase in the hydrodynamic radius the result of the DOSY analysis favoured the hypothesis of an intramolecular H-bond interaction.

To further prove the importance of the NH in this equilibrium the methylated derivative **29-32** were synthesized. In the tertiary anilides is populated the both *E* and *Z* conformation of the amide, while in the secondary is populated only the *Z*. The ¹H-NMR of **32** at room temperature displays a series of bands in the N-Me and CH₃CO region correlated to different interconverting conformers generated by the *E/Z* isomerism of the tertiary amide moiety. Once **32** was cooled down the ¹H-NMR spectrum showed the splitting of many signals in a large set of peaks related to the high number of conceivable stereoisomer (up to 9, Figure 7.3.2) with 14 related CH₃ peaks (Figure 4.3.11 right). Unfortunately, due to partial overlapping of peaks and low populated stereoisomers was difficult to establish the exact number of conformers present. Although the system is complicated by the equilibria of different species related to the *E/Z* isomerism the absence of the NH moiety made impossible to the system to generate an H-bond interaction and therefore **29-32** have a stereodynamic behaviour related to the one observed for **24**.

References

- ¹ a) Sigaloc M. V., Pylaeva S. A., Tolstoy P. M. *J. Phys. Chem. A* **2016**, *120*, 2737-2748; b) Loera D., Liu F., Houk K. N., Garcia-Garibay M. A. *J. Org. Chem.* **2013**, *78*, 11623-11626; c) Lunazzi L., Macciantelli D., Cerioni G. *J. Org. Chem.*, **1982**, *42*, 4579-4581.
- ² a) Lunazzi L., Mazzanti A., Spagnolo P. *J. Org. Chem.* **1997**, *62*, 2263-2266; b) Lunazzi L., Mazzanti A., Alvarez A. M. *J. Org. Chem.* **2000**, *62*, 3200-3206; c) Wolf C., Tumambac G. E. *J. Phys. Chem. A*, **2003**, *107*, 815-817; d) Ghosh M. W., Wolf C. *J. Org. Chem.* **2011**, *76*, 3888-3897; e) Lunazzi L., Mazzanti A., Minzoni M. *J. Org. Chem.* **2006**, *71*, 9297-9301; f) Surya Prakash G. K., Wang F., Ni C., Shen J., Haiges R., Yudin A. K., Mathew T., Olah G. A. *J. Am. Chem. Soc.* **2011**, *133*, 9992-9995; g) Flos M., Lameiras P., Denhez C., Mirand C., Berber H. *J. Org. Chem.* **2016**, *81*, 2392-2382; d) Belot V., Farran D., Jean M., Albalat M., Vanthuyne N., Roussel C., *J. Org. Chem.* **2017**, *82*, 10188-10200.
- ³ Ruzziconi R., Lepri S., Buonerba F., Schlosser M., Mancinelli M., Ranieri S., Prati L., Mazzanti A., *Org. Lett.* **2015**, *17* 2740-2743.
- ⁴ a) Winstein S., N. J. Holness, *J. Am. Chem. Soc.* **1955**, *77*, 5562-5578. b) J.A. Hirsch, *Top. Stereochem.* **1967**, *1*, 199-222, c) E. Kleinpeter, F. Taddei, P. Wacker, *Chem. Eur. J.*, **2003**, *9*, 1360-1368
- ⁵ G. Bott, L.D. Field, S. Sternhell, *J. Am. Chem. Soc.*, **1980**, *102*, 5618-5626
- ⁶ a) Ruzziconi, R., Spizzichino, S., Lunazzi, L., Mazzanti, A., Schlosser, M. *Chem – Eur. J.* **2009**, *15*, 2645-2652. b) Lunazzi, L., Mancinelli M., Mazzanti, A., Lepri, S., Ruzziconi, R., Schlosser, M., *Org. Biomol. Chem.* **2012**, *10*, 1847-1855; c) Ruzziconi, R., Spizzichino, S., Mazzanti, A., Lunazzi, L., Schlosser, M., *Org. Biomol. Chem.* **2010**, *8*, 4463-4471; d) Mazzanti A., Lunazzi L., Minzoni M., Anderson J. E. *J. Org. Chem.* **2006**, *71*, 5474-5481.
- ⁷ Mazzanti A., Lunazzi L., Lepri S., Ruzziconi R., Schlosser M. *Eur. J. Org. Chem.* **2011**, 6725–6731.
- ⁸ Dahlgren M. K., Schyman P., Tirado-Rives J., Jorgensen W. L. *J. Chem. Inf. Model*, **2013**, *53*, 1191-1199.
- ⁹ Ziegler K., Zeiser K., *Ber. Dtsch. Chem. Ges.* **1930**, *63*, 1847-1851.
- ¹⁰ Miyaura N., Suzuki A. *Chem Rev.* **1995**, *95*, 2457–2483.
- ¹¹ Ward M. D., Raithby P. R. *Chem. Soc. Rev.* **2013**, *42*, 1619-1636.
- ¹² Boga C., Cino S., Micheletti G., Padovan D., Prati L., Mazzanti A., Zanna N. *Org. Biomol. Chem.*, **2016**, *14*, 7061.
- ¹³ Forlani L., Boga C., Mazzanti A., Zanna N. *Eur. J. Org. Chem.*, **2012**, 1123.
- ¹⁴ Lowry T. H., Richardson K. S. *Mechanism and Theory in Organic Chemistry* 3rd Ed., Harper Row, Publ., New York **1987**.
- ¹⁵ A) Takahashi Y., Ikeda H., Kanase Y., Makino K., Tabata H., Oshitari T., Inagaki S., Otani Y., Natsugari H., Takahashi H., Ohwada T. *J. Org. Chem.* Article ASAP DOI: 10.1021/acs.joc.7b01759; b) Adams R., Gordon J. R. *J. Am. Chem. Soc.* **1950**, *72*, 2454–2457; c) Clayden J., Lund A., Vallverdu L., Helliwell M. *Nature* **2004**, *431*, 966–971.
- ¹⁶ PAC, **1995**, *67*, 1307 (Glossary of class names of organic compounds and reactivity intermediates based on structure (IUPAC Recommendations 1995)) on page 1317.

¹⁷ a) Curran D. P., Liu W., Chen C. H. T. *J. Am. Chem. Soc.* **1999**, *121*, 11012-11013; b) Bruch A., Ambrosius A., Fröhlich R., Studer A., Guthrie D. B., Zhang H., Curran D. P. *J. Am. Chem. Soc.* **2010**, *132*, 11452-11454; c) Curran D. P., Chen C. H. T., Geib S. J., Lapierre A. J. B. *Tetrahedron* **2004**, *60*, 4413-4424.

¹⁸ Clayden J. *Angew. Chem. Int. Ed Engl* **1997**, *36*(9), 949-951.

¹⁹ Ilieva S., Hadjieva B., Galabov B. *J. Mol. Struct.* **1999**, *508*, 73-80.

²⁰ Mazzanti A., Chiarucci M., Bentley K. W., Wolf C. *J. Org. Chem.* **2014**, *79*, 3725-3730.

²¹ Mazzanti A., Chiarucci M., Prati L., Bentley K.W., Wolf C. *J. Org. Chem.* **2016**, *81*, 89.

²² To correlate one molecule with a two molecules system in DFT is necessary to consider a counterpoise correction. In this case was adopted the one proposed by Bernardi and Boys: a) Boys S. F., Bernardi F. *Mol. Phys.* **1970**, *19*, 553; (b) Simon S., Duran M., Dannenberg J. J. *J. Chem. Phys.* **1996**, *105*, 11024-11031.

²³ The gain in energy were calculated by the difference between the BSSE counterpoise corrected energy of the adduct and the energy of the single components (the bisanilide was considered in **C₂-NH-*in*** conformation).

²⁴ Gradient strength goes from 1 to 62 G/cm and with diffusion delay of 50 ms. The radius was measured by comparison with the solvent radius.

5 Chase for new atropisomers

Dynamic stereochemistry investigations on small organic molecule can elucidate long-range electronic (Paragraphs 4.1 and 4.2) or H-bond interaction (Paragraph 4.3) and more other interactions occurring between two or more exchanging conformers. They can occur in particular structures that are somehow sensible to the electronic, steric or thermal environment.

At the high energy limit of the stereodynamic processes there are stable compound in which the exchange barrier is high enough to avoid interconversion between different stereoisomers of the molecules. As reported in Paragraph 1.5, chiral axes can display both stereodynamic and stereostable behaviour in function of some internal parameter (steric hindrance and electronic conjugation) and some external as the temperature.

Herein are discussed the attempts to produce stable conformations in which the rotation around a single bond is inaccessible at room temperature, and stable atropisomers¹ are therefore produced. The final aim of these works is to introduce chirality, through stable atropisomers, in scaffolds that cannot bear an ordinary stereogenic centre (*i.e.* quaternary carbon). The introduction of stereogenic axes in achiral scaffolds is nowadays pursued with particular interest in order to generate atropisomers and diastereoisomers in molecules already known for their usefulness in a wide range of areas (from pharmaceutical to asymmetric synthesis).

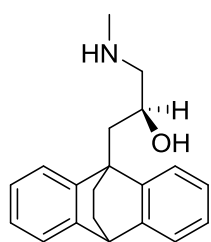
5.1 Conformational Analysis and Absolute Configuration of Axially Chiral 1-aryl and 1,3-diaryl-xanthines.²

Specular chiral molecular system can generate different biological responses. More often, only one of the two enantiomers exhibits a pronounced biological effect. In this cases in medicinal chemistry the enantiomer displays *stereoselectivity* due to its preferential interaction with the recognition site (chiral environment). It is intuitive that the most active stereoisomer (*eutomer*) reaches the best steric and electronic complementary interaction in respect to the less active stereoisomer (*distomer*). Despite this clear picture, that can be also simulated *in silico* with docking studies, in real biological environment the situation is not this straightforward. In fact, *in vivo* the difference in activity observed are not exclusively related to the fitness of the acceptor-ligand. In a real biological environment, also the distribution and all the process related to the pharmacokinetic of the drug are chiral. In other words, the *in vivo* difference of activity between the *eutomer* and *distomer* is a combination of interactions with different biologic chiral acceptors, in which the fit into the recognition site is just accounted as the last of them.

The activity difference between the two enantiomers is usually described with the Eudismic ratio (ER) or with the Eudismic index (EI). The ER is usually calculated as the ratio between the EC_{50} (Half maximal Effective Concentration) or the IC_{50} (Half maximal Inhibitory Concentration) of the *eutomer* (Affinity- E_u) and the respective EC_{50} or IC_{50} of the *distomer* (Affinity- Dis). While the EI is calculated as the logarithm of the ER (Figure 5.1.1).^{3,4,5}

$$EI = \log \frac{Affinity_{Eutomer}}{Affinity_{Distomer}}$$

$$ER = \frac{Affinity_{Eutomer}}{Affinity_{Distomer}}$$

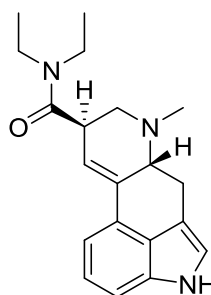


S(+)-Oxaprotiline

IC_{50} value for noradrenaline uptake into rat brain synaptosomes

ER

$$Aff_S / Aff_R = 1000$$

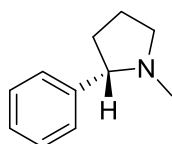


(+)-Lysergide

Binding on rat forebrain suspension

ER

$$Aff_{(+)} / Aff_{(-)} = 24000$$



S(-)-Nicotine
(naturally occurring)

Affinity constant for rat brain thalamus sites

ER

$$Aff_S / Aff_R = 35$$

The eudismic index or ratio is related to a specific activity of biologically active substance.

For a chiral molecule is it possible to have an EI or ER for each activity or affinity presented by the compound

Figure 5.1.1 Definitions of Eudesmic Index and Eudismic Ratio and some examples of biological active molecules where the activity of one enantiomer differ from the other

Although, in biological environment there are several chiral interactions of the *eutomer* other than the one in the recognition site, the difference in activity of the two stereoisomers were related to different models considering merely the interaction of the *eutomer* with the binding site. The three point contact model firstly suggested by Easson, Stedman and Beckett^{6,7} was modelled on the binding of the *R*(-)-epinephrine with its receptor. The *R*(-)-epinephrine undergoes to three interactions with its receptor thus implying a very specific molecular orientation that can be obtained only with the *R* enantiomer and not with the *S* (it undergoes only to two interaction), Figure 5.1.2.

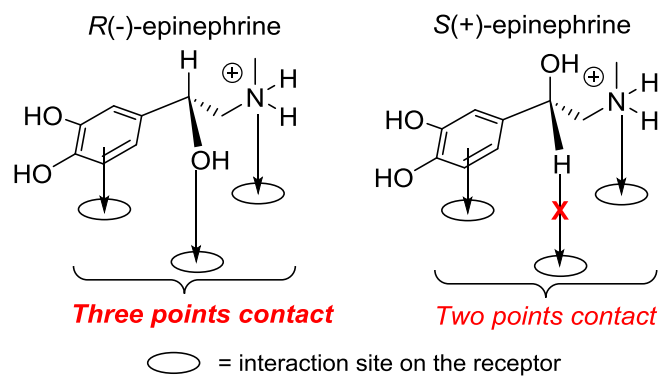


Figure 5.1.2 Interaction of *R*(-) and *S*(+) epinephrine with the receptor. Only the *R* enantiomer can achieve three interactions.

The three points contact model has some limitations: it required a perfect understanding of the environment of the interactive site and moreover found some limitation when more than one stereogenic element is present. Pursuing a more general rule, Pfeiffer⁸ stated an empirical rule “the greater the difference between the pharmacological activity of the *R* and *S* isomers, the greater is the potency of the *eutomer*”. Although this rule is very general and finds only few exceptions,⁹ it does not provide a useful tool to foresee the EI of a couple of enantiomers.

Therefore, the most common way to evaluate the difference in potency of two enantiomers is a separate synthesis and biological screening. Four possibilities can arise comparing the ratio between the affinity of the *eutomer* (A_{eu}) and the racemate (A_{rac}):^{10,11}

1. $A_{eu} / A_{rac} = 2$. The *eutomer* is the only active. The *distomer* does not contribute in any way to the affinity. The chiral compound is highly stereoselective.
2. $A_{eu} / A_{rac} > 2$. In this situation in the racemate the *distomer* counteracts the effect of the *eutomer* leading to an overall attenuated activity in the racemate.
3. $A_{eu} / A_{rac} < 2$. Both the stereoisomers are active. The *distomer* presents smaller activity than the *eutomer* indicating a smaller stereoselectivity of the active principle.
4. $A_{eu} / A_{rac} = 1$. In this case there is no stereoselectivity and it is not observed differences in the activity of the two stereoisomers. This behaviour is not uncommon and can be related to three factors, a) the stereogenic unit is not involved in the interaction with the receptor; b) the mechanism of interaction of the molecule is not specific for the receptor; c) the interaction with the receptor involves only two points of contact not discriminating between the two different chiral centres.

The latter case is related only to classic stereogenic centre in which an asymmetric tetra-substituted atom is involved, on the other hand stereogenic axis and helix can display different stereoselective interaction with the biological receptor. In fact, these stereogenic units generate enantiomers that need less than three contact points to be discriminated. Moreover, these particular stereogenic units can be

introduced in rigid bioactive scaffolds that does not allow the presence of a conventional stereogenic centre.

The generation of enantiomers in previously achiral biological active scaffold can be useful to enhance the known activity and to generate pharmacologically different compounds. In fact, enantiomers can differ in the magnitude of the activity toward a certain substrate but also in the effects (Figure 5.1.3).^{12,13,14,15} The (+)-*N*-methyl-3-methoxy morphinane is an analgesic and present addictive proprieties while the levo-stereoisomer is non-addictive and shows only antitussive proprieties. The same behaviour is displayed by the enantiomers of the propoxyphene, where the dextro-isomers is well-known for its analgesic proprieties while the levopropoxyphene retains antitussive effect.

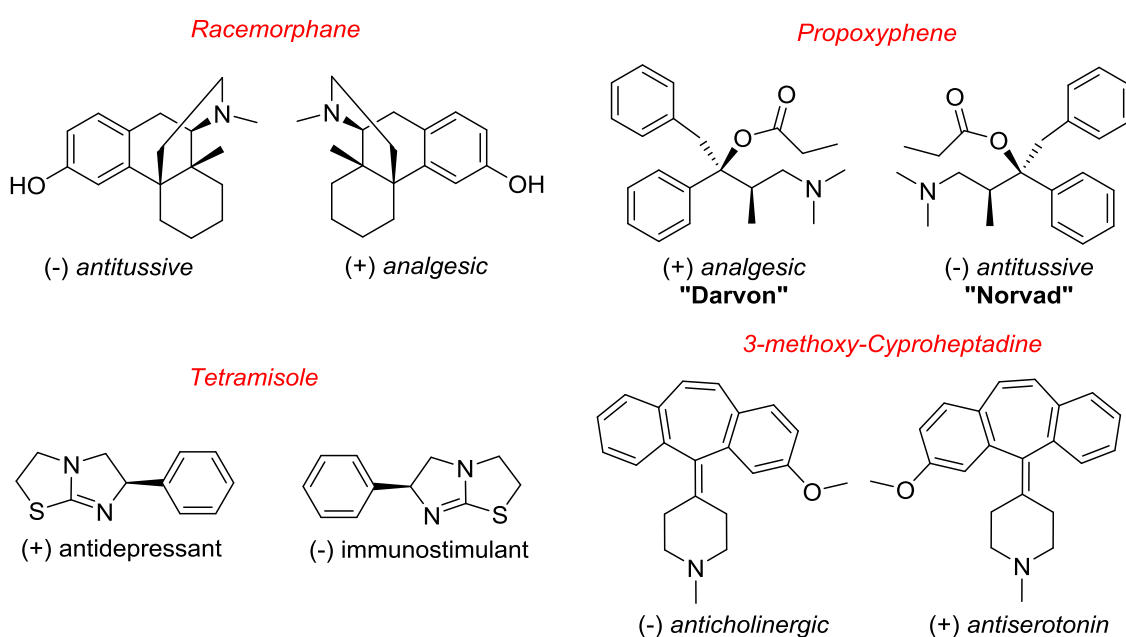


Figure 5.1.3 Differences in pharmacological profile of couple of enantiomers

Therefore, the introduction of chiral axis in biological active scaffolds that cannot bear an ordinary centre of chirality can, on one side enhance the pharmaco-related effect and on the other differentiate the activity of the two newly obtained enantiomers. Moreover, atropisomers are free from the need of three points of contact to exerts a stereoselective interaction.

On this regard $C_{sp^2}-N$ are one of the most common bonds in biological environment, moreover they are present in different class of molecule in which the insertion of chiral axis can be valuable in order to insert chirality in biological active scaffold.

Several organic scaffolds such as: imides,¹⁶ lactames¹⁷, oxazolidine-2-one¹⁸ and thiazolidine-2-thiones¹⁹, pyrrole,²⁰ indole,²¹ pyrazole,²² 1,2,4-triazole²³ are eligible for the insertion of stereogenic axis (Figure 5.1.4 A). Among them, barbiturates are well known for their biological activity and are one of the most studied biological active compound in which is conceivable the insertion of a $C_{sp^2}-N$

stereogenic axis.²⁴ The biological effect of barbiturates is related to the resemblance of this scaffold to the pyrimidine nitrogen bases. Following the same rationale the xanthine scaffold is analogous to the purine nucleobases and is well known to be the forefather of a class of biological active molecules (Figure 5.1.4 B).²⁵

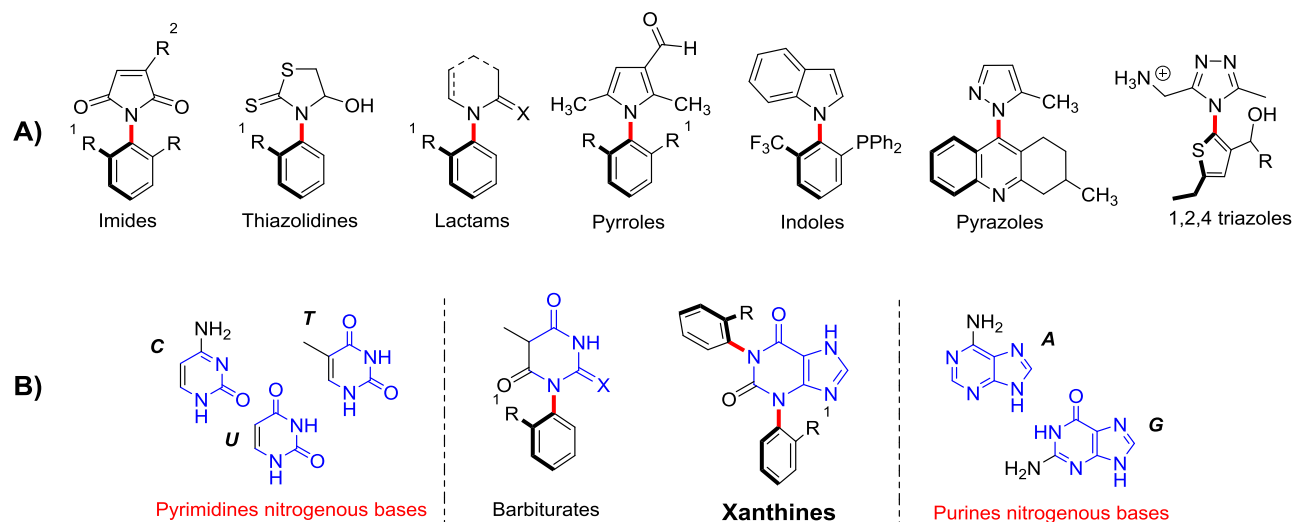


Figure 5.1.4 A stable atropisomeric compound that carry a C_{sp^2} -N stereogenic axis. B Nitrogenous bases and their respective biological active synthetic analogue bearing a N-aryl stereogenic axis.

However, despite its biological activity, poor attention has been given to the dynamic conformations of this scaffold. The motivation of this lack of studies has to be ascribed in the chemistry of the scaffold itself: it is not possible to install an ordinary stereogenic element without modify one of its essential functional groups, while it is possible to install stereogenic axes.

The xanthine scaffold is planar and an aryl substituent linked to the nitrogen in positions 1 or 3 would be skewed out of the plane of the xanthine plane due to steric hindrance caused by the two carbonyls or by one carbonyl and the imidazole moiety.

If the aryl substituents lack of local C_2 symmetry and the rotation around the C_{sp^2} -N is hindered (depending on the steric bulkiness of the aryl-substituents) the resulting conformational enantiomers would be either stereo labile or configurationally stable.

In order to evaluate the steric requirement to conceive stable atropisomers on the xanthine scaffold, an *in silico* evaluation was firstly carried out. The starting point was the known structure of 1-phenyl xanthine,²⁶ that arranges the aryl ring skewed (79.5°) with respect to the planar xanthine scaffold. However, some modification to this structure are needed. To have atropisomer related to the hindered rotation around the C_{sp^2} -N1 the aryl ring needs to be locally asymmetric (*i.e.* does not have a local C_2 symmetry axis). If an analogous situation is simultaneously introduced on the nitrogen in position 3, the combination of two stereogenic axes generates four stereoisomers. As a theoretical model it was considered the introduction of two *o*-tolyl groups in 1 and 3 positions (1,3-di-*o*-tolyl xanthine).

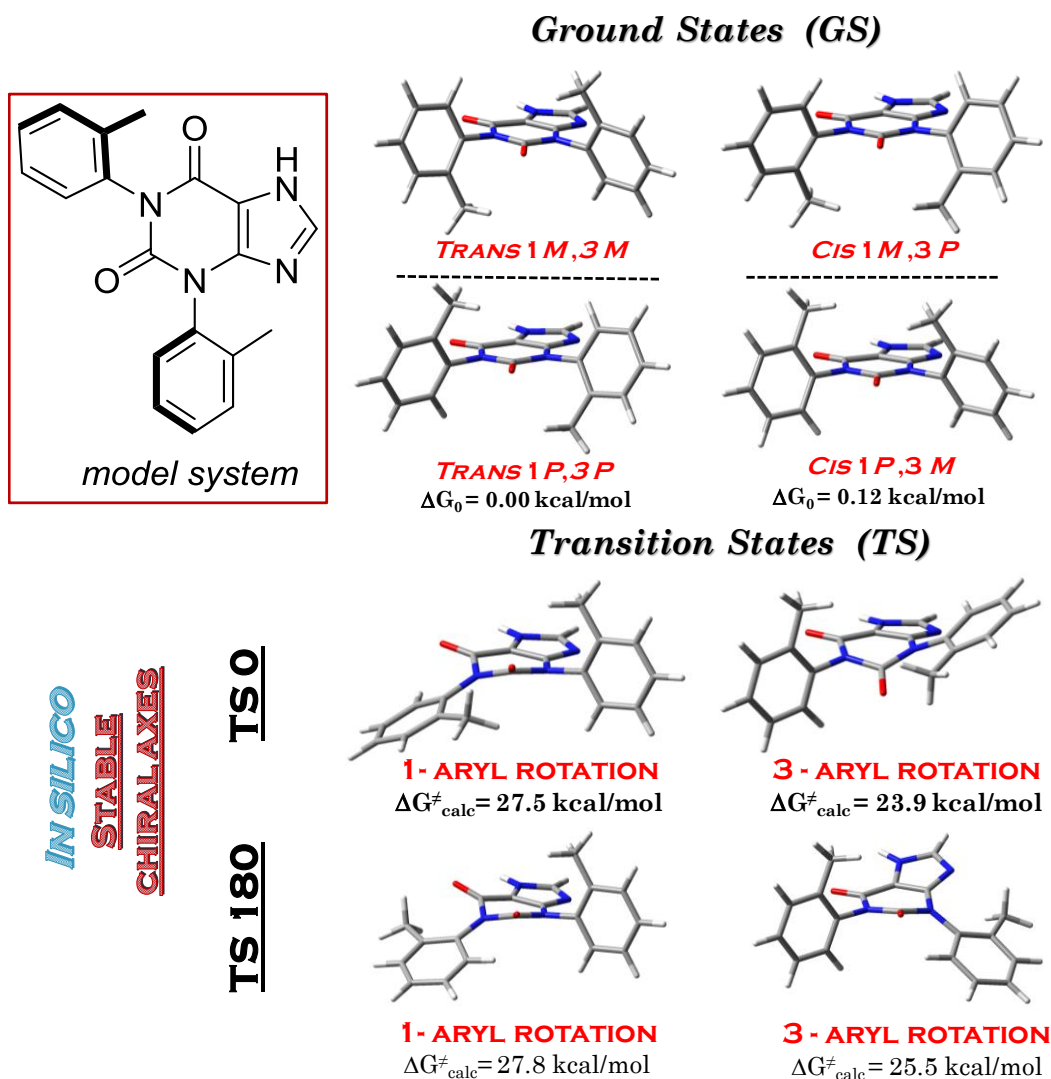


Figure 5.1.5 Theoretical studies performed at the B3LYP/6-31G(d) level of theory on the model system (1,3-ditolyl-xanthine). Ground states showed the existence of two populated diastereoisomers, while the analysis on the transition states evaluate the stability of the rotational stereoisomers. [Reprinted (adapted) with permission from *J. Org. Chem.* **2017**, *82*, 6874-6885. Copyright (2017) American Chemical Society].

The two diastereoisomers were optimized at the B3LYP/6-31G(d) level of theory, however due to the imperfect orthogonality of the *o*-tolyl moiety two conformations need to be accounted for each diastereoisomer leading to a total of eight conformers. The most stable Ground State (GS) of each diastereoisomer are presented in Figure 5.1.5. Obviously, the corresponding enantiomer of *cis* and *trans* diastereoisomer have the same energy. To evaluate the entity of the rotational barrier (and therefore the thermal stability of the atropisomer itself) the Transition States (TS) were calculated. As happens in most of the cases where a chiral axis is involved the interconversion pass through a TS in which the two aryl moieties are coplanar (Paragraph 1.5). Analogously to the biphenyls in Figure 1.5.3 each aryl in 1 or in 3 positions can be coplanar with the xanthine scaffold forming a $\approx 0^\circ$ dihedral angle (TS0), where the *o*-tolyl of the rotating ring points towards the carbonyl in position 2, or forming a $\approx 180^\circ$ dihedral angle (TS180) when the aryl rotates in the other direction (*i.e.* towards the

carbonyl in 9 for the N1-aryl and towards the imidazole for the N3-aryl). The calculated energy barriers related to the rotation for the N1-aryl and N3-aryl were 27.5 kcal/mol and 23.9 kcal/mol respectively having both the TS0 geometry as the most stable TS. Due to the higher steric constrain exerted by the carbonyls in 2 and in 9 the rotation of the *o*-tolyl in position 1 results higher enough with respect to the one in position 3 to observe the two rotations independently. Following the definition of Oki¹ and the LaPlante chart (see Paragraph 1.5 and Figure 1.5.2 there reported) these rotational barriers are high enough to develop slow to very slow interconverting atropisomer (Figure 5.1.5).

At least, *in silico*, the *o*-tolyl moiety in both the 1 and 3 positions has been proved bulky enough to generates stable conformational diastereoisomers. To experimentally prove these theoretical barriers a series of xanthine bearing a chiral axis in 1 and in 3 positions were synthesized (**34-42**, Figure 5.1.6).

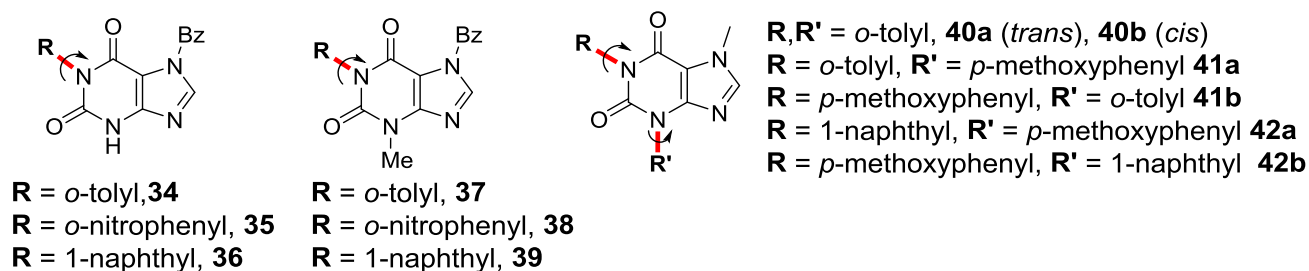


Figure 5.1.6 N1-aryl and N1-N3 bisaryl xanthine synthesized

The synthesis of the 1-aryl xanthines (**34-39**) (Figure 5.1.8)²⁷ differs from the procedure used to introduce an aryl also in 3 position (**40-42**) (Figure 5.1.7).²⁸ The latter were synthesized starting from the appropriate aryl-substituted isocyanate and aniline yielding an 1,3-diarly urea²⁹ that can be cyclized with malonyl chloride giving the respective pyrimidine-trione.³⁰ The chlorination of one of the carboxyl moieties was performed with POCl₃ and afforded the compounds **VII**, **VIII**, **IX**, in which the latter two were used as mixture of regioisomers that was separated in **41a-41b** and **42a-42b** only on the last stage of the synthesis. The amination of the vinyl chloride with MeNH₂ followed by the insertion in the alpha position of a nitroso group lead to compounds **XIII**, **XIV** and **XV**. The ring closure and the formation of the xanthine **40-42** were achieved by dehydration at high temperature followed by one-pot methylation of the imidazole ring (Paragraph 7.4.2).

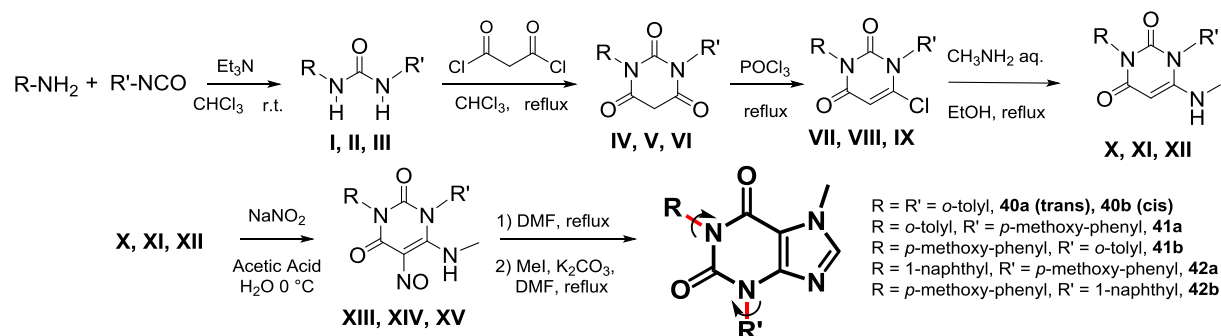


Figure 5.1.7 Synthetic procedure to obtain 40-42.

The 1-aryl xanthine (Figure 5.1.8) could be synthesized starting by the commercially available **XIX**, but the amount needed requested an in-house synthesis. Compound **XIX** derives from ethylbenzylglycinate (**XVI**) and ethyl (*E*)-*N*-cyanoformimidate (**XVII**) through the cyano-immino derivate **XVIII** that can be cyclized to the imidazole **XIX** with a base that allows the cyano group to attack the alpha position of the ester moiety. The synthesis goes on with the addition of the appropriate isocyanate to **XIX** and the formation of the urea derivatives **XX a-c** that can be easily cyclized with a base and the elimination of ethanol to form the xanthine scaffold **34-36** subsequently methylated with MeI to yield **37-39** (Paragraph 7.4.2).

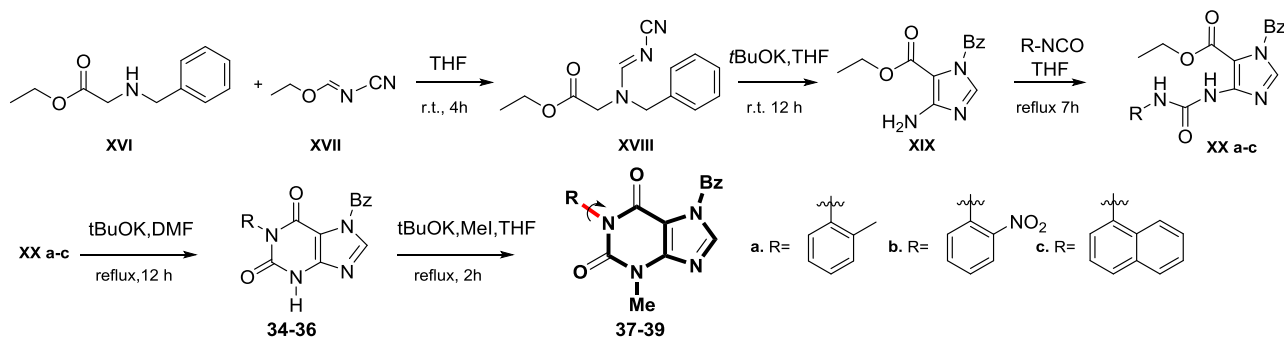


Figure 5.1.8 Synthetic procedure to obtain 34-39.

The determination of the rotational barrier can be carried out with different methodologies (Chapter 2). In the 1-aryl series (**34-39**) the introduction of the benzyl group was designed to determine the racemization barrier with D-NMR (Paragraph 2.1), however the expected AB system of the methylene of **34** did not undergo to coalescence even when heated to 120 °C (Figure 7.4.1) suggesting a rotational barrier too high for this technique. Therefore, a kinetic study was approached (Paragraph 2.3). Unfortunately, the free NH of **34-36** made difficult the isolation of the atropisomer on HPLC columns with chiral stationary phase (CSP). To solve this issue compounds **37-39** were synthesized

where the free NH is protected with a methyl group that does not interfere with the rotation barrier on the N1 and allows a better separation on CSP column.

The single enantiomer of each compound was then heated up to a fixed temperature and aliquots taken at different times were analysed at CSP-HPLC at 25 °C to determine the amount of enantiomer generated at high temperature (**37** Figure 5.1.9 and Figure 7.4.2, **38** Figure 7.4.3 and **39** Figure 7.4.4). The fitting of the experimental data into a first order reversible kinetic equation (Eq 2.3) allowed the determination of the kinetic constant for each kinetic study performed and therefore through the Eyring equation (Eq 2.2) the rotational barrier involved in the racemization.

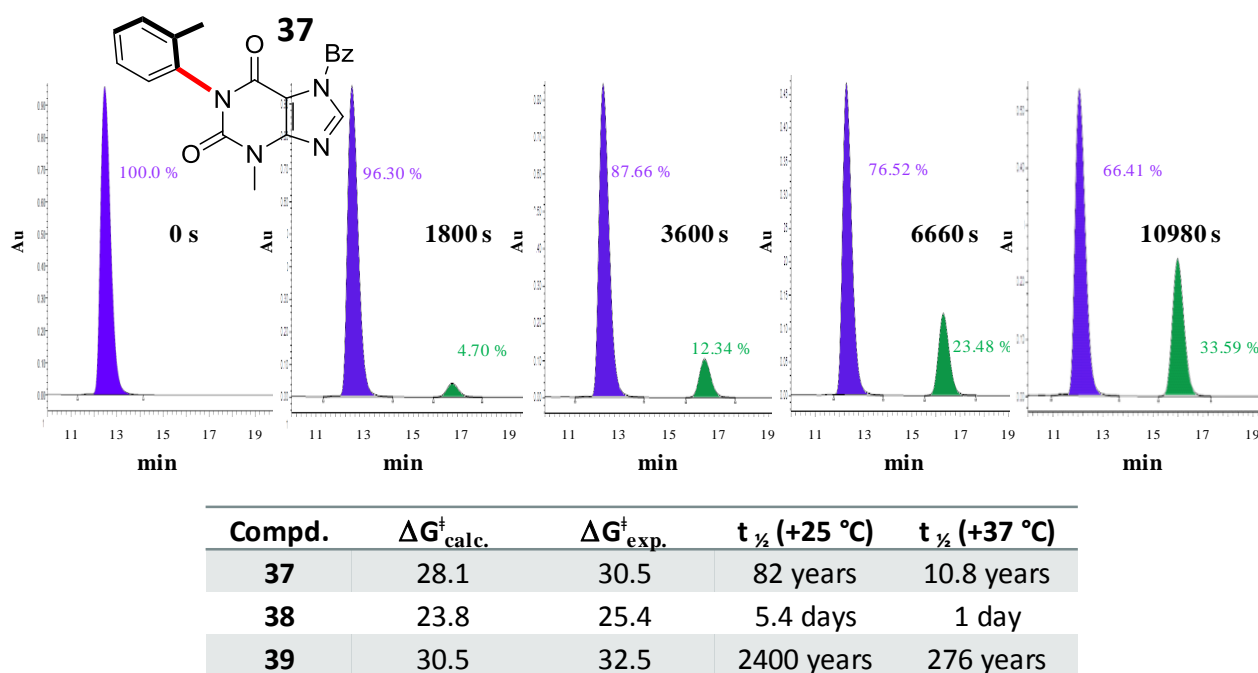


Figure 5.1.9 Racemization of enantiopure **37** (performed at +115 °C in $\text{C}_2\text{D}_2\text{Cl}$) followed by CSP-HPLC analysis recorded at room temperature. The same procedure on **38** and **39** leads to their racemization barrier displayed in the Table among the half-life time of each enantiomer at 25 °C and at 37 °C and the calculated racemization barrier. [Reprinted (adapted) with permission from *J. Org. Chem.* **2017**, 82, 6874-6885. Copyright (2017) American Chemical Society].

The experimental values determined are even higher than the theoretical ones and in the case of **37** and **39** they display a very long half-life time (both at 25 °C and 37 °C). It is noteworthy that although the nitro group and the methyl are considered almost isosteric,³¹ compound **38** shows a 5 kcal/mol lower rotational barrier. This effect has an electrostatic nature and corresponds to a stabilization of the TS due to the formation of a NO/CO interaction that facilitate the rotation around the $\text{C}_{\text{sp}^2}\text{-N}$ axis (Figure 1.5.6 C).³²

Given the very high barriers determined for **37-39** for the rotation of the aryl in position 1 the presence of the chiral probe was no longer necessary, and therefore the benzyl moiety was substituted with a methyl for the preparation of the 1,3-bisaryl xanthenes **40-42**.

This series is composed by a compound bearing two chiral axes (**40**) and two compounds that have an *ortho* substituted aryl ring in position 1 and a symmetric aryl ring in position 3 (**41a**, **42a**), or *vice versa* (**41b**, **42b**). The first, very similar to the model compound, generates two diastereoisomers almost equally populated, while the latter carry only one chiral axis and it is possible to evaluate the effect on $\Delta G_{\text{rot}}^{\ddagger}$ of the same *ortho* hindered group when it is placed in position 1 or in position 3. The rotational barriers of compounds **41-42** were determined analogously to the compounds **37-39** (**41a** Figure 7.4.6, **41b** Figure 7.4.7, **42a** Figure 7.4.8 and **42b** Figure 7.4.9).

Compound **40**, bearing two chiral axes behaves *in silico* very similarly to the model compound (to which the only difference is the methyl of the imidazole ring), displaying two distinct rotational barriers for the aryl in position 1 and in position 3, where the latter is lower by 2.1 kcal/mol (at the B3LYP/6-31G(d) level). The lower energy rotation (N3-aryl) should yield diastereomerization (interconversion *trans-cis*) while the higher (N1-aryl) should lead to racemization.

The room temperature NMR of **40** showed four methyl peaks ascribable to the two diastereoisomer (in 57:43 ratio) and the four stereoisomers could be completely resolved on amylose CSP column (Figure 5.1.10).

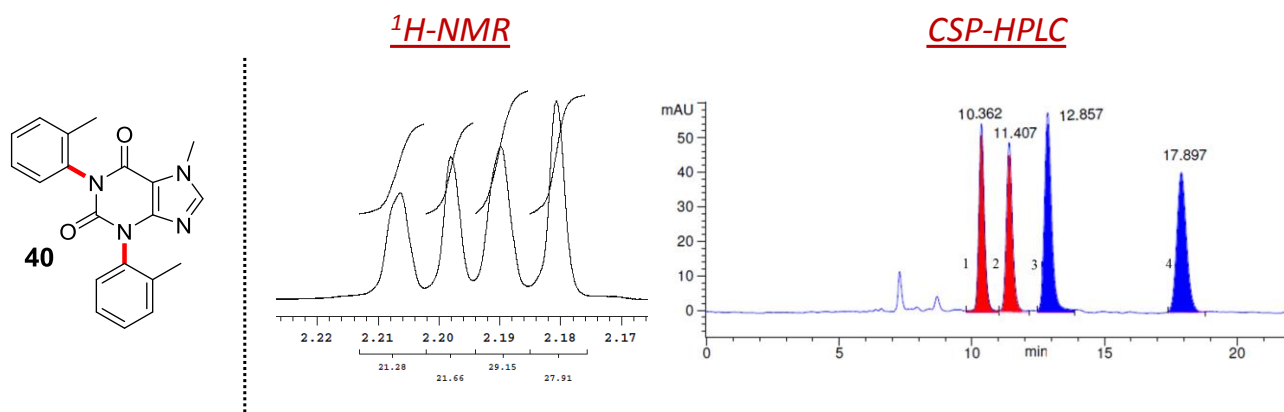


Figure 5.1.10 Left: $^1\text{H-NMR}$ spectrum (300 MHz in CDCl_3) of the mixture of the diastereoisomers of compound **40** (57:43 ratio). The signal of the *ortho*-methyl signals is shown. Right: CSP-HPLC of **40** (Chiralpak AD-H, 10 μm , 250 x 20 mm, 20 mL/min hexane/*i*PrOH 80/20 v/v) showing the four available stereoisomers. [Reprinted (adapted) with permission from *J. Org. Chem.* **2017**, 82, 6874-6885. Copyright (2017) American Chemical Society].

The NMR analysis performed individually on each chromatographic peak of **40** allowed to assign the first two eluted peaks to one diastereoisomer, while the last two to the other diastereoisomer (the first two and the last two of eluted stereoisomers have the same NMR spectra respectively).

NMR-NOE spectra were performed to determine the relative configuration of the two diastereoisomers. In fact, DFT calculations suggested that the *cis* diastereoisomer should arrange the two *ortho*-methyls near enough ($\approx 3.5 \text{ \AA}$) to provide a detectable NOE enhancement. Unfortunately, in both the diastereoisomers the methyls have very similar chemical shift (less than 10 Hz from one peak to the other), therefore a fully selective irradiation was not conceivable. Instead, the ^{13}C satellites

of both methyls were saturated simultaneously to detect the NOE effect on the ^{13}C signals (Figure 5.1.11). While this experiment performed on the mixture of first and second eluted stereoisomers did not produce any detectable NOE effect, the same experiment performed on the third and fourth stereoisomers yielded a detectable NOE enhancement on the ^{13}C signals, straightforwardly assigning to the 3+4 eluted couple the *cis* configuration (**40b**) and the 1+2 couple to the *trans* configuration (**40a**), Figure 5.1.11.

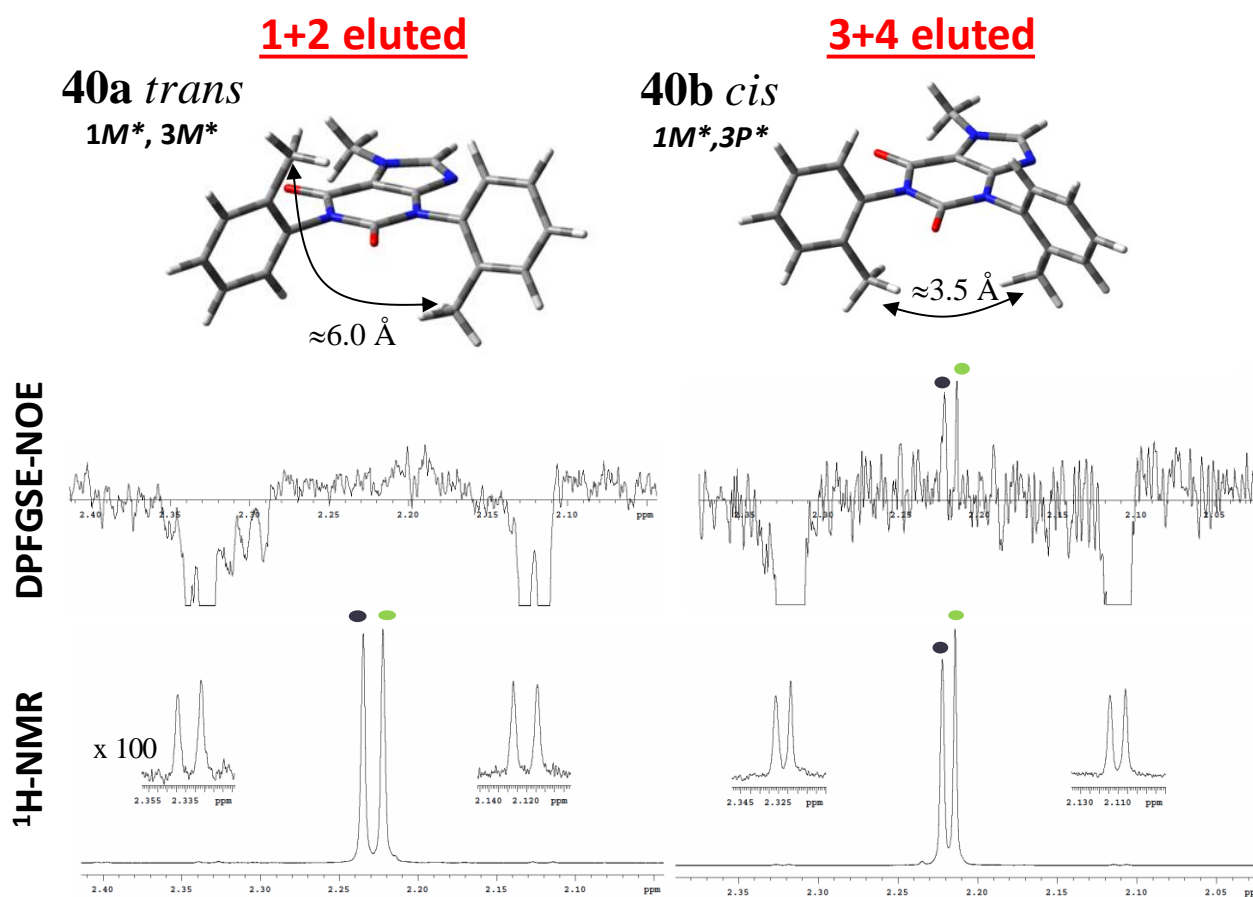


Figure 5.1.11 DPFGE-NOE for compound **40**, on saturation of the ^{13}C satellites of both methyls (600 MHz in CDCl_3). Left: first two eluted stereoisomer. Right: third and fourth eluted stereoisomer. Bottom: ^1H -NMR control spectra. [Reprinted (adapted) with permission from *J. Org. Chem.* **2017**, *82*, 6874-6885. Copyright (2017) American Chemical Society].

The diastereomerization process can be easily followed with NMR without the presence of a chiral probe. In the case of **40**, the diastereomerization barrier was measured starting from an enantiopure sample at +77 °C and +82 °C with NMR, monitoring the increase of the other diastereoisomer (Top of Figure 5.1.12). The fitting of the data with a first kinetic reversible equation lead to a rotational barrier of 26.0 kcal/mol. On the other hand, the enantiomerization was followed by CSP-HPLC heating at different temperature a sample composed by an equilibrated mixture of two diastereomer having the same chirality on the most stable chiral axis (first and fourth eluted in bottom of Figure 5.1.12).

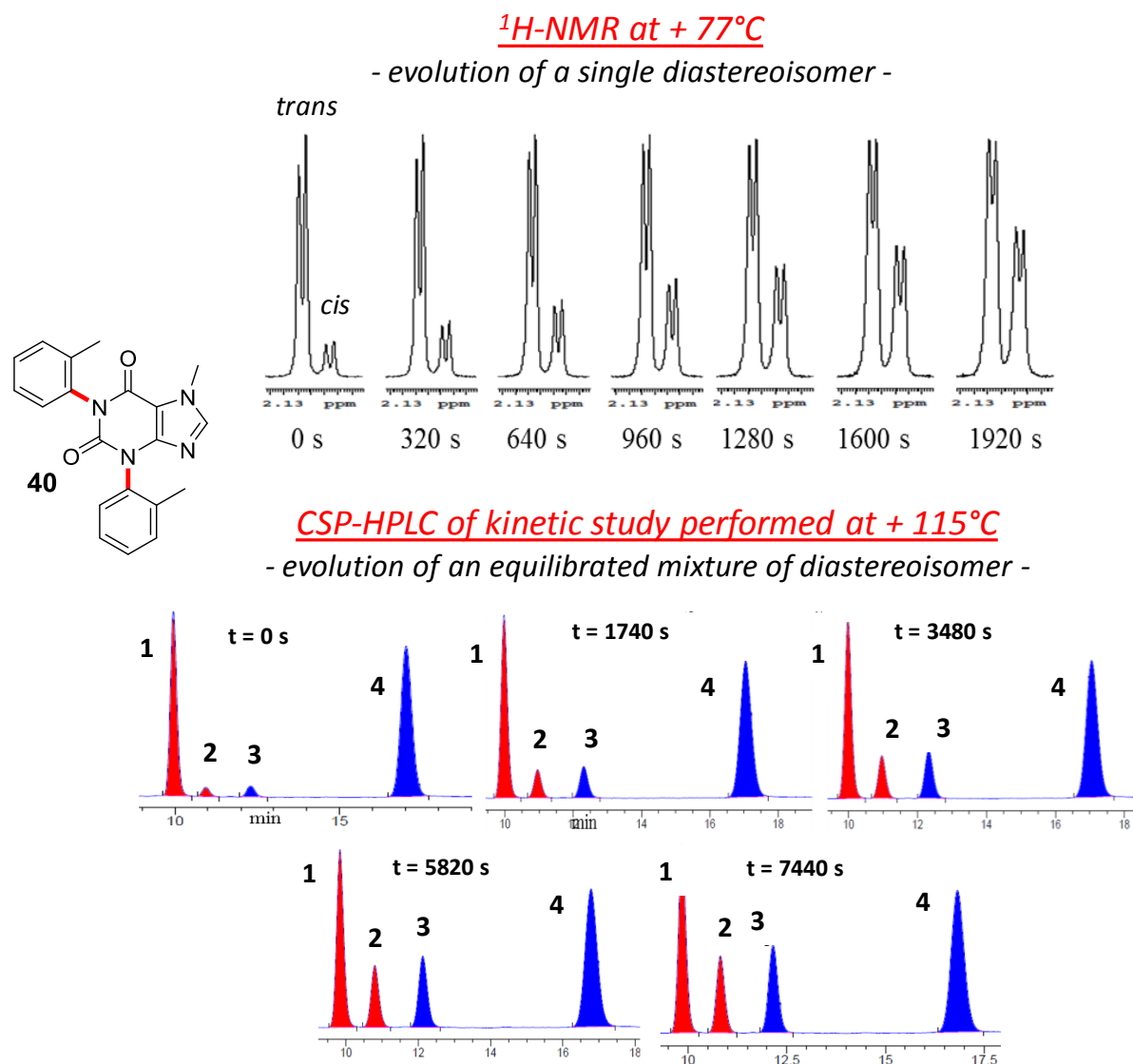


Figure 5.1.12 Top: Kinetic diastereomerization of compound **40** observed with ¹H NMR (600 MHz in DMSO) at + 77 °C. Bottom: kinetic measurement of enantiomerization rate of compound **7** by HPLC (Chiralpak AD-H, eluent hexane/*i*PrOH 80/20 v/v), starting from the two thermodynamically equilibrated diastereoisomers 1+4, kept at +115 °C in C₂D₂Cl. [Reprinted (adapted) with permission from *J. Org. Chem.* **2017**, *82*, 6874-6885. Copyright (2017) American Chemical Society].

Treating the sum of the enantiomers generated (second and third) as a single compound involved in a simple racemization the racemization barrier derived was 30.4 kcal/mol (Figure 7.4.5), perfectly compatible with the one already determined for **37**.

All the stereoisomers analysed by kinetic studies showed a rotational barrier high enough to be considered stable atropisomer at room temperature and in physiological condition as had been previously foreseen by DFT calculations (Table 5.1.1, Paragraph 7.4.1). Despite these studies, the absolute configuration (AC) of the atropisomers of **37-42** remains undisclosed. Unfortunately, these molecules do not contain any heavy atom suitable to the assignment of the absolute configuration by anomalous dispersion X-ray diffraction. It was then straightforward to choose the comparison of

computed ECD spectra (TD-DFT method) with the one experimentally recorded for each enantiomer.³³

Table 5.1.1 Experimental and computed energy barrier (in kcal/mol) for the rotation around the Csp²-N axis of **40-42** and corresponding half-life times at +37 °C.

Compd.	1-aryl rotation (kcal/mol)			3-aryl rotation (kcal/mol)		
	$\Delta G^\ddagger_{\text{calc.}}$	$\Delta G^\ddagger_{\text{exp.}}$	$t_{1/2}$ (+37 °C)	$\Delta G^\ddagger_{\text{calc.}}$	$\Delta G^\ddagger_{\text{exp.}}$	$t_{1/2}$ (+37 °C)
40	27.5	30.4	9.1 years	23.5	26.0	2.6 days
41a	27.5	30.5	10.7 years	-	-	-
41b	-	-	-	23.7	26.2	4.6 days
42a	30.1	32.8	422 years	-	-	-
42b	-	-	-	25.6	28.4	0.4 year

As discussed in Paragraph 2.5.2 this method involves the simulation of the ECD spectra for each populated ground state of the enantiomer. The final computed spectrum results as a linear combination of the single ground state spectrum weighted by their Boltzmann population.

The 1 aryl-xanthenes **37-39**, bearing a benzyl group have a wider conformational space (*i.e.* more ground states). In fact, the benzyl group can arrange on the same side of the *ortho* substituent (*syn* conformers) or on the opposite side (*anti* conformers). Although these are not stable conformers, both their simulated ECD spectra needed to be taken into account to correctly determine the AC of the compounds (**37-39**). In Figure 5.1.13A are shown the calculated ECD spectra of each stable ground state of **39** with the four different functional (for data redundancy) CAM-B3LYP, BH&HLYP, M06-2X, ω B97XD and the same basis set 6-311++G(2d,p), while in Figure 5.1.13 B are displayed the Boltzmann weighted ECD spectra for each functional with the experimental one for the second eluted enantiomer. The direct comparison of the weighted calculated ECD spectra for the *M* atropisomer with the experimental one led to the assignment of the *M* configuration to the second eluted enantiomer of **39**, Table 5.1.2.

An analogous approach was used to determine the AC of **40-42** (Table 5.1.2). The absence of the benzyl group reduces the degree of freedom of the molecules and only the geometries deriving from the imperfect orthogonality of the aryl substituent have to be considered (also the *p*-anisole although present a local C₂ symmetry axis have two conformations that must be taken into account) Figure 5.1.14.

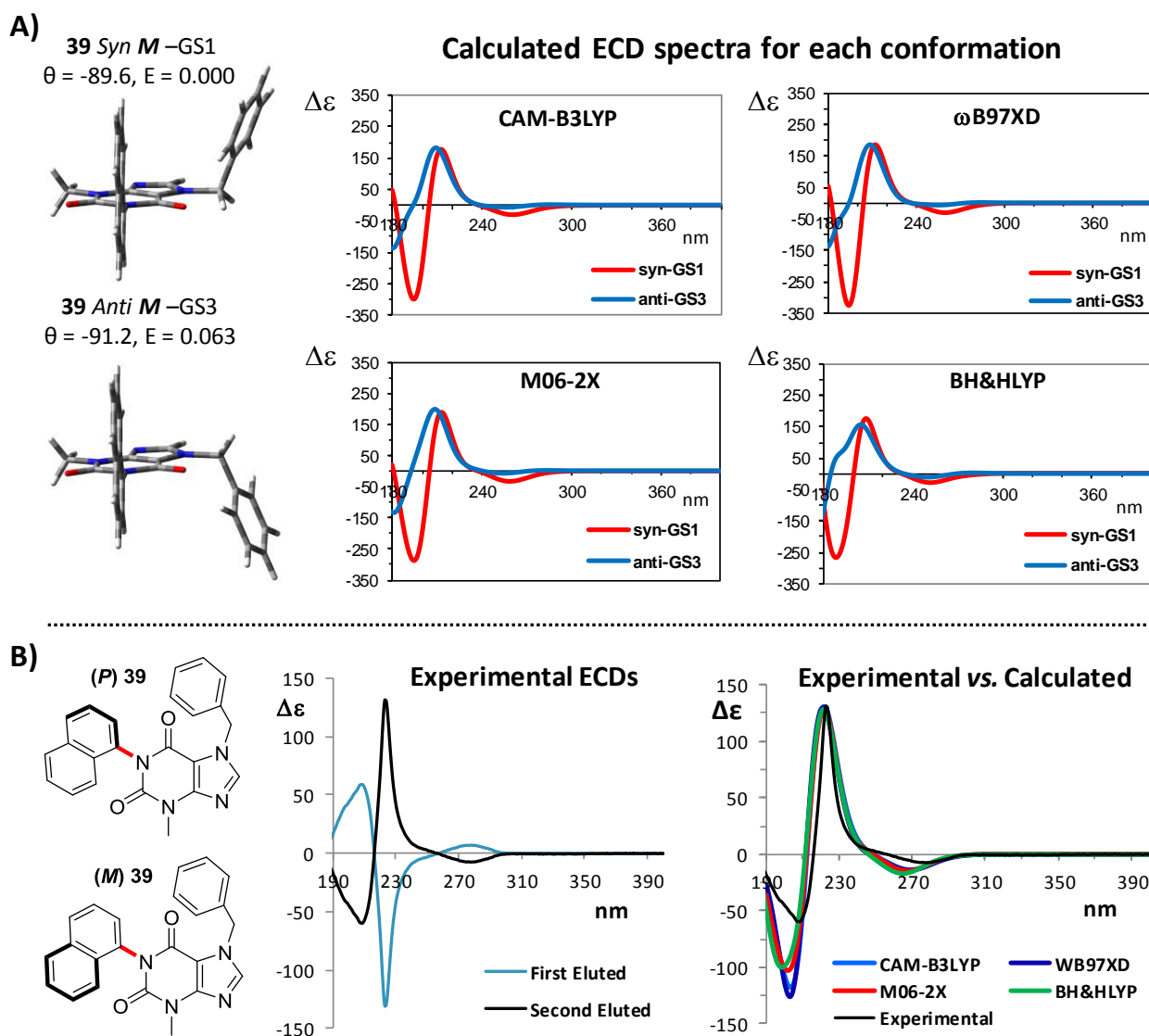


Figure 5.1.13 A) Left: Conformers of **39** generated by the *syn* or *anti* disposition of the benzyl moiety respect the hindered aryl substituent. Right: Calculated ECD spectra with four different functional (CAM-B3LYP, BH&HLYP, M06-2X, ω B97XD) with the same basis set, 6-311++G(2d,p), of each conformer of **39**. B) Left Atropisomers of **39**. Centre: Experimental ECD recorded in ACN (path length 0.2 cm) of the first and second eluted atropisomer of **39**. Right: comparison between the second eluted experimental ECD spectra and the computed ones with the four functionals. The calculated ECD spectra are red-shifted by 10, 10, 1 and 14 nm and multiplied by a factor 0.75, 0.72, 0.70 and 0.80 respectively for each functional. [Reprinted (adapted) with permission from *J. Org. Chem.* **2017**, *82*, 6874-6885. Copyright (2017) American Chemical Society].

The introduction of stereogenic axes in the xanthine scaffold produced stable atropisomers that can be easily simulated, synthesized and resolved. The good agreement between the computed and the experimental rotational barrier and computed spectra demonstrated the reliability of the DFT calculations into foreseen the steric requirement needed to produce stable atropisomers and in the AC assignment. The stability of the atropisomers generated spans from day to years in physiological conditions (+37 °C). The introduction of chirality in this biological active molecule could open to the opportunity to differentiate the effect of the two stereoisomers and to enhance the activity of one over

the other, introducing the concept of ER (or EI) also for this widely diffused biologically active scaffold.

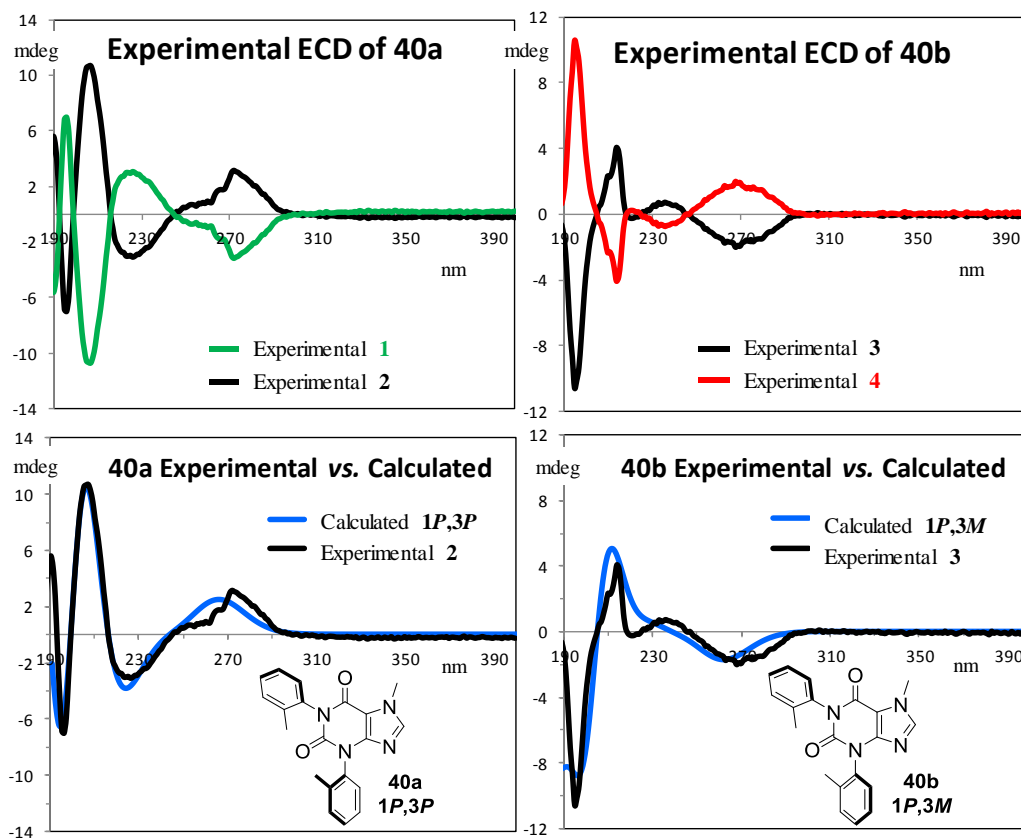


Figure 5.1.14 Top: experimental ECD of: **40a** (left) and **40b** (right) recorded in ACN (path length 0.2 cm). Bottom: comparison of the experimental ECD spectra of the second eluted (left) and third eluted (right) atropisomers with the calculated one for **40** *1P,3P* and *1P,3M* respectively at CAM-B3LYP/6-311++G(2d,p) level of theory. [Reprinted (adapted) with permission from *J. Org. Chem.* **2017**, *82*, 6874-6885. Copyright (2017) American Chemical Society].

Table 5.1.2 Absolute configuration of compounds **37-42** derived from the ECD spectra and the CSP-HPLC column employed to resolve the atropisomers.

Absolute Configuration					
Compd.	CSP-HPLC Column	1° eluted	2° eluted	3° eluted	4° eluted
37	ChiralPak AD-H	<i>1M</i>	<i>1P</i>		
38	Lux Cellulose-2	<i>1M</i>	<i>1P</i>		
39	ChiralPak AD-H	<i>1P</i>	<i>1M</i>		
40a	ChiralPak AD-H	<i>1M, 3M</i>	<i>1P, 3P</i>		
40b				<i>1P, 3M</i>	<i>1M, 3P</i>
41a	ChiralPak AD-H	<i>1M</i>	<i>1P</i>		
41b	ChiralPak AD-H	<i>3M</i>	<i>3P</i>		
42a	Lux Cellulose-2	<i>1P</i>	<i>1M</i>		
42b	Lux Cellulose-2	<i>3M</i>	<i>3P</i>		

5.2 Tetrasubstituted cyclopentadienones as suitable enantiopure ligands with axial chirality.³⁴

Over the last three decades the organic chemistry has been facing a continue and increasing demands of new, efficient and robust procedure to achieve enantiomerically pure compounds. The increasing demand comes in major instance from the life science related disciplines, where the absolute configuration of organic compound is intrinsically related to their biological activity. Various international entity such as FDA (Food and Drug Administration) or EMA (European Medical Agency) now require to any company submitting a licence request for a novel racemic Active Pharmaceutical Ingredient (API) to establish the activity of each enantiomer separately. Moreover, most of the drugs now present on the market are chiral and a large part of them are commercialized as single enantiomer. This imply the development of methods to obtain enantiopure molecules.

Nowadays three approaches exist to obtain pure enantiomers:

1) The use of natural chiral pool as reagents source to synthesize the target enantiomer. However, this method implies the perfect knowledge of the stereochemistry of the native natural product and the employment of reactions that do not imply racemization. 2) The resolution of racemic mixture. This procedure simplifies the synthesis of the desired product and enables the use of more efficient procedures. On the other hand, the separation of the enantiomers can be far from trivial, especially in a large scale production. In fact, most of the resolution are performed by co-crystallization with enantiopure chiral salt (*i.e.* citric acid, tartaric acid, mandelic acid) or with Chiral Stationary Phase (CSP) HPLC column. Both methods are time consuming, optimized by *trial and error* approach and in order to be sustainable, large purification apparatus are needed (as the simulated moving bed (SMB) for an industrial CSP-HPLC apparatus). 3) The asymmetric synthesis accomplishes the synthesis of the desired product with extremely high enantioselectivity and are usually performed by the use of enantiopure reagent or auxiliaries and a large amount of well-established methods are available.³⁵ Although this approach can be time consuming to optimize and with a restricted scope, the main advantages is the use of the enantiopure component with catalytic loading to produce large quantity of enantiopure molecules.

The role of the enantiopure catalyst is to generate a diastereomeric transition states energetically favoured over the others, thus generating an enantioselective reaction path. The extend of this stabilization is directly proportional to the enantio-selection.³⁶ The nature of the chiral auxiliary can be organic, metallo-organic³⁷ or enzymatic.³⁸

Although these catalyst are usually appealing in terms of turnover number and enantioselectivity the use of rare and expensive metal often limits their usage in industries. On this regard, both academia

and industries are striving to develop metallo-organic catalyst with common metals such as Fe or Zn. In this framework metallo-organic catalyst are now presenting a valuable option to scale up the production of enantiopure molecule.

In particular, during the synthesis design, transition-metal-mediated asymmetric hydrogenation represent a preferred way to introduce a stereogenic unit into the desired scaffold. In fact, this procedure can be easily applied to alkenes, imines, ketones using simply H₂ as reagent.³⁹ Over than a broad scope it is one of the asymmetric procedures with the highest reactivity, regio- and enantioselectivity and the lowest production of waste (generally it stoichiometrically produces H₂O as byproduct).

Unfortunately, the design of the metallo-organic compounds relies mostly on a *trial and error* approach. Since 1968, when Knowles and Horner⁴⁰ reported the first chiral version of the Wilkinson's Ruthenium catalyst, an incredibly wide number of chiral ligands have been successfully employed. In particular some of them represent (Figure 5.2.1) the forefathers of entire class of asymmetric metallo-organic ligands providing extremely valuable insights into ligand design. Among them can be noted two atropisomeric compounds.

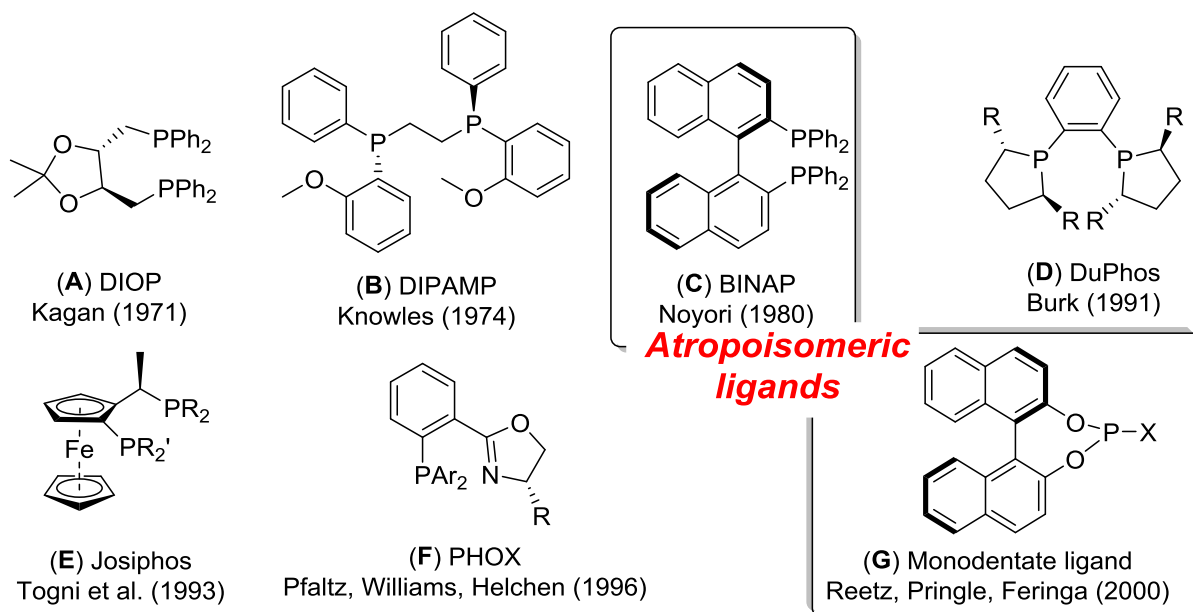


Figure 5.2.1 Important chiral ligands for asymmetric hydrogenation. C and G present a stereogenic axis.

The first in the time (C) designed by Noyori represented a major breakthrough because of the novel metal-ligand bifunctional system operating with ruthenium and an axially chiral 2,2'-bis(diphenylphosphino)-1,1'-binaphthyl (BINAP)⁴¹ that expand the scope of this asymmetric reaction from olefins to the carboxylic moieties either functionalized or not. Together with Knowles, Noyori were appointed the Nobel Prize in 2001 for its ground-breaking contribution to the field of asymmetric hydrogenation.

More recently also monodentate phosphorous atropisomeric molecules have proved that not only bidentate ligands can be valid candidates as enantiopure ligands in asymmetric reaction (Figure 5.2.1 **G**).⁴²

It is worth reminding that the difficulties into *a priori* design of the ligands are located to the fact that a simple energy difference of 2 kcal/mol between the two conceivable diastereomeric adduct metal-organic complex / substrate (transition states) can be responsible for a 95% enantiomer excess. The same activation barrier can be found in the rotation of the ethane, thus the prediction of what kind of ligand structures will be effective is far from predictable.

The use of phosphorous seems to be widespread in the asymmetric ligand design; its affinity relies on the electron availability in orbitals that easily overlap with second or third row transition metals. Recently, the use of less expensive transition metals is the only valuable option for the application in industry of the novel asymmetric organo-metallic catalyst. On this regard, the phosphorous ligands losses their attractiveness respect to their oxygen relatives. Moreover, atropisomeric ligands are well established as one of the most important classes of ligands for asymmetric metal catalyzed reactions.⁴³ In fact, oxygen related ligands are now taken in consideration (Figure 5.2.2). Namely, the Mn epoxidation catalyst **A** possesses two axially chiral binaphthyl subunits embedded in a sterically demanding backbone.⁴⁴ and more recently, attention has been focused on non- C_2 -symmetric biaryl compounds such as the tertiary aminophenol or binaphthylazepine structure (**B**), which catalyzes the enantioselective addition of diethylzinc to aldehydes.^{45,43d}

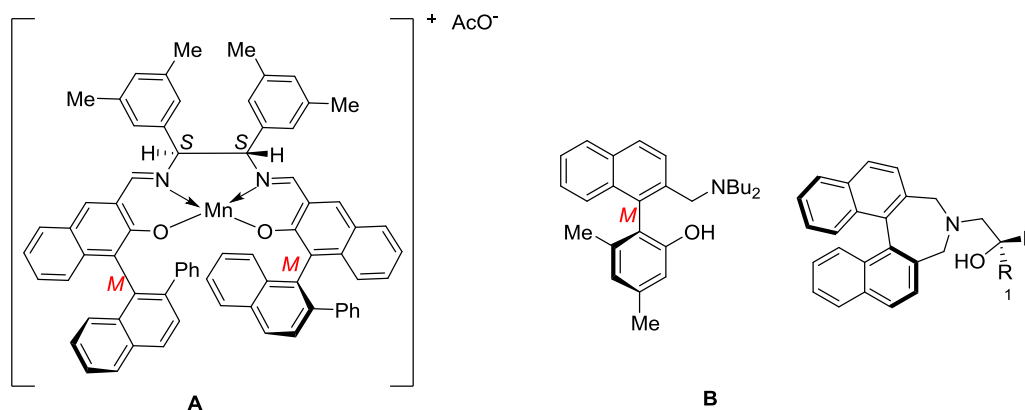


Figure 5.2.2 Axially chiral ligands without phosphorus used to perform asymmetric reactions with first row transition metals.

The Shvo catalyst has been extensively studied as hydrogenation catalyst (Figure 5.2.3 Top).⁴⁶ In this framework it represents, also for its good tolerance of first row transition metals, a valuable hydrogenation catalyst to become enantioselective with an appropriate enantiopure ligand. However, in the Shvo catalyst the election ligand is a tetraphenylcyclopentadienone where an ordinary stereogenic centre is difficult to be installed. As previously discussed atropisomeric ligands for the asymmetric hydrogenation was proved to be very effective, therefore the introduction of axial

chirality into the tetraphenylcyclopentadienone scaffold was a straightforward choice to introduce a stereogenic unit into this ligand. In fact, if any of the aryl rings lacks local C_2 symmetry and the rotation around the $C_{sp^2}-C_{sp^2}$ is frozen atropisomers arise and the ligand (and the derived metal-organic catalyst) becomes chiral.

However, the presence of one or more stereogenic axes can create geared mechanism that usually makes easier the rotation around the $C_{sp^2}-C_{sp^2}$ axis (the tetraphenylcyclopentadienone is already known to be a propeller-like motor).⁴⁷ To avoid this issue, the introduction of a 2',2'' bond between the two phenyl moieties in 4,5 positions of cyclopentadienone creates a planar and rigid phenanthrene framework fused with the cyclopentadienone that results in the formation of a so-called phencyclone (Figure 5.2.3 Bottom).⁴⁸ In this particular scaffold the aryl rings are skewed out of the planar core by 127.6° and 138.2° by the simple hindrance of the two ortho-hydrogen with the rigid framework as proved by the X-ray diffraction crystalline structure.⁴⁹

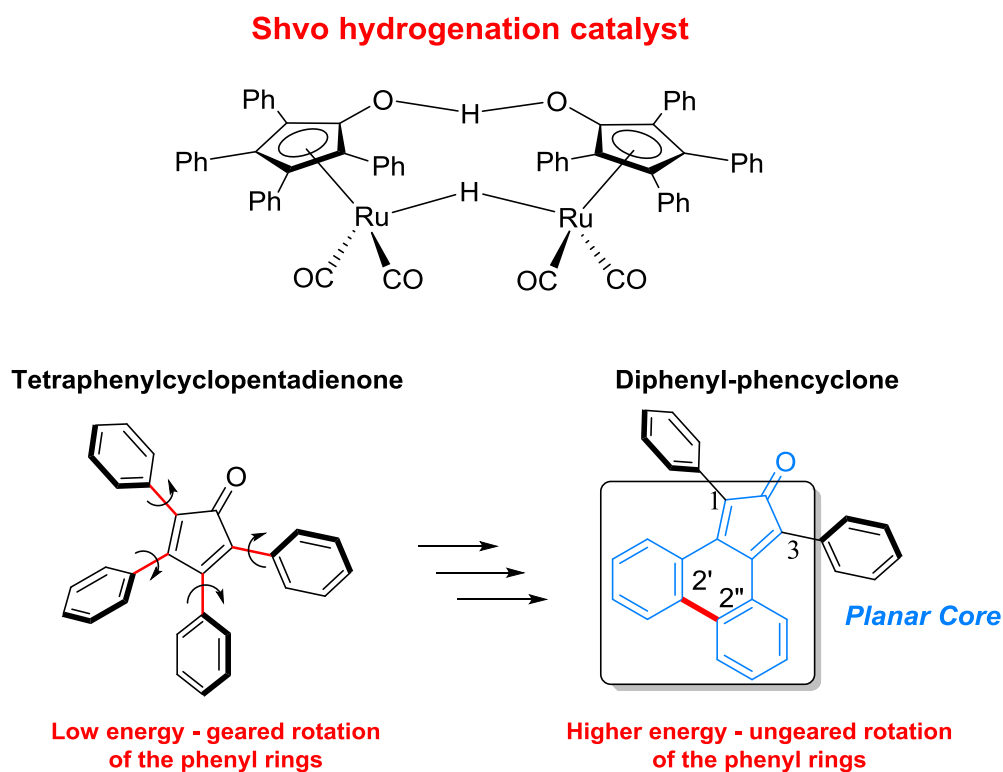


Figure 5.2.3 Top: Dimeric form of the Shvo hydrogenation catalyst. Bottom: Tetraphenylcyclopentadienone and diphenyl-phencyclone. In blue is highlighted the planar core of the phencyclone scaffold. [Reprinted (adapted) with permission from *Org. Biomol. Chem.* **2017**, *15*, 8720. Copyright (2017) Royal Society of Chemistry].

In order to evaluate the steric requirement to produce configurationally stable stereoisomers a DFT model was designed. The 1,3-di-*o*-tolyl-phencyclone **43a** structures was optimized at B3LYP/6-31G (Figure 5.2.4). This molecule carries two stereogenic axes on the 1 and 3 positions, however the *syn* conformation (M^*,P^*) where the two *ortho*-methyls are arranged on the same side with respect to the

phencyclone core, belongs to the C_s symmetry and it is an achiral *meso* form (Figure 1.2.5). On the other hand, the *anti* conformation (P^*,P^*) is a chiral structure that belongs to the C_2 symmetry group and thus two conformational enantiomers (P,P and M,M) are generated, which conformational stability relies on the entity of the rotational barrier of the ortho tolyl moieties.

As expected from the X-ray diffraction analysis on the diphenylphencyclone the DFT analysis suggested that the *o*-tolyl rings are not exactly perpendicular to the planar core. Thus, two dispositions of the aryl ring must be considered: they can conveniently be described as “*in*” conformation when the methyl of the *o*-tolyl is near the phenanthrene core and “*out*” conformation when the CH_3 is close to the carbonyl. Adding this to the presence of two asymmetric rings the conceivable conformations count to twelve, however they are halved by the *meso* combination of the *syn* conformer ending up with a total of six diastereoisomeric conformation (Figure 5.2.4). The DFT model considered all the conceivable conformer populated identifying the P^*,P^* (*anti*) *out-out* as the most stable.

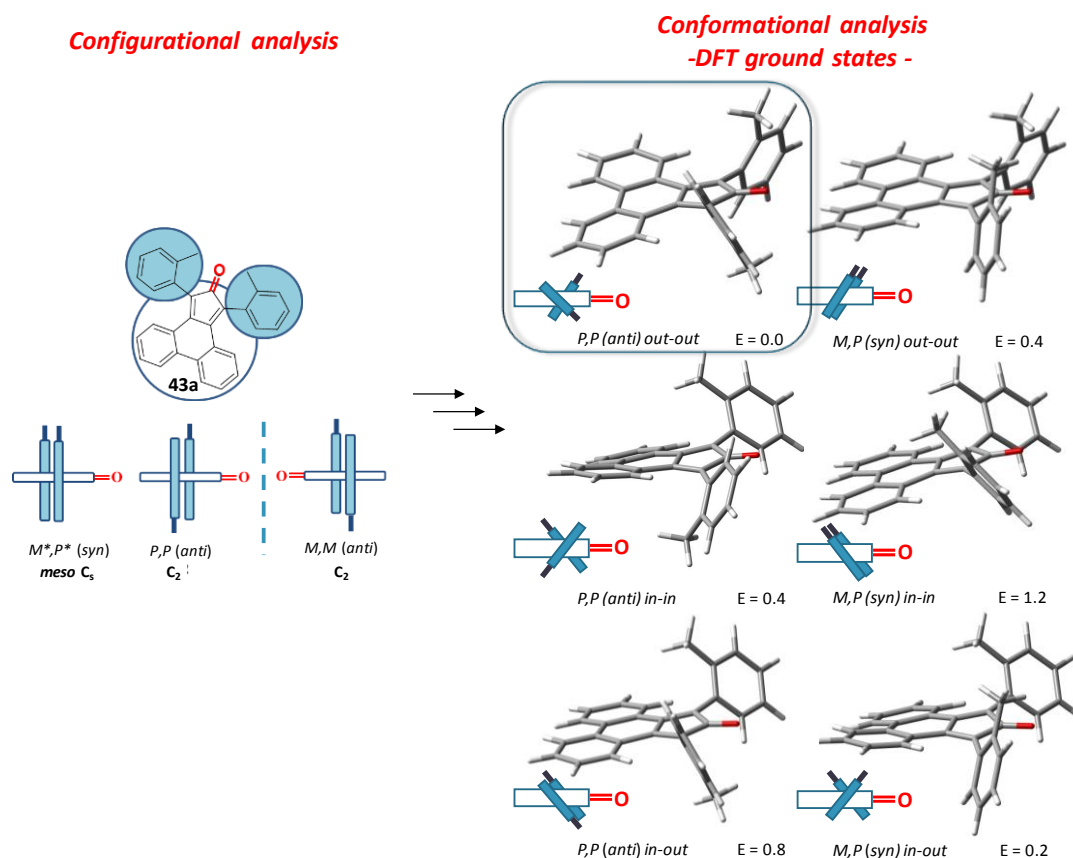


Figure 5.2.4 Left: 1,3-di-*o*-tolyl-phencyclone (**43a**) and side view of its *syn* and the *anti* conformers. Right: The six diastereoisomeric conformation of the ground states for 1,3-di-*o*-tolyl-phencyclone **43a** and their relative energy in kcal/mol. The P^*,P^* (*anti*) *out-out* conformer resulted the most stable. [Reprinted (adapted) with permission from *Org. Biomol. Chem.* **2017**, *15*, 8720. Copyright (2017) Royal Society of Chemistry].

To quantify the rotational barrier and thus the stability of the conformational stereoisomers the possible transition states energy must be calculated. The rotation about the $C_{sp^2}-C_{sp^2}$ of one *o*-tolyl moiety transforms the *anti* arrangement into the *syn*. This exchange is made possible through the

passage of the CH₃ moiety towards the phencyclone core (TS-180) or the carbonyl moiety (TS-0) (Figure 5.2.5). Computational analysis performed at B3LYP/6-31G(d) level of theory indicates that the most stable transition state rotates the methyl rotate towards the carbonyl (TS-0) with an estimated $\Delta G_{\text{rot}}^{\ddagger}$ of 17.9 kcal/mol (Table 5.2.1).

Although a barrier of this magnitude is easily detectable and measurable, the conformational stereoisomer produced are not stable, belonging to the Class 1 of LaPlante (see Paragraph 1.5, Figure 1.5.2). Therefore, to produce stable atropisomer more hindered system must be taken into account (**43b-e**, Figure 5.2.6), DFT analysis of such systems revealed that the barrier for **43d** and **43e**, with a 2-methyl-1-naphthyl as aryl substituent, should be sufficiently high ($\Delta G^{\ddagger} > 30$ kcal/mol) to obtain stable atropisomers at room temperature and above.¹

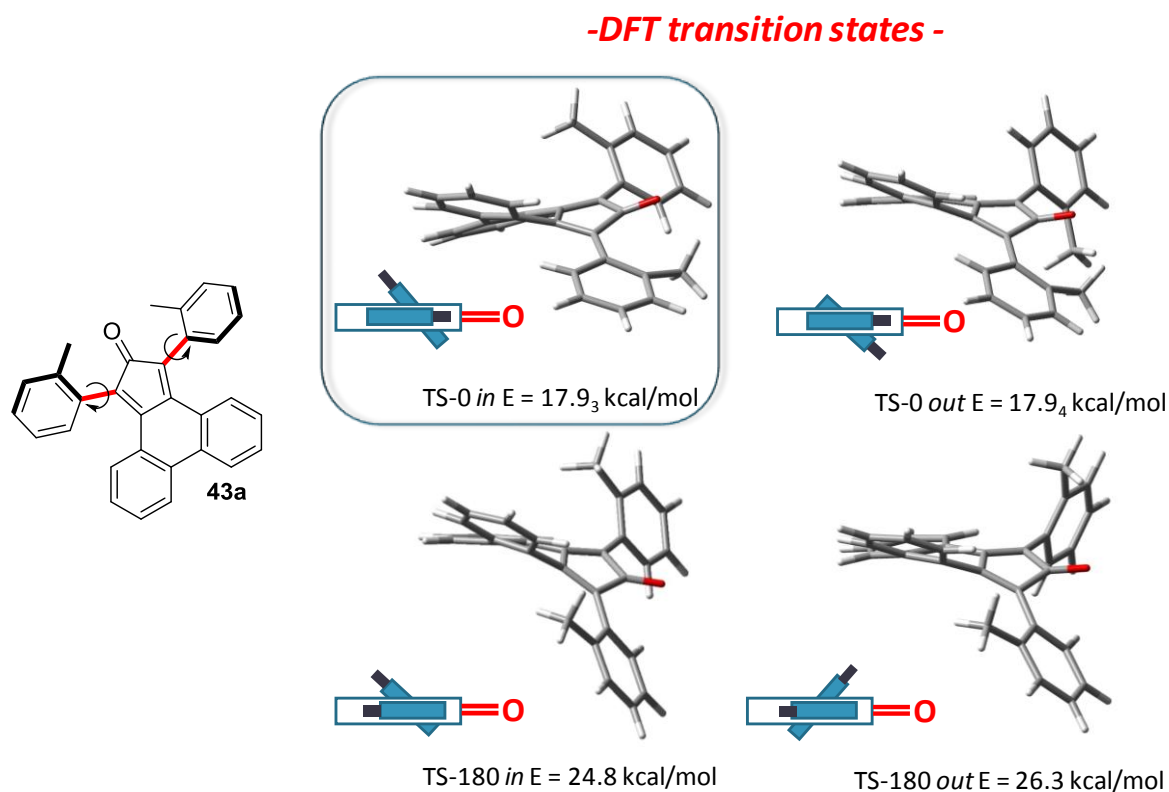


Figure 5.2.5 Transition states of **43a** optimized at B3LYP/6-31G(d) level of theory. [Reprinted (adapted) with permission from *Org. Biomol. Chem.* **2017**, *15*, 8720. Copyright (2017) Royal Society of Chemistry].

It is worth noting (Table 5.2.1) that other than the case when the aryl substituents are equivalent (**43a** and **43b**) or when there is only one stereogenic axis (**43e**), the phencyclone displays two distinct rotational barriers related to the independent rotation of each aryl substituents. The lowest barrier would be the diastereomerization barrier while the higher would racemize the system ($\Delta G_{\text{diast.}}^{\ddagger}$ and $\Delta G_{\text{enant.}}^{\ddagger}$ respectively).

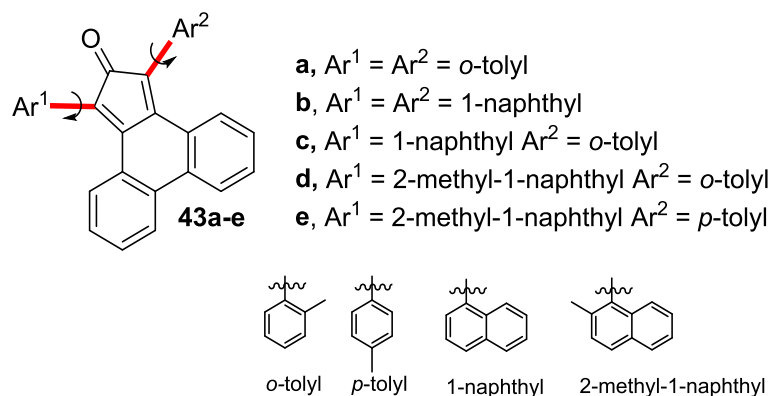


Figure 5.2.6 Phenacyclone derivatives (**43a-e**) considered during the DFT analysis. [Reprinted (adapted) with permission from *Org. Biomol. Chem.* **2017**, *15*, 8720. Copyright (2017) Royal Society of Chemistry].

To provide an experimental support to the DFT analysis the synthesis of compounds **43a-e** were performed. The synthetic approach involved a key-step double aldol condensation of the 9,10-phenanthrenequinone with a suitable 1,3-diaryl-propan-2-ones.

Table 5.2.1 Calculated energy barriers for rotation of the aryl substituents of compounds **43a-e**. In parenthesis is reported the geometry of the most stable transition state (values in kcal/mol at the B3LYP/6-31G(d) level of theory).

Compound	$\Delta G^{\ddagger}_{\text{diast}}$ (kcal/mol)	$\Delta G^{\ddagger}_{\text{enant}}$ (kcal/mol)
43a	17.9 (TS-0)	-
43b	19.6 (TS-0)	-
43c	17.7 (TS-0)	19.6 (TS-0)
43d	18.3 (TS-0)	31.8 (TS-0)
43e	31.1 (TS-0)	-

While 1,3-diphenyl-2-propanone is commercially available, the remaining ketones were synthesized following two different synthetic strategies: 1) sequential double Corey-Seebach reaction⁵⁰ on 1,3-dithiane with the appropriate benzyl derivatives, followed by mild deprotection with I₂/NaHCO₃;⁵¹ 2) opening of the appropriate epoxide with a Grignard reagent and catalysed by CuBr·S(CH₃)₂,⁵² followed by oxidation of the resulting alcohol performed with Dess-Martin periodane (DMP), Figure 5.2.7.

The X-ray diffraction on a single crystal of **43a** confirmed the geometries calculated by DFT calculation. The structure experimentally determined, in fact, displayed the so-called *anti in-in* disposition with both the methyl pointing towards the phenanthrene planar core, one of the most stable structure determined at B3LYP/6-31G(d) level of theory (Figure 5.2.8).

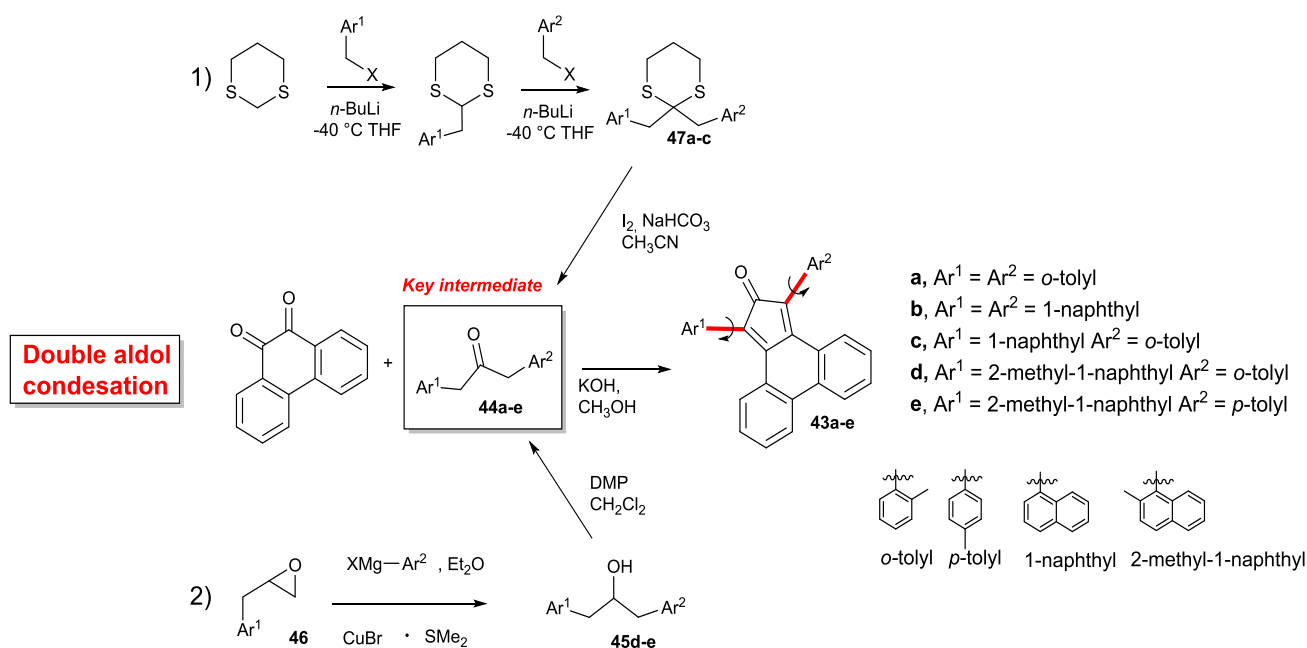


Figure 5.2.7 Synthetic pathways followed for the preparation of 1,3 diaryl-phencyclones **43a-e**. [Reprinted (adapted) with permission from *Org. Biomol. Chem.* **2017**, *15*, 8720. Copyright (2017) Royal Society of Chemistry].

It is worth mention that this structure is not the one foreseen as the most stable by DFT calculation (P^*, P^* (*anti*) *out-out*), this can be rationalized taking into account that the DFT calculations were run in gas phase while the X-ray analysis returns the most stable geometry in solid state where packing effect and other weak interaction plays an important role. Nonetheless the DFT hypothesis of not orthogonality of the *o*-tolyl rings was confirmed by the experimental X-ray data.

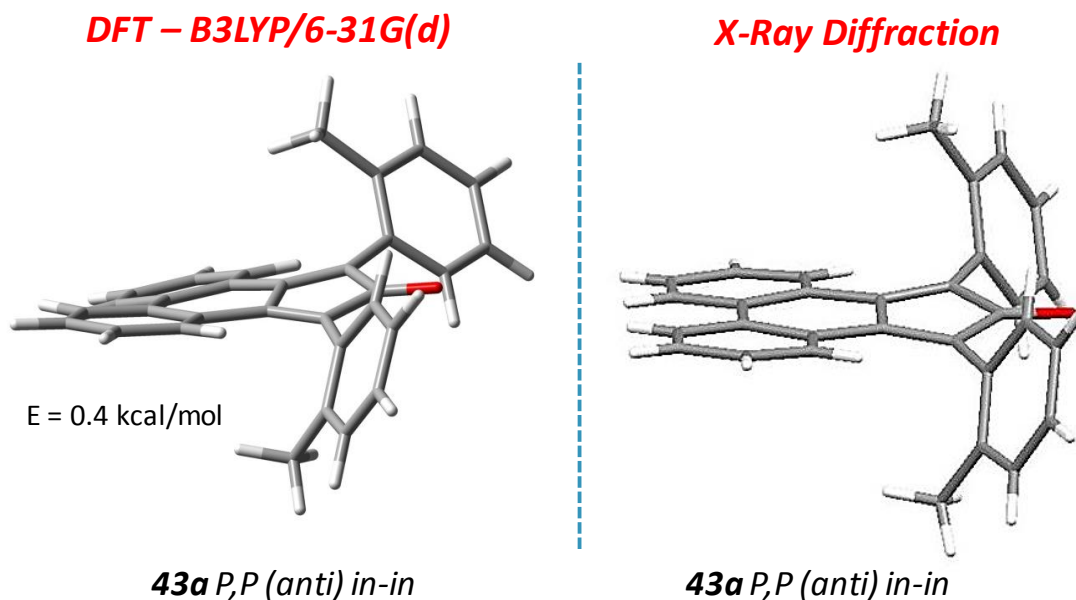


Figure 5.2.8 Compound **43a** P,P (*anti*) *in-in*. Left: Calculated structure (B3LYP/6-31G(d)). Right: X-Ray determined structure. [Reprinted (adapted) with permission from *Org. Biomol. Chem.* **2017**, *15*, 8720. Copyright (2017) Royal Society of Chemistry].

The rotational barrier can be evaluated with dynamic analysis such as D-HPLC and D-NMR. When both enantiomerization and diastereomerization barrier are present (**43c** and **43d**), the latter can be

used to determine the diastereomerization (*i.e.* the lowest) while the first (with CSP) is needed to evaluate the enantiomerization barrier.

Compound **43c** (1-(naphth-1-yl), 3-(*o*-tolyl)) bearing two different asymmetric aryl group in 1 and 3 position displays two distinct rotational barriers where the lowest is the one involved in the rotation of the *o*-tolyl as foreseen by DFT analysis, and the highest (by about 2.0 kcal/mol) rotates the 1-naphthyl (Table 5.2.2). The room temperature $^1\text{H-NMR}$ on this compound showed two well-resolved peaks, corresponding to the methyls of each diastereoisomer, P^*,P^* and M^*,P^* respectively. This is related to the sufficiently slow rotation of the aryl rings in the NMR time.

When a D-NMR analysis was performed on **43c** the aryl rings started to rotate faster until the diastereoisomers are no longer detectable by the NMR (*i.e.* when coalescence is reached) at +110 °C (Figure 5.2.9). The line shape simulation of the $^1\text{H-NMR}$ spectra recorded at different temperatures, allowed to determine the kinetic constant related to the diastereomerization process and the respective $\Delta G^\ddagger_{\text{rot}}$ by Eyring equation (21.2 kcal/mol, Table 5.2.2).

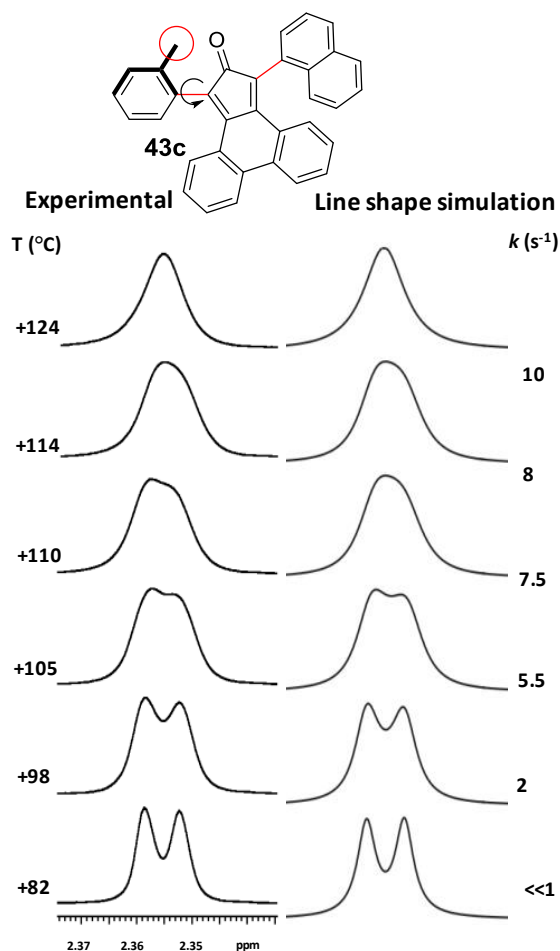


Figure 5.2.9 Left: ^1H NMR methyl signals of the two diastereoisomers of compound **43c** at different temperatures (600 MHz in $\text{C}_2\text{D}_2\text{Cl}_4$). Right: line shape simulations obtained with the corresponding rate constants. [Reprinted (adapted) with permission from *Org. Biomol. Chem.* **2017**, *15*, 8720. Copyright (2017) Royal Society of Chemistry].

Analogously, **43a** and **43d** were analysed by D-NMR (Figure 7.5.1) and the relative rotational barrier were determined.

Alternatively, the compound **43b** was more conveniently analysed by D-HPLC on achiral silica column (Figure 5.2.10 Left). The procedure involved a series of HPLC analysis at different temperature (+5 °C, 10 °C, 15 °C and 20 °C) to detect the evolution of the *syn/anti* exchange with the temperature. Likewise, the D-NMR analysis, is possible to determine the kinetic constant and the $\Delta G_{\text{rot}}^{\ddagger}$ by line shape simulation of the chromatograms (Figure 5.2.10 Left, red dotted line) and therefore the rotational energy barrier involved (21.1 kcal/mol).

When the HPLC trace of **43b** was recorded at +4 °C using CSP-HPLC, while the two *anti* enantiomers showed two opposite ECD bands (coupled to the UV-Vis chromatogram), the *syn* diastereoisomer, being a *meso* form, was straightforwardly identified by the lack of ECD signal (Figure 5.2.10 Right).

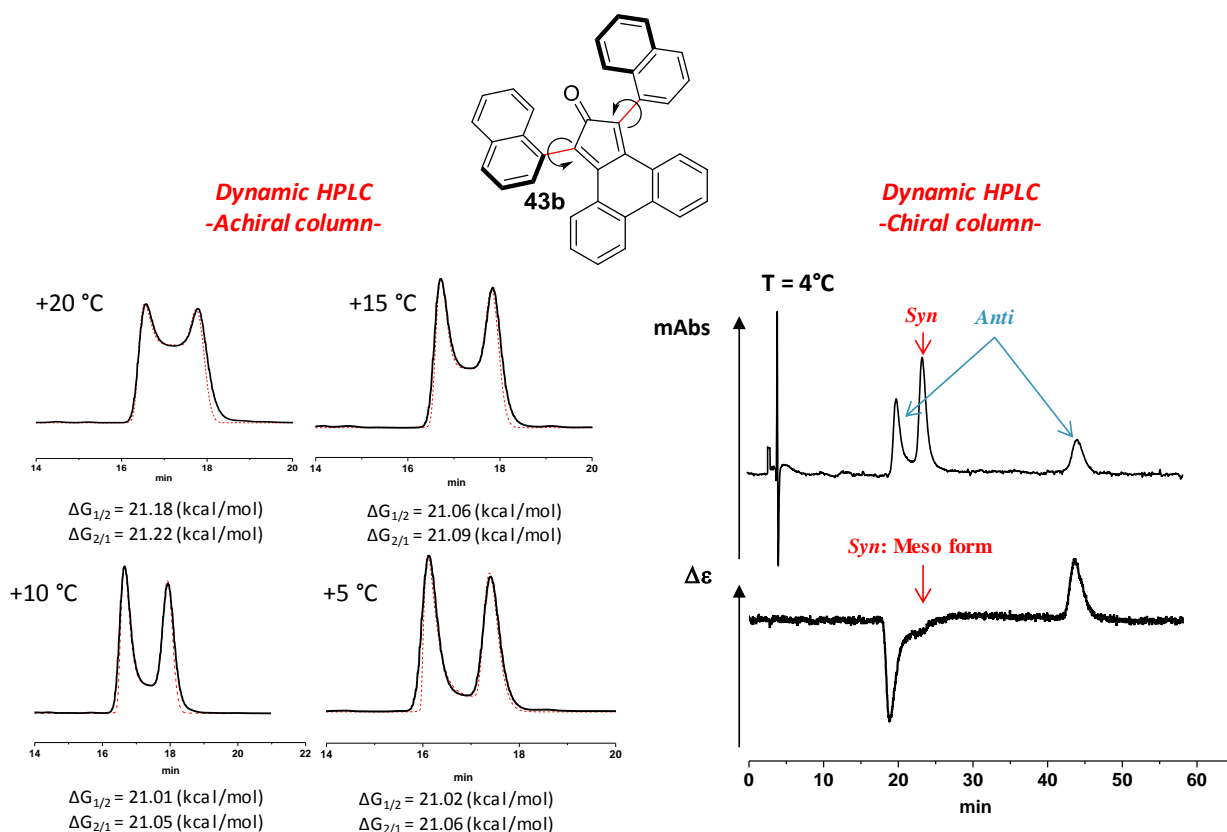


Figure 5.2.10 Left: Chromatogram of **43b** on Nova-pak Silica column, 6 μm , 19x300 mm, *n*-hexane/ CH_2Cl_2 92/8, 20 mL/min. Right: CSP-HPLC of **43b** at +4 °C (Chiralpak IA 250 x 4.6 mm eluent *n*-hexane/ CH_2Cl_2 98/2 + 0.05% EtOH, 1.0 mL/min, UV detection at 280 nm) and the relative ECD detection at 280 nm. [Reprinted (adapted) with permission from *Org. Biomol. Chem.* **2017**, 15, 8720. Copyright (2017) Royal Society of Chemistry].

The CSP-HPLC was used also to evaluate the highest rotational barrier (i.e. enantiomerization) of the compound **43c**, related to the rotation of the 1-naphthyl ring.

At room temperature, this rotation occurs partially during elution on CSP column showing an elution profile with two peaks with a plateau in between (Figure 7.5.2). To determine the enantiomerization barrier a lower temperature is therefore needed.

At -20 °C the chromatogram showed four peaks corresponding to the four stereoisomers as confirmed by the ECD profile, however the D-HPLC analysis cannot be performed with four interconverting peaks (Figure 7.5.3). Then, the dynamic analysis was performed in a temperature range where the rotation of *o*-tolyl is fast and therefore the system collapse into a simple couple of enantiomer of which is possible to determine the enantiomerization barrier related to the 1-naphthyl rotation by line shape simulation.

Compounds **43d** and **43e** presented a bulkier system such as the 2-methyl-1-naphthyl group and DFT analysis have foreseen that stable atropisomers would arise. CSP-HPLC chromatograms of **43d-e** showed two peaks related to the presence of an atropisomeric couple due to the hindered rotation of the 2-methyl-1-naphthyl aromatic substituent. The related ECD spectra of each eluted peaks showed the expected opposite profile (Figure 5.2.11).

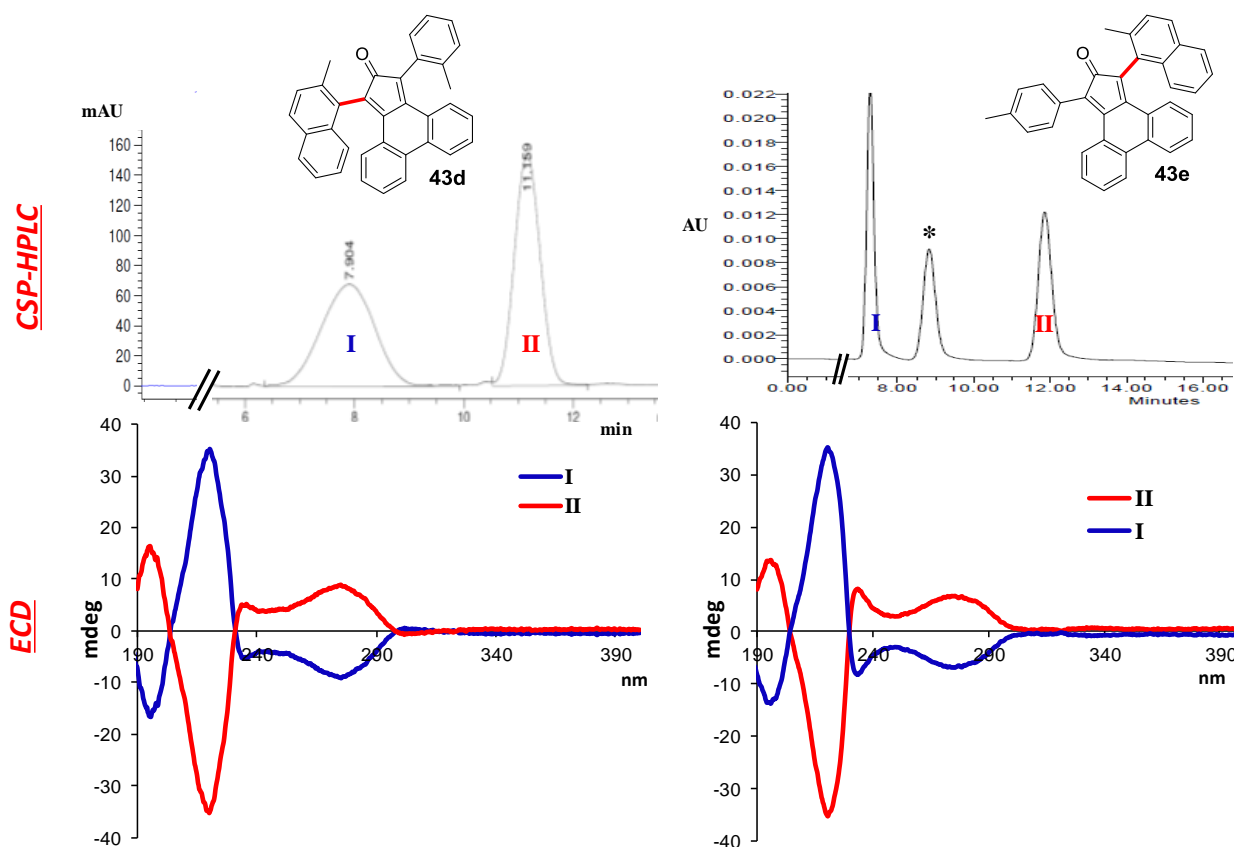
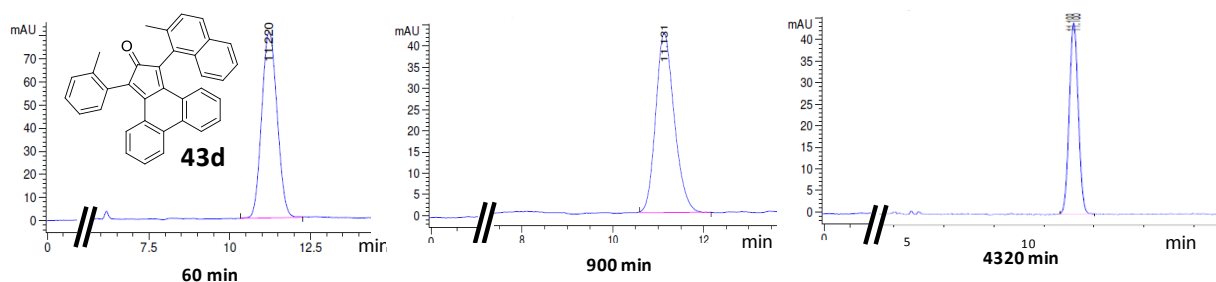


Figure 5.2.11 Top: Chromatogram of **43d** on CSP-HPLC (ChiralPak AD-H, *n*-hexane/*i*-PrOH, 92/8, +35 °C 1 mL/min) and **43e** (Chiral AD-H *n*-hexane/*i*-PrOH, 70/30 at +25 °C). Bottom: ECD spectra in acetonitrile of the relative atropisomers (first eluted in blue and the second eluted in red). * impurity. [Reprinted (adapted) with permission from *Org. Biomol. Chem.* **2017**, *15*, 8720. Copyright (2017) Royal Society of Chemistry].

Due to the high stability of the atropisomers of **43d-e** it was not possible to obtain the enantiomerization barrier with D-HPLC or D-NMR as previously performed for **43a-c** (compound **43d** was already analysed by D-NMR but to determine the barrier for the *o*-tolyl rotation, in other words the diastereomerization barrier). Once the atropisomers were physically separated on CSP-HPLC they were subjected to kinetic studies at high temperature (several hours at +147 °C in refluxing 1,1,2,2-tetrachloroethane) to evaluate the racemization barrier. Interestingly in these conditions, both **43d** and **43e** (Figure 5.2.12), did not undergo racemization, confirming the high energy barrier for racemization and the thermal stability of these compounds. From these data, it has been estimated a barrier larger than 35 kcal/mol. In fact, the racemization process can be described with a kinetic of the first order and so the half-life time ($t_{1/2}$) is independent from the concentration and is a function of the kinetic constant ($t_{1/2} = \ln 2/k$). A racemization barrier of 35 kcal/mol implies that at +147 °C the half-life time is 2154 min (~36h). In the case of **43d-e** the chromatograms did not show any trace of the second enantiomer after 48 hours at +147 °C, thus the real enantiomerization barrier is surely larger than 35 kcal/mol.

+147 °C



+147 °C

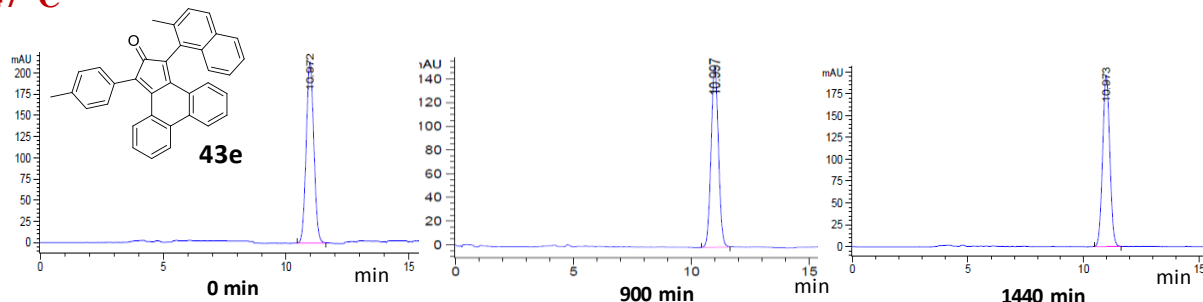


Figure 5.2.12 Chromatogram of enantiopure **43d** and **43e** eluted after having been left at +147 °C in $C_2D_2Cl_4$ for different times. (Chiral AD-H, *n*-hexane/*i*PrOH, 92/8, 1 mL/min for **43d** and Chiral AD-H *n*-hexane/*i*-PrOH, 70/30 at +25 °C for **43e**).

A close inspection of the experimentally determined rotational barrier of compounds **43a-e** revealed a difference in the ΔG_{rot}^\ddagger of **43a** with respect to **43c** and **43d** related to the rotation of the same aryl group (*i.e.* *o*-tolyl group) (Table 5.2.2). This apparent contradiction has to be attributed to a statistical effect. In compounds **43c** and **43d**, that have different substituent in 1 and in 3 position the diastereomerization takes place with the rotation of the unique *o*-tolyl ring. On the contrary, the compound **43a** has the *o*-tolyl in both 1 and 3 positions and the diastereomerization process that can

occur by rotation of one of the two *o*-tolyl rings. This doubles the probability to rotate an aryl group and so doubles the experimental rate constant, thus it lowers the related diastereomerization barrier by ≈ 0.5 kcal/mol ($RT \ln 2$ at the coalescence temperature). Considering this effect, the energy to rotate an *o*-tolyl ring is the same in **43a**, **43c** and **43d**. The analogous effect occurs for the energy barrier related to the rotation of 1-naphthyl in **43b** and **43c**, when the molecule is symmetric (**43b**) it shows a lower experimental barrier with respect to the asymmetric one (**43c**).

Compounds **43d-e** displayed a racemization barrier over the 35 kcal/mol generating highly stable atropisomers. Even if each enantiomer has been separated the absolute configuration (AC) of each one of them is not straightforwardly determined.

Table 5.2.2 Calculated and experimental diastereoisomeric ratio and calculated and experimental energy barriers for rotations of aryl substituents of phencyclones **43a-e** (values in kcal/mol at the B3LYP/6-31G(d) level of theory).

Compd.	<i>d.r.</i> (<i>P</i> *, <i>P</i> *: <i>P</i> *, <i>M</i> *) Calc./Exptl.	Diastereomerization		Enantiomerization	
		ΔG^\ddagger calc.	ΔG^\ddagger exp.	ΔG^\ddagger calc.	ΔG^\ddagger exp.
43a	57:43 / 50:50	17.9	20.7 \pm 0.3 ^a	-	-
43b	69:31 / 52:48	19.6	21.1 \pm 0.2 ^b	-	-
43c	52:48 / 51:49	17.7	21.2 \pm 0.3 ^a	19.6	21.7 \pm 0.2 ^b
43d	53:47 / 52:48	18.3	21.2 \pm 0.3 ^a	31.8	$\geq 35^c$
43e	-	-	-	31.1	$\geq 35^c$

^a by D-NMR analysis; ^b by D-HPLC analysis; ^c Kinetic studies;

The classical approach using X-ray diffraction of the single enantiomer cannot be used in the determination of the AC of **43d-e** due to the lack of suitable heavy atoms. Then to determine the AC was chosen the ECD method. This procedure consists as discussed in Paragraph 2.5.2, in the comparison of computed ECD spectra (TD-DFT method) with the one experimentally recorded for each enantiomer.

To correctly compute the ECD for each enantiomer is necessary to determine the populations of the ground state conformations. In fact, the overall spectrum is generated by combination of the ECD spectra of the single conformers weighted by their relative stability. The four conformers of **43d** are related to the possibility of the *o*-tolyl: 1) to arrange itself on the same side (*syn*) or on the opposite side (*anti*) respect to the orthogonal 2-methyl-1-naphthyl, and 2) to dispose in the “*in*” or “*out*” conformation. Each of these conformations is populated and their calculated ECD at CAM-B3LYP, BH&HLYP, M06-2X and ω B97XD / 6-311++G(2d,p) level of theory are reported in Figure 5.2.13 Top. The weighted ECD spectra calculated for the *M* configuration of the stereogenic axis is then compared to the experimental one relative to the second eluted enantiomer (Figure 5.2.13 Bottom).

The good superimposition of the experimental spectrum to the computed ones lead straightforwardly to the assign the *M* configuration to the second eluted enantiomer of **43d**.

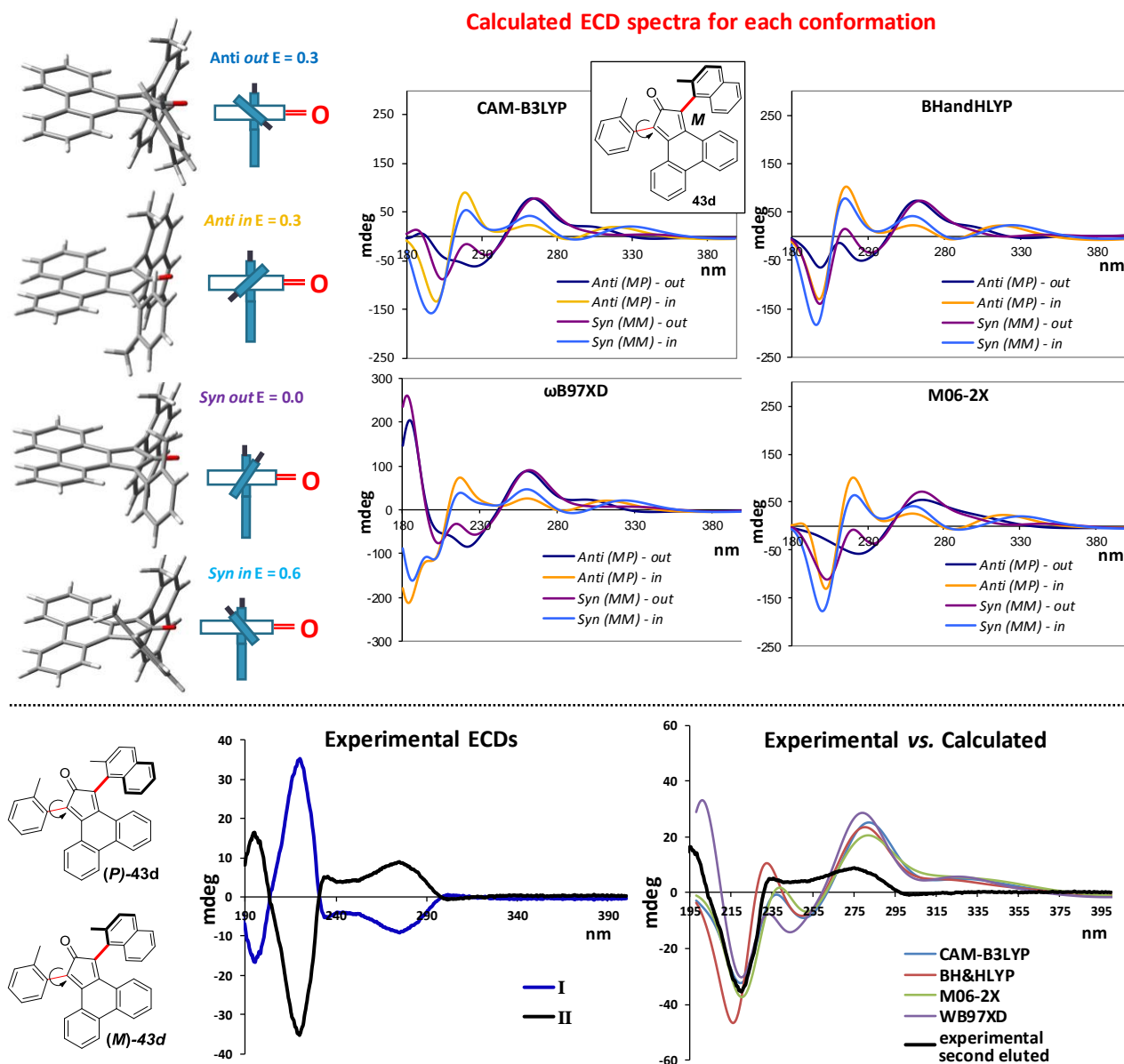


Figure 5.2.13 Top: Computed spectra (at CAM-B3LYP, BHandHLYP, M06-2X, ωB97XD / 6-311++G(2d,p) level of theory) for the four stable ground states of *M,P** atropisomer of **43d**. The conformations were red-shifted by 18 nm and scaled of a 0.4 factor in mdeg. Bottom: Experimental and calculated ECD spectra of the second eluted atropisomer of **43d**, obtained with four functionals: CAM-B3LYP (blue), BH&HLYP (red), M06-2X (green), ωB97XD (purple). [Reprinted (adapted) with permission from *Org. Biomol. Chem.* **2017**, *15*, 8720. Copyright (2017) Royal Society of Chemistry].

For **43e** the AC was assigned analogously. However, in this case the computed ECD spectrum is simplified by the fact that there are only two conformations populated generated by the *in* or *out* disposition of the *para*-tolyl (due to the local symmetry of the *p*-tolyl group the *syn* and *anti* conformers does not exist) (Figure 5.2.14).

The analysis of the stereodynamic of a series of phencylones derivative **43a-e** has led to the determination of the steric requirement needed to produce stable enantiomers carrying stereogenic

axes **43d-e**. The computations (DFT and TD-DFT methods) supported the rotational barriers experimentally evaluated and enabled the assignment of the absolute configuration of the stable axially chiral enantiomers. The latter can be used as chiral modification of the classic tetraphenylcyclopentadienone ligand of the Ruthenium based Shvo catalyst in order to perform asymmetric hydrogenations. Even though the design of the atropisomers **43d-e** came from this particular catalyst, the cyclopentadienone moiety allows these brand new molecules to be used as ligand for a wider number of organo-metallic systems.

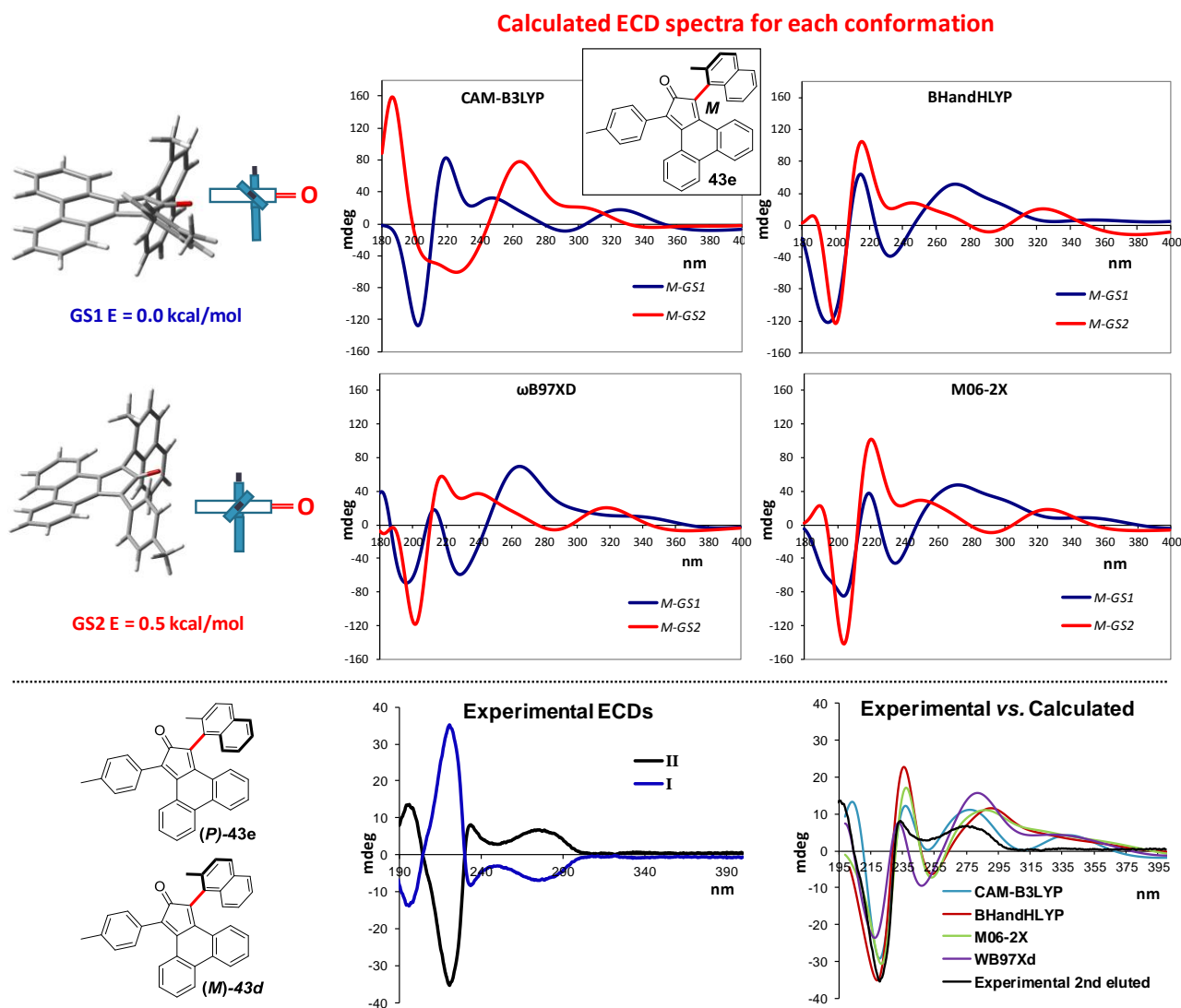


Figure 5.2.14 Top: Computed spectra (at CAM-B3LYP, BHandHLYP, M06-2X, ω B97XD / 6-311++G(2d,p) level of theory) for the two stable ground states of *M* atropisomer of **43e**. the simulated spectra were red-shifted by 18 nm, 21 nm, 18 nm, 18 nm for CAM-B3LYP, BH&HLYP, M06-2X, ω B97XD, respectively, and scaled of a 0.3 factor in mdeg for all the functionals. Bottom: Experimental and calculated ECD spectra of the second eluted atropisomer of **43d**, obtained with four functionals: CAM-B3LYP (blue), BH&HLYP (red), M06-2X (green), ω B97XD (purple). [Reprinted (adapted) with permission from *Org. Biomol. Chem.* **2017**, *15*, 8720. Copyright (2017) Royal Society of Chemistry].

References

- ¹ Oki M. *Top. Stereochem.* **1984**, *14*, 1–81.
- ² Mancinelli M., Perticarari S., Prati L., Mazzanti A. *J. Org. Chem.* **2017**, *82*, 6874–6885.
- ³ Waldmeier P. C., Baumann P. A., Hauser K., Maitre L., Storni A. *Biochem. Pharmacol.*, **1982**, *31*, 1653–1663.
- ⁴ Lovell R. A., Freedman D. X. *Mol. Pharmacol.* **1976**, *12*, 620–630.
- ⁵ Martino-Barrows A. M., Kellar K. J. *Mol. Pharmacol.* **1987**, *39*, 751–757.
- ⁶ Easson L. H., Stedman E. *Biochem J.* **1933**, *27*, 1257–1266.
- ⁷ Beckett A.H. *Stereochemical factors in biological activity*. In: Jucker E., editor. *Fortschritte der arzneimittel forschung*, Basel: Birkhäuser Verlag, **1959**, vol. I., 455–530.
- ⁸ Pfeiffer C. C. *Science* **1956**, *124*, 2931.
- ⁹ Barlow R. B. *Trends Pharmacol Sci.* **1990**, *11*, 14850.
- ¹⁰ Casy A. F. *Stereochemistry and biological activity*. In: Burger A., editor. *Medicinal chemistry*, New York: Wiley-Interscience, **1970**, vol. 1. 81107.
- ¹¹ Schröder E., Rufer C., Schmiechen R. *Arzneimittelchemie [Pharmacological chemistry]*, Stuttgart: Georg Thieme Verlag; **1976**, vol. 1., 48 [in German].
- ¹² Benson W. M., Stefko P. L., Randall L. O. *J. Pharmacol Exptl Therap* **1953**, *109*, 189200.
- ¹³ Drayer D. E. *Clin Pharmacol Ther* **1986**, *40*(2), 12533.
- ¹⁴ Bullock M. W., Hand J. J., Waletzky E. *J Med Chem.* **1968**, *11*, 1697.
- ¹⁵ Remy D. C., Rittle K. E., Hunt C. A., Anderson P. S., Engelhardt E. L., Clineschmidt B. V. *J Med Chem.* **1977**, *20*, 16814.
- ¹⁶ (a) Shimizu K. D., Freyer H. O., Adams R. D. *Tetrahedron Lett.* **2000**, *41*, 5431–5434; (b) Bennett D. J., Pickering P. L., Simpkins N. S. *Chem. Commun.* **2004**, 1392–1393.
- ¹⁷ (a) Kitagawa O., Fujita M., Kohriyama M., Hasegawa H., Taguchi T. *Tetrahedron Lett.* **2000**, *41*, 8539–8544; (b) Bennett D. J., Blake A. J., Cooke P. A., Godfrey C. R. A., Pickering P. L., Simpkins N. S., Walker M. D., Wilson C. *Tetrahedron* **2004**, *60*, 4491–4511; (c) Kitagawa O., Yoshikawa M., Tanabe H., Morita T., Takahashi M., Dobashi Y., Taguchi T. *J. Am. Chem. Soc.* **2006**, *128*, 12923–12931.
- ¹⁸ (a) Yilmaz E. M., Doğan İ. *Tetrahedron: Asymmetry* **2008**, *19*, 2184–2191; (b) Oppenheimer J., Hsung R. P., Figueroa R., Johnson W. L. *Org. Lett.* **2007**, *9*, 3969–3972.
- ¹⁹ a) Ciogli A., Kumar S. V., Mancinelli M., Mazzanti A., Perumal S., Severi C., Villani C. *Org. Biomol. Chem.* **2016**, *14*, 11137–11147; (b) Roussel C., Adjimi M., Chemplal A., Djafri A. *J. Org. Chem.* **1988**, *53*, 5076–5080; (c) Belot V., Farran D., Jean M., Albalat M., Vanthuyn N., Roussel C. *J. Org. Chem.* **2017**, *82*, 10188–10200.
- ²⁰ a) Faigl F., Fogassy K., Szucs E., Kovacs K., Keseru G. M., Harmat V., Bocskei Z., Toke L. *Tetrahedron*, **1999**, *55*, 7881; b) Vorkapic-Furac J., Mintas M., Burgemeister T., Mannschreck A., *J. Chem. Soc., Perkin Trans.*, **1989**, *2*, 713.
- ²¹ Mino T., Tanaka Y., Hattori Y., Yabusaki T., Saotome H., Sakamoto M., Fujita T. *J. Org. Chem.*, **2006**, *71*, 7346.
- ²² Frideling A., Faure R., Galy J. P., Kenz A., Alkorta I., Elguero J, *Eur. J. Med. Chem.*, **2004**, *37*, 39.
- ²³ Marubayashi N., Ogawa T., Moriwaki M., Hatake M. *Chem. Pharm. Bull.*, **1992**, *49*, 220.
- ²⁴ Oğuz S. F., Doğan İ. *Tetrahedron: Asymmetry* **2003**, *14*, 1857–1864.
- ²⁵ Kelly C. J. *American Journal of Clinical Nutrition*, **2005**, *82*, 486.
- ²⁶ He R., Ching S. M., Lam Y. *J. Comb. Chem.* **2006**, *8*, 923–928.
- ²⁷ a) Bridson P. K., Wang X. *Synthesis*, **1995**, 855–858; b) He R., Lam Y. *J. Comb. Chem.* **2005**, *7*, 916–920; c) Zavialov I. A., Dahanukar V. H., Nguyen H., Orr C., Andrews D. R. *Organic Letters* **2004**, *6*, 2237–2240.
- ²⁸ Fuchs H., Gottlieb M., Pfeleiderer W. *Chemische Berichte*, **1978**, *111*, 982–995.
- ²⁹ Busschaert N., Kirby I. L., Young S., Coles S. J., Horton P. N., Light M. E., Gale P. A. *Angew. Chem. Int. ed.*, **2012**, *51*, 4426–4430.
- ³⁰ Whithely M.A., *J. Chem. Soc.* **1907**, *91*, 138–139.
- ³¹ Lunazzi L., Mancinelli M., Mazzanti A., Lepri S., Ruzziconi R., Schlosser M. *Org. Biomol. Chem.* **2012**, *10*, 1847–1855.
- ³² Chiarucci M., Ciogli A., Mancinelli M., Ranieri S., Mazzanti A. *Angew. Chem. Int. Ed.* **2014**, *53*, 5405–5409.
- ³³ Berova N., Di Bari L., Pescitelli G. *Chem. Soc. Rev.* **2007**, *36*, 914–93.
- ³⁴ Prati L., Mancinelli M., Ciogli A., Mazzanti A. *Org. Biomol. Chem.* **2017**, *15*, 8720.
- ³⁵ (a) Izumi Y., Tai A. *Stereo-Differentiating Reactions: The Nature of Asymmetric Reactions*, Academic Press: New York, **1977**; (b) Bosnich B., Ed. *In Asymmetric Catalysis*; Nijhoff M.: New York, **1986**; (c) Ojima I., Ed. *In Catalytic Asymmetric Synthesis*; VCH: New York, **1993**; (d) Brunner H., Zettlmeier W. *Handbook of Enantioselective Catalysis*; VCH: Weinheim, **1993**; (e) Jannes G., Dubois V., Eds. *In Chiral Reactions in Heterogeneous Catalysis*; Plenum: New York, **1995**; (f) Cornils B., Herrmann W. A., Eds. *In Applied Homogeneous Catalysis with Organometallic Compounds*; VCH: Weinheim, **1996**, Vols. 1–2; (g) Beller M., Bolm C., Eds. *In Transition Metals for Organic Synthesis: Building Blocks and Fine Chemicals*; Wiley-VCH: Weinheim, **1998**, Vols. 1–2; (h) Jacobsen E. N., Pfaltz A., Yamamoto H., Eds. *In Comprehensive Asymmetric Catalysis*; Springer: Berlin, **1999**, Vol. 3; (i) Tombo G. M. R., Belluš D. *Angew. Chem., Int. Ed. Engl.* **1991**, *30*, 1193; (j) Cornils B., Herrmann W. A., Rasch M. *Angew. Chem., Int. Ed. Engl.* **1994**, *33*, 2144;

- (k) Herrmann W. A., Cornils B. *Angew. Chem., Int. Ed. Engl.* **1997**, *36*, 1048. (l) Keim W. In: *Transition Metals for Organic Synthesis: Building Blocks and Fine Chemicals*; Beller M., Bolm C., Eds.; Wiley- VCH: Weinheim, **1998**, Vol. 1, 14.
- ³⁶ Morrison J. D., Mosher M. S. *Asymmetric Organic Reaction*, American Chemical Society, Washington DC, **1976**, 35-49.
- ³⁷ For some reviews, see: (a) Kitamura M., Noyori R. In *Modern Synthetic Methods*; Scheffold, R., Ed.; Springer-Verlag: Berlin, **1989**, Vol. 5, 116-199; (b) Noyori R. In *Asymmetric Catalysis in Organic Synthesis*; Wiley: New York, **1994**; (c) Ojima I., Ed. *Catalytic Asymmetric Synthesis*, 2nd ed.; Wiley: New York, **2000**; (d) Jacobsen E. N., Pfaltz A., Yamamoto H., Eds. *Comprehensive Asymmetric Catalysis*; Springer: Berlin, **1999**, Vol. 1; (e) Brunner H. In *Topics in Stereochemistry*; Eliel E., Wilen S. H., Eds.; Wiley: New York, **1988**; Vol. 18, 129; (f) Seyden-Penne J. *Chiral Auxiliaries and Ligands in Asymmetric Synthesis*; Wiley: New York, **1995**; (g) Lin G. Q., Li Y. M., Chan A. S. C. *Principles and Applications of Asymmetric Synthesis*; Wiley: New York, **2001**; (h) Noyori R., Ohkuma T. *Angew. Chem., Int. Ed.* **2001**, *40*, 40.
- ³⁸ Wong C. H., Whitesides G. M. *Enzymes in synthetic Organic Chemistry*, Pergamon: Oxford, **1994**.
- ³⁹ (a) Tang W., Zhang X. *Chem. Rev.* **2003**, *103*, 3029–3069; (b) Zhang Z., Qian H., Longmire J., Zhang X. *J. Org. Chem.* **2000**, *65*, 6223-6226; (c) Wang S., Li J., Miao T., Wu W., Li Q., Zhuang Y., Zhou Z., Qiu L. *Org. Lett.* **2012**, *14*(8), 1966-1969.
- ⁴⁰ Knowles W. S., Sabacky M. J. *Chem. Commun.* **1968**, 1445–1446; (b) Horner L., Siegel H., Buthe H. *Angew. Chem., Int. Ed.* **1968**, *7*, 942.
- ⁴¹ (a) Noyori R., Ohkuma T. *Angew. Chem., Int. Ed.* **2001**, *40*, 40–73; (b) Noyori R. *Angew. Chem., Int. Ed.* **2002**, *41*, 2008–2022.
- ⁴² (a) Claver C., Fernandez E., Gillon A., Heslop K., Hyett D. J., Martorell A., Orpen A. G., Pringle P. G. *Chem. Commun.* **2000**, 961–962; (b) Reetz M. T., Mehler G. *Angew. Chem., Int. Ed.* **2000**, *39*, 3889–3890; (c) van den Berg M., Minnaard A. J., Schudde E. P., van Esch J., de Vries A. H. M., de Vries J. G., Feringa B. L. *J. Am. Chem. Soc.* **2000**, *122*, 11539–11540.
- ⁴³ a) Rosini C., Franzini L., Raffaelli A., Salvadori P. *Synthesis* **1992**, 503; (b) Clayden J., Johnson P., Pink J. H., Helliwell M. *J. Org. Chem.* **2000**, *65*, 7033-7040; (c) Clayden J., *Angew. Chem. Int. Ed Engl* **1997**, *36*(9), 949-951; (d) Superchi S., Mecca T., Giorgio E., Rosini C. *Tetrahedron: Asymmetry* **2001**, *12*, 1235–1239.
- ⁴⁴ Sasaki H., Irie R., Hamada T., Suzuki K., Katsuki T. *Tetrahedron* **1994**, *50*, 11827-11838.
- ⁴⁵ Bringmann G., Breuning M. *Tetrahedron: Asymmetry* **1998**, *9*, 667-679.
- ⁴⁶ Conley B. L., Pennington-Boggio M. K., Boz E., Williams T. J. *Chem. Rev.*, **2010**, *110*, 2294.
- ⁴⁷ a) Brydges S., McGlinchey M. J., *J. Org. Chem.*, **2002**, *67*, 7688; (b) Kottas G.S., Clarke L. I., Horinek D., Michl J. *Chem. Rev.*, **2005**, *105*, 1281; (c) Wolf C., “Dynamic Stereochemistry of Chiral Compounds: Principles and Applications”, RSC publishing, Cambridge, UK **2008**, *8*, 405.
- ⁴⁸ Ogliaruso M. A., Romanelli M. G., Becker E.I. *Chem. Rev.*, **1965**, *65*, 261.
- ⁴⁹ Ruffani A., Schwarzer A., Weber E. *Acta Cryst. E*, **2006**, *E62*, 2281.
- ⁵⁰ Seebach D., Corey E. J. *J. Org. Chem.*, **1975**, *40*, 231.
- ⁵¹ Geum S., Lee H. Y., *Org. Lett.*, **2014**, *16*, 2466.
- ⁵² Marotta E., Baravelli M., Maini L., Righi P., Rosini G. *J. Org. Chem.*, **1998**, *63*, 8235.

6 Appendix

6.1 Study of 1,8 naphthalene derivatives as sensors for nucleobases and chiral primary amine

The development of time-efficient and cost-effective stereoselective assays is essential in high-throughput screening (HTS).¹ In particular it can be applied in chiral reactions in order to determine: 1) the enantiopurity and stereochemical integrity, 2) the best parameters of asymmetric reactions and 3) the enantiomeric excess. Enantioselective sensing based on fluorescence spectroscopy offers a variety of advantages over NMR spectroscopy with chiral shift reagents and chiral chromatography, such as different detection modes (fluorescence quenching, enhancement, or lifetime), high sensitivity, low cost of instrumentation, waste reduction, time efficiency, and the possibility of performing real-time analysis.

Because of the high sensitivity inherent to fluorescence spectroscopy, only a very small amount of the sensor is required, which makes this technique a cost-effective and practicable alternative. To date, only few enantioselective fluorescence sensor,² including chiral macrocycles,³ dendrimers,⁴ and oligomers,⁵ have been reported.

6.1.1 Nucleobases sensing

Nucleobases are important biological structural motif and moreover their analogous have also biological activity (*i.e.* xanthine, Paragraph 5.1). Therefore, in the framework of HTS has become urgent a method to easily quantify the nucleobases present in a particular sample.

In the development of a nucleobases sensor the first step to take in consideration is the molecular design. This should incorporate:

1. a functional group able to interact with the substrate, preferentially through H-bonding;
2. a transmitter that have optical properties relatively easy to detect, like a fluorophore;
3. a rigid scaffold that arranges the transmitter and the functional group one next to the other, preferentially with a π -stacking interaction.

The designs take in consideration a naphthalene scaffold substituted in 1 and 8 positions, bearing the transmitter and the functional group (Figure 6.1.1). The functional group chosen to interact with the nucleobases is a nucleobase itself and in particular an adenine was chosen. The transmitter is a large asymmetric aromatic system that can undergo to π stacking with the adenine or the substrate. The spacer chosen allows freely conjugation between the naphthalene scaffold and the transmitter and, moreover a relatively degree of freedom for the rotation of the transmitter.

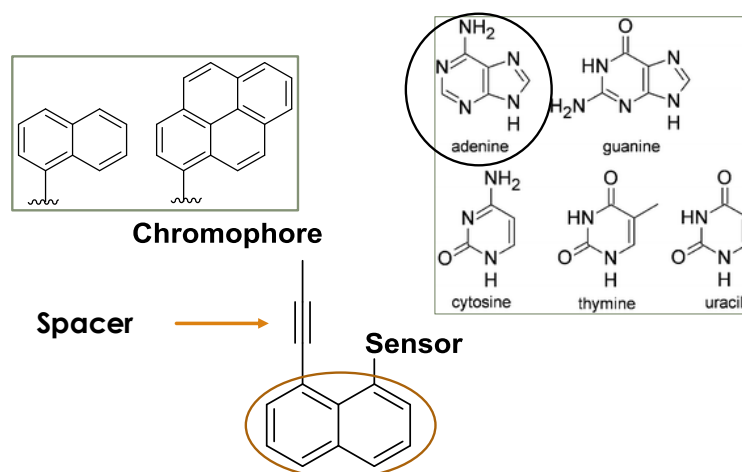


Figure 6.1.1 Molecular designs of the nucleobase sensors

The design developed was firstly tested *in silico* with the geometry optimization performed through DFT method (B3LYP/6-31g(d), Figure 6.1.2). This procedure was developed in order to verify the potential of the molecule to interact with nucleobases.

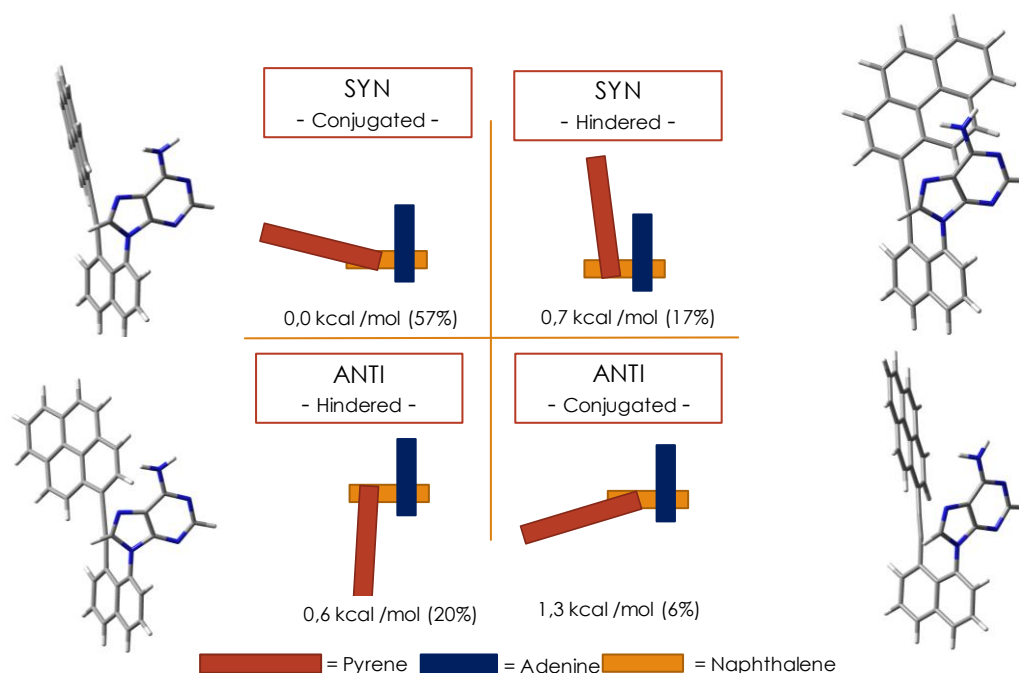


Figure 6.1.2 Ground states of pyrene sensor studied at B3LYP/6-31g(d) level of theory

Among the populated conformations the *syn*-hindered shows a good potential to sense the nucleobases due to its substituents arrangement and the relative overlap of the large π system and the adenine. The recognition of the guanine by the adenine would stabilize the already populated *syn*-hindered conformation over the conjugated ones.

Synthesis

The retrosynthetic analysis (Figure 6.1.3) shows three possible pathways for the synthesis of the molecules designed.

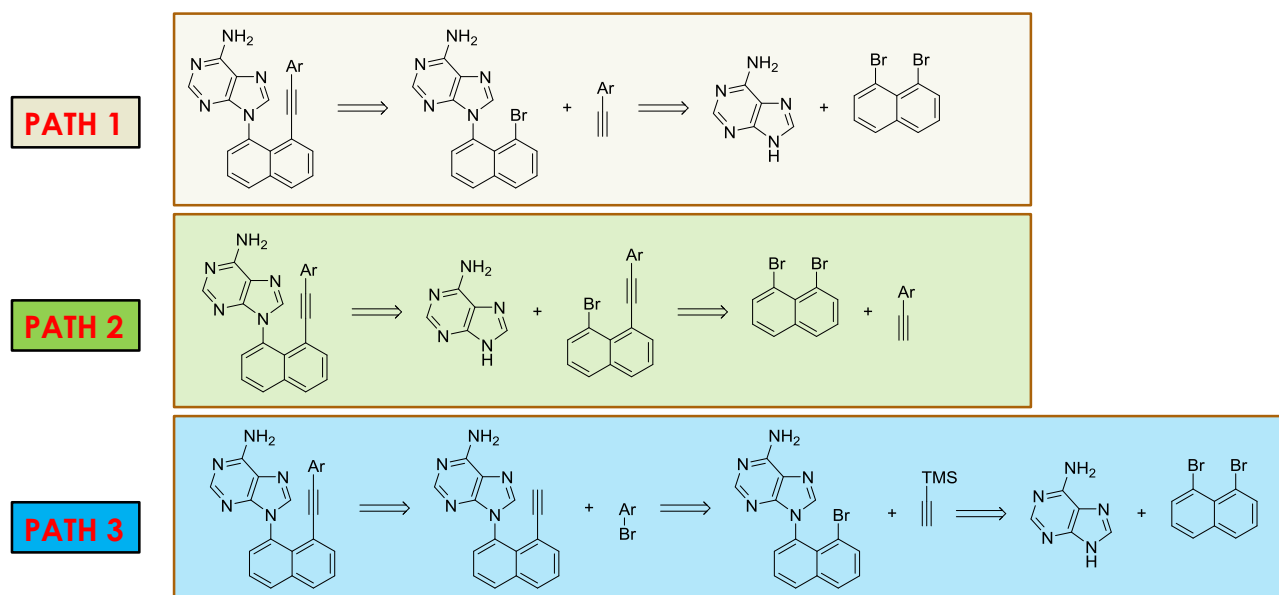


Figure 6.1.3 Retrosynthetic analysis of the sensor designed

All of these synthetic approaches were experimentally evaluated, however only **Path 1** allowed to obtain the desired product. The carefully optimized procedure (Figure 6.1.4) involved a microwave assisted C-N coupling with CuI and N^1,N^2 -dimethylethane-1,2-diamine as ligand. The subsequent Sonogashira coupling with the corresponding ethynyl derivative produced the desired product with an overall yield of close to 40%.

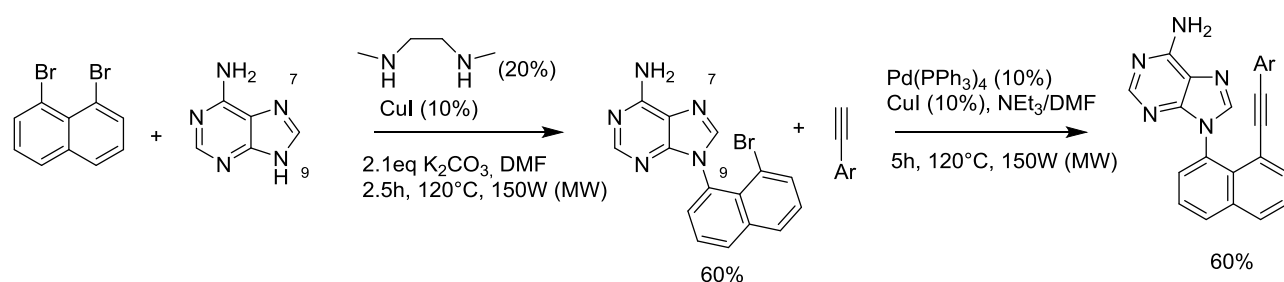


Figure 6.1.4 Synthesis of the nucleobase sensor designed

The molecules synthesized carried as Aryl group a 1-naphthalene (**H**) or a 1-pyrene (**I**). Despite the computational studies and all the efforts involved in the synthesis, the molecules **H** and **I** do not show any type of interaction with the target nucleobase (cytosine). There are no evident changes in the UV-Vis or in the fluorescence spectra upon adding cytosine to **H** or **I**. Moreover, titration experiments

were performed with cytosine and **H** and **I** at NMR. However, the $^1\text{H-NMR}$ does not reveal any type of the typical δ shifting related to an H-bond formation (Paragraph 4.3).

6.1.2 Chiral primary amine sensing

Although was not successful, the approach and the design used for the nucleobases can be translated to be used in sensing other substrates. As target was chosen primary chiral amine, that has been demonstrated to be a suitable and useful substrate to be sensed.⁶

Even if the design (Figure 6.1.5) is similar to the one used for the nucleobases, the mechanism of detection is changed. The amine, that in this case is the substrate, interacts with the sensor with the formation of a C=N bond. Enantiomeric excess and absolute configuration is determined by the interaction of the chiral amine substituents with a stereodynamic chiral axis placed on the sensor, and revealed by CD measurement.

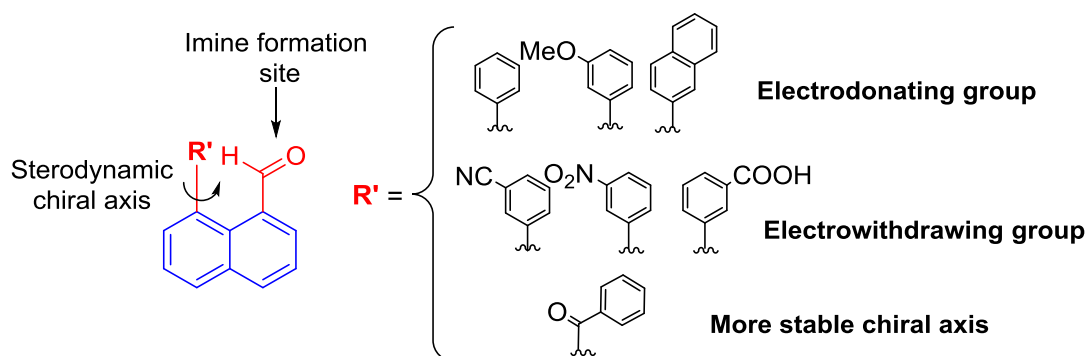


Figure 6.1.5 Molecular design of the chiral amine sensors.

Synthesis

The synthetic approach used (Figure 6.1.6) involve a monoformylation of the 1,8-dibromonaphthalene followed by a glycol protection and a Suzuki coupling with the appropriate boronic acid. Instead of the Suzuki coupling, for the benzoyl derivative was performed a lithiation of the protected monoformylated naphthalene followed by the addition of the benzoyl chloride.

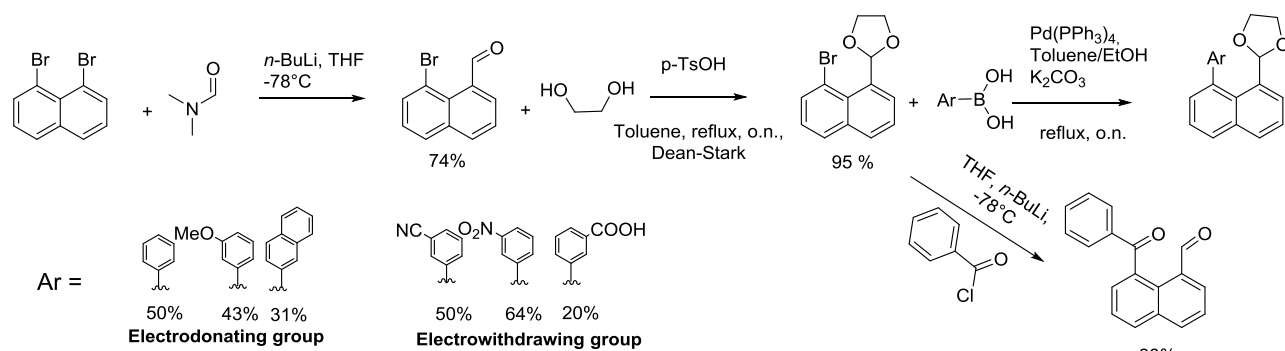


Figure 6.1.6 Synthesis of the sensors designed

In order to have a full reactivity towards the imine formation the aldehyde needs to be deprotected. The process involves a fast reaction with diluted HCl in organic solvent. However, the molecules bearing an electron-donating group shows a different behavior respect the ones that carries an electron-withdrawing group (Figure 6.1.7). While with the latter the deprotection occurs without any by-products, with the electron-donating group an intramolecular Friedel Craft acylation followed by an oxidation occurs (Figure 6.1.7). The reaction produces a planar scaffold (7*H*-benzo[*de*]anthracen-7-one) substituted in the 10 position. This unexpected reaction showed the impossibility to obtain and use the sensor designed with an electrodonating group. However, the simplicity of the reaction and the relative high yields make this pathway interesting to explore in order to synthesized the benzo-anthracene fused ring. This reaction in fact, usually involved some high reactive compound as organic periodate, radical reaction or through Pd catalysis.

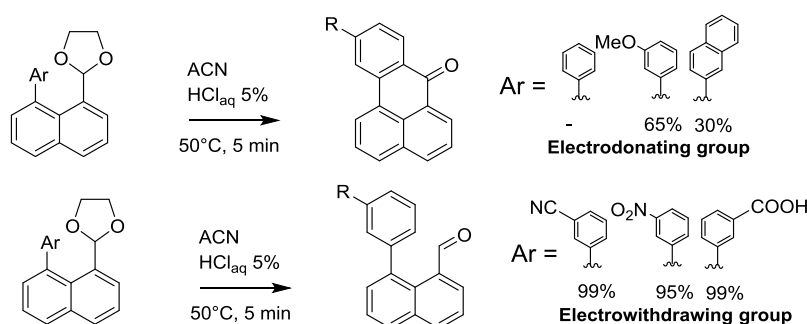


Figure 6.1.7 Reactivity of the sensors towards the acid deprotection.

Sensing

The stable deprotected Suzuki products and the benzoyl derivative were tested as sensor for the detection of an equimolar amounts of (*S*)-1-phenylethan-1-amine. The formation of the imine was checked by ¹H-NMR and the reaction appears to be quite slow (around 24h). After this period, the crude reaction mixture was analyzed with ECD in order to determine the ability of the just formed imine to amplify the chirality of the substrate (Figure 6.1.8). All the sensors synthesized are able to

detect the presence of the amine and the deriving imine shows an amplified and red-shifted ECD signal, proving a successful sensing of the amine.

Further researches will be carried out in order to produce derivative of these sensors able to enhance the CD intensity and to determine altogether the concentration of the amine in solution.

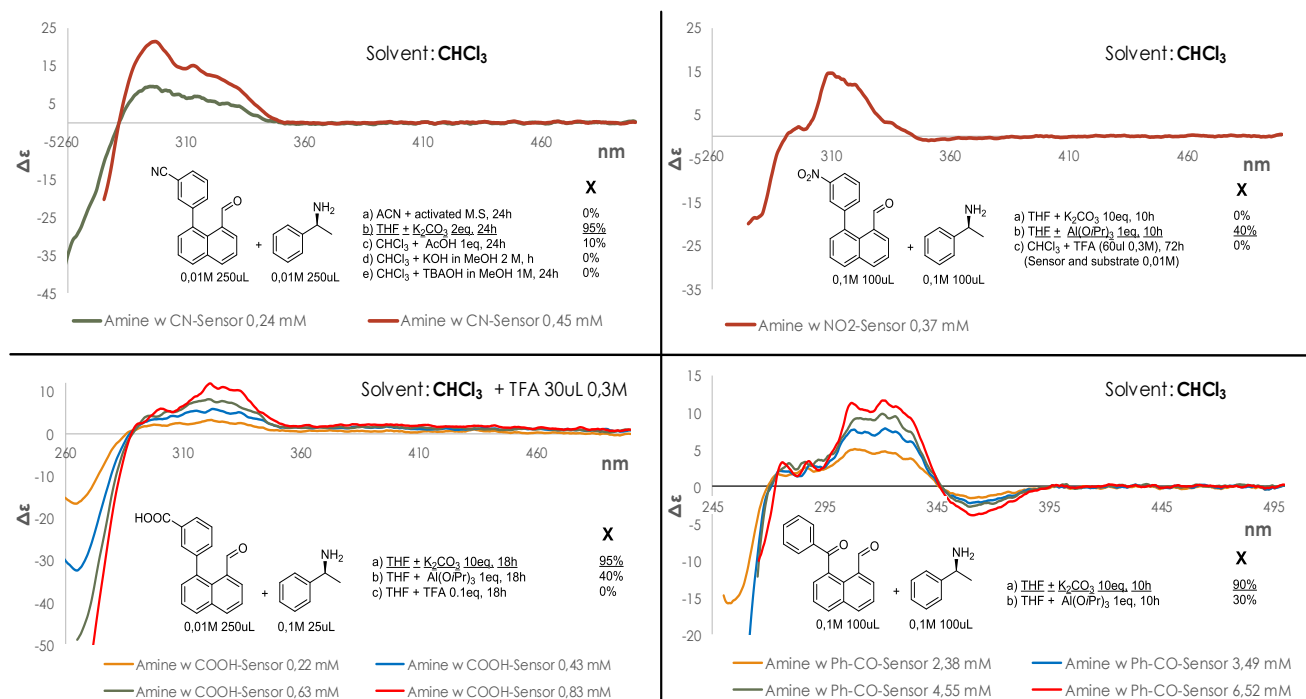


Figure 6.1.8 ECD sensing spectra of different sensor with (S)-1-phenylethan-1-amine.

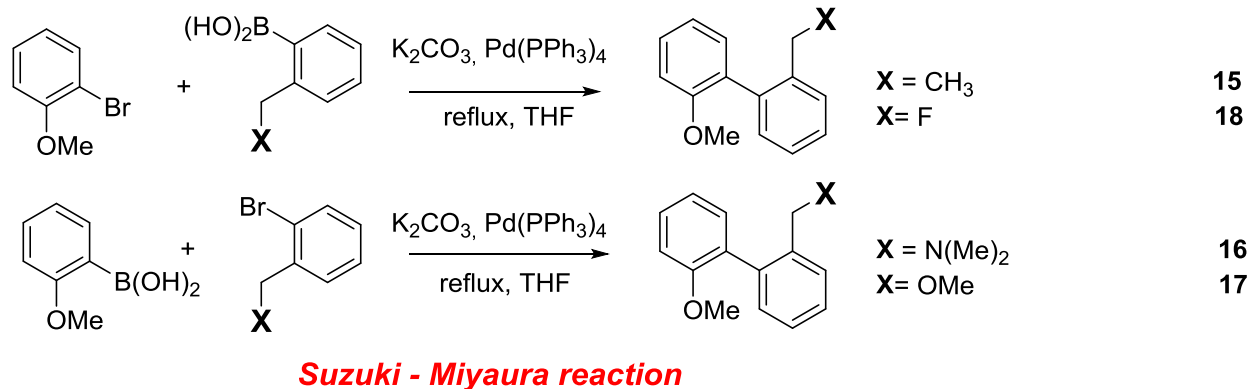
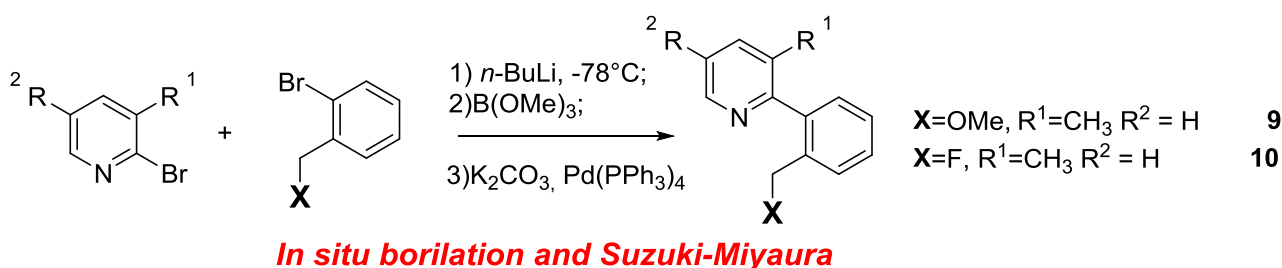
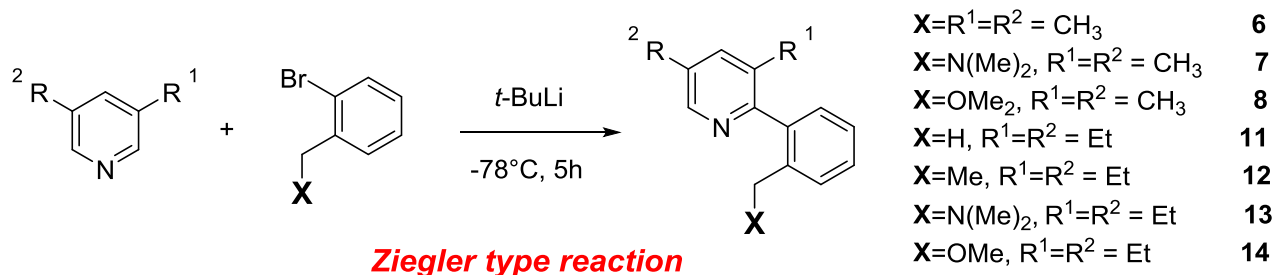
References

- Zhang X. D. "Optimal High-Throughput Screening", Cambridge University Press: London, April 2011.
- Zhao J., Fyles T. M., James T. D. *Angew. Chem., Int. Ed.* **2004**, *43*, 3461-3464.
- Lee S. J., Lin W. J. *Am. Chem. Soc.* **2002**, *124*, 4554-4555.
- Pugh V. J., Hu Q. S., Pu L. *Angew. Chem., Int. Ed.* **2000**, *39*, 3638- 3641.
- Ma L., White P. S., Lin W. J. *Org. Chem.* **2002**, *67*, 7577-7586.
- Bentley K., Wolf C. J. *Am. Chem. Soc.* **2013**, *135*, 12200-12203.

7 Experimental section

7.1 Long-Range Bonding/Nonbonding Interactions: A Donor–Acceptor Resonance Studied by Dynamic NMR

7.1.1 Synthetical procedure



Synthetical routes adopted to obtain **6-18**.

3,5-diethylpyridine.

A 100 mL steel autoclave was charged with a mixture of *N*-methylidene-*tert*-butylamine¹ (15.3 g, 0.18 mol), butanal (39.0 g, 49 mL, 0.54 mol), piperidine (6.8 g, 0.080 mol) and acetic acid (0.27 g, 0.0045 mmol) in toluene (23 mL). The autoclave was tightened and heated up to 200 °C for 2 h using an electric resistance heating jacket. After cooling at 25 °C, the autoclave was cautiously opened and the mixture was evaporated at reduced pressure (40 °C, 15 mbar) to remove the most volatile fraction. The residue was then distilled in vacuum (13 mbar) in a glass oven Kugelrohr, by collecting the fraction boiling in the 80–90 °C temperature range. Chromatography of the collected yellow oil on

silica gel (eluent, diethyl ether) allowed to recover pure 3,5-diethylpyridine⁷ (24.9 g, 34% from butanal).

¹H-NMR (400 MHz, CDCl₃) δ 1.10 (t, 6H, $J = 7.6$ Hz), 2.61 (q, 4H, $J = 7.6$ Hz), 7.32 (s, 1H), 8.28 (s, 2H). ¹³C NMR (100.6 MHz, CDCl₃) δ 15.2 (CH₃), 26.0 (CH₂), 134.5 (CH), 138.6 (Cq), 148.8 (CH). MS (70 eV) m/z (%), 135 (M⁺, 80), 134 (61), 120 (100), 106 (27), 91 (22), 77 (30).

1-bromo-2-(fluoromethyl)benzene.

To a solution of 2-bromobenzylalcohol (6.0 g, 24 mmol) in CH₂Cl₂ (20 mL) kept at -78°C, *N,N*-Diethylaminosulfur trifluoride (DAST, 4.03 g, 25 mmol) was added dropwise. After 10 minutes the solution was warmed to ambient temperature and aqueous NaHCO₃ 1M was added to quench the residual DAST. The mixture was extracted with CH₂Cl₂ and the organic phase was dried on Na₂SO₄. CH₂Cl₂ was removed by distillation at ambient pressure and the residue was purified by evaporation with a Kugelrohr apparatus (oven temp = +150°C, 18 mbar) to yield pure 1-bromo-2-(fluoromethyl)benzene as a colorless oil. Yield: 1.81 g (40% relative to 2-bromobenzylalcohol).

¹H-NMR (600 MHz, CD₃CN) δ 5.32 ppm, +25°C): δ 5.50 (d, 2H, $J_{H-F} = 47.5$ Hz), 7.33 (tt, 1H, $J = 7.8, 1.5$ Hz), 7.45 (t, 1H, $J = 7.6$ Hz), 7.53 (d, 1H, $J = 7.6$ Hz), 7.66 (d, 1H, $J = 7.6$ Hz). ¹³C-NMR (150.8 MHz, CD₃CN, 54.20 ppm, +25°C): δ 83.90 (CH₂, $J_{C-F}=165.5$ Hz), 122.61 (Cq), 128.6 (CH), 130.07 (CH, d, $J_{C-F} = 8.5$ Hz), 130.98 (CH, d, $J_{C-F} = 2.7$ Hz), 133.14 (CH), 135.80 (Cq, d, $J_{C-F} = 17.1$ Hz). MS (70 eV) m/z (%), 190 (M⁺⁺¹, 20), 188 (M⁺¹, 21), 109 (100), 90 (4), 83 (22). HRMS (EI-MS) m/z : [M]⁺ Calcd. for C₇H₆BrF: 187.9637; found: 187.9635.

1-(2-bromophenyl)-*N,N*-dimethylmethanamine.²

2-bromobenzylbromide (1.0 g, 4 mmol) and dimethylamine (33% w/w solution in ethanol, 2.15 ml, 12 mmol) were dissolved in 25 ml of dichloromethane. The stirred solution was kept for 6 hours at reflux. After this time, 20 ml of water were added. The mixture was made basic with solid NaHCO₃ (pH \approx 10-11) and it was extracted with ethyl acetate (3 x 20 ml). The collected organic layers were dried on Na₂SO₄ and evaporated. The crude was kept at high vacuum to remove excess of dimethylamine, yielding the pure compound as colorless oil. Yield: 0.65 g (76% relative to 2-bromobenzylbromide).

¹H-NMR (400 MHz, CDCl₃, +25°C): δ 2.29 (s, 3H), 3.51 (s, 2H), 7.10 (dt, $J=7.8, 1.7$ Hz, 1H), 7.27 (dt, $J=7.4, 1.3$ Hz, 1H), 7.42 (dd, $J=7.7, 1.7$ Hz, 1H), 7.53 (dd, $J=8.0, 1.2$ Hz, 1H). ¹³C-NMR (100.6 MHz, CDCl₃, +25°C): δ 45.49 (CH₃), 63.26 (CH₂), 124.68 (Cq), 127.16 (CH), 128.39 (CH), 130.91 (H), 132.70 (CH), 138.13 (Cq). MS (70 eV) m/z (%), 215 (M⁺⁺¹, 37), 213 (M⁺¹, 38), 171 (30), 169

(30), 132 (12), 91 (18), 89 (18), 58 (100). HRMS (EI-MS) m/z : $[M]^+$ Calcd. for $C_9H_{12}BrN$ 213.0153; Found: 213.0155.

***N,N*-dimethyl-1-[2-(pyridin-2-yl)phenyl]methanamine (4)**

tert-Butyllithium (1.7M in pentane, 5 mL, 8.5 mmol) was added, to *N,N*-dimethylbenzylamine (1.71 g, 8 mmol) in diethyl ether (20 mL) at 25 °C. After 70 hours a white crystalline solid precipitates and pyridine was added (0.63 g, 8.0 mmol). After 24 hours at 25 °C the mixture was concentrated, absorbed on a small quantity of silica gel and dried before being poured on a chromatography column. Elution with a 1:4 (v/v) mixture of diethyl ether and petroleum ether mixture gave a colorless oil. Analytically pure samples were obtained by semi-preparative HPLC on C18 column using Acetonitrile/H₂O+0.1% HCOOH as eluent (70:30 v/v). The elute was concentrated to remove acetonitrile and the aqueous phase was made basic (pH \approx 9) with NaOH 0.5M. Then the aqueous phase was extracted with Et₂O and the organic phase was evaporated at high vacuum (0.1 torr) to get the pure compound as colorless oil. Yield: 0.77 g (46% relative to *N,N*-dimethylbenzylamine).

¹H-NMR (600 MHz, CD₃CN, +25°C): δ 2.06 (s, 6H, NMe₂), 3.50 (s, 2H, CH₂), 7.32 (ddd, 1H, $J = 7.5, 4.8, 1.1$ Hz), 7.35-7.44 (m, 3H), 7.53 (m, 1H), 7.58 (dt, 1H, $J = 7.8, 1.1$ Hz), 7.81 (td, 1H, $J = 7.8, 1.9$ Hz), 8.64 (ddd, 1H, $J = 4.9, 1.8, 0.9$ Hz). **¹³C-NMR** (150.8 MHz, CD₃CN, +25°C): δ 44.86 (2CH₃), 61.18 (CH₂), 122.72 (CH), 124.61 (CH), 127.25(CH), 128.36 (CH), 130.24 (CH), 130.56 (CH), 136.54 (CH), 137.58 (Cq), 141.49 (Cq), 149.25(CH), 159.98 (Cq). HRMS (ESI-TOF-MS⁺) m/z : $[M+H]$ Calcd. for C₁₄H₁₇N₂: 213.1392; Found: 212.1396.

2-(2-ethylphenyl)-3,5-dimethylpyridine (6).

At -78 °C, *tert*-butyllithium (1.7M in pentane, 5 mL, 8.5 mmol) and 3,5-dimethylpyridine (0.86 g, 8.0 mmol) were added consecutively to 2-bromoethylbenzene (1.48 g, 8 mmol) in diethyl ether (20 mL). After 5 h at +25 °C the mixture was concentrated, absorbed on a small quantity of silica gel and dried before being poured on a chromatography column. Elution with a 1:4 (v/v) mixture of diethyl ether and petroleum ether mixture gave a colorless oil. Analytically pure samples were obtained by semi-preparative HPLC on C18 column (Acetonitrile/H₂O 80:20 v/v). Yield: 0.99 g (59% relative to 3,5-dimethylpyridine). **¹H-NMR** (600 MHz, CD₂Cl₂, 5.32 ppm, +25°C): δ 1.00 (t, $J = 7.4$ Hz, 3H), 2.04 (s, 3H), 2.35 (s, 3H), 2.39 (bs, 2H), 7.11 (d, $J = 7.7$ Hz, 1H), 7.26 (m, 2H), 7.36 (d, $J = 7.8$, 1H), 7.50 (bs, 1H), 8.30 (s, 1H). **¹³C-NMR** (150.8 MHz, CD₃CN, 118.69 ppm, +25°C): δ 14.88 (CH₃), 17.47 (CH₃), 18.64 (CH₃), 26.10 (CH₂), 125.88 (CH), 128.29 (CH), 128.95 (CH), 129.26 (CH), 131.21 (Cq), 132.23 (Cq), 138.53 (CH), 140.48 (Cq), 142.41 (Cq), 147.12 (CH), 156.94 (Cq). HRMS (ESI-TOF-MS⁺) m/z : $[M+H]$ Calcd. for C₁₅H₁₈N₁: 212.1439; Found: 212.1437.

1-[2-(3,5-dimethylpyridin-2-yl)phenyl]-*N,N*-dimethylmethanamine (7).

At $-78\text{ }^{\circ}\text{C}$, *tert*-butyllithium (1.7M in pentane, 3 mL, 5.1 mmol) and 3,5-dimethylpyridine (0.86 g, 5.0 mmol) were added consecutively to 1-(2-bromophenyl)-*N,N*-dimethylmethanamine (1.07 g, 5 mmol) in diethyl ether (15 mL). After 5 h at $+25\text{ }^{\circ}\text{C}$ the mixture was concentrated, absorbed on a small quantity of silica gel and dried before being poured on a chromatography column. Elution with a 1:4 (v/v) mixture of diethyl ether and petroleum ether mixture gave a colorless oil. Analytically pure samples were obtained by semi-preparative HPLC on C18 column using Acetonitrile/ $\text{H}_2\text{O}+0.1\%$ HCOOH as eluent (75:25 v/v). The eluate was concentrated to remove acetonitrile and the aqueous phase was made basic (pH \approx 9) with NaOH 0.5M. Then the aqueous phase was extracted with Et_2O and the organic phase was evaporated at high vacuum (0.1 torr) to get the pure compound as colorless oil. Yield: 0.58 g (48% relative to 3,5-dimethylpyridine).

$^1\text{H-NMR}$ (600 MHz, CD_2Cl_2 , 5.32 ppm, $+25\text{ }^{\circ}\text{C}$): δ 2.04 (s, 9H), 2.35 (s, 3H), 3.17 (s, 2H), 7.11 (d, $J = 7.1$ Hz, 1H), 7.29 (t, $J = 7.1$ Hz, 1H), 7.36 (t, $J = 7.1$ Hz, 1H), 7.39 (bs, 1H), 7.56 (d, $J = 7.7$ Hz, 1H), 8.28 (s, 1H). **$^{13}\text{C-NMR}$** (150.8 MHz, CD_2Cl_2 , $+25\text{ }^{\circ}\text{C}$): δ 17.38 (CH_3), 18.76 (CH_3), 45.14 (2CH_3), 60.64 (CH_2), 126.34 (CH), 127.50 (CH), 128.76 (CH), 129.26 (CH), 130.97 (Cq), 131.43 (Cq), 13.51 (Cq) 137.93 (CH), 141.210 (Cq), 146.64 (CH), 156.36 (Cq). MS (70 eV) m/z (%), 240 (M^+ , 7), 225 (17), 196 (73), 182 (100), 152 (8), 58 (5). HRMS (ESI-TOF- MS^+) m/z : [$\text{M}+\text{H}$] Calcd. for $\text{C}_{16}\text{H}_{21}\text{N}_2$: 241.1705; Found: 241.1706.

2-[2-(methoxymethyl)phenyl]-3,5-dimethylpyridine (8).

At $-78\text{ }^{\circ}\text{C}$, *tert*-butyllithium (1.7M in pentane, 3 mL, 5.1 mmol) and 3,5-dimethylpyridine (0.86 g, 5.0 mmol) were added consecutively to 1-Bromo-2-(methoxymethyl)benzene (1.00 g, 5 mmol) in diethyl ether (15 mL). After 5 h at $+25\text{ }^{\circ}\text{C}$ the mixture was concentrated, absorbed on a small quantity of silica gel and dried before being poured on a chromatography column. Elution with a 1:4 (v/v) mixture of diethyl ether and petroleum ether mixture gave a colorless oil. Analytically pure samples were obtained by semi-preparative HPLC on C18 column (Acetonitrile/ H_2O 80:20 v/v). Yield: 0.59 g (52% relative to 3,5-dimethylpyridine).

$^1\text{H-NMR}$ (600 MHz, CD_3CN , $+25\text{ }^{\circ}\text{C}$): δ 2.05 (s, 3H), 2.35 (s, 3H), 3.16 (s, 3H), 4.20 (bs, 2H), 7.18 (dd, 1H, $J = 7.5, 1.3$ Hz), 7.37 (td, 1H, $J = 7.5, 1.3$ Hz), 7.43 (td, 1H, $J = 7.5, 1.3$ Hz), 7.50 (m, 1H), 7.53 (d, 1H, $J = 7.7$ Hz), 8.29 (bs, 1H). **$^{13}\text{C-NMR}$** (150.8 MHz, CD_3CN , $+25\text{ }^{\circ}\text{C}$): δ 17.47 (CH_3), 18.62 (CH_3), 57.72 (CH_3), 71.86 (CH_2), 127.52 (CH), 128.08 (CH), 128.53 (CH), 129.28 (CH), 131.42 (Cq), 132.38 (Cq), 137.01 (Cq), 138.56 (CH), 140.24 (Cq), 147.06 (CH), 156.02 (Cq). MS (70 eV) m/z (%), 227 (M^+ , 2), 212 (100), 184 (16), 106 (5), 45 (1). HRMS (ESI-TOF- MS^+) m/z : [$\text{M}+\text{H}$] Calcd. for $\text{C}_{15}\text{H}_{18}\text{NO}$: 228.1388; Found: 228.1387.

2-[2-methoxymethyl]phenyl]-3-methylpyridine (9).

2-(methoxymethyl)bromobenzene (1.0 g, 5.0 mmol) was dissolved in dry THF (20 mL), under nitrogen flux and kept at -78°C. At this solution *n*-BuLi (1.6M in hexane, 4.7 ml, 7.5 mmol) was added dropwise and the solution was kept stirred at -78°C for 1 hour. At the same temperature, trimethylborate (1.54 g, 15 mmol) was added dropwise. The reaction was kept stirred overnight reaching the ambient temperature, then the resulting 0.2M solution of dimethyl(2-(methoxymethyl)phenyl)boronate was used for the next step without any further work up. 3-Methyl-2-bromopyridine (110 µL, 1 mmol, 1 eq) was added to dimethyl(2-(methoxymethyl)phenyl)boronate (7.5 mL of the 0.2M solution in THF, 1.5 mmol), under nitrogen flux. Then K₂CO₃ (2M solution, 0.69 g, 5 mmol) and Pd(PPh₃)₄ (11.5 mg, 0.01 mmol) were added. The solution was kept stirred at reflux for 2 hours, then H₂O was added and the solution was extracted three times with dichloromethane. The organic layer was dried (Na₂SO₄), filtered on silica gel and concentrated at reduced pressure. The crude was pre-purified by flash chromatography on silica gel (7:3 petroleum ether/ethyl acetate). Analytically pure samples were obtained by semi-preparative HPLC on Synergi Hydro-RP 10x250 mm (acetonitrile/H₂O 80:20 v/v). Yield: 102 mg (48% relative to 2-(methoxymethyl)bromobenzene). ¹H-NMR (600 MHz, CD₂Cl₂, +25°C): δ 2.09 (s, 3H), 3.20 (s, 3H), 4.21 (s, 2H), 7.18 (d, 1H, *J* = 7.9 Hz), 7.22 (dd, 1H, *J* = 7.5, 7.2 Hz), 7.38 (t, 1H, *J* = 7.5 Hz), 7.42 (t, 1H, *J* = 7.5 Hz), 7.54 (d, 1H, *J* = 7.5 Hz), 7.62 (d, 1H, *J* = 7.9 Hz), 8.46 (d, 1H, *J* = 4.3 Hz). ¹³C-NMR (150.8 MHz, CD₂Cl₂, +25°C): δ 19.72 (CH₃), 58.74 (CH₃), 71.62 (CH₂), 123.05 (Cq), 127.92 (CH), 128.64 (CH), 128.94 (CH), 129.42 (CH), 132.59 (Cq), 137.25 (CH), 138.48 (CH), 140.39 (Cq), 147.09 (CH), 159.34 (Cq). HRMS (ESI-TOF-MS⁺) *m/z*: [M+H] Calcd. for C₁₄H₁₆NO: 214.1232; Found: 214.1237.

2-[(2-fluoromethyl)phenyl]-3-methylpyridine (10).

2-(Fluoromethyl)bromobenzene (0.94 g, 5.0 mmol) was dissolved in dry THF (20 mL), under nitrogen flux and kept at -78°C. At this solution *n*-BuLi (1.6M in hexane, 4.7 ml, 7.5 mmol) was added dropwise and the solution was stirred at -78°C for 1 hour. At the same temperature, trimethylborate (1.54 g, 15 mmol) was added dropwise and the solution was kept for 3 hour at -78°C. The reaction was stirred overnight allowing the temperature to raise to ambient temperature, then the resulting 0.2M solution of dimethyl(2-(fluoromethyl)phenyl)boronate was used for the next step without any further work up. 3-Methyl-2-bromopyridine (0.11 mL, 1 mmol, 1 eq) and dimethyl-(2-fluoromethyl)phenyl)boronate (7.5 mL of the 0.2 M solution in THF, 1.5 mmol), were stirred under nitrogen flux, then K₂CO₃ (2 M solution, 0.69 g, 5 mmol, 5 eq) and Pd(PPh₃)₄ (11.5 mg, 0.01 mmol) were added, and the solution was kept at reflux for 2 hours. Water was then added and the solution was extracted three times with dichloromethane. The organic layer was dried (Na₂SO₄), filtered on

silica gel and concentrated at reduced pressure. The crude was then purified by silica flash chromatography (7:3 petroleum ether/ethyl acetate) to yield a slightly green oil. Yield: 147 mg (49 % relative to 2-(fluoromethylbromobenzene).

¹H-NMR (600 MHz, CD₃CN, +25°C): δ 2.12 (s, 3H), 5.22 (d, 2H, $J_{\text{H-F}} = 48.5$ Hz, CH₂F), 7.3 (m, 2H), 7.47-7.53 (m, 2H), 7.61 (m, 1H), 7.71 (m, 1H), 8.46 (d, 1H, $J = 4.9$ Hz). **¹⁹F-NMR** (564.3 MHz, CD₃CN, +25°C): δ -209.06 (t, $J_{\text{H-F}} = 48.5$ Hz). **¹³C-NMR** (150.8 MHz, CD₃CN, +25°C): δ 18.80 (CH₃), 82.73 (d, $J_{\text{C-F}} = 162.5$ Hz, CH₂F), 123.10 (CH), 128.60 (CH, d, $J_{\text{C-F}} = 1.4$ Hz), 128.95 (CH, d, $J_{\text{C-F}} = 3.0$ Hz), 129.08 (CH, d, $J_{\text{C-F}} = 7.6$ Hz), 129.49 (CH, d, $J_{\text{C-F}} = 1.6$ Hz), 132.24 (Cq), 134.71 (Cq, d, $J_{\text{C-F}} = 16.5$ Hz), 138.43 (CH), 140.4 (Cq, d, $J_{\text{C-F}} = 4.4$ Hz), 146.78 (CH), 158.05 (Cq). HRMS (ESI-TOF-MS⁺) m/z : [M+H] Calcd. for C₁₃H₁₃NF: 202.1032; Found: 202.1037.

3,5-diethyl-2-(2-methylphenyl)pyridine (11)

At -78 °C, *tert*-butyllithium (1.7M in pentane, 5 mL, 8.5 mmol) and 3,5-diethylpyridine (1.08 g, 8.0 mmol) were added consecutively to 2-bromotoluene (1.37 g, 8 mmol) in diethyl ether (20 mL). After 5 h at +25 °C the mixture was concentrated, absorbed on a small quantity of silica gel and dried before being poured on a chromatography column. Elution with a 1:4 (v/v) mixture of diethyl ether and petroleum ether mixture gave a colorless oil. Analytically pure samples were obtained by semi-preparative HPLC on C18 column (Acetonitrile/H₂O 75:25 v/v). Yield: 0.99 g (55 % relative to 3,5-diethylpyridine).

¹H-NMR (600 MHz, CD₃CN +25°C): δ 1.03 (t, 3H, $J = 7.6$ Hz), 1.30 (t, 3H, $J = 7.6$ Hz), 2.05 (s, 3H), 2.40 (bs, 2H), 2.70 (q, 2H, $J = 7.6$ Hz), 7.15 (d, 1H, $J = 8.3$ Hz), 7.26 (m, 1H), 7.32 (m, 2H), 7.58 (d, 1H, $J = 2.5$ Hz), 8.35 (d, 1H, $J = 2.5$ Hz). **¹³C-NMR** (150.8 MHz, CD₃CN, +25°C): δ 14.59 (CH₃), 15.28 (CH₃), 19.24 (CH₃), 25.47 (CH₂), 25.85 (CH₂), 125.81 (CH), 128.11 (CH), 129.25 (CH), 130.38 (CH), 136.07 (CH), 136.37 (Cq), 137.20 (Cq), 138.60 (Cq), 140.95 (Cq), 146.59 (CH), 156.80 (Cq). MS (70 eV) m/z (%) 225 (M⁺, 22), 224 (52), 210 (100), 196 (53), 180 (21), 77 (10). HRMS (ESI-TOF-MS⁺) m/z : [M+H] Calcd. for C₁₆H₂₀N: 226.1596; Found: 226.1591

3,5-diethyl-2-(2-ethylphenyl)pyridine (12)

At -78 °C, *tert*-butyllithium (1.7M in pentane, 5 mL, 8.5 mmol) and 3,5-diethylpyridine (1.08 g, 8.0 mmol) were added consecutively to 2-bromoethylbenzene (1.48 g, 8 mmol) in diethyl ether (20 mL). After 5 h at +25 °C the mixture was concentrated, absorbed on a small quantity of silica gel and dried before being poured on a chromatography column. Elution with a 1:4 (v/v) mixture of diethyl ether and petroleum ether mixture gave a colorless oil. Analytically pure samples were obtained by semi-

preparative HPLC on C18 column (Acetonitrile/H₂O 80:20 v/v). Yield: 0.82 g (53 % relative to 3,5-diethylpyridine).

¹H-NMR (600 MHz, CD₃CN, +25°C): δ 1.02 (t, 3H, J = 7.6 Hz), 1.05 (t, 3H, J = 7.7 Hz), 1.29 (t, 3H, J = 7.7 Hz), 2.34 (broad, 4H), 2.70 (q, 2H, J = 8.3 Hz), 7.12 (d, 1H, J = 7.7, 0.9 Hz), 7.25 (m, 1H), 7.37 (m, 2H), 7.59 (bs, 1H), 8.32 (d, 1H, J = 1.9 Hz). **¹³C-NMR** (150.8 MHz, CD₃CN, 118.69 ppm, +25°C): δ 14.47 (CH₃), 14.86 (CH₃), 15.18 (CH₃), 25.44 (CH₂), 25.78 (CH₂), 26.17 (CH₂), 125.72 (CH), 128.34 (CH), 128.78 (CH), 129.36 (CH), 136.058 (CH), 137.29 (Cq), 138.63 (Cq), 140.18 (Cq), 142.42 (Cq), 146.23 (CH), 156.59 (Cq). MS (70 eV) m/z (%) 239 (M⁺, 13), 223 (3), 210 (100), 195 (20), 180 (12), 77 (4). HRMS (ESI-TOF-MS⁺) m/z : [M+H] Calcd. for C₁₇H₂₂N: 240.1752; Found: 240.1749

1-[2-(3,5-diethylpyridin-2-yl)phenyl]-N,N-dimethylmethanamine (13)

At ambient temperature, *tert*-butyllithium (1.7M in pentane, 5 mL, 8.5 mmol) was added to 1-(2-bromophenyl)-N,N-dimethylmethanamine (1.71 g, 8 mmol) in diethyl ether (20 mL). After 70 hours a white crystalline solid precipitates and 3,5-diethylpyridine was added (1.08 g, 8.0 mmol). After 24 hours at ambient temperature the mixture was concentrated, absorbed on a small quantity of silica gel and dried before being poured on a chromatography column. Elution with a 1:4 (v/v) mixture of diethyl ether and petroleum ether mixture gave a colorless oil. Analytically pure samples were obtained by semi-preparative HPLC on C18 column using acetonitrile/H₂O+0.1% HCOOH as eluent (75:25 v/v). The eluate was concentrated to remove acetonitrile and the aqueous phase was made basic (pH \approx 9) with NaOH 0.5M. Then the aqueous phase was extracted with Et₂O and the organic phase was evaporated at high vacuum (0.1 torr) to get the pure compound as colorless oil. Yield: 0.96 g (45 % relative to 3,5-diethylpyridine).

¹H-NMR (600 MHz, CD₂Cl₂, 5.32 ppm, +25°C): δ 1.05 (t, 3H, J = 7.6 Hz), 1.30 (t, 3H, J = 7.6 Hz), 2.02 (s, 6H), 2.40 (bs, 2H), 2.71 (q, 2H J = 7.7 Hz), 3.17 (bs, 2H), 7.14 (dd, 1H, J = 7.6, 1.2 Hz, 1H), 7.31 (td, 1H, J = 7.2, 1.3 Hz), 7.40 (dt, 1H, J = 7.7, 1.2 Hz), 7.57 (m, 2H), 8.31 (d, 1H, J = 2.1 Hz). **¹³C-NMR** (150.8 MHz, CD₃CN, +25°C): δ 15.39 (CH₃), 16.26 (CH₃), 26.40 (CH₂), 26.82 (CH₂), 46.19 (CH₃), 62.00 (CH₂), 127.62 (CH), 128.97 (CH), 130.37 (CH), 130.42 (CH), 136.70 (CH), 138.41 (Cq), 139.14 (Cq), 139.46 (Cq), 141.88 (Cq), 147.14 (CH), 157.43 (Cq). MS (70 eV) m/z (%) 268 (M⁺, 6), 253 (20), 224 (68), 210 (100), 196 (41), 180 (7), 58 (15). HRMS (ESI-TOF-MS⁺) m/z : [M+H] Calcd. for C₁₈H₂₅N₂: 269.2018; Found: 269.2015.

3,5-diethyl-2-[2-(methoxymethyl)phenyl]pyridine (14)

At $-78\text{ }^{\circ}\text{C}$, *tert*-butyllithium (1.7M in pentane, 5 mL, 8.5 mmol) and 3,5-diethylpyridine (1.08 g, 8.0 mmol) were added consecutively to 1-bromo-2-(methoxymethyl)benzene (1.61 g, 8 mmol) in diethyl ether (20 mL). After 5 h at $+25\text{ }^{\circ}\text{C}$ the mixture was concentrated, absorbed on a small quantity of silica gel and dried before being poured on a chromatography column. Elution with a 1:4 (v/v) mixture of diethyl ether and petroleum ether mixture gave a colorless oil. Analytically pure samples were obtained by semi-preparative HPLC on C18 column (acetonitrile/H₂O 80/20 v/v). Yield: 1.20 g (59 % relative to 3,5-diethylpyridine).

¹H-NMR (600 MHz, CD₃CN, $+25\text{ }^{\circ}\text{C}$): δ 1.04 (t, 3H, $J = 7.3$ Hz), 1.30 (t, 3H, $J = 7.9$ Hz), 2.41 (q, 2H, $J = 7.3$ Hz), 2.71 (q, 2H, $J = 7.3$ Hz), 3.17 (s, 3H), 4.18 (s, 2H), 7.18 (dd, 1H, $J = 7.8, 1.2$ Hz), 7.36 (td, 1H, $J = 7.5, 1.1$ Hz), 7.43 (td, 1H, $J = 7.7, 1.2$ Hz), 7.54 (d, 1H, $J = 7.8$ Hz), 7.59 (m, 1H), 8.33 (d, 1H, $J = 2.1$ Hz). **¹³C-NMR** (150.8 MHz, CD₃CN, $+25\text{ }^{\circ}\text{C}$): δ 14.40 (CH₃), 15.16 (CH₃), 25.38 (CH₂), 25.77 (CH₂), 57.85 (CH₃), 71.87 (CH₂), 127.34 (CH), 128.08 (Cq), 128.34 (CH), 129.37 (CH), 135.99 (CH), 137.17 (Cq), 137.41 (Cq), 138.73 (Cq), 140.05 (Cq), 146.33 (CH), 155.75 (Cq). MS (70 eV) m/z (%) 255 (M⁺, 3), 240 (100), 224 (3), 212 (7), 196 (13), 180 (7), 77 (3). HRMS (ESI-TOF-MS⁺) m/z : [M+H] Calcd. for C₁₇H₂₂NO: 256.1701; Found: 256.1697.

2-ethyl-2'-methoxy-1,1'-biphenyl (15)

A mixture of 2-bromoanisole (0.1 ml, 0.8 mmol) and 2-ethylphenylboronic acid (0.150 g, 1 mmol, 1.25 eq), under nitrogen flux, were dissolved in a 8:3 mixture of toluene/ethanol (0.15M). Then K₂CO₃ (1 M solution, 4 mL, 4 mmol) and Pd(PPh₃)₄ (11.5 mg, 0.01 mmol) were added and the stirred solution was kept at reflux for 3 hours. Water was then added and the solution was extracted three times with CH₂Cl₂. The organic layer was dried (Na₂SO₄), filtered on silica gel and concentrated at reduced pressure. The crude was then purified by semi-preparative HPLC on Luna C18 column (acetonitrile/H₂O 90:10 v/v). Yield: 96 mg (57 % relative to 2-bromoanisole).

¹H-NMR (600 MHz, C₂D₂Cl₄, $+25\text{ }^{\circ}\text{C}$): δ 1.11 (t, 3H, $J = 7.6$ Hz, 3H), 2.49 (bs, 2H), 3.79 (s, 3H), 7.01 (d, 1H, $J = 8.6$ Hz), 7.05 (td, 1H, $J = 7.3, 0.8$ Hz), 7.19 (dd, 1H, $J = 8.7, 1.4$ Hz), 7.20 (d, 1H, $J = 8.2$ Hz), 7.26 (m, 1H), 7.35 (m, 2H), 7.39 (td, 1H, $J = 7.9, 1.7$ Hz). **¹³C-NMR** (150.8 MHz, C₂D₂Cl₄, $+25\text{ }^{\circ}\text{C}$): δ 15.06 (CH₃), 26.20 (CH₂), 55.56 (CH₃), 110.83 (CH), 120.50 (CH), 125.42 (CH), 125.41 (CH), 127.36 (CH), 127.92 (CH), 128.64 (CH), 130.44 (CH), 130.65 (Cq), 132.35 (CH), 138.31 (Cq), 142.91 (Cq), 156.60 (Cq). HRMS (ESI-TOF-MS⁺) m/z : [M+H] Calcd. for C₁₅H₁₇O₁: 213.1279; Found: 213.1278.

1-(2'-methoxy-[1,1'-biphenyl]-2-yl)-*N,N*-dimethylmethanamine (16)

A mixture of 1-(2-bromophenyl)-*N,N*-dimethylmethanamine (0.250 g, 1.04 mmol) and 2-methoxyphenylboronic acid (237 mg, 1.56 mmol), under nitrogen flux, were dissolved in a 8:3 mixture of toluene/ethanol (0.10M). Then K₂CO₃ (2M solution, 2 mL, 4 mmol) and Pd(PPh₃)₄ (23.0 mg, 0.02 mmol) were added. The stirred solution was kept at reflux for 2.5 hours. Water was then added and the solution was extracted three times with CH₂Cl₂. The organic layer was dried (Na₂SO₄), filtered and concentrated at reduced pressure. The crude was then purified by a silica plug (dichloromethane + triethylamine 0.5%). Analytically pure samples were obtained by semi-preparative HPLC on C18 column using acetonitrile/H₂O+0.1% HCOOH as eluent (80:20 v/v). The eluate was concentrated to remove acetonitrile and the aqueous phase was made basic (pH ≈ 9) with NaOH 0.5M. Then the aqueous phase was extracted with Et₂O and the organic phase was evaporated at high vacuum (0.1 torr) to get the pure compound as colorless oil. Yield: 100 mg (40 % relative to 1-(2-bromophenyl)-*N,N*-dimethylmethanamine).

¹H-NMR (600 MHz, CD₃CN, +25°C): δ 2.08 (s, 6H), 3.16 (broad doublet, 1H, *J* = 13.5 Hz), 3.36 (broad doublet, 1H, *J* = 13.5 Hz) 3.73 (s, 3H), 7.03 (dt, 1H, *J* = 7.4, 1.1 Hz), 7.06 (d, 1H, *J* = 8.4 Hz), 7.13 (m, 2H), 7.30 (td, 1H, *J* = 7.4, 1.3 Hz), 7.36 (td, 1H, *J* = 7.6, 1.4 Hz), 7.39 (ddd, 1H, *J* = 9.2, 7.5, 1.8 Hz), 7.62 (d, 1H, *J* = 7.8). ¹³C-NMR (150.8 MHz, CD₃CN, +25°C): δ 45.80 (CH₃), 55.29 (CH₃), 60.72 (CH₂), 111.18 (CH), 120.71 (CH), 126.96 (CH), 127.66 (CH), 129.18 (CH), 129.29 (CH), 130.34 (Cq), 130.48 (CH), 131.27 (CH), 137.65 (Cq), 139.19 (Cq), 156.97 (Cq). HRMS (ESI-TOF-MS⁺) *m/z*: [M+H] Calcd. for C₁₆H₂₀NO: 242.1545; Found: 242.1544.

2-methoxy-2'-(methoxymethyl)-1,1'-biphenyl (17).

A mixture of 2-methoxyphenylboronic acid (152 mg, 1 mmol) and 1-bromo-2-(methoxymethyl)benzene (201 mg, 1 mmol) were dissolved in 5 mL of THF. Then K₂CO₃ (2M solution, 1 mL, 2 mmol) and Pd(PPh₃)₄ (11.5 mg, 0.01 mmol) were added and the mixture was stirred at reflux for 2 hours. Then water was added and the aqueous phase was extracted three times with CH₂Cl₂. The organic phase was dried, filtered and concentrated under reduced pressure. The crude was then purified by semi-preparative HPLC on C18 column (acetonitrile/H₂O 90:10 v/v). Yield: 139 mg (61 % relative to 1-bromo-2-(methoxymethyl)benzene).

¹H-NMR (600 MHz, CD₃CN, +25°C): δ 3.25 (s, 3H), 3.77 (s, 3H), 4.27 (bs, 2H), 6.97 (d, *J* = 8.4 Hz, 1H), 7.03 (t, 1H, *J* = 7.5), 7.18 (dd, 1H, *J* = 7.4, 1.7 Hz), 7.23 (d, 1H, *J* = 7.2 Hz), 7.33 (t, 1H, *J* = 7.2 Hz), 7.38 (t, 1H, *J* = 7.2 Hz), 7.53 (d, 1H, *J* = 7.5 Hz). ¹³C-NMR (150.8 MHz, CD₃CN, +25°C): δ 55.35 (CH₃), 57.72 (CH₃), 72.13 (CH₂), 111.28 (CH), 120.77 (CH), 127.41 (CH), 127.69 (CH), 127.83 (CH), 129.44 (CH), 129.76 (Cq), 130.50 (CH), 131.19 (CH), 137.61 (Cq), 138.21 (Cq), 156.95 (Cq). HRMS (ESI-TOF-MS⁺) *m/z*: [M+H] Calcd. for C₁₅H₁₇O₂: 229.1229; Found: 229.1225.

2-(fluoromethyl)-2'-methoxy-1,1'-biphenyl (18)

2-bromoanisole (0.12 ml, 1 mmol) and dimethyl (2-fluoromethyl)phenyl boronate (7.5 mL of a 0.2M solution in THF, 1.5 mmol, see compound **10**) were mixed under nitrogen flux, Then K_2CO_3 (2 M solution, 2 mL, 4 mmol) and $Pd(PPh_3)_4$ (11.5 mg, 0.01 mmol) were added, and the stirred solution was kept at reflux for 2 hours. Water was then added and the solution was extracted three times with CH_2Cl_2 . The organic layer was dried (Na_2SO_4), filtered on silica gel and concentrated at reduced pressure. The crude was then pre-purified by silica flash chromatography (9:1 petroleum ether/ethyl acetate). Analytically pure samples were obtained by semipreparative HPLC on C18 column (acetonitrile/ H_2O 80:20 v/v). Yield: 118 mg (55 % relative to 2-bromoanisole).

1H -NMR (600 MHz, CD_3CN +25°C): δ 3.74 (s, 3H), 5.18 (broad dd, 2H, $J = 11$ Hz, $J_{H-F} = 48.6$ Hz), 7.06 (td, 1H, $J = 7.4$ Hz, 1.0 Hz), 7.09 (dd, 1H, $J = 8.4$, 1.0 Hz), 7.18 (dd, 1H, $J = 7.4$, 1.8 Hz), 7.25 (m, 1H), 7.40-7.47 (m, 3H), 7.56 (m, 1H). **^{19}F -NMR** (564.3 MHz, CD_3CN , +25°C): δ -208.48 (t, $J = 48.0$ Hz). **^{13}C -NMR** (150.8 MHz, CD_3CN , +25°C): δ 55.40 (CH_3), 83.14 (CH_2 , d, $J_{C-F} = 163.5$ Hz), 111.37 (CH), 120.91 (CH), 128.01 (CH), 128.35 (CH, d, $J_{C-F} = 7.4$ Hz), 128.89 (CH, d, $J_{C-F} = 3.3$ Hz), 128.94 (Cq), 129.80 (CH), 130.85 (CH), 131.35 (CH), 135.43 (Cq, d, $J_{C-F} = 16.0$ Hz), 138.33 (Cq, d, $J_{C-F} = 5.2$ Hz), 156.83 (Cq). HRMS (ESI-TOF-MS⁺) m/z: [M+H] Calcd. for $C_{14}H_{14}OF$: 217.1029; Found: 217.1034

7.1.2 Dynamic NMR

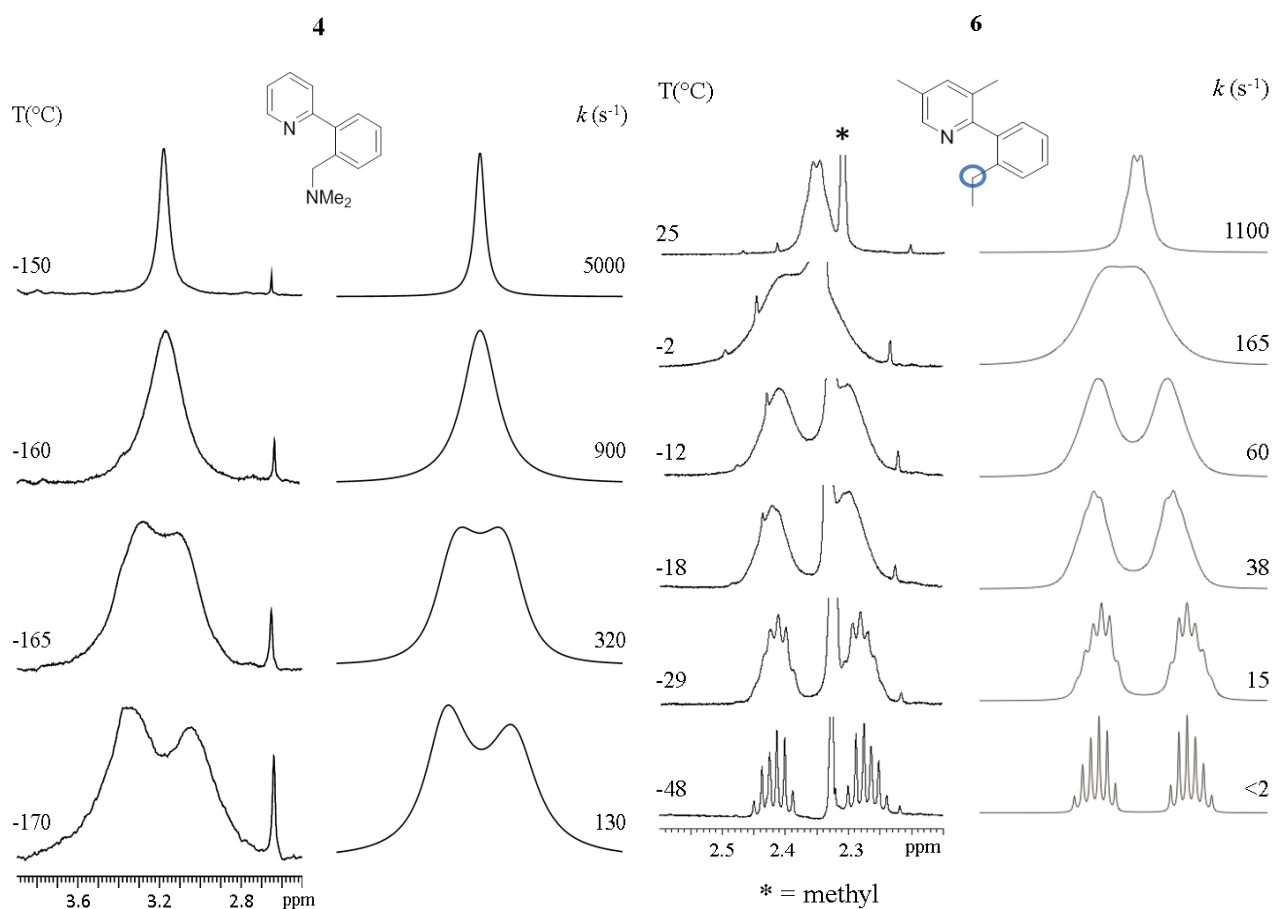


Figure 7.1.1 Dynamic ^1H -NMR spectra of compound **4** (CH_2 signal) and **6** (CH_2 signal) respectively at 600 MHz in $\text{CDCl}_2/\text{CHF}_2\text{Cl}$ and CD_2Cl_2 . On the right of the experimental spectra is reported the line shape simulations and the corresponding rate constants.

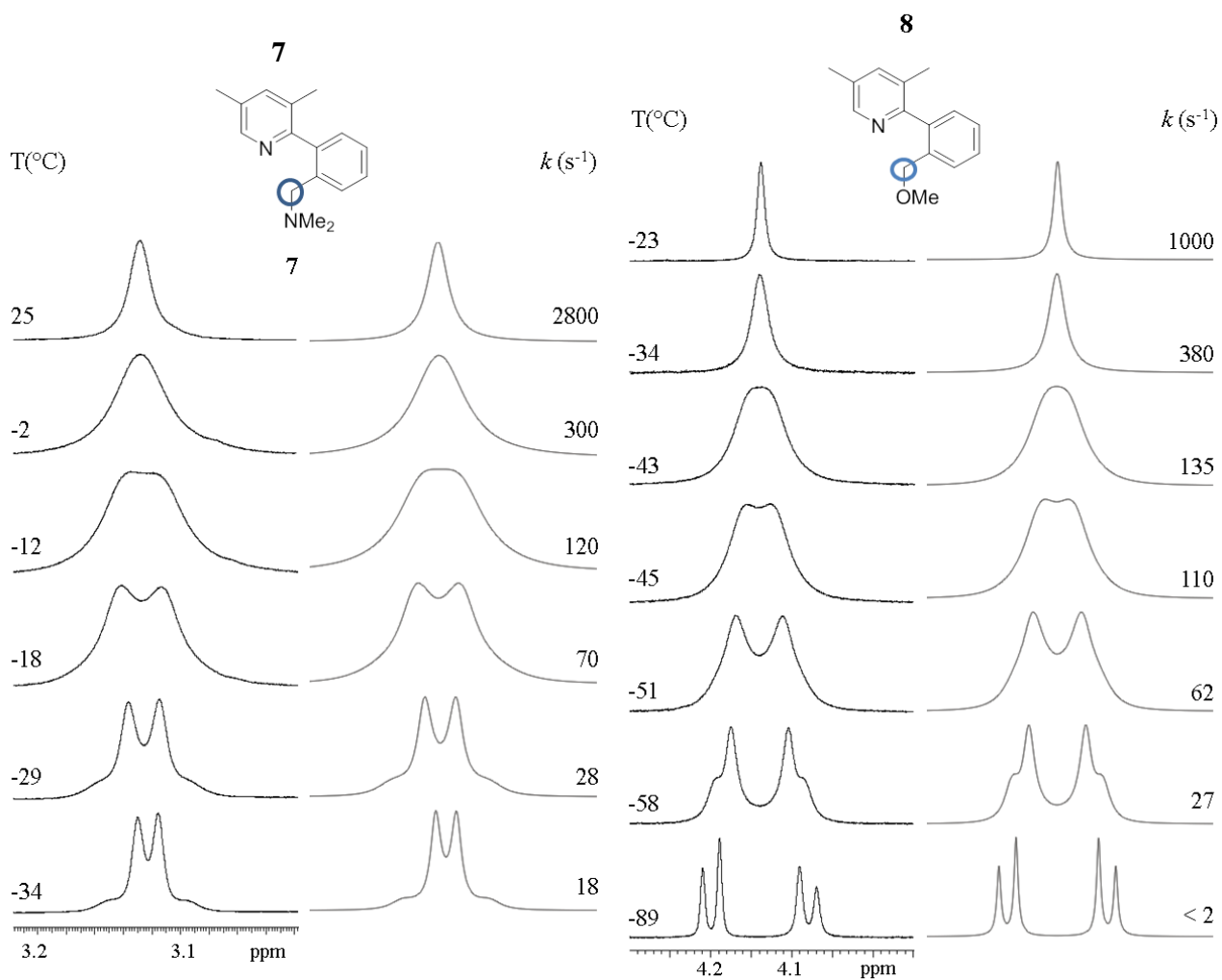


Figure 7.1.2 Dynamic $^1\text{H-NMR}$ spectra of compound **7** (CH_2 signal) and **8** (CH_2 signal) at 600 MHz in CD_2Cl_2 . On the right of the experimental spectra is reported the line shape simulations and the corresponding rate constants.

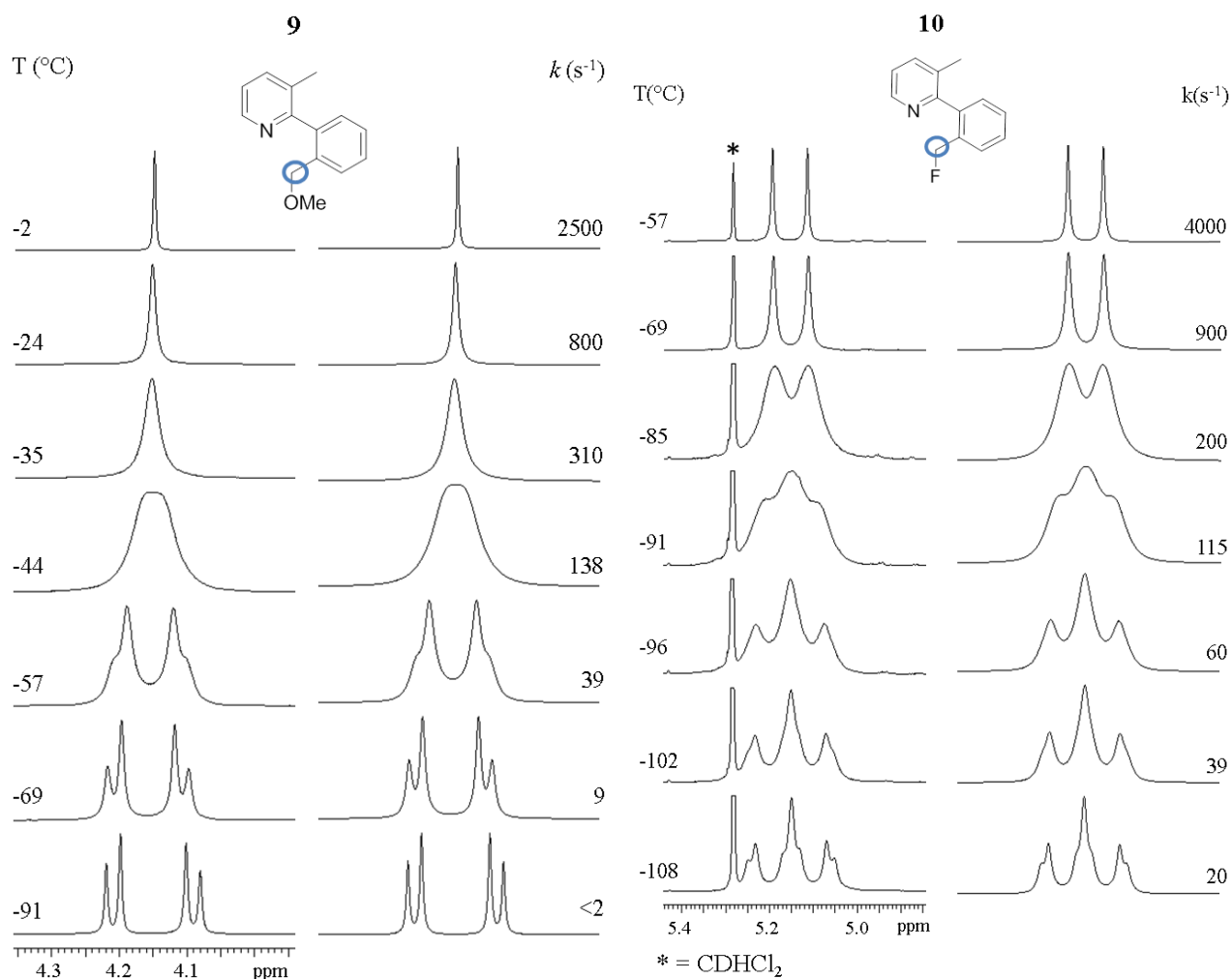


Figure 7.1.3 Dynamic ^1H -NMR spectra of compound **4** (CH_2 signal) and **6** (CH_2 signal) at 600 MHz in CD_2Cl_2 . On the right of the experimental spectra is reported the line shape simulations and the corresponding rate constants.

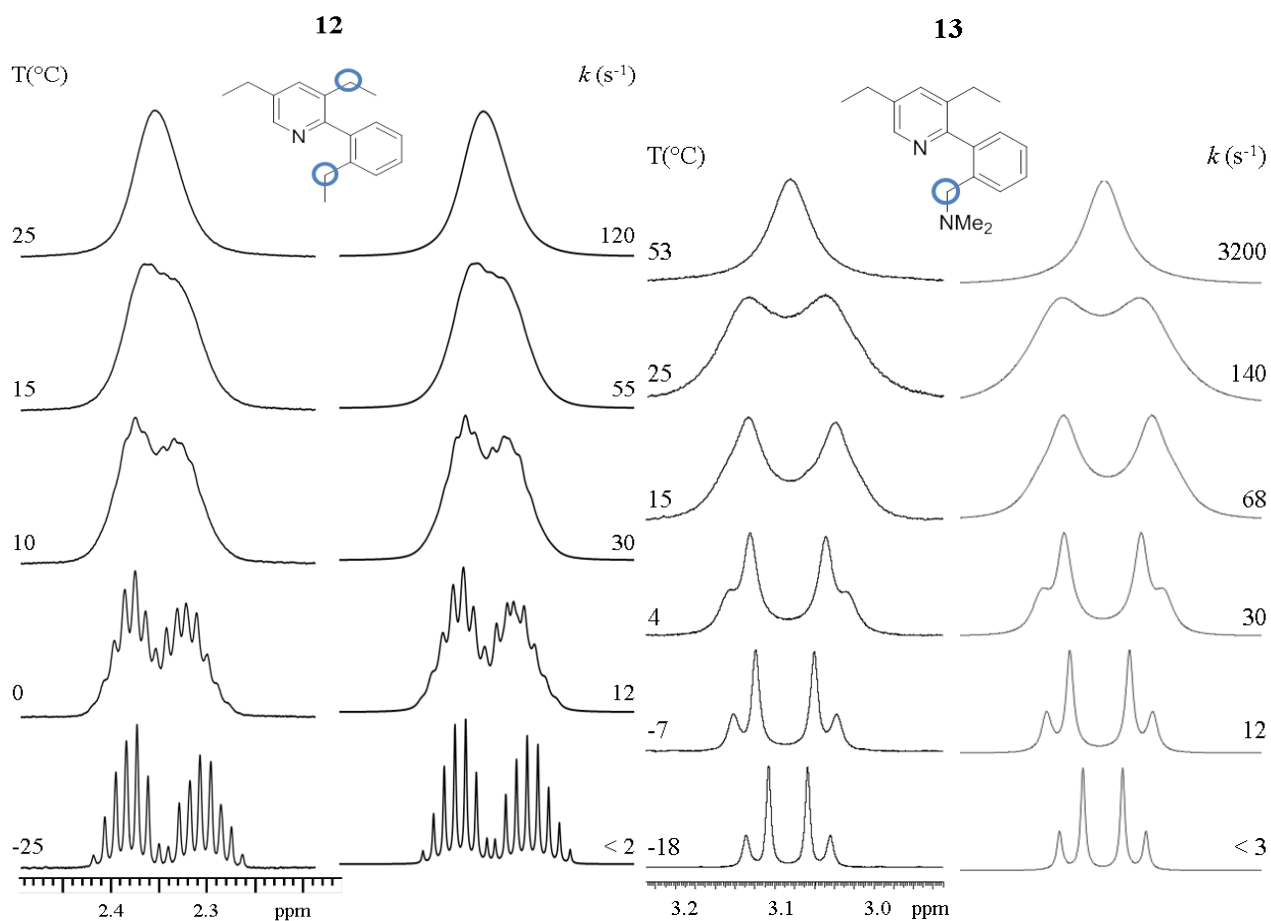


Figure 7.1.4 Dynamic ^1H -NMR spectra of compound **12** (signal of the two diastereotopic CH_2 signals) and **13** (CH_2 signals) at 600 MHz respectively in CD_2Cl_2 and CDCl_3 . On the right of the experimental spectra is reported the line shape simulations and the corresponding rate constants. In the case of **12** the number of the lines exceeded the software limit. For this reason, the full line shape simulation was obtained by the point to point sum of two ABX_3 systems.

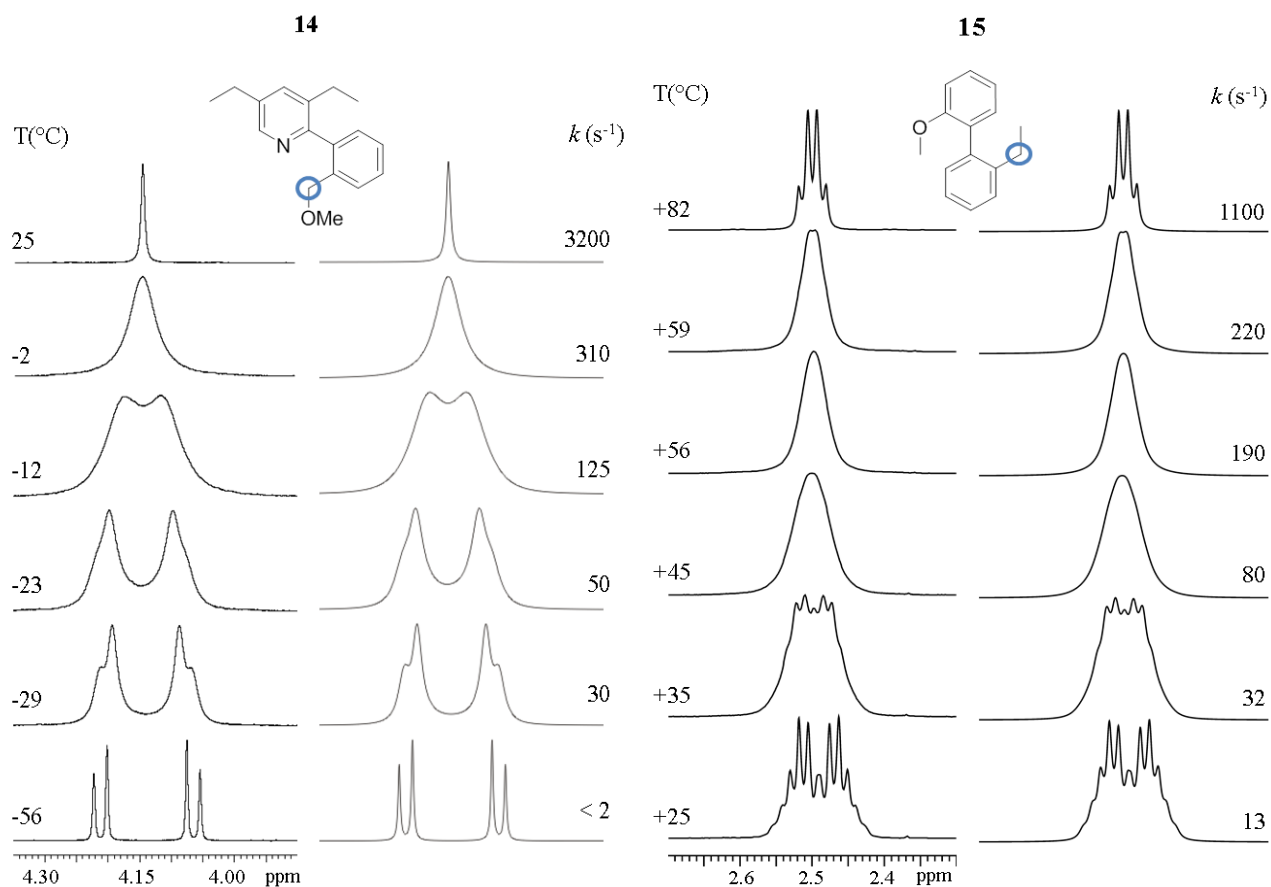


Figure 7.1.5 Dynamic ¹H-NMR spectra of compound **14** (CH₂ signal) and **15** (CH₂ signal) at 600 MHz respectively in CD₂Cl₂ and C₂D₂Cl₄. On the right of the experimental spectra is reported the line shape simulations and the corresponding rate constants.

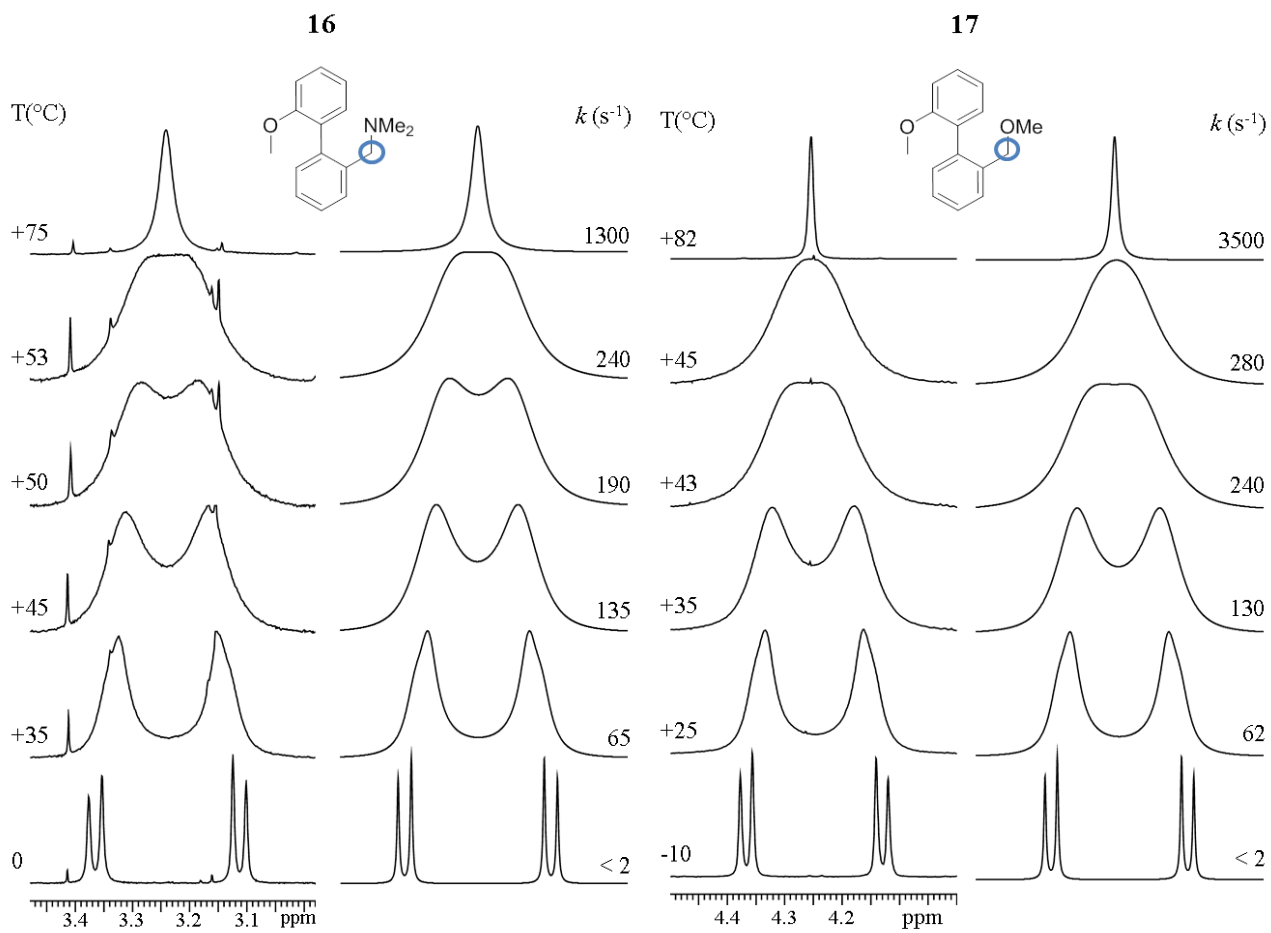


Figure 7.1.6 Dynamic ¹H-NMR spectra of compound **14** (CH₂ signal) and **15** (CH₂ signal) at 600 MHz in C₂D₂Cl₄. On the right of the experimental spectra is reported the line shape simulations and the corresponding rate constants.

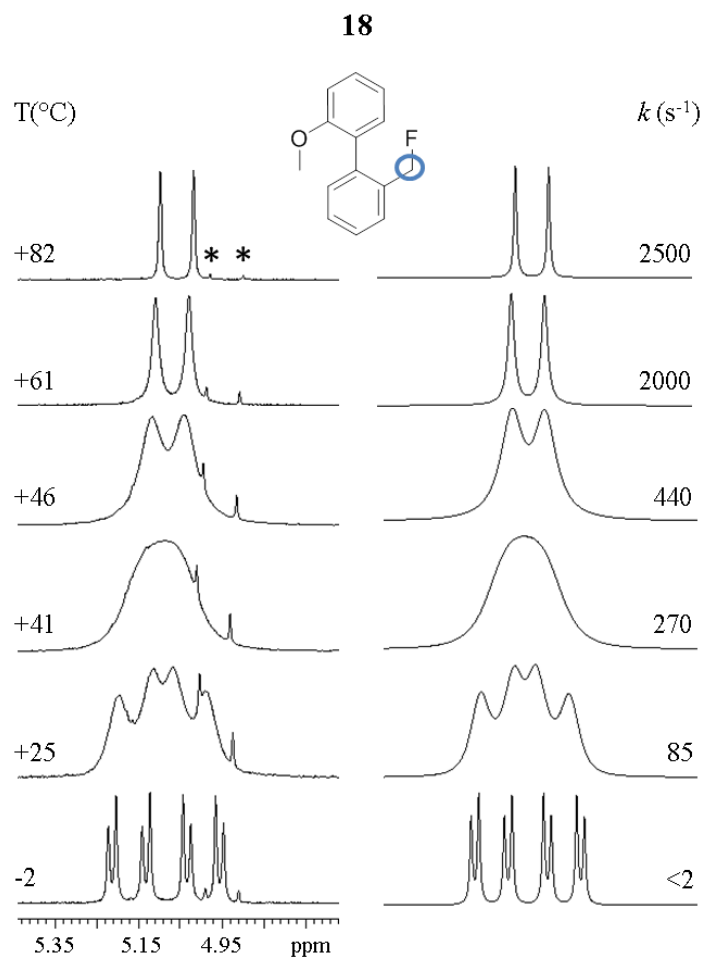


Figure 7.1.7 Dynamic ^1H -NMR spectra of compound **14** (CH_2 signal) and **15** (CH_2 signal) at 600 MHz in $\text{C}_2\text{D}_2\text{Cl}_4$ (Asterisks mark an impurity). On the right of the experimental spectra is reported the line shape simulations and the corresponding rate constants. Note: the doublet at +82 °C is due to the coupling with fluorine.

¹ Vijn R. J., Arts H. J., Green R., Castelijns A. M. *Synthesis*, **1994**, 573–578.

² Mahmud T., Iqbal J., Imran M., Mckee V. *J. Appl. Sciences* **2007**, 7, 1347–1350

7.2 New azo-decorated N-pyrrolidinylthiazoles: synthesis, properties and an unexpected remote substituent effect transmission

7.2.1 Dynamic NMR

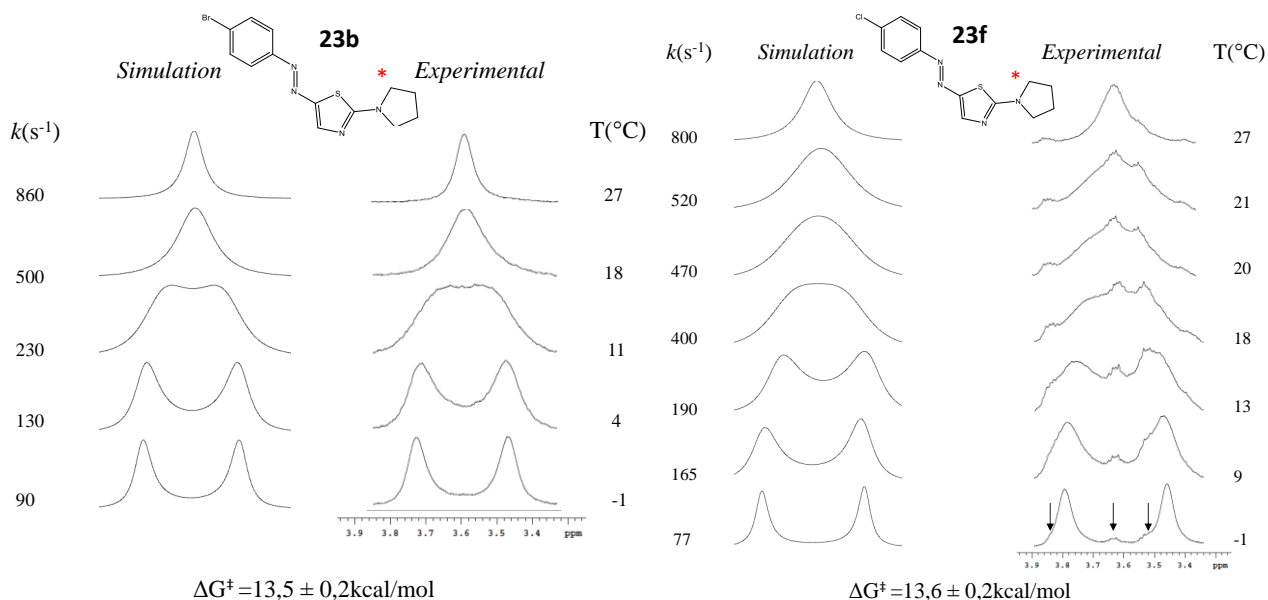


Figure 7.2.1 Methylene dynamic ¹H-NMR spectra in CDCl₃ and line shape simulations and correspondent kinetic constant for **23b** and **23f**. Black arrows indicates impurity.

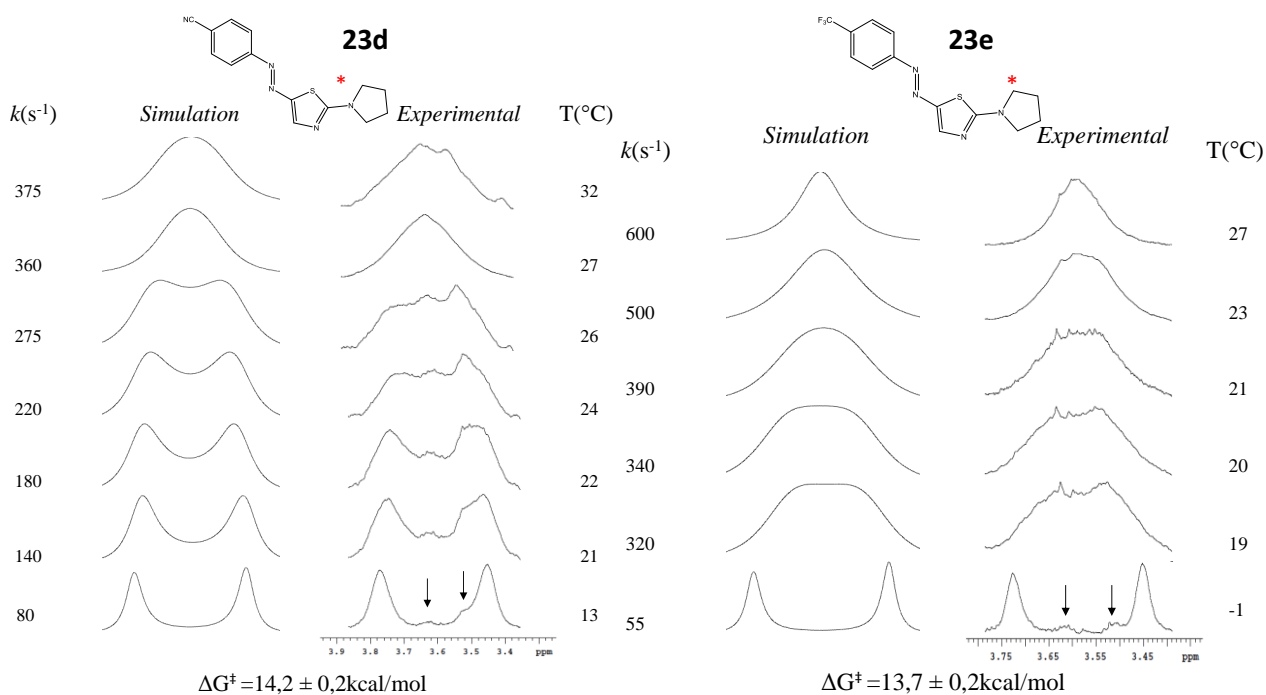


Figure 7.2.2 Methylene dynamic ¹H-NMR spectra in CDCl₃ and line shape simulations and correspondent kinetic constant for **23d** and **23e**. Black arrows indicates impurity.

7.3 Computational and DNMR Analysis of the Conformational Isomers and Stereodynamics of Secondary 2,2'-Bisanilides

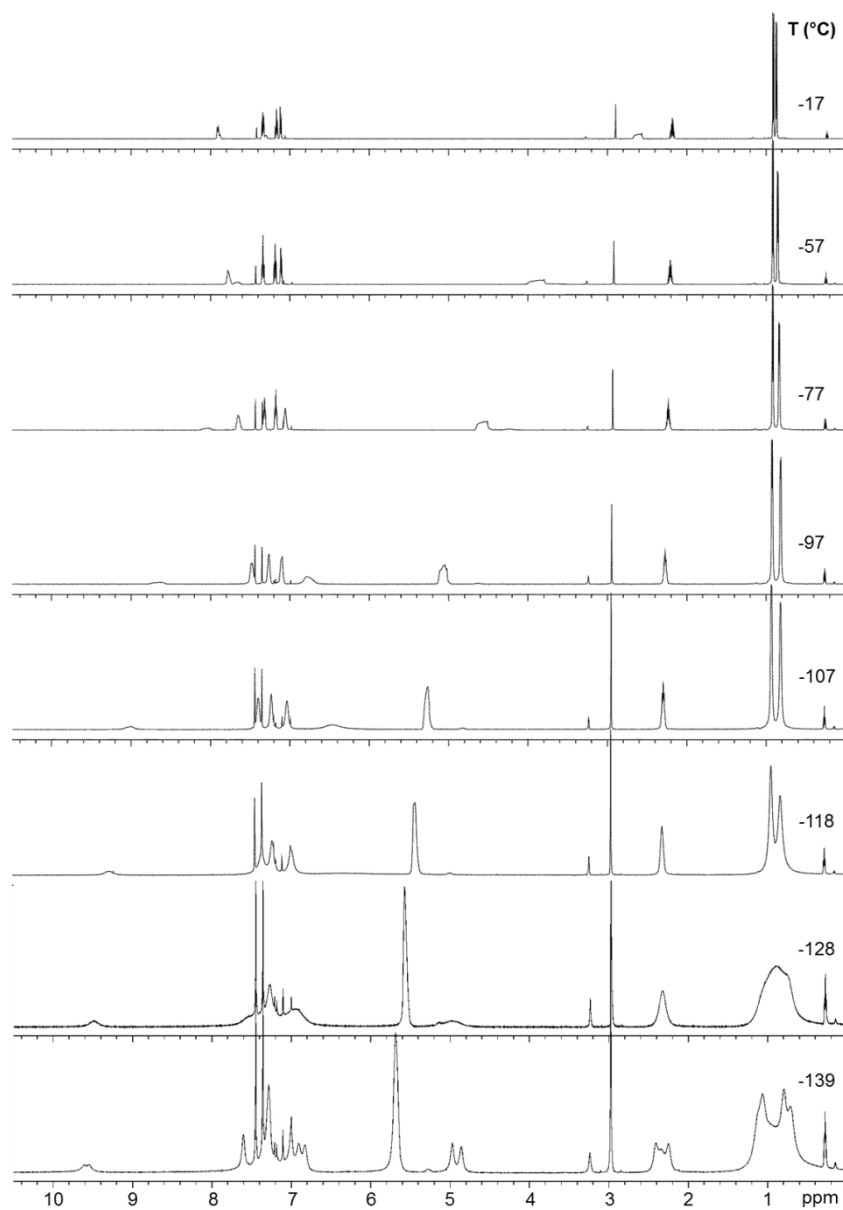


Figure 7.3.1 Temperature dependence of the ¹H NMR spectra of compound **25** (CDFCl₂:CDF₂Cl 5:1, 600 MHz) in presence of 3 equivalent of CD₃OD.

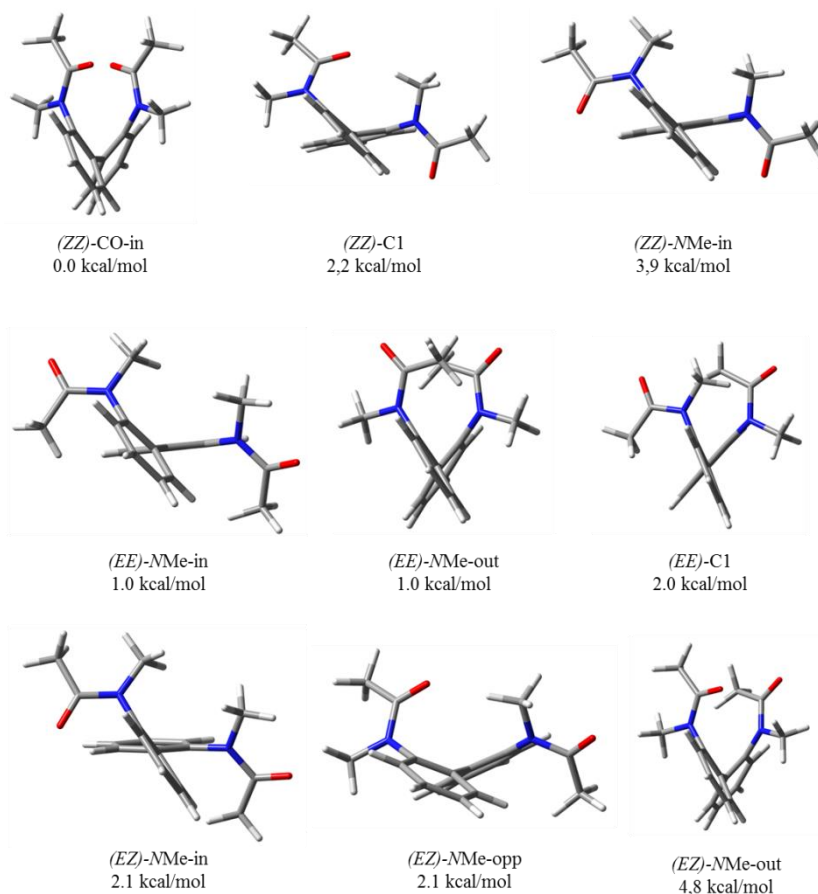
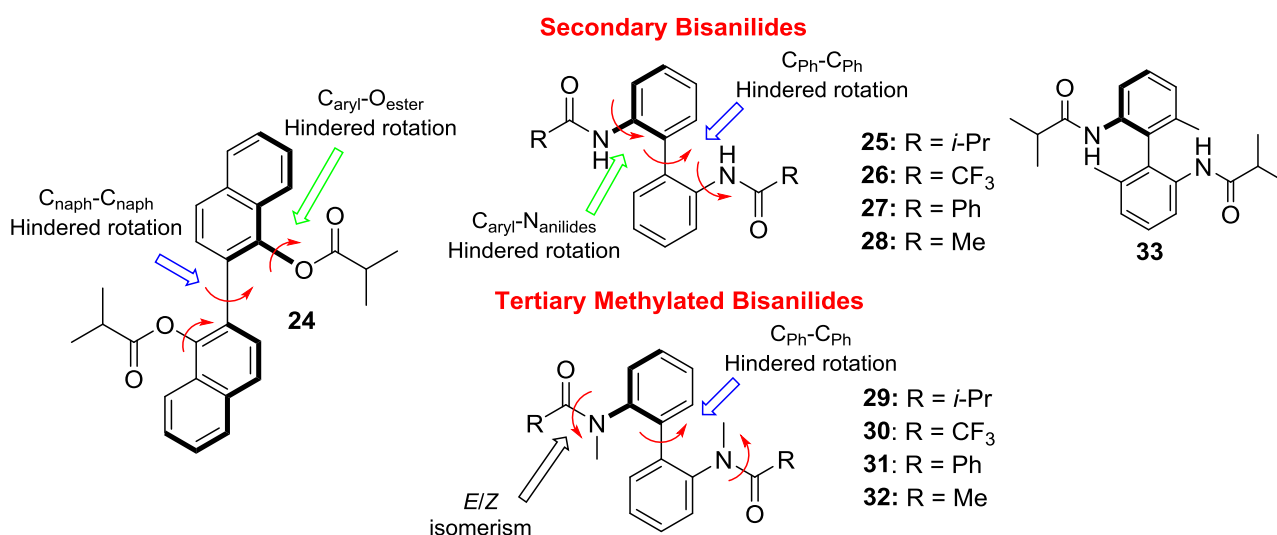


Figure 7.3.2 Possible conformers for **32**. Optimized geometries and relative energies were calculated at the B3LYP/6-31G(d) level.

7.3.1 Synthetical procedure



Structure of 2,2'-binaphthalene-1,1'-diol diisobutyrate **24**, and structural analogues bisanilides **25-33** investigated.

1,1'-Biphenyl-2,2'-diamine diisobutyramide, **25**.

2,2'-Diaminobiphenyl (50 mg, 0.27 mmol, 1 eq) and NEt_3 (94 μL , 0.68 mmol, 2.5 eq) were dissolved in 5 mL of dichloromethane and cooled to 0 °C. Isobutyryl chloride (68 μL , 0.65 mmol, 2.4 eq) was added and the mixture was slowly warmed to room temperature and stirred for 2 hours. The reaction was quenched with water and extracted with dichloromethane. The combined organic layers were dried over MgSO_4 and concentrated *in vacuo*. Purification by flash chromatography on silica gel (CH_2Cl_2 :EtOAc 85:15) afforded 85 mg (0.26 mmol, 95%) of a white solid. Crystals suitable for X-ray diffraction were obtained by slow evaporation of a CHCl_3 solution.

$^1\text{H NMR}$ (600 MHz, CD_3CN , +25 °C): δ = 0.91 (d, J = 6.8 Hz, 6H), 0.96 (d, J = 6.8 Hz, 6H), 2.28 (septet, J = 6.8 Hz, 2H), 7.18 (dd, J = 7.6 Hz, 1.7 Hz, 2H), 7.27 (dd, J = 7.6 Hz, 8.1 Hz, 2H), 7.42 (dd, J = 8.1 Hz, 7.6 Hz, 2H), 7.63 (s, 2H), 7.77 (d, J = 8.1 Hz, 2H). $^{13}\text{C NMR}$ (150 MHz, CD_3CN , +25 °C): δ = 19.4 (2 CH_3), 19.5 (2 CH_3), 36.3 (2CH), 125.8 (2CH), 126.2 (2CH), 129.4 (2CH), 131.4 (2CH), 133.6 (2Cq), 136.9 (2Cq), 176.8 (2CO). Anal. Calcd. for $\text{C}_{20}\text{H}_{24}\text{N}_2\text{O}_2$: C, 74.05; H, 7.46; N, 8.63. Found: C, 74.01; H, 7.73; N, 8.59.

1,1'-Biphenyl-2,2'-diamine bis(trifluoromethylacetamide) 26.¹

2,2'-Diaminobiphenyl (60 mg, 0.33 mmol, 1 eq) and NEt_3 (95 μL , 0.68 mmol, 2 eq) were dissolved in 5 mL of dichloromethane and cooled to 0 °C. Trifluoroacetic anhydride (114 μL , 0.82 mmol, 2.5 eq) was added and the mixture was slowly warmed to room temperature and stirred for 4 hours. The reaction was quenched with water and extracted with dichloromethane. The combined organic layers were dried over MgSO_4 and concentrated *in vacuo*. Purification by flash chromatography on silica gel (CH_2Cl_2 : EtOAc 85:15) afforded 92 mg (0.24 mmol, 75%) of a brown solid. Crystals suitable for X-ray diffraction were obtained by slow evaporation of a CHCl_3 solution.

$^1\text{H NMR}$ (600 MHz, CD_3CN , +25 °C): δ = 7.30 (d, J = 7.6 Hz, 2H), 7.45 (dd, J = 7.6 Hz, 7.9 Hz, 2H), 7.54 (dd, J = 7.9 Hz, 7.6 Hz, 2H), 7.69 (d, J = 7.9 Hz, 2H), 8.71 (bs, 2H). $^{13}\text{C NMR}$ (150 MHz, CD_3CN , +25 °C): δ = 116.8 (q, J_{CF} = 288 Hz, 2 CF_3), 126.7 (2CH), 128.5 (2CH), 130.3 (2CH), 131.7 (2CH), 133.5 (2Cq), 134.5 (2Cq), 156.6 (2CO). $^{19}\text{F NMR}$ (376 MHz, CDCl_3): δ = -76.1.

1,1'-Biphenyl-2,2'-diamine dibenzamide, 27.²

2,2'-Diaminobiphenyl (80 mg, 0.43 mmol, 1 eq) and NEt_3 (150 μL , 1.09 mmol, 2.5 eq) were dissolved in 5 mL of dichloromethane and cooled to 0 °C. Benzoyl chloride (106 μL , 0.91 mmol, 2.1 eq) was added and the mixture was slowly warmed to room temperature and stirred for 2 hours. The reaction was quenched with water and extracted with dichloromethane. The combined organic layers were dried over MgSO_4 and concentrated *in vacuo*. Purification by flash chromatography on silica gel (CH_2Cl_2 :EtOAc 85:15) afforded 130 mg (0.33 mmol, 75%) of a white solid.

¹H NMR (600 MHz, CD₃CN, +25 °C): δ = 7.28-7.33 (m, 4H), 7.41-7.48 (m, 6H), 7.53 (m, 2H), 7.66 (m, 4H), 7.81 (d, *J* = 7.4Hz, 2H), 8.58 (s, 2H). **¹³C NMR** (150 MHz, CD₃CN, +25 °C): δ = 126.6 (2CH), 126.8 (2CH), 127.9 (4CH), 129.5 (4CH), 129.6 (2CH), 131.4 (2CH), 132.7 (2CH), 135.1 (2Cq), 135.3 (2Cq), 136.8 (2Cq), 167.1 (2CO).

1,1'-Biphenyl-2,2'-diamine acetamide, 28.

2,2'-Diaminobiphenyl (612 mg, 0.33 mmol, 1 eq) and 4-aminopyridine (40 mg, 0.033 mmol, 1 eq) were dissolved in 4 mL (40 mmol, 12 eq) of acetic anhydride. The dark orange mixture was stirred for 1 hour at 75 °C. The reaction was quenched with 20 mL of HCl (0.2M). The solution was diluted with 20 mL of dichloromethane and the organic phase was separated. The aqueous phase was extracted with DCM (3 x 15 mL); the combined organic layers were washed with a saturated aqueous solution of NaHCO₃ (20 mL) and brine (20 mL), then dried over Na₂SO₄. Purification by flash chromatography on silica gel (hexane:ethyl acetate 80:20) afforded 680 mg (2.54 mmol, 76%) of a white solid. Crystal suitable for X-ray diffraction were obtained by slow evaporation of an acetonitrile solution.

¹H NMR (600 MHz, CD₃CN, +25 °C): δ = 1.84 (s, 6H), 7.21 (dd, *J* = 7.6Hz, 1.6Hz, 2H), 7.27 (dd, *J* = 7.6 Hz, 7.6 Hz, 2H), 7.42 (dd, *J* = 7.6Hz, 8.1Hz, 2H), 7.62 (s, 2H), 7.83 (d, *J* = 8.1Hz, 2H). **¹³C NMR** (150 MHz, CD₃CN, +25 °C): δ = 23.7 (2CH₃), 125.5 (2CH), 126.1 (2CH), 129.4 (2CH), 131.8 (2CH), 132.5 (2Cq), 136.9 (2Cq), 170.0 (2CO). Anal. Calcd. for C₁₆H₁₆N₂O₂: C, 71.62; H, 6.01; N, 10.44. Found: C, 71.36; H, 5.73; N, 10.32.

***N,N'*-(6,6'-dimethyl-[1,1'-biphenyl]-2,2'-diyl)bis(2-methylpropanamide) 33 and (*M*)-*N,N'*-(6,6'-dimethyl-[1,1'-biphenyl]-2,2'-diyl)bis(2-methylpropanamide) (*M*)-33.**

In an oven-dried two-necked round bottomed flask 6,6'-dimethyl-2,2'-diaminobiphenyl³ or (*M*)-6,6'-dimethyl-2,2'-diaminobiphenyl (0.24 mmol, 1 eq.) was dissolved in 2 mL of anhydrous dichloromethane and the solution was cooled at 0 °C. Triethylamine (1.44 mmol, 6 eq.) and isobutyryl chloride (0.96 mmol, 4 eq) were added in sequence. The solution was stirred at room temperature until complete consumption of the starting material (TLC, 3 hours). The reaction mixture was diluted with dichloromethane (10 mL) and quenched with 1M HCl (5 mL) at 0 °C. The organic layer was washed with brine (10 mL) and saturated aqueous solution of NaHCO₃ (2 x 5 mL). The organic phase was dried over Na₂SO₄ and the solvent was removed under reduced pressure to afford the product as a pale brown solid in 82 % yield (69 mg, 0.19 mmol).

¹H NMR (600 MHz, CDCl₃, +25 °C) δ = 0.92 (d, *J* = 6.6 Hz, 6H), 0.97 (d, *J* = 6.6 Hz, 6H), 1.97 (s, 6H), 2.23 (septet, *J* = 6.6 Hz, 2H), 6.98 (bs, 2H), 7.15 (d, *J* = 7.8 Hz, 2H), 7.34 (dd, *J* = 7.8 Hz, 7.9

Hz, 2H), 8.03 (d, $J = 7.8$ Hz, 2H). ^{13}C NMR (150 MHz, CDCl_3 , +25 °C) $\delta = 19.0$ (2 CH_3), 19.1 (2 CH_3), 19.5 (2 CH_3), 36.2 (2CH), 120.3 (2CH), 126.4 (2CH), 127.1 (2Cq), 129.0 (2CH), 135.7 (2Cq), 137.0 (2Cq), 175.4 (2CO). GC-MS (m/z): 352 (25) $[\text{M}]^+$, 309 (5) $[\text{M-iPr}]^+$, 282 (25), 239 (25), 212(20), 195 (100), 180 (15), 71(15). Anal. Calcd. for $\text{C}_{22}\text{H}_{28}\text{N}_2\text{O}_2$: C, 74.97; H, 8.01; N, 7.95. Found: C, 74.78; H, 8.39; N, 7.85.

N,N' -([1,1'-Biphenyl]-2,2'-diyl)bis(N -methyl-2-dimethylpropanamide) 29.

In an oven-dried round balloon purged with nitrogen a solution of N,N' -dimethyl-2,2'-diaminobiphenyl (0.47 mmol, 1 eq.) in dichloromethane (4 mL) was cooled at 0 °C and 5.7 mmol (12 eq) of TEA was added. Isobutyryl chloride (3.8 mmol, 8 eq) was added dropwise and the reaction mixture was stirred and allowed to return to the room temperature in 3h. The reaction was quenched with HCl (1M), and the phases were separated. The aqueous phase was extracted with DCM (3 x 10 mL). The combined organic layers were washed with a saturated aqueous solution of NaHCO_3 (20 mL) and brine (20 mL), and dried over Na_2SO_4 . The solvent was removed under reduced pressure and the desired product was obtained as a white solid (113 mg, 0.32 mmol) by semi-preparative HPLC in 70% yield. Column: LUNA-C18 (250 x 21.20 mm), MeCN/ H_2O 80/20, 20 ml/min, λ 254 nm, t_{R} : 4.72 min. mp 152-154 °C.

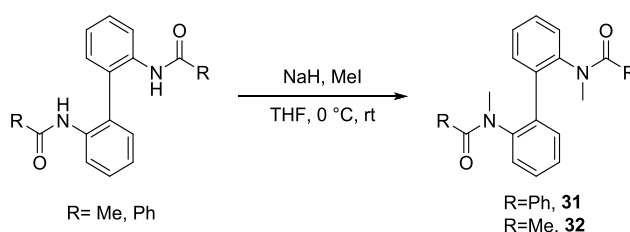
^1H NMR (600 MHz, CDCl_3 , +25 °C): $\delta = 0.80$ (bs, 1H), 1.4 (d, $J = 6.7\text{Hz}$, 1H), 1.08 (d, $J = 6.7\text{Hz}$, 4H), 1.14 (d, $J = 6.7\text{Hz}$, 4H), 1.17-1.27 (bs, 2H). 2.25 (bs, 0.3H) 2.39 (sept, $J = 6.7\text{Hz}$, 0.3H), 2.59 (sept, $J = 6.7\text{Hz}$, 1.4H), 2.79-2.87 (bs, 4H), 2.95 (bs, 0.7H), 3.07 (bs, 1H), 3.37 (bs, 0.3H), 7.24 (bs, 1H), 7.29 (bm, 2.6H), 7.33 (bm, 0.6H), 7.39 (bm, 2.2H), 7.43(bm, 1.4H), 7.47 (bs, 0.2H). ^{13}C NMR (150 MHz, CDCl_3 , +25 °C): $\delta = 18.8$, 19.0, 19.6, 20.3, 20.7 (b), 30.4, 31.4, 31.6 (b), 35.6 (b), 128.1, 128.2, 128.7, 129.27, 129.34, 129.4, 129.5, 130.9, 131.2, 134.0, 134.7, 141.4, 141.8, 177.5, 177.8 (b). Anal. Calcd. for $\text{C}_{22}\text{H}_{28}\text{N}_2\text{O}_2$: C, 74.97; H, 8.01; N, 7.95. Found: C, 74.57; H, 8.43; N, 7.83.

N,N' -([1,1'-biphenyl]-2,2'-diyl)bis(2,2,2-trifluoro- N -methylacetamide) 30.

A solution of 1.0 mL of trifluoroacetic anhydride was cooled to 0 °C and 0.1 mmol (1 eq.) of N,N' -dimethyl-[1,1'-biphenyl]-2,2'-diamine were added. The solution was stirred for 1 hour at room temperature and then diluted with ethyl acetate and quenched with HCl (1M, 10 mL). The organic layer was washed with brine (10 mL) and a saturated aqueous solution of NaHCO_3 (10 mL). The organic phase was dried over Na_2SO_4 and the solvent was evaporated under reduced pressure to afford a sticky solid. A sample was purified by preparative HPLC on the LUNA-C18 phase (250 x 21.20 mm), MeCN/ H_2O 70/30, 20 ml/min, λ 254 nm, t_{R} : 9.14 min. The HPLC purification gave 32mg (0.08 mmol,80%) of a sticky solid.

¹H NMR (600 MHz, CDCl₃, +25 °C) δ = 2.80 (s, 1.2H), 2.86 (bs, 0.6H), 2.95-3.07 (bm, 1.8H), 3.15 (bs, 0.9H), 3.54-3.66 (bs, 1.5H), 7.24-7.52 (bm, 8H). **¹⁹F NMR** (564 MHz, CDCl₃, +25 °C) δ = -66.1, -66.2, -67.2, -70.2, -70.3, -70.6, -70.8. **¹³C NMR** (150 MHz, CDCl₃, +25 °C) δ = 37.1, 37.4 (b), 39.7 (b), 116.4 (q, *J* = 291.7Hz, CF₃), 127.2 (b), 128.4, 128.9, 129.1 (b), 129.7, 129.8, 130.0 (b), 130.5, 131.0, 133.4 (b), 134.0 (b), 134.7, 138.2, 140.0 (b), 140.7 (b), 156.1(b), 157.4, 157.6, 157.8, 158.1. HRMS (ESI-QTOF) Calcd for C₁₈H₁₅F₆N₂O₂: 405.1032. Found: 405.1038. Anal. Calcd. for C₁₈H₁₄F₆N₂O₂: C, 53.47; H, 3.49; N, 6.93. Found: C, 53.12; H, 3.85; N, 6.69.

General procedure for the preparation of tertiary amides **31** and **32**.



In an oven dried Schlenk tube under nitrogen atmosphere 0.2 mmol (1 eq.) of amide was dissolved in 1 mL of anhydrous THF and the solution was cooled at 0 °C. NaH (60% dispersion in mineral oil, 0.5 mmol, 2.5 eq.) was added and the reaction mixture was stirred for 15 minutes at ambient temperature, then MeI (0.6 mmol, 3 eq.) was added at 0 °C. The reaction mixture was stirred at ambient temperature until complete consumption of the starting material (TLC, 2-6 hours) and then quenched with a saturated solution of NH₄Cl (5 mL). The aqueous phase was extracted with ethyl acetate (3 x 5 mL), the combined organic layers were washed with brine (10 mL) and then dried over Na₂SO₄. The solvent was removed under reduced pressure to afford the desired product which was used as is or purified by semi-preparative HPLC for the VT-NMR analysis.

N,N'-([1,1'-Biphenyl]-2,2'-diyl)bis(*N*-methylbenzamide) **31**.

Using **27** in the protocol described above, were obtained 56 mg (67% yield) of a white solid. Mp 157-159 °C.

¹H NMR (600 MHz, CDCl₃, +25 °C) δ = 1.98 (s, 0.4H), 3.07 (bs, 2.9H), 3.56 (s, 2.7H), 5.95 (bs, 1.3H), 6.85 (bdd, *J* = 6.0 Hz, *J* = 6.0 Hz, 0.8H), 7.03-7.20 (bm, 4.2H), 7.20-7.69 (bm, 9.1H). **¹³C NMR** (150 MHz, CDCl₃, +25 °C) δ = 37.7, 125.6, 126.5 (b), 127.1, 127.2, 127.6, 128.2, 128.4, 128.7, 129.3, 129.5, 129.8, 130.9 (b), 132.5, 135.0, 135.2, 135.3, 136.0 (b), 141.2, 142.0, 168.9, 169.7, 172.0 (b). Anal. Calcd. for C₂₈H₂₄N₂O₂: C, 79.98; H, 5.75; N, 6.66. Found: C, 79.53; H, 5.65; N, 6.66.

N,N'-([1,1'-biphenyl]-2,2'-diyl)-bis(*N*-methylacetamide) **32**.

Using **28** in the protocol described above, were obtained 38 mg (63% yield) of a white solid. Mp 173-175 °C. Crystals suitable for X-ray analysis were obtained by slow evaporation of a CDCl₃ solution. ¹H NMR (600 MHz, CDCl₃, +25 °C) δ = 1.85 (s, 1.2H), 2.01 (bs, 4.1H), 2.16 (bs, 0.7H), 2.77 (bs, 4.1H), 2.87 (bs, 0.5H), 2.96 (s, 1.5H), 3.37 (bs, 0.7H), 7.24 (bd, 1.9H), 7.27 (d, J = 7.2Hz, 1.4H), 7.31 (bd, 0.6H), 7.37 (bm, 0.5H), 7.41-7.44 (bm, 3.5H). ¹³C NMR (150 MHz, CDCl₃, +25 °C) δ = 22.0, 22.5, 22.6, 22.7, 35.4, 36.6, 127.9, 128.1, 128.2, 129.1, 129.2, 129.3, 131.2, 132.4, 135.0, 136.1, 141.8, 142.1, 170.7, 170.9, 171.0. Anal. Calcd. for C₁₈H₂₀N₂O₂: C, 72.95; H, 6.80; N, 9.45. Found: C, 72.57; H, 6.49; N, 9.85.

¹ Zhang S., Zhang D., Liebeskind L. S. *J. Org. Chem.* **1997**, *62*, 2312-2313.

² Ames D. E., Opalko A. *Tetrahedron* **1984**, *40*, 1919-1925.

³ Gillerspie K. M., Sanders C. J., Westmoreland I., Thickitt C. P., Scott P. *J. Org. Chem.*, **2002**, *67*, 3450-3458

7.4 Conformational Analysis and Absolute Configuration of Axially Chiral 1-aryl and 1,3-diaryl-xanthenes

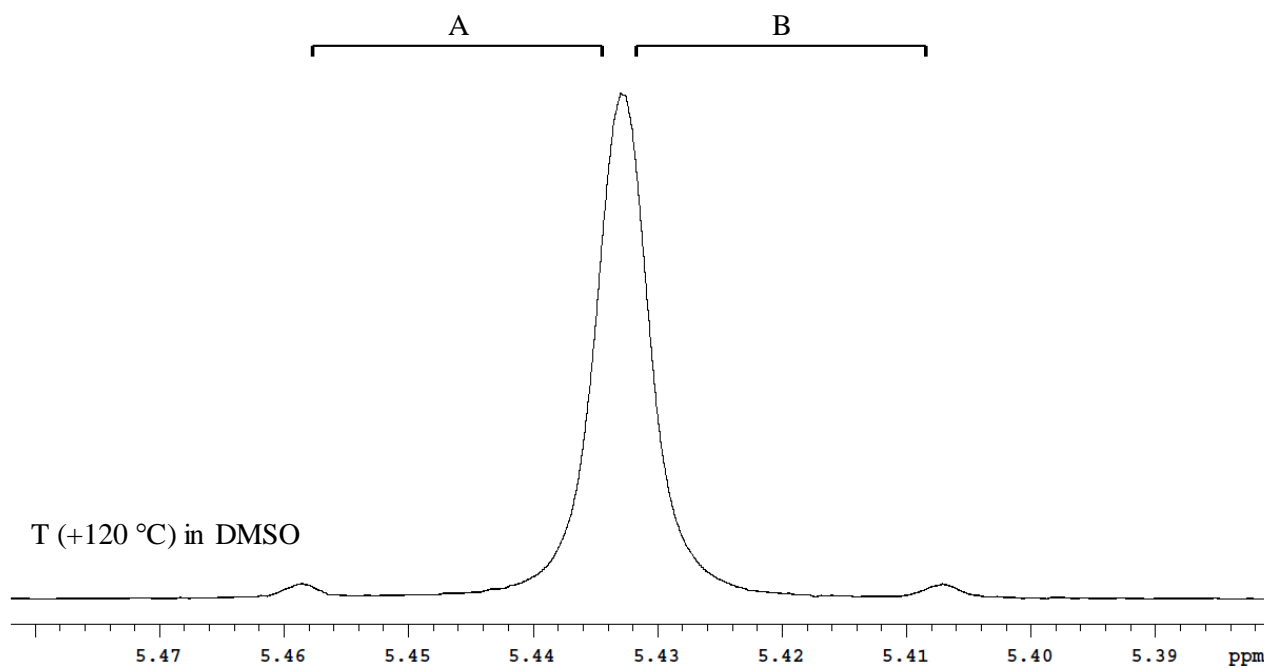


Figure 7.4.1 ¹H NMR spectrum of compound **34** for the benzyl signal at +120 °C in DMSO at 600 MHz.

7.4.1 Kinetic studies

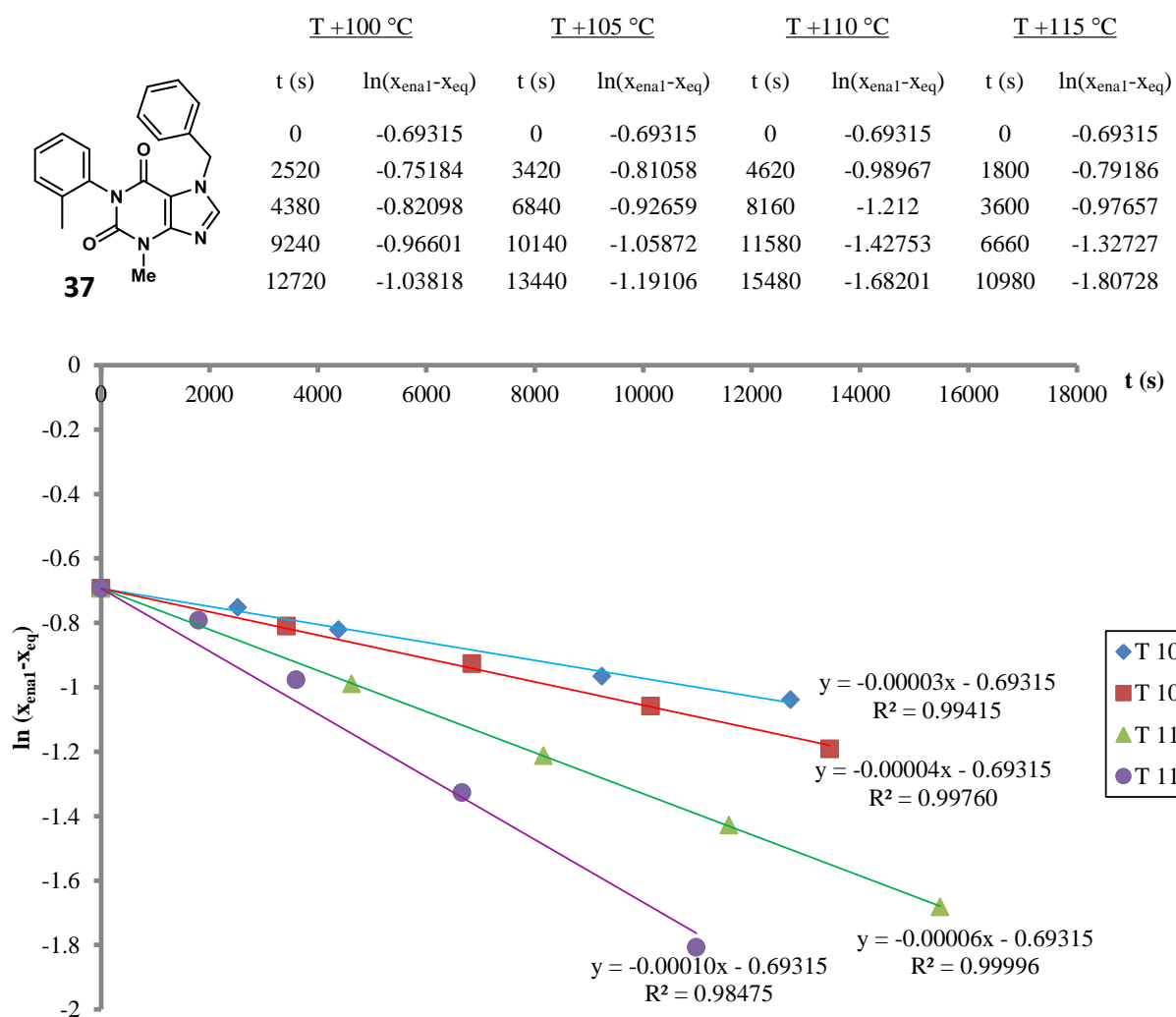
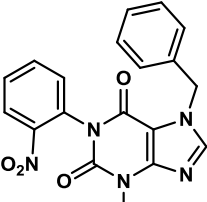


Figure 7.4.2 First Order Kinetics of Compound **37** at +100 °C, +105 °C, +110 °C and +115 °C in C₂D₂Cl₄. The slope gives the sum of the kinetic constant at each temperature.

	T +30 °C		T +50 °C		T +56 °C		T +58 °C	
	t (s)	ln(x _{ena1} -x _{eq})	t (s)	ln(x _{ena1} -x _{eq})	t (s)	ln(x _{ena1} -x _{eq})	t (s)	ln(x _{ena1} -x _{eq})
	0	-0,90042	0	-0,73397	0	-0,81803	0	-0,90189
	74700	-1,59554	2280	-0,95946	1680	-1,09602	3540	-1,48281
	97860	-1,81523	5880	-1,25702	5100	-1,77078	7920	-2,29066
			9120	-1,5616	8760	-2,4986	10020	-2,752
			12660	-1,86821				
			14340	-2,04022				

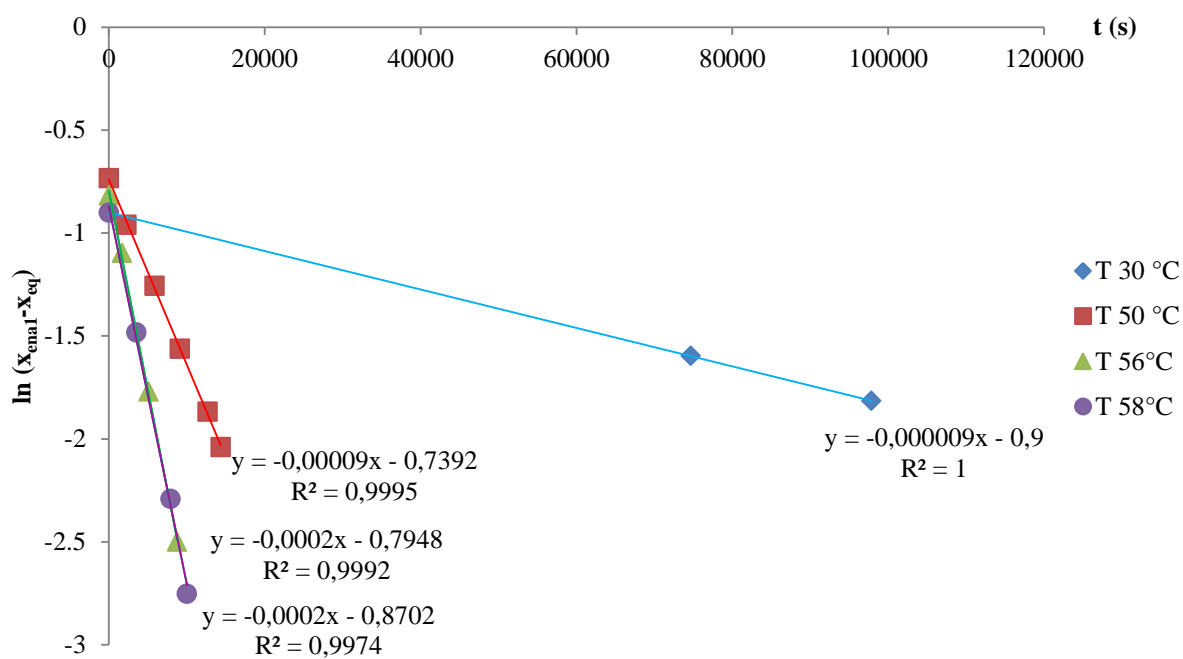
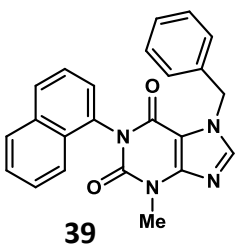


Figure 7.4.3 First Order Kinetics of Compound **38** at +30 °C, +50 °C, +56 °C and +58 °C in C₂D₂Cl₄. The slope gives the sum of the kinetic constant at each temperature.

	T +100 °C		T +110 °C		T +120 °C		T +130 °C	
	t (s)	ln(x _{ena2} -x _{eq})	t (s)	ln(x _{ena2} -x _{eq})	t (s)	ln(x _{ena2} -x _{eq})	t (s)	ln(x _{ena2} -x _{eq})
 <p>39</p>	0	-0,7529	0	-0,7529	0	-0,7546	0	-0,7546
	18720	-0,77653	13860	-0,80386	3900	-0,81622	4860	-0,89575
	79200	-0,85637	22980	-0,86917	8460	-0,93777	9960	-1,07646
	93180	-0,87156			11940	-1,00731	13080	-1,19733
					14340	-1,05354	16800	-1,3356
				66960	-1,7043	21360	-1,50328	

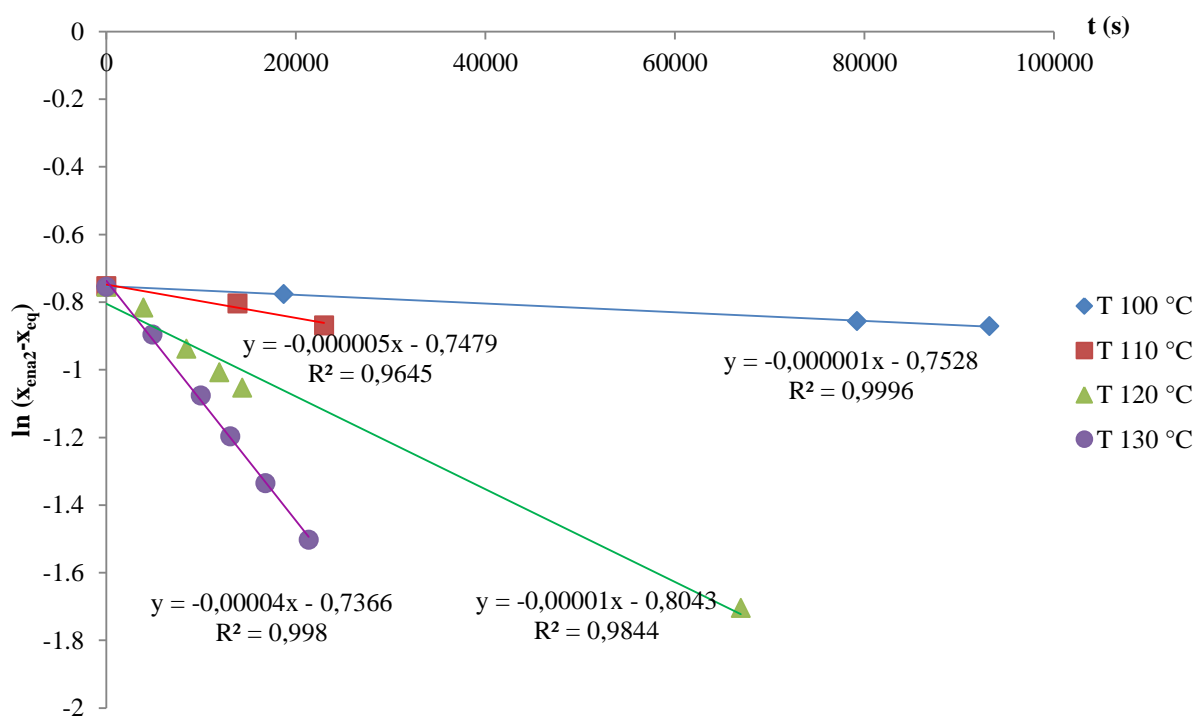


Figure 7.4.4 First Order Kinetics of Compound **39** at +100 °C, +110 °C, +120 °C and +130 °C in C₂D₂Cl₄. The slope gives the sum of the kinetic constant at each temperature.

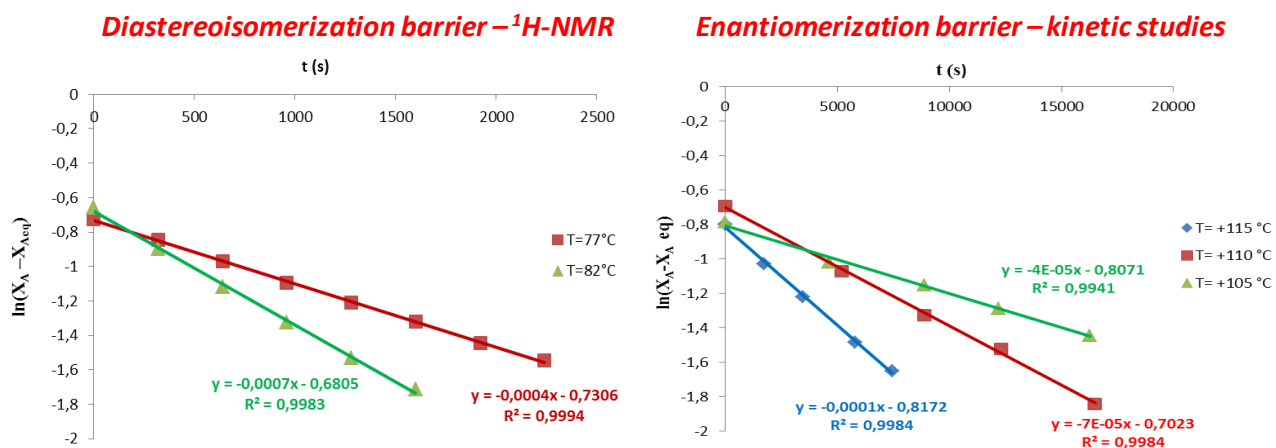
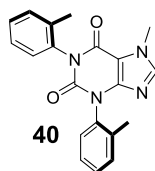


Figure 7.4.5 Left: First order kinetics at +77 °C and +82 °C obtained at ¹H-NMR of **40**. The slope provides the sum of the kinetic constants at each temperature. Right: First Order Kinetic treatment at +105 °C, +110 °C and +115 °C of **40**. The slope gives the sum of kinetic rate constants at each temperature.

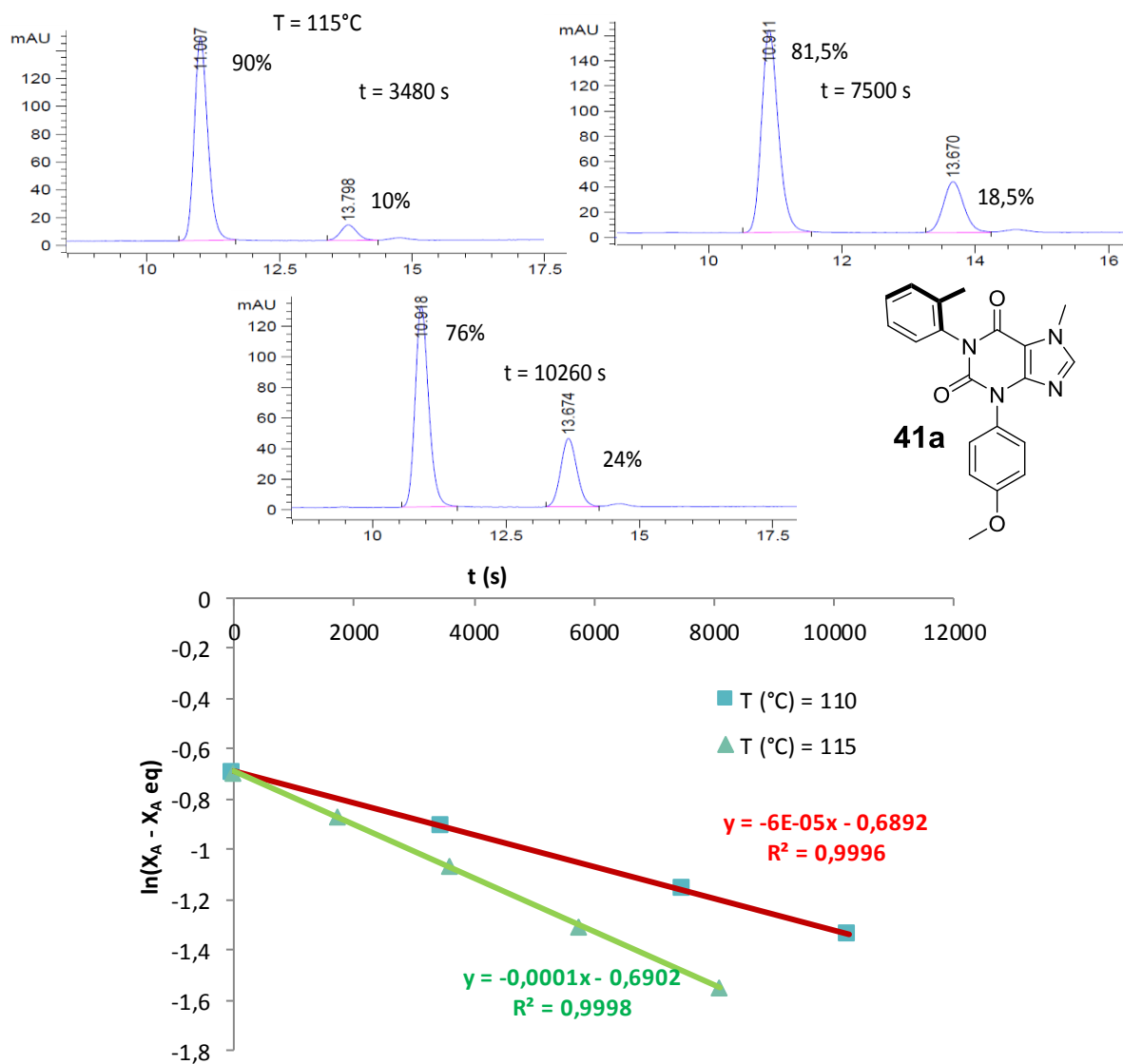
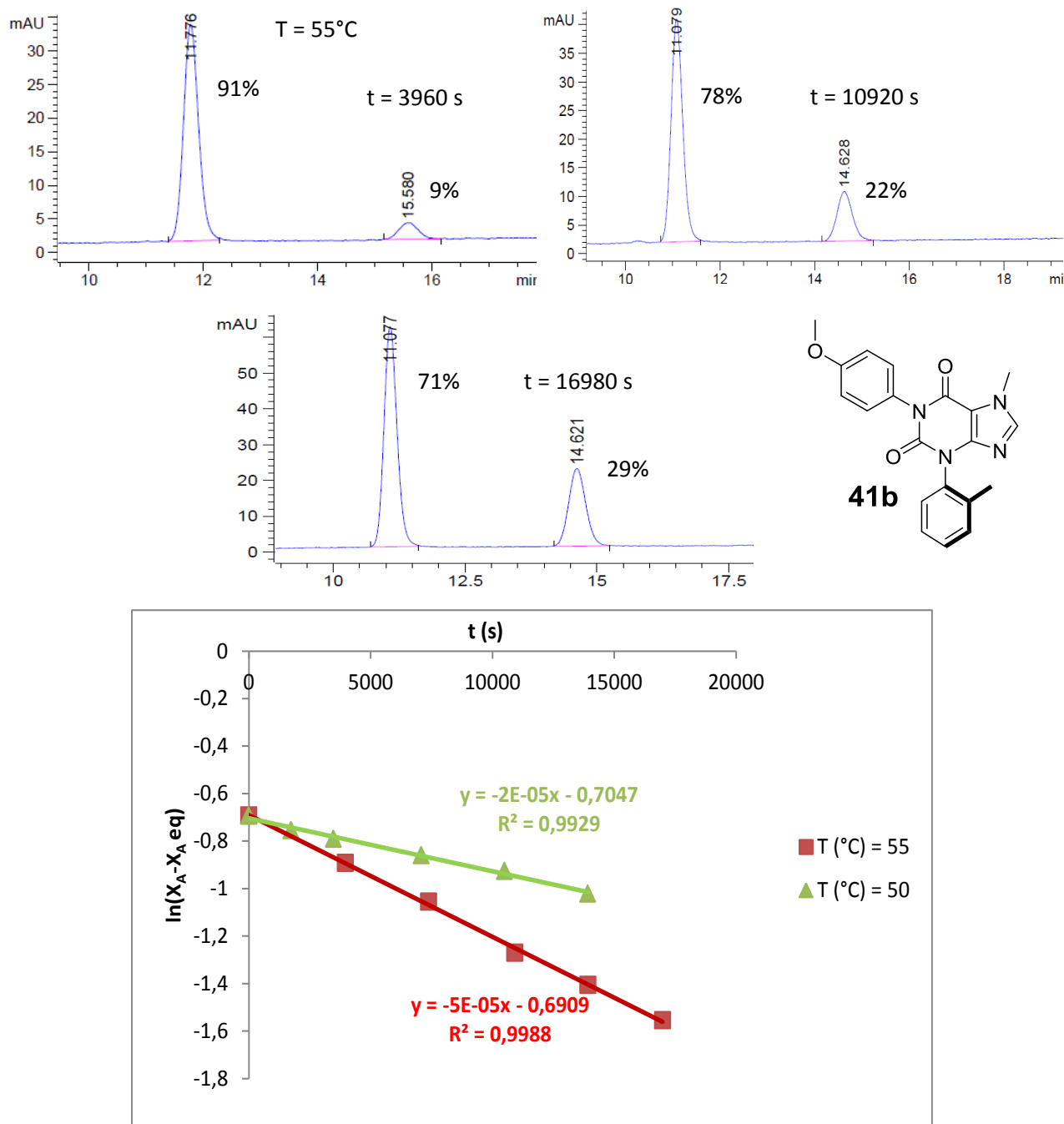


Figure 7.4.6 Top: kinetic measurement of enantiomerization rate of compound **41a** by HPLC (Chiralpak AD-H, eluent hexane/*i*PrOH 70/30 v/v, 0.8 mL/min), starting from one enantiomer kept at +115 °C in $\text{C}_2\text{D}_2\text{Cl}_4$ Bottom: first order kinetic treatment at +115 °C and +110 °C. The slope provides the sum of kinetic rate constant at each temperature.



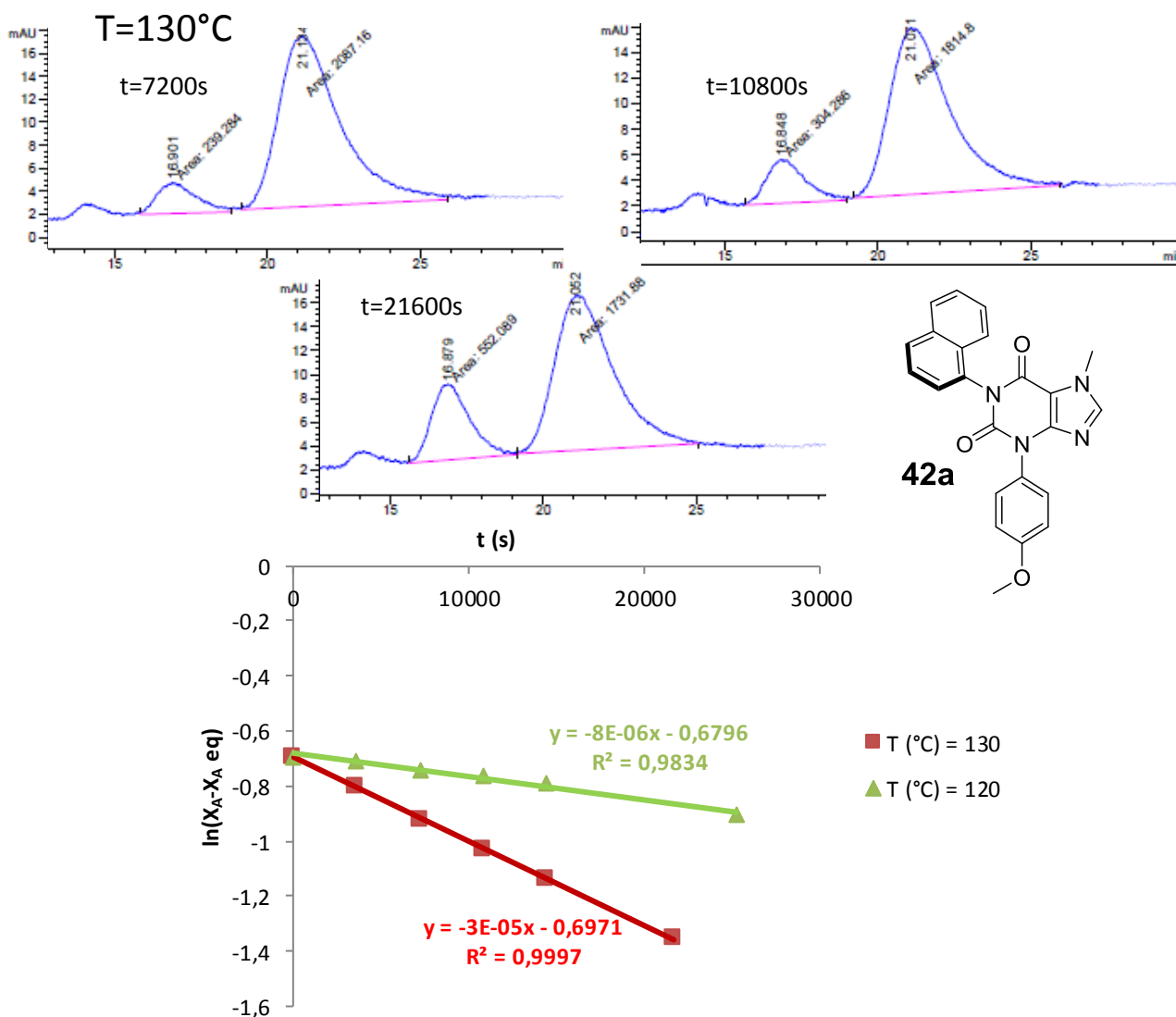


Figure 7.4.8 Top: kinetic measurement of enantiomerization rate of compound **42a** by HPLC (Chiralpak AS-H, eluent hexane/*i*PrOH 50/50 v/v, 0.6 mL/min), starting from one enantiomer kept at +130 °C in C₂D₂Cl₄. Bottom: first order kinetic treatment at +130 °C and +120 °C. The slope provides the sum of kinetic rate constant at each temperature.

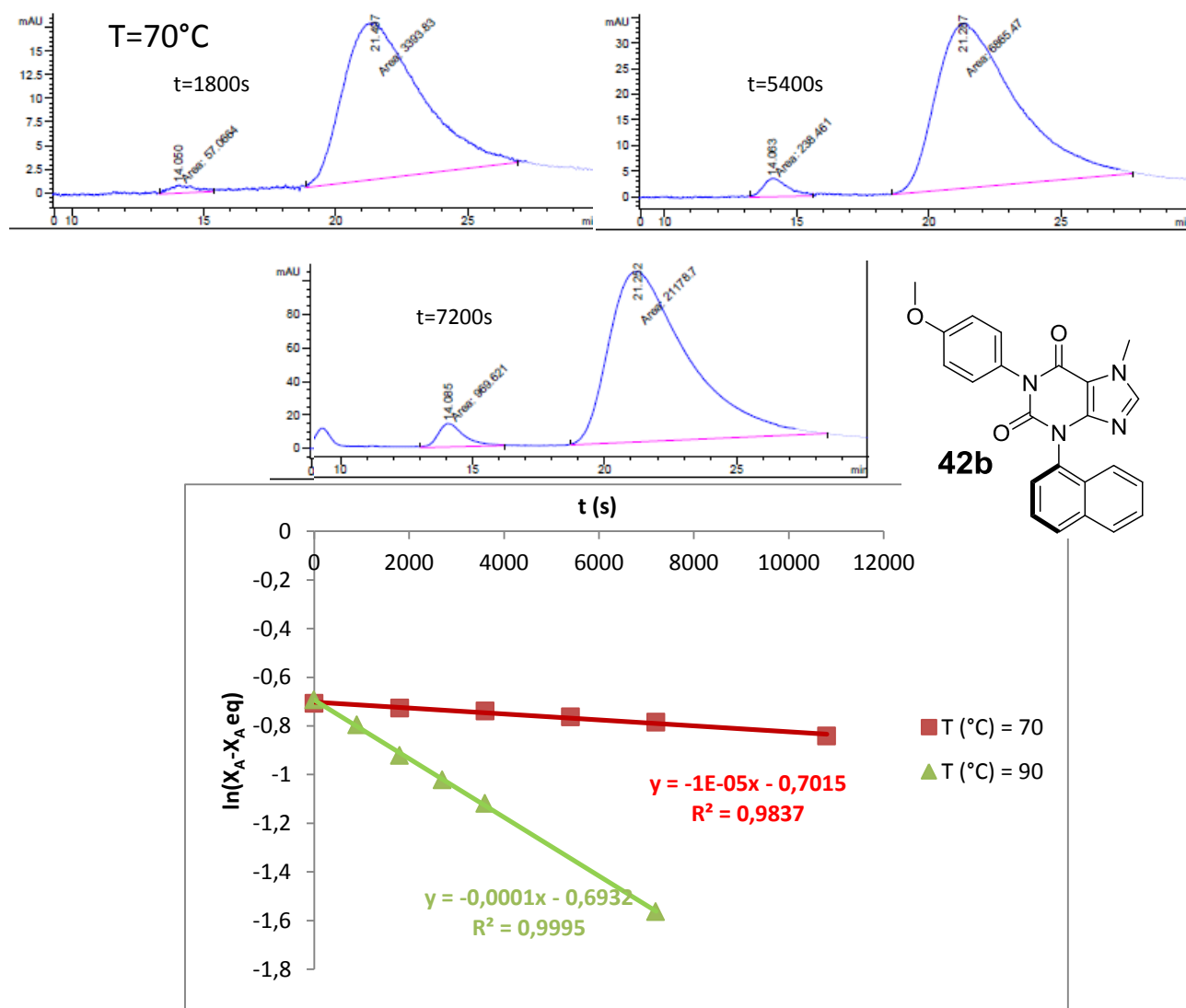
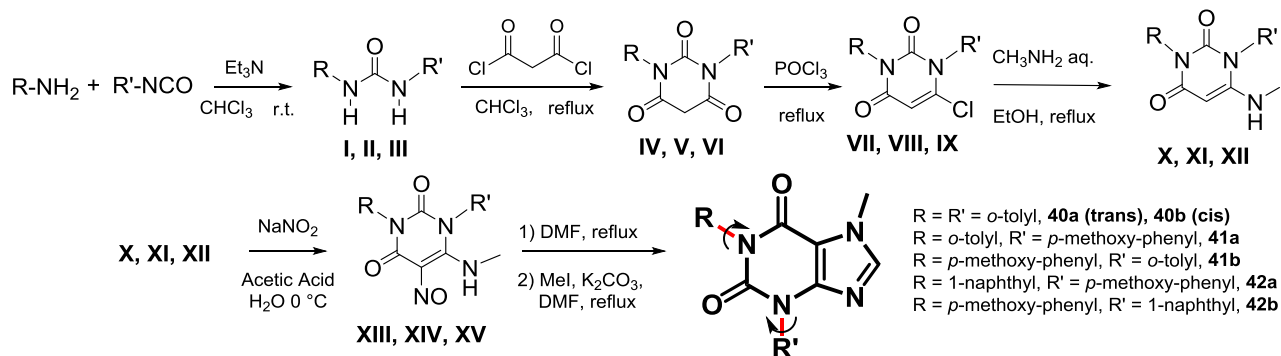


Figure 7.4.9 Top: kinetic measurement of enantiomerization rate of compound **42b** by HPLC (Chiralpak AS-H, eluent hexane/*i*PrOH 50/50 v/v, 0.6 mL/min), starting from one enantiomer kept at +70 °C in $\text{C}_2\text{D}_2\text{Cl}_4$. Bottom: first order kinetic treatment at +90 °C and +70 °C. The slope provides the sum of kinetic rate constant at each temperature.

7.4.2 Synthetic procedures

1,3-diary-xanthenes



R = R' = *o*-tolyl, **I, IV, VII, X, XIII**

R = *o*-tolyl, R' = *p*-methoxy-phenyl, **II, V, and VIII, XI, XIV as mixture of regioisomers**

R = 1-naphthyl, R' = *p*-methoxy-phenyl, **III, VI, and IX, XII, XV as mixture of regioisomers**

Figure 7.4.10 synthetic pathway followed for molecules **40-42**

General procedure for the synthesis of compounds **I-III**.¹

In a round bottom flask equipped with a stir bar were added the appropriate isocyanate (8 mmol) in $CHCl_3$ (50 mL, 0.16 M), while stirring were added the appropriate aryl amine (12 mmol) and Et_3N (18.4 mmol, 2.6 mL). The mixture was stirred at room temperature from 3 h to overnight until complete disappearance of the isocyanate. The products were filtrated and washed with $CHCl_3$ and isolated as white precipitate.

1,2-di-*o*-tolylurea (**I**, CAS Number: 617-07-2).

Yield 93% (1.79 g, 7.45 mmol). ¹H-NMR (400 MHz, DMSO- d_6 , 2.54 ppm, +25 °C) δ 2.31 (s, 6H, CH_3), 6.98 (td, $J = 7.5, 1.2$ Hz, 2H), 7.14-7.24 (m, 4H), 7.84 (dd, $J = 8.1, 0.9$ Hz), 8.27 (bs, 2H, NH). ¹³C-NMR (100 MHz, DMSO- d_6 , 40.45 ppm, +25 °C): δ 18.9 (CH_3), 122.4 (CH), 123.6 (CH), 127.0 (CH), 128.6 (Cq), 131.1 (CH), 138.4 (Cq), 153.9 (CO).

1-(4-methoxyphenyl)-3-(*o*-tolyl)urea (**II**, CAS Number: 106106-60-9).

Yield 78% (1.6 g, 6.25 mmol). ¹H-NMR (600 MHz, DMSO- d_6 , 2.54 ppm, +25 °C): δ 2.23 (s, 3H, CH_3), 3.71 (s, 3H, CH_3), 6.87 (m, 2H), 6.92 (dd, $J = 7.2$ Hz, 7.2 Hz, 1H), 7.13 (dd, $J = 7.9$ Hz, 7.2 Hz, 1H), 7.16 (d, $J = 7.2$ Hz, 1H), 7.36 (m, 2H), 7.81 (s, 1H, NH), 7.83 (d, $J = 7.9$ Hz, 1H), 8.82 (s, 1H, NH). ¹³C-NMR (150.8 MHz, DMSO- d_6 , 40.45 ppm, +25 °C): δ 18.3 (CH_3), 55.6 (CH_3), 114.5 (CH), 120.2 (CH), 121.3 (CH), 122.8 (CH), 126.6 (CH), 127.7 (Cq), 130.6 (CH), 133.4 (Cq), 138.0 (Cq), 153.3 (Cq), 154.8 (Cq).

1-(4-methoxyphenyl)-3-(naphthalen-1-yl)urea (**III**).²

Yield 82% (1.92 g, 6.56 mmol). ¹H-NMR (600 MHz, DMSO-d₆, 2.54 ppm, +25 °C): δ 3.73 (s, 3H, CH₃), 6.90 (m, 2H), 7.43 (m, 2H), 7.47 (dd, *J*=8.0 Hz, 8.1 Hz, 1H), 7.54 (dd, *J*=7.5 Hz, 7.3 Hz, 1H), 7.57-7.63 (m, 2H), 7.92 (d, *J*=8.0 Hz, 1H), 8.04 (d, *J*=7.3 Hz, 1H), 8.13 (d, *J*=8.1 Hz, 1H), 8.69 (s, 1H, NH), 8.87 (s, 1H, NH). ¹³C-NMR (600 MHz, DMSO, 40.45 ppm, +25 °C): δ 55.6 (CH₃), 114.5 (2CH), 117.6 (CH), 120.3 (2CH), 121.7 (CH), 123.1 (CH), 126.1 (CH), 126.2₇ (Cq), 126.3 (CH), 126.3₄ (CH), 128.9 (CH), 133.3 (Cq), 134.2 (Cq), 135.0 (Cq), 153.5 (Cq), 154.9 (Cq).

General procedure for the synthesis of compounds IV-VI.³

In an oven dried round bottom flask purged with N₂ was dissolved the appropriate urea (**I-III**, 3.11 mmol) in anhydrous CHCl₃ (0.39 M, 8 mL); successively malonyl chloride (3.11 mmol, 0.3 mL) was added dropwise. The reaction mixture was refluxed for 5 h. After the solvent was removed *in vacuo* the crude solid was washed with *i*-PrOH until the mother liquors were clear of the product. The mother liquors were purified by a chromatographic column to afford products **IV-VI** as yellowish solids. A small sample for each product were purified by semi-preparative HPLC for characterization purpose.

1,3-di-*o*-tolylpyrimidine-2,4,6(1H,3H,5H)-trione (**IV**, CAS Number: 184589-06-8).

Compound **IV** was prepared as described by the general procedure except the addition of 0.33 eq of malonyl chloride (1.03 mmol, 0.1 mL) after 5 h and a longer reaction time (12 h). The product was purified by chromatographic column (DCM:MeOH = 95:5 with gradient to 90:10) to afford **IV** with 92% yield (882 mg, 2.86 mmol). Further purification was performed by semi-preparative HPLC on a Luna C18 column (10 μm, 250 x 21.2 mm, 20 mL/min, *t_r* = 5.45 min, ACN:H₂O = 70:30 v/v).

¹H-NMR (600 MHz, CD₃CN, 1.96 ppm, +25 °C): Mixture *syn* 57.2% + *anti* 42.8%: δ 2.22₉ (s, 6H, *syn*), 2.23₃ (s, 6H, *anti*), 3.98 (d, *J*=21.2 Hz, 1H, *syn*), 4.00 (s, 2H, *anti*), 4.05 (d, 2H, *J*=21.2 Hz, *syn*), 7.24-7.28 (m, 4H, *syn+anti*), 7.32-7.36 (m, 4H, *syn+anti*), 7.36-7.40 (m, 8H, *syn+anti*). ¹³C-NMR (150.8 MHz, CD₃CN, 118.3 ppm, +25 °C): Mixture *syn* + *anti*: δ 17.5 (CH₃), 17.6 (CH₃), 41.4 (CH₂), 41.6 (CH₂), 127.8₇ (CH), 127.9₁ (CH), 129.7 (CH), 129.7₅ (CH), 130.1₆ (CH), 130.1₇ (CH), 131.8 (2 CH), 135.3 (Cq), 135.4 (Cq), 137.5 (Cq), 137.8 (Cq), 151.9₈ (Cq), 152.0 (Cq), 166.3 (Cq), 166.3₄ (Cq).

1-(4-methoxyphenyl)-3-(*o*-tolyl)pyrimidine-2,4,6(1H,3H,5H)-trione (**V**).

Yield 91% (915 mg, 2.82 mmol). The compound was purified by chromatographic column on silica gel (DCM:MeOH = 95:5). Further purification was performed by semi-preparative HPLC on a Luna C18 column (10 μm, 250 x 21.2 mm, 20 mL/min, *t_r* = 6.23 min, ACN:H₂O = 65:35 v/v).

¹H-NMR (600 MHz, CDCl₃, 7.26 ppm, +25 °C): δ 2.18 (s, CH₃), 3.80 (s, CH₃), 3.94 (m, CH₂), 6.97 (m, 2H), 7.12 (m, 3H), 7.27-7.37 (m, 3H). **¹³C-NMR** (150.8 MHz, CDCl₃, 77.0 ppm, +25 °C): δ 17.4 (CH₃), 55.4 (CH₃), 40.2 (CH₂), 114.6 (CH), 126.2 (Cq), 127.1 (CH), 128.3 (CH), 129.2 (CH), 129.5 (CH), 131.1 (Cq), 133.1 (Cq), 135.6 (Cq), 150.3 (Cq), 159.8 (Cq), 164.0 (Cq), 164.7 (Cq). **HRMS(ESI-QTOF)**. Calcd. for C₁₈H₁₇N₂O₄⁺ 325.1183. Found 325.1188.

1-(4-methoxyphenyl)-3-(naphthalen-1-yl)pyrimidine-2,4,6(1H,3H,5H)-trione (VI).

Yield 92% yield (1.03 g, 2.86 mmol). The compound was purified by chromatographic column on silica gel (DCM:MeOH = 95:5 with gradient to 90:10). Further purification was performed by semi-preparative HPLC on a Luna C18 column (10 μm, 250 x 21.2 mm, 20 mL/min, t_r = 5.82 min, ACN:H₂O = 60:40 v/v).

¹H-NMR (600 MHz, CDCl₃, 7.26 ppm, +25 °C): δ 3.82 (s, CH₃), 4.12 (d, *J*=22.0 Hz, 1H), 4.17 (d, *J*=22.0 Hz, 1H), 6.99 (m, 2H), 7.21 (m, 2H), 7.41 (d, *J*=7.4 Hz, 1H), 7.52-7.63 (m, 4H), 7.94 (d, *J*=8.2 Hz, 1H), 7.97 (d, *J*=7.8 Hz, 1H). **¹³C-NMR** (150.8 MHz, CDCl₃, 77.0 ppm, +25 °C) δ: 40.5 (CH₂), 55.5 (CH₃), 114.7 (2CH), 121.0 (CH), 125.4 (CH), 126.2 (Cq), 126.6 (CH), 126.8 (CH), 127.5 (CH), 128.9 (CH), 129.3 (2CH), 129.7 (Cq), 130.1 (CH), 130.6 (Cq), 134.5 (Cq), 151.2 (Cq), 159.9 (Cq), 164.3 (Cq), 164.7 (Cq). **HRMS(ESI-QTOF)**. Calcd. for C₂₁H₁₇N₂O₄⁺ 361.1183. Found 361.1174.

General procedure for the synthesis of compounds VII-IX.

In a test tube with a Teflon pressure-resistant cap was added the opportune bis-aryl barbituric acid (**IV-VI**, 2.80 mmol), H₂O (8.96 mmol, 160 μL), and slowly dropwise POCl₃ (19.6 mmol, 1.83 mL). Once the heat produced was dissipated the reaction mixture was refluxed overnight. The excess of POCl₃ was removed *in vacuo* and the reaction was quenched with ice. The aqueous phases were extracted with EtOAc (30 mL) five times. The combined organic layers were dried on Na₂SO₄, filtered and concentrated under reduced pressure. The crude was purified by chromatographic column and semi-preparative HPLC.

6-chloro-1,3-di-*o*-tolylpyrimidine-2,4(1H3H)-dione (VII).

Compound **VII** was obtained starting from **IV** (2.8 mmol, 863 mg). The product was purified by a chromatographic column on silica gel (petroleum ether : EtOAc 70:30) affording a yellow solid in 22% yield (201 mg, 0.616 mmol). Further purification was performed by semi-preparative HPLC on a Luna C18 column (10 μm, 250 x 21.2 mm, 20 mL/min, t_r = 6.46 min, ACN:H₂O = 80:20 v/v with 0.05% HCOOH as acid modifier).

¹H-NMR (600 MHz, CD₃CN, 1.96 ppm, +25 °C): Mixture **a** 57,0% + **b** 43,0%: δ 2.18 (s, 3H, **b**), 2.19 (s, 3H, **a**) 2.25 (s, 3H, **b**), 2.27 (s, 3H, **a**), 7.24 (s, 1H, **b**), 7.25 (s, 1H, **a**), 7.33-7.46 (m, 16 H, **a** + **b**). **¹³C-NMR** (150.8 MHz, CD₃CN, 118.3 ppm, +25 °C) Mixture **a** + **b** δ 17.4₁ (CH₃), 17.4 (CH₃), 17.4₇ (CH₃), 17.4₈ (CH₃), 103.1 (CH) 103.1₄ (CH), 118.3 (Cq), 127.9 (CH), 128.0 (CH), 128.2 (CH), 128.2₃ (CH), 129.5 (CH), 129.6 (CH), 130.0 (CH), 130.0₇ (CH), 130.1 (CH), 131.0₄ (CH), 131.0₅ (CH), 131.8 (CH), 132.0 (CH), 135.5₈ (Cq), 135.6 (Cq), 136.9 (Cq), 137.1₀ (Cq), 137.1₁ (Cq), 137.2 (Cq), 137.7 (Cq), 138.0 (Cq), 147.5 (Cq), 147.5₃ (Cq), 150.9 (Cq), 150.9₃ (Cq), 161.7 (Cq), 161.7₄ (Cq). **HRMS(ESI-QTOF)**. Calcd. for C₁₈H₁₆ClN₂O₂⁺ 327.0895. Found 327.0889.

6-chloro-1-(4-methoxyphenyl)-3-(o-tolyl)pyrimidine-2,4(1H,3H)-dione (VIIIa) and 6-chloro-3-(4-methoxyphenyl)-1-(o-tolyl)pyrimidine-2,4(1H,3H)-dione (VIIIb).

The two regioisomers of compound **VIII** were obtained starting from **V** (2.8 mmol, 910 mg). The mixture was purified by a chromatographic column on silica gel (petroleum ether : EtOAc 70:30) affording a yellow solid in 48% yield (1.34 mmol, 460 mg). Further purification was performed by semi-preparative HPLC on a Luna C18 column (10 μm, 250 x 21.2 mm, 20 mL/min, t_r = 7.91 min, ACN:H₂O = 70:30 v/v with 0.05% HCOOH as acid modifier).

¹H-NMR (600 MHz, CDCl₃, 7.26 ppm, +25 °C) mixture **a** 60.3% + **b** 39.7%: δ 2.20 (s, 3H, CH₃, **a**), 2.25 (s, 3H, CH₃, **b**), 3.82 (s, 3H, CH₃, **a**), 3.84 (s, 3H, CH₃, **b**), 6.15 (s, 1H, CH, **b**), 6.17 (s, 1H, CH, **a**), 6.98 (m, 4H, **a** + **b**), 7.15-7.24 (m, 8H, **a** + **b**), 7.28-7.39 (m, 8H, **a** + **b**). **¹³C-NMR** (150.8 MHz, CDCl₃, 77.0 ppm, +25 °C) mixture **a** + **b** : δ 17.3₆ (CH₃), 17.4₄ (CH₃), 55.4 (CH₃), 55.5 (CH₃), 102.3₉ (CH), 102.4₄ (CH), 126.8 (Cq), 127.0 (CH), 127.2 (CH), 128.2 (CH), 128.8 (CH), 128.9 (C1), 129.1 (CH), 129.3 (CH), 129.9 (CH), 130.0 (CH), 131.1 (CH), 131.2 (CH), 133.7 (Cq), 135.5 (Cq), 135.6 (Cq), 136.3 (Cq), 146.4 (Cq), 147.0 (Cq), 150.4 (Cq), 150.5 (Cq), 159.7 (Cq), 160.3 (Cq), 160.5 (Cq), 161.2 (Cq). **HRMS(ESI-QTOF)**. Calcd. for C₁₈H₁₆ClN₂O₃⁺ 343.0844. Found 343.0843.

6-chloro-3-(4-methoxyphenyl)-1-(naphthalen-1-yl)pyrimidine-2,4(1H,3H)-dione (IXa) and 6-chloro-1-(4-methoxyphenyl)-3-(naphthalen-1-yl)pyrimidine-2,4(1H,3H)-dione (IXb).

The two regioisomers of compound **IX** were obtained starting from **VI** (2.8 mmol, 1010 mg). The mixture products **18** were purified by a chromatographic column on silica gel (petroleum ether : EtOAc 70:30) affording a yellow solid in 40% yield (1.12 mmol, 424 mg). Further purification was performed by semi-preparative HPLC on a Luna C18 column (10 μm, 250 x 21.2 mm, 20 mL/min, t_r = 8.76 min, ACN:H₂O = 70:30 v/v with 0.05% HCOOH as acid modifier).

¹H-NMR (600 MHz, CDCl₃, 7.26 ppm, +25 °C) mixture **a** 62.0% + **b** 38.0%: δ 3.80 (s, 3H, CH₃, **a**), 3.84 (s, 3H, CH₃, **b**), 6.22 (s, 1H, CH, **b**), 6.25 (s, 1H, CH, **a**), 6.98 (m, 4H, **a** + **b**), 7.22 (m, 2H, **a**), 7.26 (m, 2H, **b**), 7.44 (d, *J*=7.9 Hz, 1H, **b**), 7.48-7.65 (m, 9H, **a** + **b**), 7.68 (d, *J*=8.5 Hz, 1H, **b**), 7.89-7.95 (m, 2H, **a** + **b**), 7.98 (d, *J*=8.8 Hz, 1H, **a**). **¹³C-NMR** (150.8 MHz, CDCl₃, 77.0 ppm, +25 °C) mixture **a** + **b**: δ 55.4 (CH₃), 55.5 (CH₃), 102.5 (CH), 102.6 (CH), 114.6 (2CH), 121.1 (CH), 121.4 (CH), 125.3 (CH), 125.5 (CH), 126.3 (CH), 126.5 (CH), 126.7 (Cq), 126.8 (CH), 127.3 (CH), 127.4 (CH), 128.0 (CH), 128.6₇ (CH), 128.7₄ (Cq), 128.8 (Cq), 129.2 (2CH), 129.5 (Cq), 129.7 (CH), 129.8 (CH), 129.9 (CH), 130.2 (Cq), 130.5 (CH), 131.2 (Cq), 132.8 (Cq), 134.3 (Cq), 134.5 (Cq), 147.0 (Cq), 147.3 (Cq), 150.8₇ (Cq), 150.8₉ (Cq), 159.7 (Cq), 160.2 (Cq), 160.9 (Cq), 161.2 (Cq). **HRMS(ESI-QTOF)**. Calcd. for C₂₁H₁₆ClN₂O₃⁺ 379.0844. Found 379.0849.

General procedure for the synthesis of compounds X-XII.

In a round bottom flask were dissolved the opportune chloro-derivative (**VII-IX**, 0.61 mmol) in EtOH (1M, 0.61 mL) and were added CH₃NH₂ 40% aq (6.1mmol, 0.47 mL). The reaction mixture was heated to reflux overnight. Once removed the EtOH at reduced pressure the crude was quenched with H₂O and extracted with EtOAc. The combined organic layers were dried on Na₂SO₄, filtered and concentrated. The crude products **X-XII** were used without further purification in the next steps of the synthesis. Eventually a semi-preparative HPLC purification were carried out in order to obtain analytically pure sample for characterization.

6-(methylamino)-1,3-di-*o*-tolylpyrimidine-2,4(1H,3H)-dione (**X**).

Compound **X** was obtained as a yellow solid in 97% yield (0.59 mmol, 190 mg). Further purification was performed by semi-preparative HPLC on a Luna C18 column (10 μm, 250 x 21.2 mm, 20 mL/min, *t_r* = 4.15 min, ACN:H₂O = 60:40 v/v with 0.05% HCOOH as acid modifier). Due to hindered rotation of the two aryl ring, two conformational diastereoisomer are present in a 61:39 mixture (**a**:**b**). **¹H-NMR** (600 MHz, DMSO-*d*₆, 2.54 ppm, +25°C): δ 2.12 (s, 3H, **a**), 2.13 (s, 3H, **b**), 2.15 (s, 3H, **a**), 2.17 (s, 3H, **b**), 2.68 (s, 3H, **a**), 2.69 (s, 3H, **b**), 4.86 (m, 2H, **a** + **b**), 5.81-5.83 (m, 2H, **a** + **b**), 7.13-7.15 (d, 1H, *J* = 7,5 Hz, **b**), 7.16-7.17 (d, 1H, *J* = 7,5 Hz, **a**), 7.27-7.37 (m, 8H, **a** + **b**), 7.39-7.42 (m, 2H, **a** + **b**), 7.46-7.47 (m, 4H, **a** + **b**). **¹³C-NMR** (150.8 MHz DMSO-*d*₆, 40.45 ppm, +25 °C) mixture **a** + **b** δ 17.6 (CH₃), 17.7 (CH₃), 17.9 (CH₃), 18.1 (CH₃), 30.4 (CH₃), 73.9 (CH), 73.9₄ (CH), 127.3₃ (Cq), 127.3₄ (CH), 128.6 (CH), 128.9 (CH), 130.2 (CH), 130.2₃ (CH), 130.7 (Cq), 130.7₃ (CH), 130.7₆ (CH), 130.8 (CH), 131.1 (CH), 132.2₆ (CH), 132.3 (CH), 133.7 (Cq), 133.7₃ (Cq), 136.4 (Cq), 136.7 (Cq), 136.9 (Cq), 137.7 (Cq), 137.9 (Cq), 150.8 (Cq), 150.9 (Cq), 154.8 (Cq), 154.9 (Cq), 162.5 (Cq), 162.5₄ (Cq). **HRMS(ESI-QTOF)**. Calcd. for C₁₉H₂₀N₃O₂⁺ 322.1550. Found 322.1544.

1-(4-methoxyphenyl)-6-(methylamino)-3-(o-tolyl)pyrimidine-2,4(1H,3H)-dione (XIa) and 3-(4-methoxyphenyl)-6-(methylamino)-1-(o-tolyl)pyrimidine-2,4(1H,3H)-dione (XIb).

The mixture of compounds **XI** were obtained as a yellow solid in 70% yield (0.427 mmol, 144 mg). Further purification was performed by semi-preparative HPLC on a Luna C18 column (10 μ m, 250 x 21.2 mm, 20 mL/min, t_r = 4.92 min, ACN:H₂O = 60:40 v/v with 0.05% HCOOH as acid modifier).

¹H-NMR (600 MHz, CD₃CN, 1.96 ppm, +25 °C) mixture **a** 60.2% + **b** 40.8%: δ 2.15 (s, 3H, CH₃, **a**), 2.18 (s, 3H, CH₃, **b**), 2.66 (m, 6H, N-CH₃, **a** + **b**), 3.82 (s, 3H, CH₃, **a**), 3.85 (s, 3H, CH₃, **a**), 4.60 (bs, 1H, NH, **a**), 4.71 (bs, 1H, NH, **b**), 4.83 (s, 1H, CH, **b**), 4.84 (s, 1H, CH, **a**), 6.98 (m, 2H, **a**), 7.10 (m, 2H, **b**), 7.16 (m, 4H), 7.25-7.32 (m, 6H), 7.30-7.46 (m, 2H). **¹³C-NMR** (150.8 MHz, CD₃CN, 118.3 ppm, +25 °C) mixture **a** + **b**: δ 16.3 (CH₃), 16.7 (CH₃), 28.8₂ (CH₃), 28.8₄ (CH₃), 55.2 (CH₃), 55.4 (CH₃), 73.4₇ (CH), 73.5₃ (CH), 114.0 (CH), 115.4 (CH), 115.5 (CH), 126.5 (Cq), 126.6 (CH), 127.9 (CH), 128.3 (CH), 129.3 (CH), 129.4 (Cq), 129.8 (CH), 130.1₆ (CH), 130.1₈ (CH), 130.5 (CH), 130.9 (CH), 131.0 (CH), 131.7 (CH), 133.1 (Cq), 136.2 (Cq), 136.7 (Cq), 137.9 (Cq), 151.3 (Cq), 151.4 (Cq), 154.2 (Cq), 155.1 (Cq), 159.2 (Cq), 160.6 (Cq), 162.5 (Cq), 163.1 (Cq). **HRMS(ESI-QTOF)**. Calcd. for C₁₉H₂₀N₃O₃⁺ 338.1499. Found 338.1493.

3-(4-methoxyphenyl)-6-(methylamino)-1-(naphthalene-1-yl)pyrimidine-2,4(1H,3H)-dione (XIIa) and 1-(4-methoxyphenyl)-6-(methylamino)-3-(naphthalene-1-yl)pyrimidine-2,4(1H,3H)-dione (XIIb).

The mixture of compounds **XII** were obtained as a yellow solid in 80% yield (0.487 mmol, 182 mg). Further purification was performed by semi-preparative HPLC on a Luna C18 column (10 μ m, 250 x 21.2 mm, 20 mL/min, t_r = 3.65 min, ACN:H₂O = 80:20 v/v with 0.05% HCOOH as acid modifier).

¹H-NMR (600 MHz, CD₃CN, 1.96 ppm, +25 °C) mixture **a** 77.2% + **b** 22.8%: δ 2.59 (d, J =5.3 Hz, 3H, N-CH₃, **a**), 2.73 (d, J =5.3 Hz, 3H, N-CH₃, **b**), 3.82 (s, 3H, CH₃, **a**), 3.85 (s, 3H, CH₃, **b**), 4.69 (bs, 1H, NH, **a**), 4.83 (bs, 1H, NH, **b**), 4.92 (s, 1H, CH, **b**), 4.93 (s, 1H, CH, **a**), 6.99 (m, 2H, **a**), 7.11 (m, 2H, **b**), 7.35 (m, 2H, **b**), 7.45 (d, J =7.5 Hz, 1H, **b**), 7.55-7.69 (m, 8H, **a** + **b**), 7.80-7.85 (m, 2H, **a** + **b**), 7.99 (m, 2H, **b**), 8.06 (m, 2H, **a** + **b**), 8.11 (d, J =8.2 Hz, 1H, **a**). **¹³C-NMR** (150.8 MHz, CD₃CN, 118.3 ppm, +25 °C) mixture **a** + **b**: δ 29.5 (CH₃), 29.7 (CH₃), 56.0 (CH₃), 56.2 (CH₃), 74.3 (CH), 74.5 (CH), 114.8 (CH), 116.2 (CH), 116.3 (CH), 122.6 (CH), 123.3 (CH), 126.6 (CH), 127.0₇ (CH), 127.1₁ (CH), 127.2 (Cq), 127.7 (CH), 127.8 (CH), 127.9 (CH), 128.6 (CH), 129.1 (CH), 129.3₀ (CH), 129.3₄ (CH), 129.4 (CH), 130.1 (Cq), 131.0 (CH), 131.2 (CH), 131.4 (Cq), 131.6 (Cq), 131.7 (CH), 131.8 (CH), 134.6 (Cq), 135.0 (Cq), 135.7 (Cq), 152.6₀ (Cq), 152.6₄ (Cq), 155.5 (Cq), 156.1 (Cq), 160.0

(Cq), 161.4 (Cq), 163.8 (Cq), 164.0 (Cq). **HRMS(ESI-QTOF)**. Calcd. for $C_{22}H_{20}N_3O_3^+$ 374.1499. Found 374.1488.

General procedure for the synthesis of compounds XIII-XV.

The appropriate methyl-amino derivative (**X-XII**, 1 eq, 0.4 mmol) and $NaNO_2$ (2eq, 0.8 mmol, 55 mg) were dissolved in H_2O (11.2 mL) and acetic acid (1.5 mL). The reaction mixture was left stirring at 0 °C overnight and the product was collected as a bright pink precipitate and washed twice with cold water. The mother liquors were eventually extracted with EtOAc to fully recover the product. The combined organic layers were dried on Na_2SO_4 , filtered and the solvent was removed at reduced pressure. The crude product was used without further purification in the next steps of the synthesis. Eventually a semi-preparative HPLC purification were carried out in order to obtain analytically pure samples for characterization.

6-(methylamino)-5-nitroso-1,3-di-*o*-tolylpyrimidine-2,4-(1H,3H)-dione (XIII).

The product **XIII** was obtained in 57.5% yield (pink solid, 0.23 mmol, 81 mg). Further purification was performed by semi-preparative HPLC on a Luna C18 column (10 μ m, 250 x 21.2 mm, 20 mL/min, t_r = 7.08 min, ACN: H_2O = 60:40 v/v with 0.05% $HCOOH$ as acid modifier). Due to hindered rotation of the two aryl rings, two conformational diastereoisomer are present in a 57:43 mixture (**a:b**).

1H -NMR (600 MHz, $DMSO-d_6$, 2.54 ppm, +25 °C) δ 2.22 (s, 6H, **a + b**), 2.24 (d, 3H, $J=4.9$ Hz, **a**), 2.25 (d, 3H, $J=4.9$ Hz, **b**), 2.29 (s, 3H, **a**), 2.31 (s, 3H, **b**), 7.35-7.45 (m, 14H, **a + b**), 7.49-7.50 (m, 2H, **a + b**), 7.62 (d, 1H, $J=8.1$ Hz, **a**), 7.70 (d, 1H, $J=8.1$ Hz, **b**). **^{13}C -NMR** (150.8 MHz, $DMSO-d_6$, 40.45 ppm, +25 °C) mixture **a + b** δ 17.9 (CH_3), 18.0 (CH_3), 18.0₁ (CH_3), 18.1 (CH_3), 31.1 (CH_3), 31.1₅ (CH_3), 127.5₇ (CH), 127.6 (CH), 127.7₆ (CH), 127.8 (CH), 129.6₉ (CH), 129.7₁ (CH), 129.9₆ (CH), 130.0₁ (CH), 130.9 (CH), 131.0 (CH), 131.3 (CH), 131.4 (CH), 131.5 (CH), 131.7₇ (CH), 131.8₂ (CH), 135.0 (Cq), 135.1 (Cq), 135.2 (Cq), 135.3 (Cq), 135.7 (Cq), 137.2 (Cq), 138.7 (Cq), 139.0 (Cq), 139.5 (Cq), 139.6 (Cq), 147.8₆ (Cq), 147.9 (Cq), 149.4 (Cq), 149.4₄ (Cq), 160.2 (Cq), 160.3 (Cq). **HRMS(ESI-QTOF)**. Calcd. for $C_{19}H_{19}N_4O_3^+$ 351.1452. Found 351.1444.

1-(4-methoxyphenyl)-6-(methylamino)-5-nitroso-3-(*o*-tolyl)pyrimidine-2,4-(1H,3H)-dione

(**XIVa**) 3-(4-methoxyphenyl)-6-(methylamino)-5-nitroso-1-(*o*-tolyl)pyrimidine-2,4-(1H,3H)-dione (**XIVb**).

The mixed products **XIV** were obtained in 50% yield (pink solid, 0.2 mmol, 73 mg). Further purification was performed by semi-preparative HPLC on a Luna C18 column (10 μ m, 250 x 21.2 mm, 20 mL/min, t_r = 5.88 min, ACN:H₂O = 50:50 v/v with 0.05% HCOOH as acid modifier).

¹H-NMR (600 MHz, CD₃CN, 1.96 ppm, +25 °C) mixture **a** 60.0% + **b** 40.0%: δ 2.23 (s, 3H, CH₃, **b**), 2.25 (d, 3H, J =5.3 Hz N-CH₃, **a**), 2.29 (s, 3H, CH₃, **a**), 2.34 (d, 3H, J =5.3 Hz N-CH₃, **b**), 3.85 (s, 6H, OCH₃, **a** + **b**), 7.05 (m, 4H, **a** + **b**), 7.29 (m, 3H, **a** + **b**), 7.34-7.49 (m, 7H, **a** + **b**). **¹³C-NMR** (150.8 MHz, CD₃CN, 118.3 ppm, +25 °C) mixture **a** + **b**: δ 17.5 (CH₃), 17.8 (CH₃), 31.1 (CH₃), 31.8 (CH₃), 56.1 (CH₃), 56.3 (CH₃), 115.3 (CH), 115.5 (CH), 127.8 (CH), 128.0 (CH), 128.2 (Cq), 128.9 (CH), 129.8, (CH) 130.0 (CH), 130.8 (CH), 130.9 (CH), 131.5 (CH), 131.7 (CH), 132.1 (CH), 132.3 (Cq), 135.3 (Cq), 135.7 (Cq), 137.5, (Cq) 139.4 (Cq), 139.5 (Cq), 139.7 (Cq), 147.8 (Cq), 148.4 (Cq), 150.6 (Cq), 150.8 (Cq). **HRMS(ESI-QTOF)**. Calcd. for C₁₉H₁₉N₄O₄⁺ 367.1401. Found 367.1392.

1-(4-methoxyphenyl)-6-(methylamino)-3-(naphthalen-1-yl)-5-nitrosopyrimidine-2,4-(1H,3H)-dione (XVa) and 3-(4-methoxyphenyl)-6-(methylamino)-1-(naphthalen-1-yl)-5-nitrosopyrimidine-2,4-(1H,3H)-dione (XVb).

The mixture of compounds **XV** were obtained in 56% yield (pink solid, 0.224 mmol, 90 mg). Further purification was performed by semi-preparative HPLC on a Luna C18 column (10 μ m, 250 x 21.2 mm, 20 mL/min, t_r = 7.04 min, ACN:H₂O = 50:50 v/v with 0.05% HCOOH as acid modifier).

¹H-NMR (600 MHz, CD₃CN, 1.96 ppm, +25 °C) mixture **a** 79.9% + **b** 20.1: δ 1.99 (d, J =4.8Hz, 3H, N-CH₃, **a**), 2.39 (d, J =5.0Hz, 3H, N-CH₃, **b**), 3.85 (s, 6H, CH₃, **a** + **b**), 7.06 (m, 2H, **a**), 7.35 (m, 2H, **b**), 7.48 (bs, 1H, **b**), 7.53 (bs, 1H, **a**), 7.60-7.70 (m, 3.8H, **a** + **b**), 7.75 (d, J =8.0Hz, 1H, **a**), 8.00 (m, 1H, **b**), 8.06 (m, 2H, **a** + **b**), 8.14 (d, J =8.5Hz, 1H, **a**). **¹³C-NMR** (150.8 MHz, CD₃CN, 118.3 ppm, +25 °C) mixture **a** + **b**: δ 31.5 (CH₃), 32.2 (CH₃), 56.5 (CH₃), 56.7 (CH₃), 115.6 (CH), 115.8 (CH), 123.3 (CH), 123.6 (CH), 126.7 (CH), 127.1 (CH), 127.8, (CH) 128.3 (CH), 128.5 (CH), 129.2 (CH), 129.5₄ (CH), 129.5₆ (CH) 129.7 (CH), 129.9 (CH), 130.6 (CH), 131.1 (CH), 131.6 (Cq), 132.2, (CH) 132.5 (Cq), 132.7 (Cq), 133.0 (Cq), 133.6 (Cq), 135.2 (Cq), 135.5 (Cq), 140.0, (Cq) 148.8 (Cq), 151.5 (Cq), 161.0 (Cq), 161.7 (Cq), 162.1 (Cq). **HRMS(ESI-QTOF)**. Calcd. for C₂₂H₁₉N₄O₄⁺ 403.1401. Found 403.1386.

General procedure for compounds 40-42.

The opportune nitroso-pyrimidine-dione (**XIII-XV**, 1eq, 0.2 mmol) was refluxed for 3 hours in 1 mL of DMF until complete disappearance of the bright pink colour. Then to the reaction mixture cooled at room temperature was added K₂CO₃ (6 eq, 1.2 mmol, 166 mg) and CH₃I (10 eq, 2.00 mmol, 0.12 mL). Then the solution was heated at +50 °C for further 3 hours. The work up proceeds with H₂O

and extraction with EtOAc. The combined organic layers were dried on Na₂SO₄, filtered and the solvent was removed at reduced pressure. The crude products were purified by semi-preparative HPLC in high yields as separate isomers.

7-methyl-1,3-di-*o*-tolyl-1H-purine-2,6(3H,7H)-dione (40).

The mixture of **40a** and **40b** was obtained in ratio 45:55 respectively with overall 98% yield (white solid, 0.196 mmol, 68 mg, m.p. 213.3-215.5 °C). **HRMS(ESI-QTOF)**. Calcd. for C₂₀H₁₉N₄O₂⁺ 347.1502. Found 347.1493. The mixture of stereoisomers was resolved using ChiralPak AD-H column (10 μm, 250 x 20 mm, 20 mL/min, hexane:*i*PrOH = 80:20 v/v).

40a (trans) ¹H-NMR (600 MHz, CD₃CN, 1.96 ppm, +25 °C) δ 2.19 (s, 3H), 2.20 (s, 3H), 3.94 (s, 3H), 7.24-7.25 (m, 1H), 7.33-7.43 (m, 7H), 7.62 (s, 1H). ¹³C-NMR (150.8 MHz, CD₃CN, 118.3 ppm, +25 °C) □□17.5 (CH₃), 17.7 (CH₃), 34.0 (CH₃), 108.8 (Cq), 127.7 (CH), 127.9 (CH), 129.7 (CH), 130.2 (CH), 130.2₃ (CH), 130.2₄ (CH), 131.6 (CH), 131.9 (CH), 135.8 (Cq), 136.4 (Cq), 137.7 (Cq), 137.9 (Cq), 143.7 (CH), 150.2 (Cq), 151.3 (Cq), 156.0 (Cq).

The atropisomers were resolved with t_r = 10.36 min and t_r = 11.41 min, respectively.

40b (cis). ¹H-NMR (600 MHz, CD₃CN, 1.96 ppm, +25 °C) δ 2.17 (s, 3H), 2.18 (s, 3H), 3.93 (s, 3H), 7.25-7.26 (m, 1H), 7.35-7.43 (m, 7H), 7.62 (s, 1H). ¹³C-NMR (150.8 MHz, CD₃CN, 118.3 ppm, +25 °C) δ 17.4 (CH₃); 17.6 (CH₃), 34.0 (CH₃), 108.7 (Cq), 127.8 (CH), 128.0(CH), 129.7 (CH), 130.1 (CH), 130.2 (CH), 130.2₅ (CH), 131.6 (CH), 131.9 (CH), 135.7 (Cq), 136.4 (Cq), 137.5 (Cq), 137.8 (Cq), 143.7 (CH), 150.2 (Cq), 151.3 (Cq), 156.1 (Cq).

The atropisomers were resolved with t_r = 12.86 min and t_r = 17.89 min, respectively.

Compounds 41a and 41b.

The mixture of **41a** and **41b** was obtained in ratio 42:58 respectively with overall 99% yield (white solid, 0.199 mmol, 72 mg, m.p. 204.5-205.3 °C). The two compounds were isolated by semi-preparative HPLC on a Luna C18 column (10 μm, 250 x 21.2 mm, 20 mL/min, ACN:H₂O = 60:40 v/v) with t_r = 9.88 min (**41a**) and t_r = 9.34 min (**41b**).

3-(4-methoxyphenyl)-7-methyl-1-(*o*-tolyl)-1H-purine-2,6(3H,7H)-dione (41a).

¹H-NMR (600 MHz, DMSO-*d*₆, 2.54 ppm, +25 °C): δ 2.14 (s, 3H, CH₃), 3.85 (s, 3H, CH₃), 3.93 (s, 3H, CH₃), 7.08 (m, 2H), 7.27-7.41 (m, 6H), 8.01 (s, 1H). ¹³C-NMR (150.8 MHz, DMSO-*d*₆, 40.45 ppm, +25 °C): δ 18.0 (CH₃), 34.1 (CH₃), 56.3 (CH₃), 108.0 (Cq), 115.1 (CH), 127.5 (CH), 128.8 (Cq), 129.3 (CH), 130.3 (CH), 130.7 (CH), 131.3 (CH), 136.1 (Cq), 137.0 (Cq), 143.9 (Cq), 150.2 (Cq),

151.2 (Cq), 155.2 (Cq), 159.9 (Cq). **HRMS(ESI-QTOF)**. Calcd. for C₂₀H₁₉N₄O₃⁺ 363.14517. Found 363.1462.

The racemic mixture was resolved with ChiralPak AD-H column (10 μm, 250 x 20 mm, 20 mL/min, hexane:*i*PrOH = 72:28 v/v) with *t_r* = 10.04 min and *t_r* = 13.74 min.

1-(4-methoxyphenyl)-7-methyl-3-(*o*-tolyl)-1H-purine-2,6(3H,7H)-dione (41b).

¹H-NMR (600 MHz, DMSO-*d*₆, 2.54 ppm, +25 °C): δ 2.14 (s, 3H, CH₃), 3.83 (s, 3H, CH₃), 3.94 (s, 3H, CH₃), 7.04 (m, 2H), 7.26 (m, 2H), 7.37-7.43 (m, 6H), 7.99 (s, 1H). **¹³C-NMR** (150.8 MHz, DMSO-*d*₆, 40.45 ppm, +25 °C): δ 18.1 (CH₃), 34.1 (CH₃), 56.2 (CH₃), 108.0 (Cq), 114.9 (CH), 127.7 (CH), 129.3 (Cq), 129.8 (CH), 130.2 (CH), 131.2 (CH), 131.6 (CH), 135.5 (Cq), 137.2 (Cq), 143.9 (Cq), 149.4 (Cq), 151.3 (Cq), 155.9 (Cq), 159.7 (Cq). **HRMS(ESI-QTOF)**. Calcd. for C₂₀H₁₉N₄O₃⁺ 363.1452. Found 363.1456.

The racemic mixture was resolved with ChiralPak AD-H column (10 μm, 250 x 20 mm, 20 mL/min, hexane:*i*PrOH = 72:28 v/v) with *t_r* = 10.91 min and *t_r* = 14.10 min.

Compounds 42a and 42b.

The mixture of **42a** and **42b** was obtained in ratio 17:83 respectively with overall 99% yield (white solid, 0.198 mmol, 79 mg, m.p. 194.6-195.7 °C). The two compounds were isolated by semi-preparative HPLC on a Luna C18 column (10 μm, 250 x 21.2 mm, 20 mL/min, ACN:H₂O = 35:65 v/v) with *t_r* = 18.58 min (**42a**) and *t_r* = 17.54 min (**42b**). Single enantiomers were separated by Lux Cellulose 2 column (5 μm, 250 x 10 mm), or ChiralPak AS-H column (5 μm, 150 x 4.6 mm, 50/50 *n*-hexane/*i*PrOH 0.6 mL/min).

3-(4-methoxyphenyl)-7-methyl-1-(naphthalene-1-yl)-1H-purine-2,6(3H,7H)-dione (42a).

¹H-NMR (600 MHz, CDCl₃, 7.26 ppm, +25 °C): δ 3.83 (s, 3H, CH₃), 4.01 (s, 3H, CH₃), 7.02 (m, 2H), 7.43 (m, 2H), 7.50 (m, 3H), 7.56 (s, 1H), 7.59 (dd, *J*=8.3 Hz, *J*=8.3 Hz, 1H), 7.69 (m, 1H), 7.94 (m, 2H). **¹³C-NMR** (150.8 MHz, CDCl₃, 77.0 ppm, +25 °C): δ 33.6 (CH₃), 55.5 (CH₃), 108.0 (Cq), 114.6 (CH), 121.6 (CH), 125.6 (Cq), 126.3 (CH), 127.0 (CH), 127.2 (CH), 127.3 (Cq), 128.7 (CH), 129.2 (CH), 129.4 (CH), 130.3 (Cq), 132.0 (Cq), 134.6 (Cq), 141.9 (CH), 149.8 (Cq), 151.2 (Cq), 155.5 (Cq), 159.7 (Cq). **HRMS(ESI-QTOF)**. Calcd. for C₂₃H₁₉N₄O₃⁺ 399.1452. Found 399.1445.

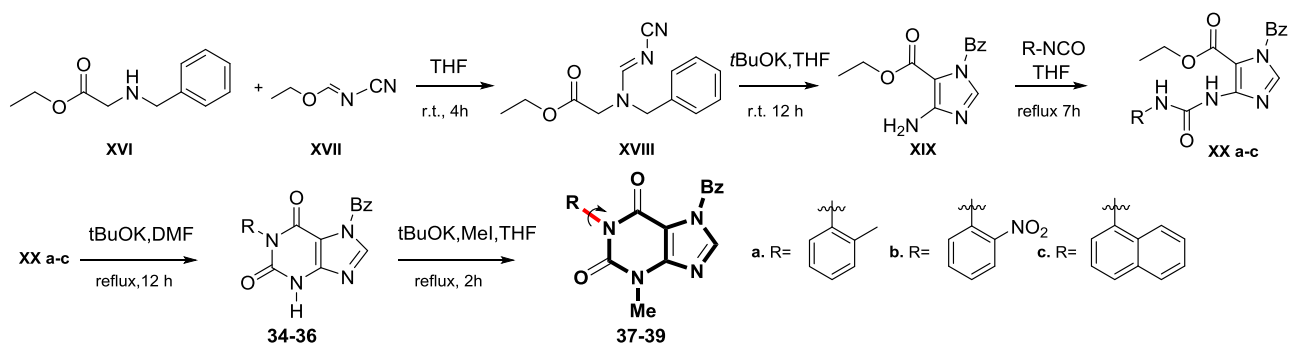
The racemic mixture was resolved with Lux Cellulose 2 column (32/68 *n*-hexane/*i*PrOH, 5 mL/min) with *t_r* = 18.63 min and *t_r* = 31.20 min, respectively. Kinetic studies were performed in ChiralPak AS-H column with *t_r* = 16.85 min and *t_r* = 21.07 min.

1-(4-methoxyphenyl)-7-methyl-3-(naphthalene-1-yl)-1H-purine-2,6(3H,7H)-dione (42b).

¹H-NMR (600 MHz, CDCl₃, 7.26 ppm, +25 °C): δ 3.75 (s, 3H, CH₃), 3.94 (s, 3H, CH₃), 6.94 (m, 2H), 7.21 (m, 2H), 7.37 (s, 1H), 7.43 (m, 2H), 7.54 (m, 3H), 7.86 (d, *J*=8.5 Hz, 1H), 7.92 (m, 1H).

¹³C-NMR (150.8 MHz, CDCl₃, 77.0 ppm, +25 °C): δ 33.6 (CH₃), 55.5 (CH₃), 107.8 (Cq), 114.6 (CH), 122.0 (CH), 125.6 (Cq), 126.5 (CH), 127.0 (CH), 127.3 (CH), 127.6 (Cq), 128.7 (CH), 129.7 (CH), 130.07 (CH), 130.1 (Cq), 131.4 (Cq), 134.7 (Cq), 142.1 (CH), 149.8 (Cq), 151.4 (Cq), 155.8 (Cq), 159.5 (Cq). **HRMS(ESI-QTOF)**. Calcd. for C₂₃H₁₉N₄O₃⁺ 399.14517. Found 399.1447.

The racemic mixture was resolved with Lux Cellulose 2 (40/60 *n*-hexane/*i*PrOH, 5 mL/min) column with *t_r* = 40.65 min and *t_r* = 50.19 min, respectively. Kinetic studies were performed in ChiralPak AS-H column with *t_r* = 14.06 min and *t_r* = 21.22 min respectively.

1-aryl-xanthineFigure 7.4.11 Synthetic pathway followed to synthesized molecules **34-39**.**General procedure for the synthesis of compounds 34-36**

The appropriate aryl isocyanate (0.4 mmol) was added to a solution of ethyl-4-amino-1-benzyl-1H-imidazole-5-carboxylate (**XIX** 0.2 mmol) in THF (4.7 mL) and the reaction mixture was stirred under reflux conditions for 7h. The resulting mixture, containing **XX a-c**, was concentrated under reduced pressure conditions and then dissolved in 5 mL of DMF. *t*-BuOK (0.067g, 0.6mmol) were added to this solution. The mixture was stirred under reflux overnight. Subsequently, the mixture was quenched with an aqueous solution of HCl and extracted with EtOAc. The combined organic layer was dried with Na₂SO₄, filtered, concentrated under reduced pressure and purified by column chromatography (EtOAc : Hexane = 2:1 with gradient to 1:0) to afford products **34-36** with a 80% (white amorphous solid, 53 mg, 0.16 mmol), 65% (white amorphous solid, 47 mg, 0.13 mmol), and 80% yield (white amorphous solid, 58 mg, 0.157 mmol), respectively.

7-benzyl-1-(*o*-tolyl)-1H-purine-2,6(3H,7H)-dione (34).

¹H-NMR (600 MHz, CD₃CN, 1.96 ppm, +25 °C): δ 2.07 (s, 3H), 5.46 (s, 2H), 7.15 (d, *J*=7.8 Hz, 1H), 7.29-7.38 (m, 8H), 7.85 (s, 1H), 9.87 (NH). ¹³C-NMR (150.8 MHz, CD₃CN, 118.3 ppm, +25 °C): δ 17.4 (CH₃), 50.5 (CH₂), 107.8 (Cq), 127.7 (CH), 128.7 (CH), 129.1 (CH), 129.6 (CH), 129.7₅ (CH), 130.3 (CH), 131.6 (CH), 136.1 (Cq), 137.6 (Cq), 137.8 (Cq), 143.4 (CH), 149.3 (Cq), 151.8 (Cq), 156.2(Cq). HRMS(ESI-QTOF). Calcd. for C₁₉H₁₇N₄O₂⁺ 333.1346. Found 333.1348.

7-benzyl-1-(2-nitrophenyl)-1H-purine-2,6(3H,7H)-dione (35).

Compound **35** was further purified by semipreparative HPLC on a Luna C18 column (10 μm, 250 x 21.2 mm, 20 mL/min, ACN:H₂O = 63:37 v/v).

¹H-NMR (600 MHz, CD₃CN, 1.96 ppm, +25 °C): δ 5.42 (d, *J*= 15.2 Hz, 1H), 5.45 (d, *J*=15.2 Hz, 1H), 7.32-7.38 (m, 5H), 7.52 (dd, *J*=7.9, 1.5 Hz, 1H), 7.69 (ddd, *J*=8.2, 7.6, 1.5 Hz, 1H), 7.84 (ddd, *J*=7.9, 7.6, 1.5 Hz, 1H), 7.9 (s, 1H), 8.16 (dd, *J*=8.2, 1.5 Hz, 1H), 9.52 (NH). ¹³C-NMR (150.8 MHz,

CD₃CN, 118.3 ppm, +25 °C) : δ 50.6 (CH₂), 107.6 (Cq), 126.2 (CH), 128.6 (CH), 129.2 (CH), 129.8 (CH), 130.4 (Cq), 131.0 (CH), 133.3 (CH), 135.4 (CH), 137.5 (Cq), 144.0 (CH), 147.7 (Cq), 149.6 (Cq), 151.4 (Cq), 155.8 (Cq). **HRMS(ESI-QTOF)**. Calcd. for C₁₈H₁₄N₅O₄⁺ 364.1040. Found 364.1044.

7-benzyl-1-(naphthalene-1-yl)-1H-purine-2,6(3H,7H)-dione (36).

Compound **36** was further purified by semipreparative HPLC on a Luna C18 column (10 μ m, 250 x 21.2 mm, 20 mL/min, ACN:H₂O = 90:10 v/v).

¹H-NMR (600 MHz, CD₃CN, 1.96 ppm, +25 °C): δ 5.45 (d, *J* = 15.2 Hz, 1H), 5.47 (d, *J* = 15.2 Hz, 1H), 7.31-7.38 (m, 5H), 7.45 (d, *J*=7.4 Hz, 1H), 7.49-7.51 (m, 1H), 7.55-7.58 (m, 1H), 7.61-7.63 (m, 1H), 7.66 (d, *J*=8.2 Hz, 1H), 7.88 (s, 1H), 8.01 (dd, *J*=8.2, 2.4 Hz, 2H), 9.73 (NH). **¹³C-NMR** (150.8 MHz, CD₃CN, 118.3 ppm, +25 °C) : δ 50.5 (CH₂), 107.9 (Cq), 123.1 (CH), 126.7 (CH), 127.4 (CH), 128.0 (CH), 128.3 (CH), 128.7 (CH), 129.1 (CH), 129.3 (CH), 129.8 (CH), 129.9 (CH), 131.7 (Cq), 133.8 (Cq), 135.2 (Cq), 137.8 (Cq), 143.5 (CH), 149.5 (Cq), 152.1 (Cq), 156.7 (Cq). **HRMS(ESI-QTOF)**. Calcd. for C₂₂H₁₇N₄O₂⁺ 369.1346. Found 369.1345

General Procedure for the synthesis of compounds 37-39.

Products **34-36** (0.1 mmol) were dissolved in 2.5 mL THF and t-BuOK (18 mg, 0.16 mmol) followed by MeI (d = 2.28 g/mL, 0.01 mL, 0.16 mmol) were added. The mixture was stirred under reflux conditions for 2h and after that, it was extracted with EtOAc. The combined organic layer was dried with Na₂SO₄, filtered and concentrated under reduced pressure to give the compounds **37-39** with 98% (white amorphous solid, 34 mg, 0.098 mmol), 97% (white solid, 36.5 mg, 0.097 mmol), 98% yield (white amorphous solid, 37.5 mg, 0.098 mmol), respectively.

7-benzyl-3-methyl-1-(*o*-tolyl)-1H-purine-2,6(3H,7H)-dione (37).

¹H-NMR (600 MHz, CD₃CN, 1.96 ppm, +25 °C): δ 2.06 (s, 3H), 3.51 (s, 3H), 5.48 (s, 2H), 7.13 (d, *J*=7.8 Hz, 1H), 7.30-7.37 (m, 8H), 7.89 (s, 1H). **¹³C-NMR** (150.8 MHz, CD₃CN, 118.3 ppm, +25 °C): δ 17.5 (CH₃), 30.1 (CH₃), 50.6 (CH₂), 107.8 (Cq), 127.7 (CH), 128.8 (CH), 129.2 (CH), 129.6 (CH), 129.8 (CH), 130.2 (CH), 131.6 (CH), 136.7 (Cq), 137.6 (Cq), 137.8 (Cq), 143.1 (CH), 151.0 (Cq), 152.1 (Cq), 155.7(Cq). **HRMS(ESI-QTOF)**. Calcd. for C₂₀H₁₉N₄O₂⁺ 347.1503. Found 347.1507.

The atropisomers of compound **37** were resolved by ChiralPak AD-H column (10 μ m, 250 x 20 mm, 20 mL/min, hexane:*i*PrOH = 80:20 v/v).

7-benzyl-3-methyl-1-(2-nitrophenyl)-1H-purine-2,6(3H,7H)-dione (38).

m.p. 176.0-179.0 °C, ¹H-NMR (600 MHz, CD₃CN, 1.96 ppm, +25 °C): δ 3.52 (s, 3H), 5.45 (d, *J*= 15.4 Hz, 1H), 5.47 (d, *J*= 15.4 Hz, 1H), 7.32-7.38 (m, 5H), 7.49 (dd, *J*=8.0, 1.4 Hz, 1H), 7.70 (td, *J*=8.1, 1.4 Hz, 1H), 7.84(td, *J*=7.7, 1.5 Hz, 1H), 7.93(s, 1H), 8.16 (dd, *J*=8.2, 1.6 Hz, 1H). ¹³C-NMR (150.8 MHz, CD₃CN, 118.3 ppm, +25 °C) : δ 30.2 (CH₃), 50.8 (CH₂), 107.7 (Cq), 126.2 (CH), 128.7 (CH), 129.2 (CH), 129.8 (CH), 130.9 (Cq), 130.9_s (CH), 133.2 (CH), 135.4 (CH), 137.5 (Cq), 143.7 (CH), 147.7 (Cq), 151.2 (Cq), 151.9 (Cq), 155.3 (Cq). **HRMS(ESI-QTOF)**. Calcd. for C₁₉H₁₆N₅O₄⁺ 378.1197. Found 378.1201.

The atropisomers of compound **38** were resolved by Lux Cellulose 2 column (5 μm, 250 x 10 mm, 5 mL/min, hexane:*i*PrOH = 50:50 v/v).

7-benzyl-3-methyl-1-(naphthalene-1-yl)-1H-purine-2,6(3H,7H)-dione (39).

¹H-NMR (600 MHz, CD₃CN, 1.96 ppm, +25 °C): δ 3.56 (s, CH₃), 5.46 (d, *J*= 15.3 Hz, 1H), 5.49 (d, *J*= 15.3 Hz, 1H), 7.31-7.38 (m, 5H), 7.45 (d, *J*=7.4 Hz, 1H), 7.47-7.51 (m, 1H), 7.54-7.58 (m, 1H), 7.61-7.64 (m, 1H), 7.65 (d, *J*=8.2 Hz, 1H), 7.94 (s, 1H), 8.01 (dd, *J*=8.2, 2.4 Hz, 2H). ¹³C-NMR (150.8 MHz, CD₃CN, 118.3 ppm, +25 °C) : δ 30.2 (CH₃), 50.6 (CH₂), 108.0 (Cq), 123.2 (CH), 126.7 (CH), 127.3 (CH), 127.9 (CH), 128.2 (CH), 128.7 (CH), 129.1 (CH), 129.3 (CH), 129.7₆ (CH), 129.8 (CH), 131.6 (Cq), 134.3 (Cq), 135.2 (Cq), 137.8 (Cq), 143.3 (CH), 151.2 (Cq), 152.6 (Cq), 156.2 (Cq). **HRMS(ESI-QTOF)**. Calcd. for C₂₃H₁₉N₄O₂⁺ 383.1503. Found 383.1504.

The atropisomers of compound **39** were purified by ChiralPak AD-H column (10 μm, 250 x 20 mm, 20 mL/min, hexane:*i*PrOH = 76:24 v/v).

7.4.3 Assignment of absolute configuration

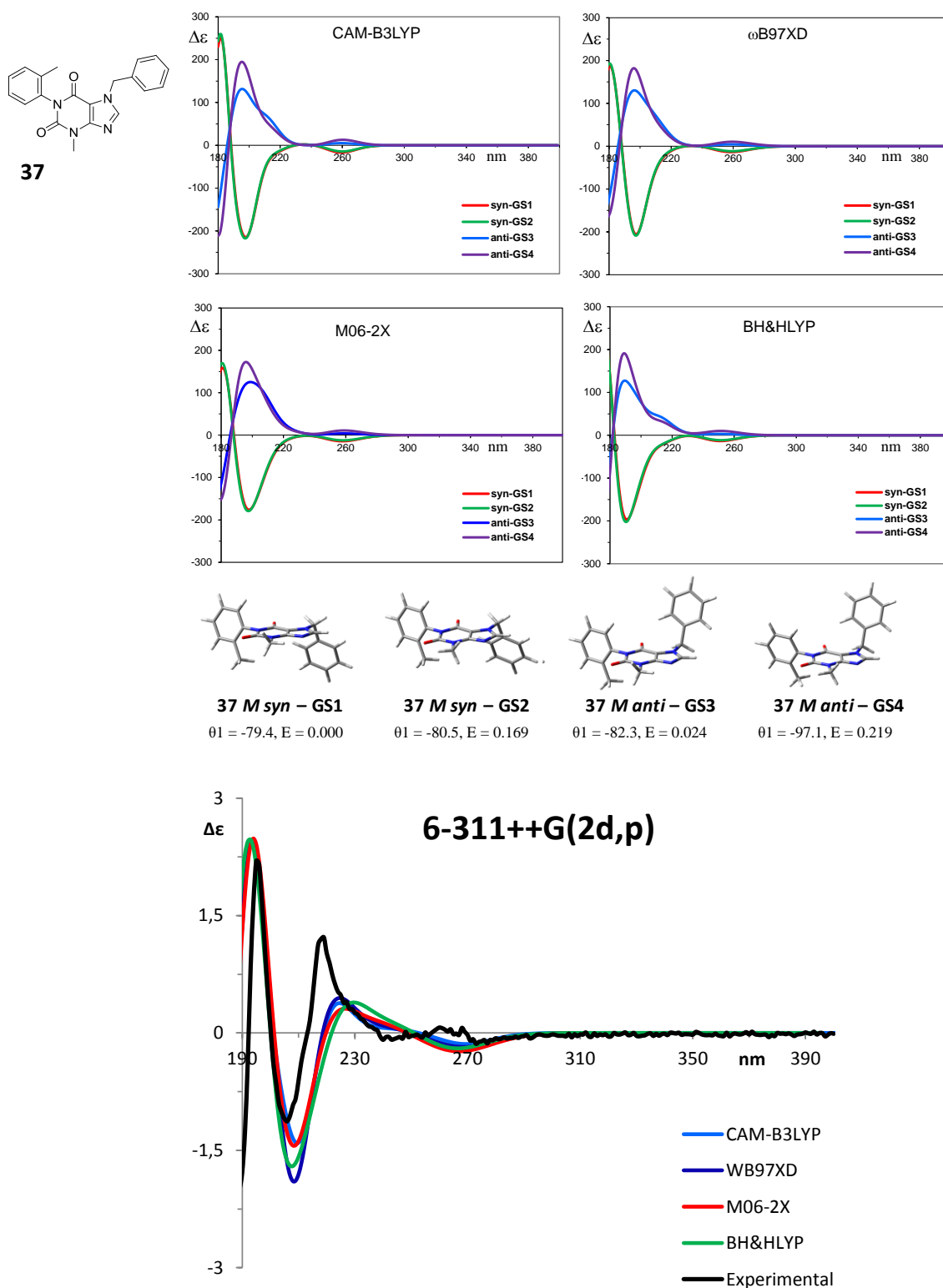


Figure 7.4.12 Top. Calculated ECD spectra for the four conformations with different dihedral angles and different benzyl disposition of compound **37-M** using 4 different functionals and 6-311++G(2d,p) as basis set. Bottom: Experimental ECD spectra of 1° eluted CSP-HPLC, compared with calculated ECD sum spectra of the four conformations of compound **37** using four different functionals (CAM-B3LYP, ωB97XD, M06-2X, BH&HLYP) and 6-311++G(2d,p) as basis set. The calculated ECD spectra are shifted by 10 nm, 10 nm, 10 nm and 15 nm and multiplied by a factor of 0.035, 0.055, 0.065, 0.055, respectively.

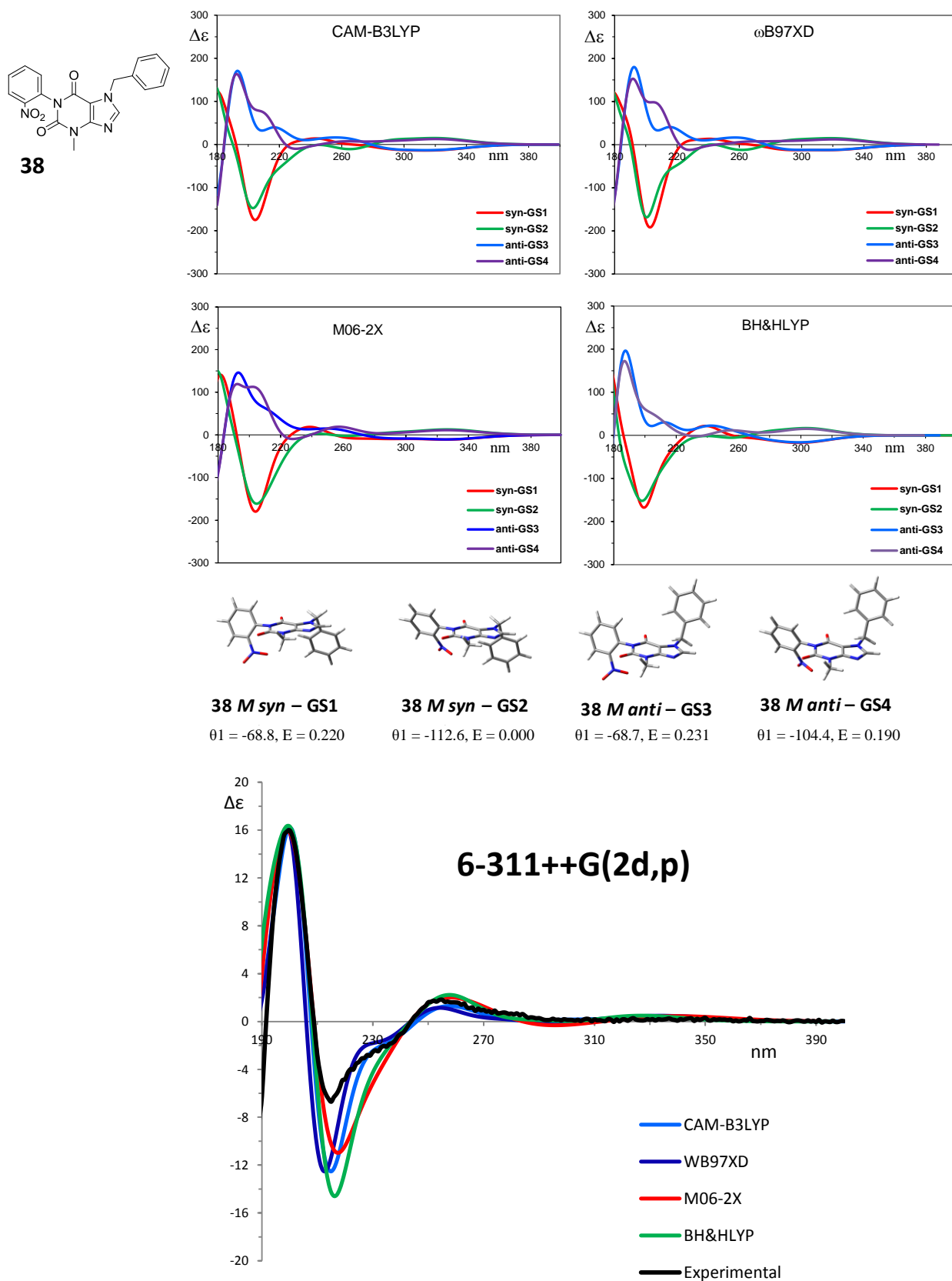


Figure 7.4.13 Experimental ECD spectra of 1° eluted CSP-HPLC, compared with calculated ECD sum spectra of the four conformations of compound **38-M** using four different functionals (CAM-B3LYP, ω B97XD, M06-2X, BH&HLYP) and 6-311++G(2d,p) as basis set. The calculated ECD spectra are shifted by 10 nm, 10 nm, 12 nm and 16 nm and multiplied by a factor of 0.22, 0.21, 0.22, 0.23, respectively.

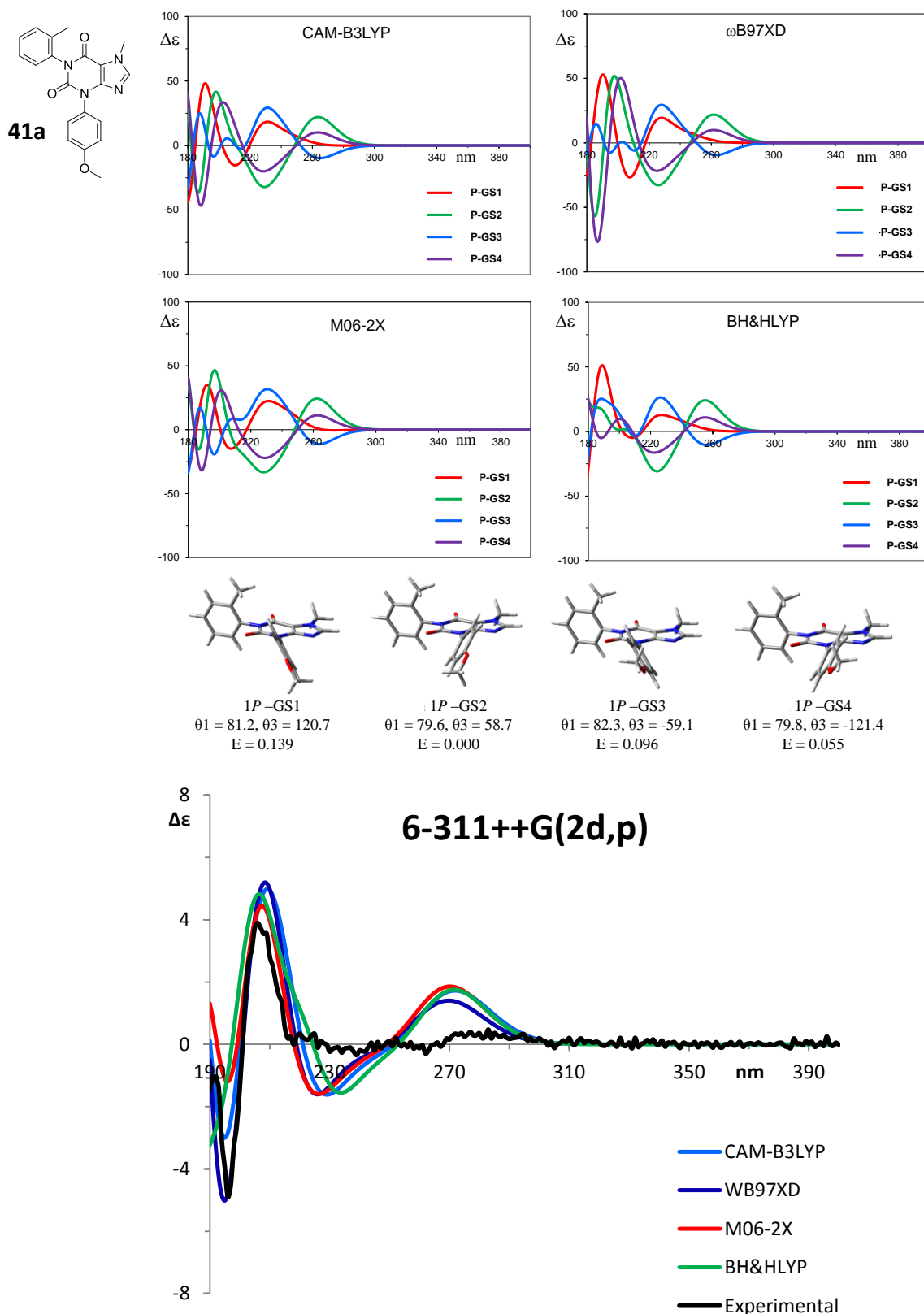


Figure 7.4.14 Top: Calculated ECD spectra for the four conformations with different dihedral angles and different *p*-OMe dispositions of compound **41a** 1^P using 4 different functionals and 6-311++G(2d,p) as basis set. Bottom: Experimental ECD spectra of 2° eluted CSP-HPLC, compared with calculated ECD sum spectra of the four conformations of compound **41a** 1^P using 4 different functionals (CAM-B3LYP, ω B97XD, M06-2X, BH&HLYP) and 6-311++G(2d,p) as basis set. The calculated ECD spectra are shifted by 10 nm, 10 nm, 10 nm and 18 nm and multiplied by a factor of 0.25, 0.2, 0.25, 0.23, respectively.

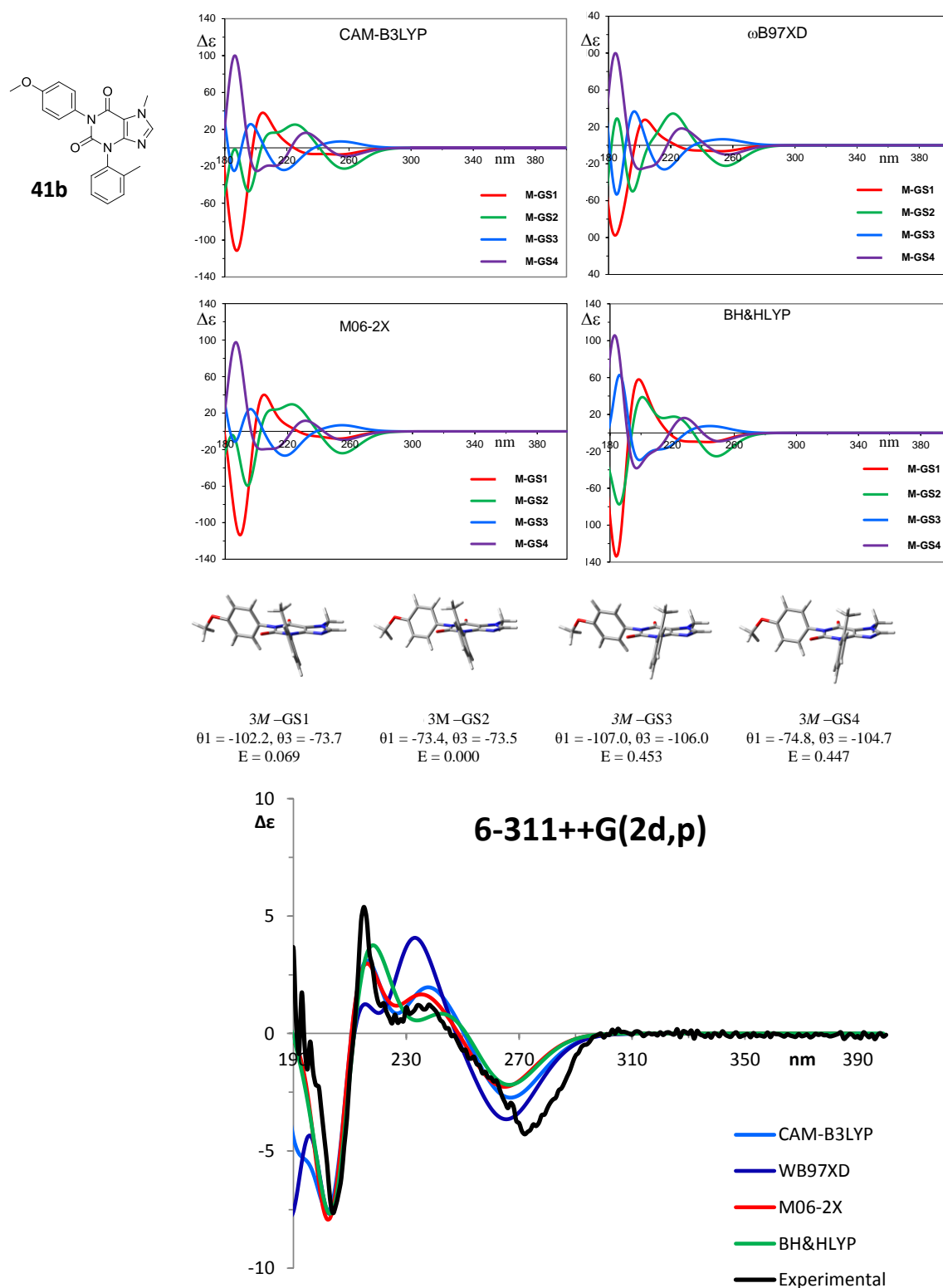


Figure 7.4.15 Top: Calculated ECD spectra for the four conformations with different dihedral angles and different *p*-OMe dispositions of compound **41b** using 4 different functionals and 6-311++G(2d,p) as basis set. Bottom: Experimental ECD spectra of 1° eluted HPLC, compared with calculated ECD sum spectra of the four conformations of compound **41b** 3M using 4 different functionals (CAM-B3LYP, ωB97XD, M06-2X, BH&HLYP) and 6-311++G(2d,p) as basis set. The calculated ECD spectra are shifted by 10 nm, 10 nm, 10 nm and 18 nm and multiplied by a factor of 0.26, 0.35, 0.2, 0.18, respectively.

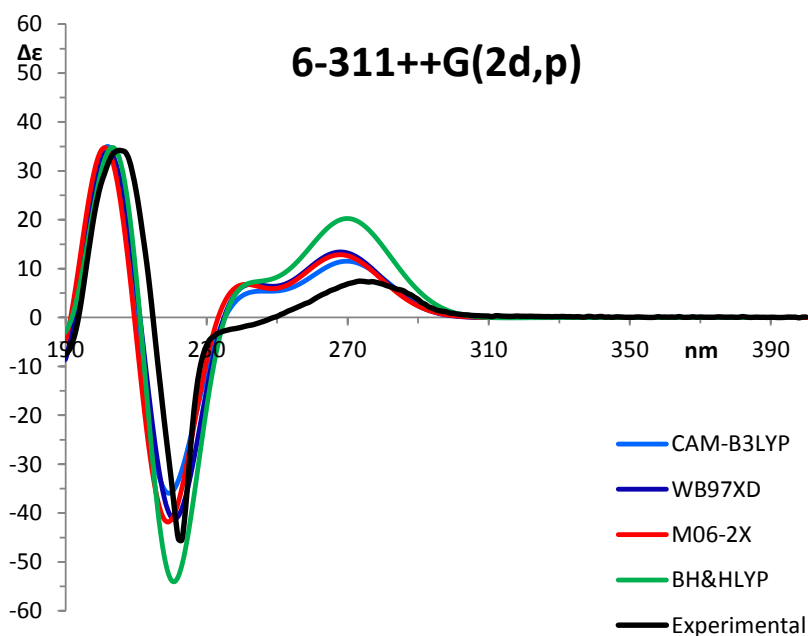
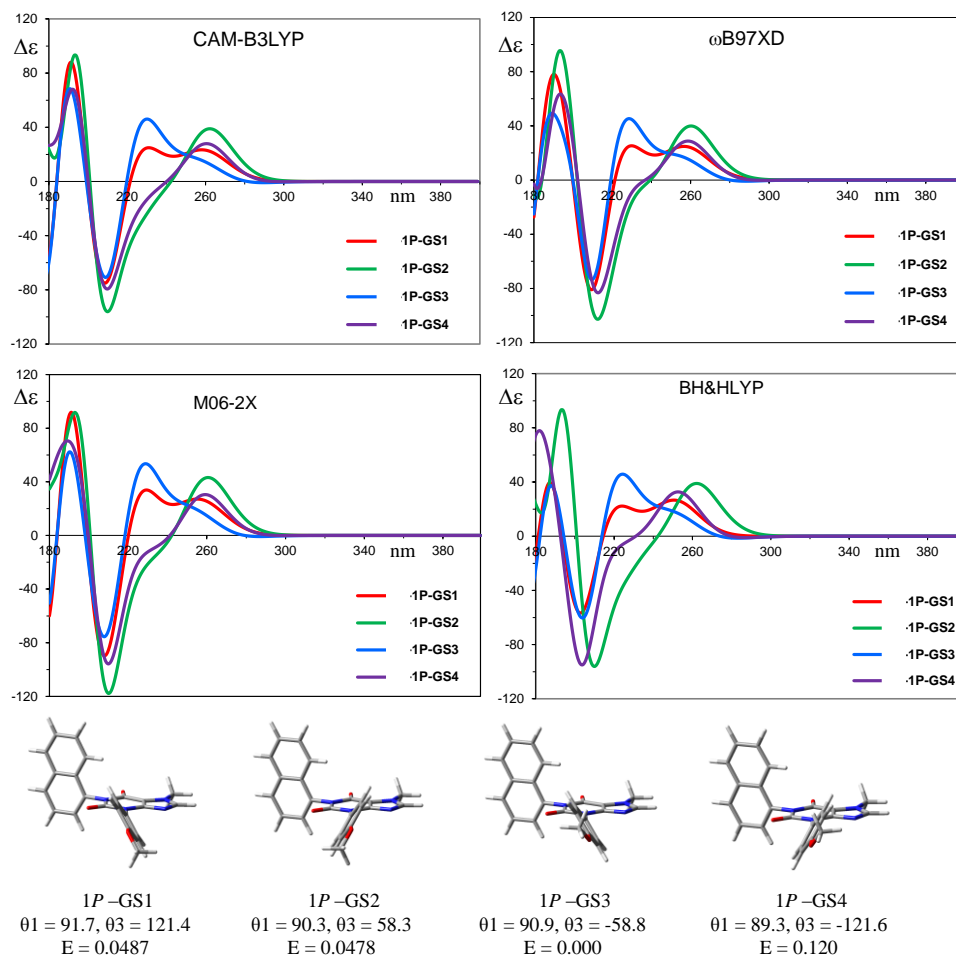
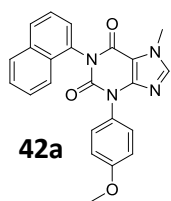


Figure 7.4.16 Top: Calculated ECD spectra for the four conformations with different dihedral angles and different *p*-OMe dispositions of compound **42a** using 4 different functionals and 6-311++G(2d,p) as basis set. Bottom: Experimental ECD spectra of 1° eluted CSP-HPLC, compared with calculated ECD sum spectra of the four conformations of compound **42a** 1P using 4 different functionals (CAM-B3LYP, ω B97XD, M06-2X, BH&HLYP) and 6-311++G(2d,p) as basis set. The calculated ECD spectra are shifted by 10 nm, 10 nm, 10 nm and 15 nm and multiplied by a factor of 0.45, 0.5, 0.45, 0.8, respectively.

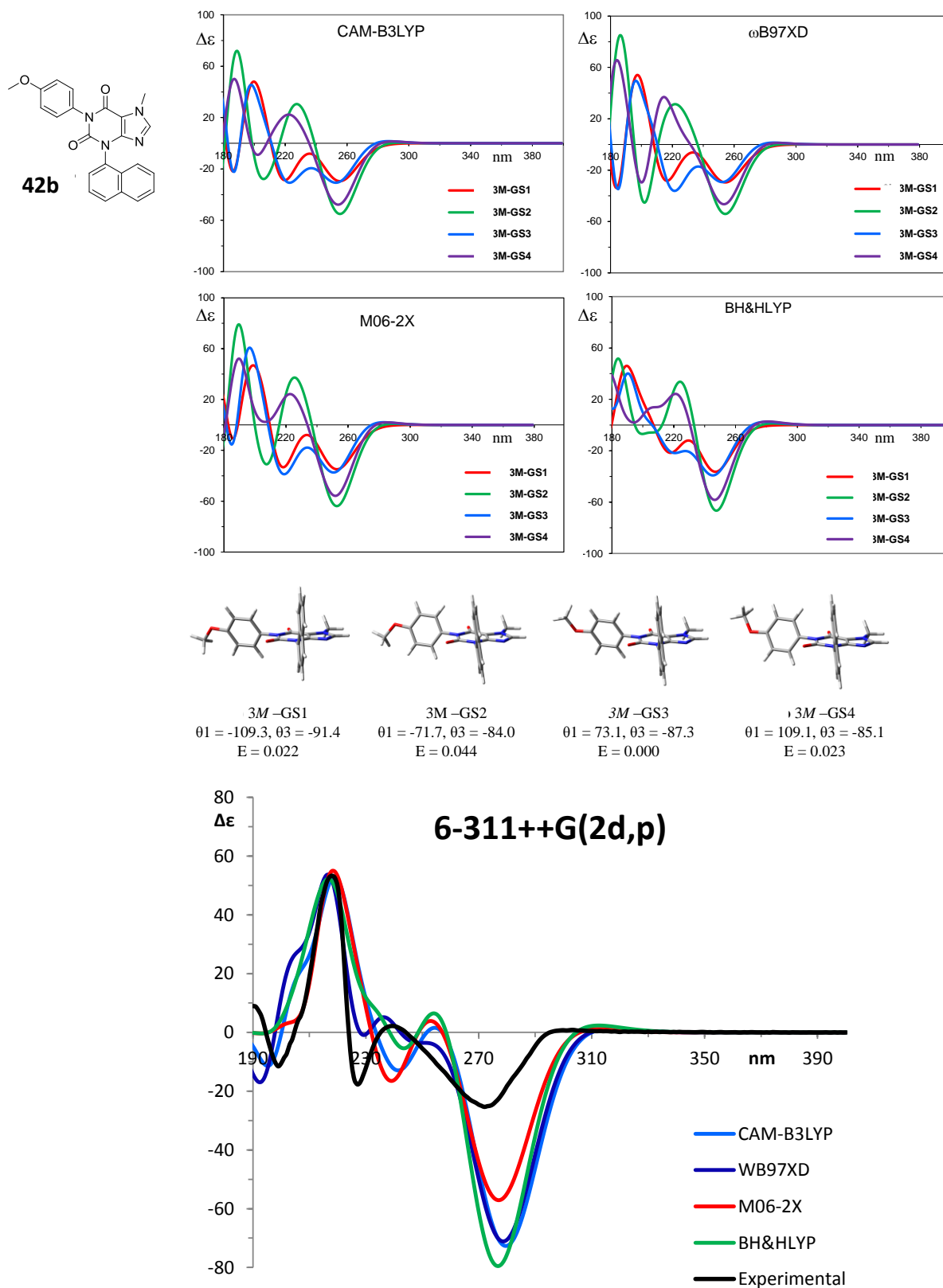


Figure 7.4.17 Top: Calculated ECD spectra for the four conformations with different dihedral angles and different *p*-OMe dispositions of compound **42b** using 4 different functionals and 6-311++G(2d,p) as basis set. Bottom: Experimental ECD spectra of 1° eluted CSP-HPLC is compared with Calculated ECD sum spectra of the four conformations of compound **42b** 3M using 4 different functionals (CAM-B3LYP, ω B97XD, M06-2X, BH&HLYP) and 6-311++G(2d,p) as basis set. The calculated ECD spectra are shifted by 25 nm, 25 nm, 25 nm and 30 nm and multiplied by a factor of 1.8, 1.8, 1.2, 1.6, respectively.

¹ Busschaert N., Kirby I. L., Young S., Coles S. J., Horton P. N., Light M. E., Gale P. A. *Angew. Chem. Int. Ed.*, **2012**, *51*, 4426-4430.

² Zhao J., Li Z., Yan S., Xu S., Wang M. A., Fu B., Zhang, Z. *Org. Lett.*, **2016**, *18*, 1736.

³ Whiteley M. A. *J. Chem. Soc., Trans.*, **1907**, *91*, 1330-1350.

7.5 Tetrasubstituted cyclopentadienones as suitable enantiopure ligands with axial chirality

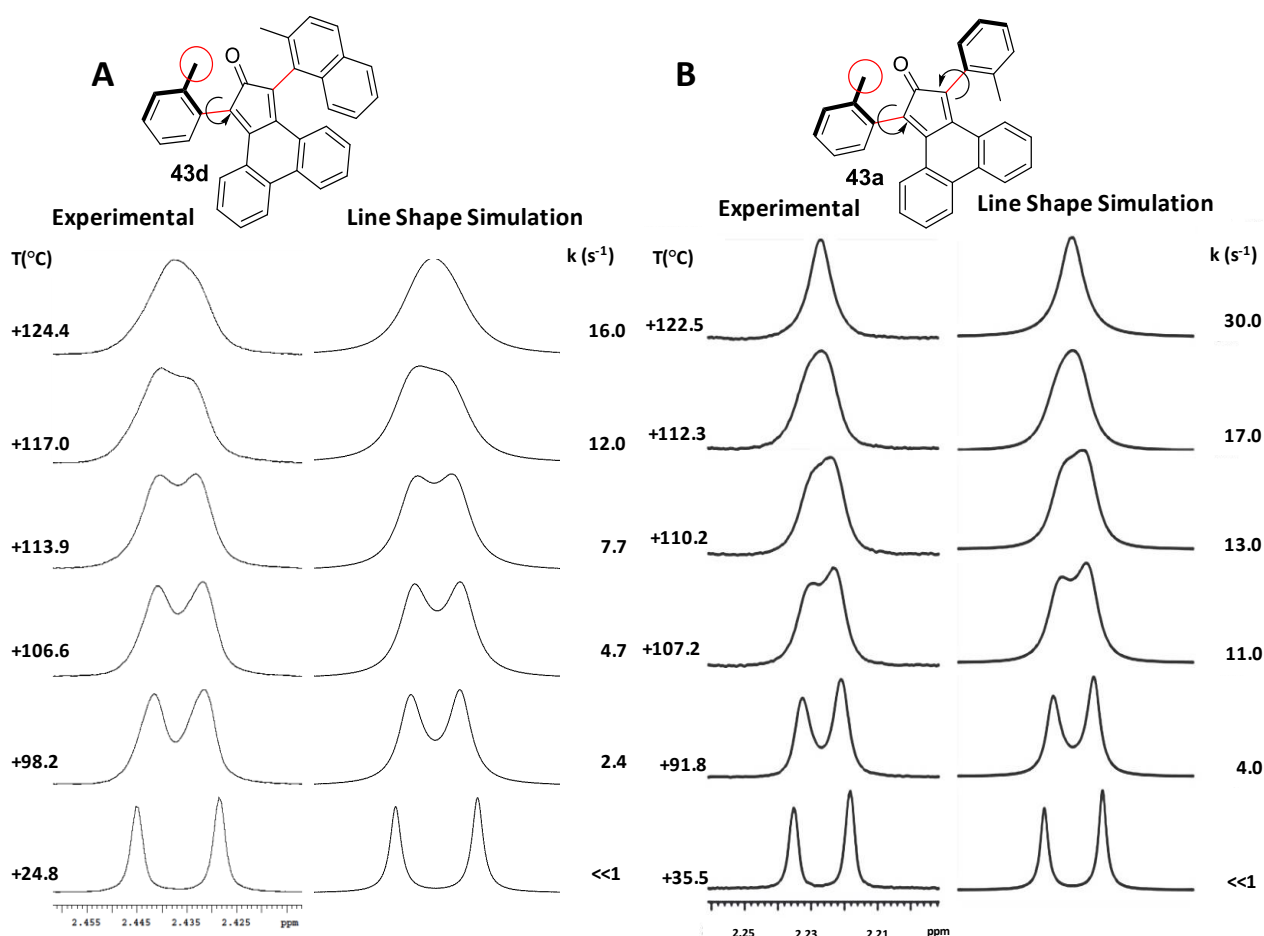


Figure 7.5.1 **A**) Left: ¹H NMR methyl signals of the two diastereoisomers of compound **43d** at different temperatures (600 MHz in C₂D₂Cl₄). Right: line shape simulations obtained with the corresponding rate constants. **B**) Left: ¹H NMR methyl signals of the two diastereoisomers of compound **43a** at different temperatures (600 MHz in C₂D₂Cl₄). Right: line shape simulations obtained with the corresponding rate constants.

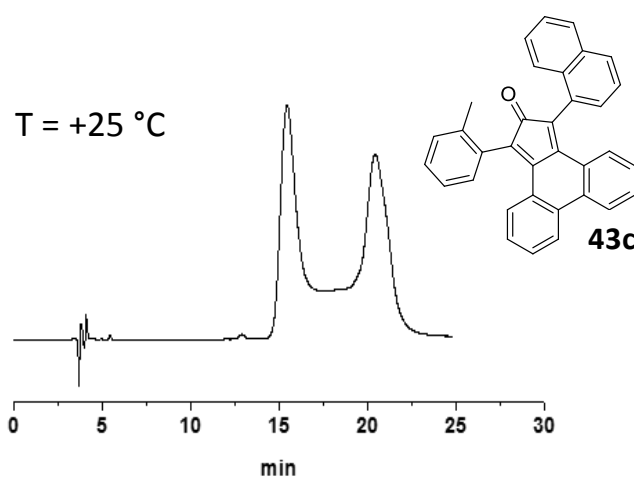


Figure 7.5.2 CSP-HPLC chromatogram of **43c** recorded at +25 °C. Chiralpak IA 250 x 4.6 mm eluent *n*-hexane/CH₂Cl₂, 98/2 + 0.05% EtOH, 1.0 mL/min, UV detection at 280 nm.

Dynamic HPLC and line shape simulation

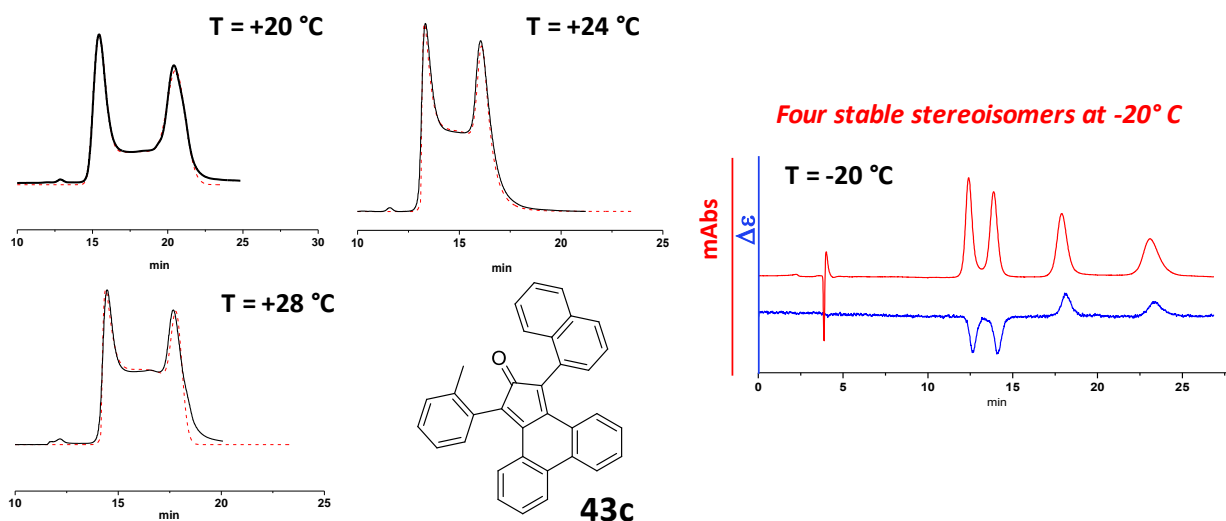
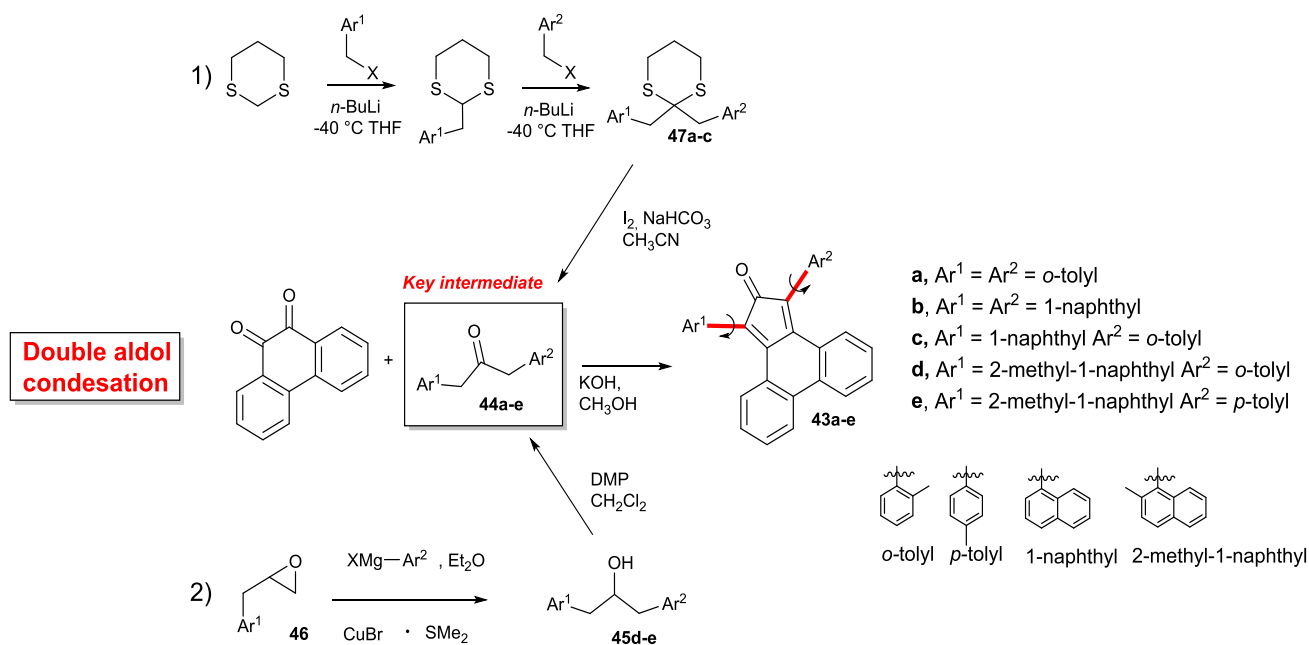


Figure 7.5.3 Right: D-CSP-HPLC chromatogram of **43c** recorded at different temperatures (Black solid line) and line shape simulation (red dotted line). Chiralpak IA 250 x 4.6 mm eluent *n*-hexane/CH₂Cl₂, 98/2 + 0.05% EtOH, 1.0 mL/min, UV detection at 280 nm. Left: CSP HPLC performed at -20 °C on **43c**, all the four stereoisomers are detectable.

7.5.1 Synthetic procedure

General procedure for the synthesis of dithianes (**47a-c**)¹

An oven dried three necked round bottomed flask kept under nitrogen atmosphere, was charged with a solution of 1,3-dithiane (15.4 mmol, 1.85 g, 1 eq.) in 60 mL of anhydrous THF (0.26 M). The resultant solution was brought to -40 °C and 15 mL of *n*-BuLi (15.4 mmol, 9.6 mL, 1 eq., 1.6 M in *n*-hexane) was added dropwise to the solution and left to stir at this temperature for 2 hours. In a

separate two-necked flask flushed with N₂ was dissolved the appropriate halide (15.4 mmol, 1 eq.) in dry THF (1.2 M). This solution was then added dropwise at -40 °C to the solution of the lithiate: the resultant deep yellow solution was allowed to return to room temperature in 2.5 hours. The raw mixture of the mono-substituted 1,3-dithiane was cooled again to -40 °C and 15 mL of *n*-BuLi (15.4 mmol, 9.6 mL, 1 eq., 1.6 M in *n*-hexane) was added dropwise. The yellow solution became transparent, then turned from emerald to deep green, and left to stir at -40 °C for 2 hours. The second halide (15.4 mmol, 1 eq.) was diluted in THF (1.2 M) and added dropwise to the reaction at -40 °C. Then the mixture was allowed to return to ambient temperature overnight. Before working up the reaction, it was partially concentrated under reduced pressure and then quenched with a saturated solution of NH₄Cl. The organic phase was separated, and the water phase was washed three times with diethyl ether. The combined organic phase was dried over MgSO₄ and the solvent removed in vacuum. The crude 2,2-diarylmethylene-1,3-dithiane was then purified by crystallization, flash chromatography on silica gel or semi-preparative HPLC.

2,2-bis(2-methylbenzyl)-1,3-dithiane (47a)

Using the general procedure, the crude product was purified through a precipitation in *n*-hexane/Et₂O 9:1. The sticky solid was used without further purification for the next step of the synthesis (2.00 g, yield = 39.5%). A small pure sample was obtained by a silica gel chromatography column (petroleum ether: EtOAc, 8:2 gradient to 6:4) and used for the characterization. **¹H NMR** (600 MHz, CDCl₃, +25 °C, TMS); δ 1.85 (m, 2H), 2.29 (s, 6H), 2.82 (m, 4H), 3.27 (s, 4H), 7.12-7.17 (m, 6H), 7.47 (m, 2H). **¹³C NMR** (150.8 MHz, CDCl₃, +25 °C, TMS); δ 20.7 (CH₃), 24.1 (CH₂), 26.7 (CH₂), 42.3 (CH₂), 56.1 (Cq), 125.1 (CH), 126.9 (CH), 130.2 (CH), 131.9 (CH), 135.0 (Cq), 137.7 (Cq).

2,2-bis(naphthalen-1-yl-methyl)-1,3-dithiane (47b).

Using the general procedure, the crude product was purified through a precipitation in *n*-hexane/Et₂O 9:1 as a sticky solid (1.54 g, yield = 25%). **¹H NMR** (600 MHz, CDCl₃, +25 °C, TMS); δ 1.77 (m, 2H), 2.76 (m, 4H), 3.75 (s, 4H), 7.40-7.47 (m, 6H), 7.64 (d, *J* = 7.3 Hz, 2H), 7.78 (d, *J* = 8.1 Hz, 2H), 7.82 (d, *J* = 8.1 Hz, 2H), 7.82 (d, *J* = 8.5 Hz, 2H). **¹³C NMR** (150.8 MHz, CDCl₃, +25 °C, TMS); δ 24.0 (CH₂), 27.0 (CH₂), 42.3 (CH₂), 55.9 (Cq), 124.7 (CH), 124.9 (CH), 125.2 (CH), 125.6 (CH), 127.8 (CH), 128.7 (CH), 129.9 (CH), 132.7 (Cq), 133.5 (Cq), 133.6 (Cq).

2-(2-methylbenzyl)-2-(naphthalen-1-ylmethyl)-1,3-dithiane (47c)

Using the general procedure, the crude product was partially purified through multiple precipitation (in *n*-hexane : EtOAc, 9:1). The crude mixture was used without further purification for the next step of the synthesis (sticky solid, 2.53 g, yield 45%). A small pure sample for the characterization was obtained by a semi-preparative HPLC purification (Phenomenex Luna C18, 10 μ m, 100 Å, 250 x 21.2 mm, CH₃CN/H₂O, 90/10, 20 mL/min, 254 nm, t_R = 14.23 min). **¹H NMR** (600 MHz, CDCl₃, +25 °C, TMS); δ 1.82 (m, 2H), 2.29 (s, 3H), 2.83 (m, 4H), 3.30 (s, 2H), 3.75 (s, 2H), 7.13-7.19 (m, 3H), 7.43-7.51 (m, 4H), 7.64 (d, J = 6.9 Hz, 1H), 7.79 (d, J = 7.7 Hz, 1H), 7.83 (m, 1H), 8.03 (m, 1H). **¹³C NMR** (150.8 MHz, CDCl₃, +25 °C, TMS); δ 20.8 (CH₃), 24.0 (CH₂), 26.9 (2CH₂), 41.8 (CH₂), 42.8 (CH₂), 56.0 (Cq), 124.6 (CH), 124.8 (CH), 125.22 (CH), 125.2₃ (CH), 125.6 (CH), 126.9 (CH), 127.7 (CH), 128.7 (CH), 129.8 (CH), 130.3 (CH), 132.0 (CH), 132.7 (Cq), 133.5 (Cq), 133.6 (Cq), 135.0 (Cq), 137.7 (Cq).

General procedure for the deprotection of dithianes (44a-44c)²

To a solution of the appropriate 2,2-diarylmethylene-1,3-dithiane (1.13 mmol, 1 eq.) in acetonitrile (107 mL) and H₂O (5.4 mL) were added sodium bicarbonate (9.08 mmol, 0.762 g, 6.6 eq.) and iodine (4 mmol, 1.01 g, 2.9 eq.) at 0 °C. The reaction mixture was stirred for 1 hour and then quenched with a saturated solution of Na₂S₂O₃. The aqueous layer was extracted twice with diethyl ether (50 mL). The combined organic layer was collected and dried over MgSO₄. The crude was then purified by flash chromatography on silica gel or semi-preparative HPLC.

1,3-di-*o*-tolylpropan-2-one (44a)

Using the general procedure the product was purified by flash chromatography on silica gel (petroleum ether : Et₂O, 9:1), as white solid (226 mg, yield = 84%). **¹H NMR** (600 MHz, CDCl₃, +25 °C, TMS); δ 2.17 (s, 6H), 3.73 (s, 4H), 7.07 (d, J = 7.3 Hz, 2H), 7.14-7.20 (m, 6H). **¹³C NMR** (150.8 MHz, CDCl₃, +25 °C, TMS); δ 19.5 (2CH₃), 47.3 (2CH₂), 126.2 (2CH), 127.4 (2CH), 130.4 (2CH), 130.5 (2CH), 132.9 (2Cq), 136.9 (2Cq), 205.6 (CO).

1,3-di(naphthalen-1-yl)propan-2-one (44b)

Using the general procedure with longer (12 h) reaction time, the crude was pass through a plug of silica gel and the product was further purified by semi-preparative HPLC (Phenomenex Synergi Polar-RP, 4 μ m, 80 Å, 250 x 21.2 mm, CH₃CN/H₂O, 68/32, 20 mL/min, 254 nm, t_R = 13.05 min) in 54% yield as white solid (190 mg). **¹H NMR** (600 MHz, CDCl₃, +25 °C, TMS); δ 4.14 (s, 4H), 7.29 (d, J = 6.5 Hz, 2H), 7.39-7.43 (m, 4H), 7.47 (dd, J = 8.6 Hz, J = 8.6 Hz, 2H), 7.70 (d, J = 8.6 Hz, 2H),

7.79 (d, $J = 8.3$ Hz, 2H), 7.86 (d, $J = 8.6$ Hz, 2H). ^{13}C NMR (150.8 MHz, CDCl_3 , +25 °C, TMS); δ 47.1 (2CH₂), 123.9 (2CH), 125.5 (2CH), 125.8 (2CH), 126.4 (2CH), 128.1 (2CH), 128.5 (2CH), 128.7 (2CH), 130.8 (2Cq), 132.2 (2Cq), 133.9 (2Cq), 206.4 (CO).

1-(naphthalen-1-yl)-3-(*o*-tolyl)propan-2-one (44c)

Using the general procedure, the crude was purified by flash chromatography on silica gel (petroleum ether: EtOAc, 8:2 gradient to 6:4). White solid (182 mg, yield = 59%). ^1H NMR (600 MHz, CDCl_3 , +25 °C, TMS) δ 2.07 (s, 3H), 3.71 (s, 2H), 4.14 (s, 2H), 7.03 (d, $J = 7.7$ Hz, 1H), 7.10-7.18 (m, 3 H), 7.31 (d, $J = 6.9$ Hz, 1H), 7.42 (dd, $J = 6.9$ Hz, $J = 7.0$ Hz, 1H), 7.45-7.50 (m, 2H), 7.79 (m, 2H), 7.86 (m, 2H). ^{13}C NMR (150.8 MHz, CDCl_3 , +25 °C, TMS) δ 19.5 (CH₃), 46.9 (CH₂) 47.4 (CH₂), 123.8 (CH), 125.5 (CH), 125.8 (CH), 126.1 (CH), 126.5 (CH), 127.3 (CH), 128.0 (CH), 128.4 (CH), 128.7 (CH), 130.4₁ (CH), 130.4₃ (CH), 130.8 (Cq), 132.2 (Cq), 132.8 (Cq), 133.9 (Cq), 137.0 (Cq), 206.0 (CO).

2-((2-methylnaphthalen-1-yl)methyl)oxirane (46)³

To an ice-cooled solution of 1-bromo-2-methylnaphthalene (16 mmol, 3.54 g, 1 eq.) in 130 mL of dry Et₂O (0.12 M) a solution of *n*-BuLi (16 mmol, 10 mL, 1 eq., 1.6M in *n*-hexane) was added over 7 minutes under N₂ atmosphere. The reaction was stirred at -5 °C for 40 minutes and 2-(chloromethyl)oxirane (16 mmol, 1.25 mL, 1 eq.) was added to the yellow solution. Stirring was continued for 90 minutes at -5 °C. The reaction was quenched with 150 mL of water, extracted with Et₂O (3 x 70 mL), and the collected organic layers washed with brine (50 mL). The product was dried under vacuum evaporation and used as crude for the subsequent reaction. The crude product was dissolved in CH₂Cl₂ (200 mL), and to the solution was added KOH (3.41 mmol, 1.91 g), and 18-crown-6 ether (0.98 mmol, 0.259 g). The reaction was stirred at room temperature overnight. Subsequent workup by filtration on a celite pad followed by evaporation of the solvent at low pressure. The product was purified by chromatography on silica gel (*n*-hexane:EtOAc, 8:2) as a yellow oil (2.57 g, overall yield = 81%). ^1H NMR (600 MHz, CDCl_3 , +25 °C, TMS); δ 2.48 (dd, $J = 4.9$ Hz, $J = 5.2$ Hz, 1H), 2.49 (s, 3H), 2.68 (dd, $J = 4.9$ Hz, $J = 5.2$ Hz, 1H), 3.20 (m, 1H), 4.31 (dd, $J = 15.0$ Hz, $J = 4.9$ Hz, 1H), 4.36 (dd, $J = 15.0$ Hz, $J = 4.9$ Hz, 1H), 7.28 (d, $J = 8.2$ Hz, 1H), 7.39 (dd, $J = 8.2$ Hz, $J = 8.2$ Hz, 1H), 7.47 (dd, $J = 8.2$ Hz, $J = 8.2$ Hz, 1H), 7.63 (d, $J = 8.2$ Hz, 1H), 7.77 (d, $J = 7.9$ Hz, 1H), 8.01 (d, $J = 8.5$ Hz, 1H). ^{13}C NMR (150.8 MHz, CDCl_3 , +25 °C, TMS) δ 20.6 (CH₃), 30.5 (CH₂), 46.9 (CH₂), 51.7 (CH-O), 123.6 (CH), 124.6 (CH), 126.1 (CH), 126.9 (CH), 128.5 (CH), 129.0 (CH), 130.0 (Cq), 132.4 (Cq), 132.7 (Cq), 134.4 (Cq).

General procedure (III) for the synthesis of 1,3 di-substituted alcohols (45d-e)⁴

An oven dried double-necked round bottomed flask (50 mL) with internal stirring, was kept under nitrogen. The flask was charged with oven dried Mg turnings (5.125 mmol, 0.125 g, 2.05 eq.) and barely covered with dry diethyl ether (10 mL). The solution was stirred overnight in order to activate the Mg turnings. A catalytic amount of dibromoethane (0.25 mmol, 20 μ L, 0.05 eq.) and iodine were added, the solution was refluxed until the brown colour disappear and then cooled to room temperature. The appropriate aryl bromide was added (5 mmol, 2 eq.) dropwise and the reaction was heated to reflux until most of the magnesium was consumed (1-2.5 hours). The aryl Grignard reagent so formed was cooled to room temperature and transferred into an oven dried three-necked round bottomed flask under nitrogen equipped with addition funnel, thermometer and septum. The solution was diluted with 10 mL of dry diethyl ether and cooled to -50 °C, then CuBr•S(CH₃)₂ (1.25 mmol, 0.257 g, 0.5 eq.) was added to the mixture that was kept stirring for 2 hours at -50 °C. A solution in Et₂O (0.33 M) of the epoxide **3** (2.5 mmol, 0.495 g, 1 eq.) was charged in the addition funnel and added dropwise at the mixture at -50 °C. The cooling bath was removed and the temperature was allowed to reach the room temperature in 1.5 hour. Subsequent work up with a saturated solution of NH₄Cl allowed to remove the copper as tetra ammonium complex (blue aqueous solution). The crude product was extracted several times with ethyl acetate and purified by flash chromatography.

1-(2-methylnaphthalen-1-yl)-3-(*o*-tolyl)propan-2-ol (45d)

Using the general procedure the product was obtained as yellowish oil (660 mg, yield = 91%) by flash chromatography on silica gel (*n*-hexane : EtOAc, 8:2). ¹H NMR (600 MHz, CDCl₃, +25 °C, TMS); δ 2.23 (s, 3H), 2.51 (s, 3H), 2.94 (m, 2H), 3.33-3.38 (m, 2H), 4.20 (m, 1H), 7.12-7.16 (m, 3H), 7.22 (m, 1H), 7.39 (dd, *J* = 8.4 Hz, *J* = 8.4 Hz, 1H), 7.43 (dd, *J* = 8.2 Hz, *J* = 8.0 Hz, 1H), 7.64 (d, *J* = 8.2 Hz, 1H), 7.80 (d, *J* = 8.0 Hz, 1H), 7.90 (d, *J* = 8.4 Hz, 1H). ¹³C NMR (150.8 MHz, CDCl₃, +25 °C, TMS); δ 19.5 (CH₃), 20.8 (CH₃), 35.7 (CH₂), 41.1 (CH₂), 72.7 (CH-OH), 123.7 (CH), 124.6 (CH), 125.9 (CH), 126.0 (CH), 126.6 (CH), 126.8 (CH), 128.6 (CH), 129.2 (CH), 130.2 (CH), 130.5 (CH), 131.9 (Cq), 132.6 (Cq), 132.7 (Cq), 134.6 (Cq), 136.5 (Cq), 136.8 (Cq).

1-(2-methylnaphthalen-1-yl)-3-(*p*-tolyl)propan-2-ol (45e)

Using the general procedure the product was obtained as yellowish oil (572 mg, yield = 79%) by flash chromatography on silica gel (hexane : EtOAc, 8:2). ¹H NMR (600 MHz, CDCl₃, +25 °C, TMS); δ 1.59 (d, *J* = 8.2, OH), 2.32 (s, 3H), 2.51 (s, 3H), 2.86-2.92 (m, 2H), 3.28-3.35 (m, 2H), 4.18

(m, 1H), 7.12 (m, 4H), 7.30 (d, $J = 8.3$ Hz, 1H), 7.39 (dd, $J = 8.3$ Hz, $J = 8.3$ Hz, 1H), 7.44 (dd, $J = 8.5$ Hz, $J = 8.3$ Hz, 1H), 7.64 (d, $J = 8.5$ Hz, 1H), 7.78 (d, $J = 8.0$ Hz, 1H), 7.93 (d, $J = 8.3$ Hz, 1H). ^{13}C NMR (150.8 MHz, CDCl_3 , +25 °C, TMS); δ 20.8 (CH_3), 21.0 (CH_3), 35.6 (CH_2), 43.5 (CH_2), 73.6 (CH-OH), 123.8 (CH), 124.6 (CH), 125.9 (CH), 126.7 (CH), 128.6 (CH), 129.2₂ (2CH), 129.2₃ (2CH), 129.3 (CH), 131.8 (Cq), 132.6 (Cq), 132.7 (Cq), 134.6 (Cq), 135.4 (Cq), 136.0 (Cq).

General procedure (IV) for the oxidation of 1,3 di-substituted alcohols (44d-e)

To a solution of the appropriate alcohol (45d-e, 2.25 mmol, 1 eq) in DCM (0.01 M), was added in one portion the Dess-Martin periodinane (3.93 eq, 1.667 g, 1.75 eq). The solution was allowed to stir at room temperature for 36 hours. The reaction was quenched with 40 mL of aqueous NaOH 1.3 M and extracted three times with DCM. The combined organic layers were collected, dried with MgSO_4 and the solvent was removed under reduced pressure.

1-(2-methylnaphthalen-1-yl)-3-(*o*-tolyl)propan-2-one (44d)

Using the general procedure IV, the product was purified by flash chromatography on silica gel (*n*-hexane : EtOAc 9:1), as a white solid (337 mg, 52% yield). ^1H NMR (400 MHz, CDCl_3 , +25 °C, TMS); δ 2.08 (s, 3H), 2.36 (s, 3H), 3.69 (s, 2H), 4.19 (s, 2H), 7.04 (m, 1H), 7.11-7.20 (m, 3 H), 7.32 (d, $J = 8.4$ Hz, 1H), 7.38-7.45 (m, 2H), 7.66 (m, 1H), 7.70 (m, 1H), 7.80 (m, 1H). ^{13}C NMR (100.56 MHz, CDCl_3 , +25 °C, TMS); δ 19.5 (CH_3), 20.5 (CH_3), 42.9 (CH_2), 47.2 (CH_2), 123.2 (CH), 124.8 (CH), 126.2 (CH), 126.5 (CH), 127.4 (CH), 127.6 (CH), 128.0 (Cq), 128.6 (CH), 129.0 (CH), 130.3 (CH), 130.4 (CH), 132.4 (Cq), 132.6 (Cq), 132.8 (Cq), 134.7 (Cq), 136.9 (Cq), 205.8 (CO).

1-(2-methylnaphthalen-1-yl)-3-(*p*-tolyl)propan-2-one (44e)

Using the general procedure IV the product was purified by flash chromatography on silica gel (*n*-hexane : EtOAc, 9:1) as a white solid (311 mg, 48% yield). ^1H NMR (600 MHz, CDCl_3 , +25 °C) δ = 2.33 (s, 3H), 2.36 (s, 3H), 3.65 (s, 2H), 4.19 (s, 2H), 7.01 (m, 2H), 7.11 (m, 2H), 7.31 (d, $J = 8.1$ Hz, 1H), 7.38-7.45 (m, 2H), 7.69 (m, 2H), 7.80 (m, 1H). ^{13}C NMR (150.8 MHz, CDCl_3 , +25 °C, TMS); δ 20.6 (CH_3), 21.1 (CH_3), 42.8 (CH_2), 48.7 (CH_2), 123.2 (CH), 124.7 (CH), 126.4 (CH), 127.5 (CH), 128.0 (Cq), 128.6 (CH), 129.1 (CH), 129.3 (2CH), 129.4 (2CH), 130.9 (Cq), 132.5 (Cq), 132.7 (Cq), 134.8 (Cq), 136.7 (Cq), 206.2 (CO).

General procedure for the synthesis of phencyclones derivatives (43a-e)

Phenanthrene-9,10-dione (0.741 mmol, 0.154 g, 1 eq.) and the appropriate ketone (0.741 mmol, 1 eq., see ESI for the preparation of the ketones) were placed in a two-necked round-bottomed flask and dissolved with 15 mL of methanol. The solution was refluxed for 1 hour until the complete dissolution of the reagents. KOH (0.590 mmol, 0.033 g, 0.8 eq.) was separately dissolved in 6.0 mL of methanol and added dropwise to the reaction mixture. The mixture was allowed to reflux from 2 to 24 hours. The mixture was cooled down to room temperature and then the crude was filtrated. The precipitate was eventually further purified with semi-preparative HPLC.

1,3-di-*o*-tolyl-2*H*-cyclopenta[*l*]phenanthren-2-one (43a)

Using the general procedure, the precipitate was purified through a plug on silica gel (*n*-hexane : EtOAc, 95:5) and subsequent semi-preparative HPLC Phenomenex Synergi Polar-RP, (4 μ m, 250 x 21.2 mm, CH₃CN/H₂O, 90/10, 20 mL/min, 254 nm, t_R = 8.87 min) yielded 152 mg (50% yield) of a deep green solid. ¹H NMR (*syn* 50% + *anti* 50% 600 MHz, CDCl₃, +25 °C, TMS) δ 2.25 (s, *syn+anti*, 6H), 6.91 (m, *syn+anti*, 2H), 7.13 (dd, *syn+anti*, J = 7.0 Hz, J = 7.0 Hz, 2H), 7.17-7.21 (m, *syn+anti*, 2H), 7.23-7.31 (m, *syn+anti*, 8H), 7.81 (d, *syn+anti*, J = 7.80 Hz, 2H). ¹³C NMR (*syn+anti*, 150.8 MHz, CDCl₃, +25 °C) δ = 20.1₉ (CH₃), 20.2₅ (CH₃), 123.1 (Cq), 123.3 (Cq), 124.1₆ (CH), 124.1₇ (CH), 126.1 (CH), 126.2 (CH), 128.2₁ (CH), 128.2₆ (CH), 128.7 (2CH), 128.9₀ (CH), 128.9₇ (2Cq), 128.9₈ (CH), 129.0 (CH), 129.8 (CH), 130.0 (CH), 130.4 (CH), 131.2₁ (CH), 131.2₄ (CH), 132.4 (Cq), 132.5 (Cq), 133.1₃ (Cq), 133.1₄ (Cq), 137.3 (Cq), 137.4 (Cq), 147.8₆ (Cq), 147.9₄ (Cq), 200.7₂ (CO), 200.7₇ (CO). HRMS (ESI-QTOF) Calcd. for C₃₁H₂₂O: 410.1671. Found: 410.1666.

1,3-di(naphthalen-1-yl)-2*H*-cyclopenta[*l*]phenanthren-2-one (43b)

Using the general procedure the precipitate was purified through a plug on silica gel (*n*-hexane : EtOAc, 95:5) and subsequent semi-preparative HPLC (Phenomenex Kinetex C18, 5 μ m, 250 x 21.2 mm, CH₃CN/H₂O, 90/10, 20 mL/min, 254nm, t_R = 12.54 min) yielded 239 mg (67% yield) of a deep green solid. ¹H NMR (52% : 48% *anti+syn*, 600 MHz, CDCl₃, +25 °C, TMS); δ 6.72 (m, *syn+anti*, 2H), 6.96 (dd, *syn+anti*, J = 8.1 Hz, J = 8.1 Hz, 2H), 7.21 (m, *syn+anti*, 2H), 7.41-7.50 (m, *syn+anti*, 6H), 7.58 (m, *syn+anti*, 2H), 7.82 (d, *syn+anti*, J = 8.7 Hz, 2H), 7.91 (d, *syn+anti*, J = 7.9 Hz, 4H), 7.96 (d, J = 8.3 Hz, 1H), 7.99 (d, J = 8.3 Hz, 1H). ¹³C NMR (*syn+anti*, 150.8 MHz, CDCl₃, +25 °C, TMS) δ 121.6 (Cq), 122.1 (Cq), 124.2 (2CH), 125.7 (CH), 125.7₄ (CH), 125.9₄ (CH), 125.9₉ (CH), 126.0₂ (CH), 126.1 (CH), 126.3₈ (CH), 126.4₀ (CH), 128.0 (CH), 128.4₄ (Cq), 128.4₇ (2CH), 128.5₂ (CH), 128.6₁ (CH), 128.6₄ (CH), 128.6₅ (Cq), 128.6₈ (CH), 130.0 (CH), 130.2 (Cq), 130.4 (Cq), 131.3₃ (CH), 131.3₅ (CH), 131.5 (Cq), 131.8 (Cq), 133.3₈ (Cq), 133.3₉ (Cq), 133.8₆ (Cq), 133.9₀ (Cq),

149.3 (2Cq), 200.7 (CO), 200.8 (CO). HRMS (ESI-QTOF) Calcd. for C₃₄H₂₂O: 482.1671. Found: 482.1665.

1-(naphthalen-1-yl)-3-(*o*-tolyl)-2*H*-cyclopenta[*l*]phenanthren-2-one (43c)

Using the general procedure, the precipitate was purified through a plug on silica gel (*n*-hexane : EtOAc, 98:2) and subsequent semi-preparative HPLC (Phenomenex Kinetex C18, 5μm, 250 x 21.2 mm, CH₃CN/H₂O, 90/10, 20 mL/min, 254 nm, t_R = 14.00 min) yielded 40 mg (12% yield) of a deep green solid. ¹H NMR (51% : 49% *anti*+*syn*, 600 MHz, CDCl₃, +25 °C, TMS); δ 2.21₈ (s, 3H), 2.22₃ (s, 3H), 6.60 (m, *syn*+*anti*, 2H), 6.83-6.89 (m, *syn*+*anti*, 4H), 7.06-7.25 (m, *syn*+*anti*, 14H), 7.30-7.42 (m, *syn*+*anti*, 6H), 7.48 (m, *syn*+*anti* 2H), 7.71 (d, *syn*+*anti*, *J* = 8.2 Hz, 2H), 7.74 (d, *syn*+*anti*, *J* = 7.9 Hz, 2H), 7.79-7.87 (m, *syn*+*anti*, 6H). ¹³C NMR (*syn*+*anti*, 150.8 MHz, CDCl₃, +25 °C, TMS); δ 20.2₈ (CH₃), 20.3₄ (CH₃), 121.5 (Cq), 121.7 (Cq), 123.3 (Cq), 123.7 (Cq), 124.1₀ (CH), 124.1₂ (CH), 124.2₁ (CH), 124.2₃ (CH), 125.6₇ (CH), 125.7₂ (CH), 125.8 (CH), 125.9₇ (CH), 126.0₀ (CH), 126.0₄ (CH), 126.1 (CH), 126.2 (CH), 126.3 (CH), 126.4 (CH), 128.0 (CH), 128.2₁ (CH), 128.2₄ (CH), 128.3 (CH), 128.4₆ (CH), 128.4₇ (2CH), 128.6₀ (2CH), 128.6₁ (CH), 128.7₀ (CH), 128.7₂ (CH), 128.9₂ (CH), 128.9₄ (Cq), 129.0 (Cq), 129.1 (CH), 129.8 (CH), 129.9₁ (CH), 129.9₃ (CH), 130.2 (CH), 130.3 (Cq), 130.4 (CH), 130.5 (CH), 131.2₆ (2CH), 131.2₈ (CH), 131.3 (CH), 131.6 (Cq), 131.7 (Cq), 132.3 (Cq), 132.5 (Cq), 133.2₂ (Cq), 133.2₃ (Cq), 133.2₈ (Cq), 133.3₀ (Cq), 133.8 (Cq), 133.9 (Cq), 137.3 (Cq), 137.4 (Cq), 148.0 (Cq), 148.1 (Cq), 149.2 (2Cq), 200.7 (CO), 200.8 (CO). HRMS (ESI-QTOF) Calcd. for C₃₄H₂₂O: 446.1671. Found: 446.1666.

1-(2-methylnaphthalen-1-yl)-3-(*o*-tolyl)-2*H*-cyclopenta[*l*]phenanthren-2-one (43d)

Using the general procedure, the precipitate was purified through a plug on silica gel (gradient hexane to *n*-hexane : EtOAc, 95:5) and subsequent semi-preparative HPLC (Phenomenex Kinetex C18, 5μm, 250 x 21.2 mm, CH₃CN/H₂O, 90/10, 20 mL/min, 254 nm, t_R = 14.22 min) yielded 27 mg (8% yield) of a deep green solid. The assignment of the signals of the *anti* and *syn* diastereoisomer was obtained by NOE-NMR spectra.

¹H NMR (53% : 47% *anti*+*syn*, 600 MHz, CDCl₃, +25 °C, TMS); δ 2.30 (s, *syn*, 3H), 2.33 (s, *anti*, 3H), 2.41 (s, *syn*, 3H), 2.43 (s, *anti*, 3H), 6.71 (m, *syn*+*anti*, 2H), 6.83 (m, *syn*+*anti*, 2H), 6.95 (m, *syn*+*anti*, 2H), 7.12-7.22 (m, *syn*+*anti*, 4H), 7.24-7.32 (m, *syn*+ *anti*, 10H), 7.37-7.44 (m, *syn*+*anti*, 6H), 7.79-7.91 7.24-7.32 (m, *syn*+ *anti*, 10H). ¹³C NMR (*syn*+*anti*, 150.8 MHz, CDCl₃, +25 °C, TMS); δ 20.2₅ (CH₃), 20.3₅ (CH₃), 20.8 (2CH₃) 121.6 (Cq), 121.7 (Cq), 123.8 (Cq), 123.9 (Cq), 124.0 (2CH), 124.2 (2CH), 125.1 (CH), 125.1₇ (CH), 125.2₁ (CH), 125.3 (CH), 126.2 (2CH), 126.4₆ (CH),

126.4₇ (CH), 128.2₅ (CH), 128.2₇ (CH), 128.2₉ (CH), 128.3₁ (CH), 128.7₂ (CH), 128.7₄ (CH), 128.8₀ (2CH), 128.8₃ (CH), 128.8₇ (CH), 128.8₈ (CH), 128.8₉ (CH), 129.0₄ (CH), 129.0₆ (CH), 129.0₈ (CH), 129.1₀ (CH), 129.1₁ (CH), 129.1₅ (CH), 129.9 (CH), 130.0 (CH), 130.4₃ (CH), 130.4₅ (CH), 131.2₇ (CH), 131.2₉ (CH), 131.3 (Cq), 132.2 (Cq), 132.3₁ (2Cq), 132.3₄ (Cq), 132.3₅ (Cq), 132.5₄ (Cq), 132.5₅ (Cq), 133.0₁ (Cq), 133.0₂ (Cq), 133.1₅ (Cq), 133.1₈ (Cq), 135.1 (Cq), 135.2 (Cq), 137.2 (Cq), 137.4 (Cq), 147.5₇ (Cq), 147.6₃ (Cq), 149.4₁ (Cq), 149.4₅ (Cq), 200.7₁ (CO), 200.7₃ (CO). **HRMS (ESI-QTOF)** Calcd. for C₃₅H₂₄O: 460.1827. Found: 460.1826.

1-(2-methylnaphthalen-1-yl)-3-(*p*-tolyl)-2*H*-cyclopenta[*I*]phenanthren-2-one (43e)

Using the general procedure, the precipitate was purified through a plug on silica gel (gradient *n*-hexane to *n*-hexane: EtOAc, 95:5) and subsequent semi-preparative HPLC (Phenomenex Synergi Polar-RP, 4μm, 250 x 21.2 mm, CH₃CN/H₂O, 90/10, 20 mL/min, 254 nm, t_R = 10.53 min) yielded 17 mg (5% yield) of a deep green solid.

¹H NMR (600 MHz, CDCl₃, +25 °C) δ = 2.40 (s, 3H), 2.41 (s, 3H), 6.71 (dd, *J* = 7.8 Hz, *J* = 7.8 Hz, 1H), 6.82 (d, *J* = 7.8 Hz, 1H), 6.99 (dd, *J* = 7.8 Hz, *J* = 7.8 Hz, 1H), 7.18 (dd, *J* = 8.0 Hz, *J* = 8.0 Hz, 1H), 7.25 (m, 2H), 7.29 (dd, *J* = 7.3 Hz, *J* = 7.8 Hz, 1H), 7.34-7.44 (m, 5H), 7.71 (d, *J* = 7.9 Hz, 1H), 7.79-7.89 (m, 5H). **¹³C NMR** (150.8 MHz, CDCl₃, +25 °C) δ = 20.8 (CH₃), 21.4 (CH₃), 121.1 (Cq), 124.0 (CH), 124.1 (Cq), 124.4 (CH), 125.1 (CH), 125.4 (CH), 126.4 (Cq), 128.2 (CH), 128.2₂ (2CH), 128.8₀ (CH), 128.8₃ (Cq), 128.9 (CH), 129.0 (CH), 129.1 (CH), 129.2 (Cq), 129.4 (2CH), 129.8 (2CH), 131.2 (CH), 131.3 (CH), 132.2₉ (Cq), 132.3₀ (Cq), 133.2 (Cq), 133.3 (Cq), 135.2 (Cq), 138.1 (Cq), 146.6 (Cq), 150.1 (Cq), 200.6 (CO). **HRMS (ESI-QTOF)** Calcd. for C₃₅H₂₄O: 460.1827. Found: 460.1829.

¹ Seebach D., Corey E. J. *J. Org. Chem.*, **1975**, *40*, 231.

² Geum S., Lee H. Y. *Org. Lett.*, **2014**, *16*, 2466.

³ Becker H. D., Amin K. A. *J. Org. Chem.*, **1989**, *54*, 3182.

⁴ Marotta E., Baravelli M., Maini L., Righi P., Rosini G. *J. Org. Chem.*, **1998**, *63*, 8235.